# annual report 2000

NEUTRONS FOR SCIENCE

# annual report 2000

## The Institut Max von Laue-Paul Langevin

The Institut Laue-Langevin (ILL) is an international research centre using neutrons to probe the microscopic structure and dynamics of a broad range of materials. The combination of the world's most powerful neutron source with dedicated instrumentation enables the study of a wide variety of scientific questions. Problems in materials science, chemistry, biology, solid-state physics and nuclear physics are investigated. For these diverse studies, the Institute offers its experimental facilities (some 30 instruments) to scientists world-wide via a peer-review system; confidential industrial experiments are also welcomed.

NEUTRONS
FOR SCIENCE

Dirk Dubbers, the ILL director, refusing to sing along with his secretary, Barbara Standke, and choosing to give an after dinner speech instead.

On 1st January 2000 the ILL launched the Millennium Programme. This ambitious programme will involve the continuous renewal of almost all ILL instruments and infrastructure over the years to come. To celebrate the New Millennium and the launch of the Millennium Programme the Directors organised a Millennium party on 21 January. All ILL people and their families were invited. After the buffet everyone danced to the sounds of the two ILL groups, the Groupe Chanson[1] and the ILL rockers[2].

[1] Barbara Standke (vocals), Gérard Grandene (electrical and electro-mechanical workshop, synthesizer), Claude Yoccoz (experimental hall and vacuum laboratory, drums).
[2] Frottage Cheese (Charles Dewhurst, instrument scientist on D22), Aphra Denmark (Andrew Wildes, instrument scientist on D17), Rock McLoonie (Ross Stewart, instrument scientist on D7) and Trouser McCoff (Trefor Roberts, polarised $^3$He project).

Barbara Standke singing one of her old favourite songs (*We are the champions*).

The Greatest Rockin' Rollin' Band.

Colin Carlile, the British director, head of the projects and techniques division, asking Eddy Lelièvre's daughter for a dance.

Claude Campos, electronics service, and Bob Pratt, reactor crew, improvise a blues.

annual report 2000

# contents

# Director's report

The year 2000 was a good one for the ILL. Our Millennium Renewal Programme got off to a prompt start on the 1st of January 2000, and the programme's first five instruments (D3, IN20, VIVALDI, the Strain Imager, and the SANS detectors) have proceeded apace over the course of the year. At the same time, six other instrument projects have been successfully completed, four of them (D4, D16, H113, D17) on schedule and the remaining two (D20, IN4) once unforeseen technical challenges had been overcome. Users have welcomed all these new instruments with great enthusiasm. IN5 and IN8, the final two instruments in this series, are on the way, for delivery as planned in the course of 2001.

As far as future projects are concerned, the Millennium Programme involves not only many more excellent propositions for instrument renwal, but also plans for an overhaul of ILL's infrastructure, including the renewal of all the old neutron guides. With a recently new reactor, strong new infrastructure, a suite of instruments comprehensively renewed and a rejuvenated workforce, the Institute could not be better prepared to face the future. The Millennium Programme has been presented and discussed, both internally in ILL's committees, and on a national and international level in a number of scientific fora; this discussion is now being extended to involve all former and potential users with a stake in the question. It is our duty to ensure that ILL maintains its rightful place in what is a rapidly evolving field. It is therefore essential that ILL's strengths, and in particular the advantages of very strong continuous neutron beams, be brought fully to bear upon those areas of research most likely to bear fruit. We must also now investigate the potential for widening the scope of neutron technology, and we are lending all our efforts in support of the project to construct the ESS, a pulsed spallation source in Europe.

At the end of 2000 more good news came in for the Institute: the UK partner has announced its intention to make successive increases over the next few years in its contribution to ILL, as well as further investment on a targeted basis in ILL-approved projects. This gives ILL the chance to start work immediately on other parts of its ambitious Millennium Programme.

On a sadder note, in the course of 2000, Professors Louis Néel and Heinz Maier-Leibnitz passed away – two of ILL's greatest pioneers whose memory will be honoured by us all.

In the past year the ILL directors have been particularly occupied with the question of the directions to be taken by science at ILL in the future - we know from experience that if the 'product' is right – and for ILL this means research of the highest quality – the rest will follow. In the following pages we present a selection of the work carried out at the Institute over the last year, and we would like to thank all those who have helped to make such fine results possible. There were also other important challenges to be met in the year – the securing of the fuel cycle, the introduction of a 35-hour week, and the resolution of intricate financial questions, to name a few – and these have been dealt with in their usual masterly fashion by ILL's technical teams. We would like to take this opportunity to thank them for their contributions.

All in all ILL has the wind in its sails. There are all the indications that over the decades to come the Institute will confirm its position in the forefront of neutron science.

*Dirk Dubbers*

# rapport du Directeur

L'an 2000 a été une bonne année pour l'ILL. Dès le 1er janvier 2000, le programme de renouvellement de l'ILL, le 'Programme Millennium', a été lancé. La réalisation des cinq premiers instruments de ce programme (D3, IN20, VIVALDI, le scanner de contrainte et les détecteurs DNPA) est en bonne voie. Parallèlement, six projets instrumentaux lancés au cours des années précédentes ont été achevés avec succès (D4, D16, H113, D17, D20, IN4), les quatre premiers dans les délais prévus, les deux derniers avec un certain retard en raison de problèmes techniques inattendus. Ces instruments ont été accueillis avec enthousiasme par les utilisateurs de l'ILL. Les deux derniers instruments de cette série (IN5, IN8) seront disponibles, comme prévu, en 2001.

Pour les années à venir, le 'Programme Millennium' comprend de nombreuses autres propositions d'excellente qualité pour le renouvellement des instruments, mais également pour un renouvellement en profondeur de l'infrastructure de l'ILL, y compris de tous les anciens guides de neutrons. Avec un réacteur pour ainsi dire neuf, une infrastructure saine, un parc instrumental entièrement rénové ainsi qu'une équipe fortement rajeunie, l'Institut est parfaitement équipé pour affronter l'avenir.

Le 'Programme Millennium' a été présenté et discuté au sein des comités de l'ILL ainsi que dans différents colloques scientifiques au niveau national et international, les discussions se poursuivent maintenant sur une base plus large au sein de la communauté des utilisateurs actuels et potentiels de neutrons. Dans un environnement qui évolue rapidement, il est de notre devoir de donner à l'ILL la place qui lui revient. Pour cela, il est essentiel de mettre en valeur les points forts de l'ILL, en particulier les avantages des faisceaux de neutrons continus et très intenses dans des domaines de recherche particulièrement prometteurs. En outre, il faut chercher à diversifier les applications possibles de la neutronique. Simultanément, l'ILL soutient fermement la pro-

position de construire la source à spallation pulsée européenne ESS.
La fin 2000 a également été marquée par une autre bonne nouvelle pour l'Institut. L'Associé britannique a décidé d'augmenter progressivement sa contribution à l'ILL au cours des prochaines années. En outre, la Grande-Bretagne a l'intention d'investir de manière ciblée dans des projets de l'ILL déjà approuvés. L'ILL sera ainsi en mesure de s'attaquer immédiatement à d'autres parties de son ambitieux 'Programme Millennium'.
En 2000, deux des grands pionniers de l'ILL, les professeurs Louis Néel et Heinz Maier-Leibnitz, ont disparu. Nous honorerons toujours leur mémoire.
Au cours de l'année écoulée, la Direction de l'ILL s'est plus particulièrement penchée sur la question de l'orientation future de la science à l'ILL. En effet, comme le montre l'expérience, lorsque le 'produit' est bon, c'est-à-dire lorsque la science est de grande qualité, tout le reste suit. Dans les pages suivantes de ce rapport, nous présentons une sélection de l'activité de l'ILL au cours de l'année 2000. Nous remercions tous ceux qui ont permis d'obtenir ces résultats scientifiques remarquables. D'autres défis importants ont été relevés, il a fallu, par exemple, assurer le cycle du combustible, mettre en œuvre la semaine de 35 heures et résoudre des problèmes de technique financière. Comme d'habitude, ces problèmes ont été maîtrisés par les spécialistes de l'ILL avec une grande efficacité. Nous voulons également profiter de cette occasion pour les remercier.
Dans l'ensemble, l'ILL a le vent en poupe et tout laisse à penser que l'Institut pourra maintenir au cours des prochaines décennies son rôle prédominant dans le domaine de la recherche neutronique.

*Dirk Dubbers*

# bericht des Direktors

Das Jahr 2000 war ein gutes Jahr für das ILL. Pünktlich mit dem 1. Januar 2000 wurde das ILL Millennium-Erneuerungsprogramm angefahren. Die ersten fünf Instrumente aus diesem Programm (D3, IN20, VIVALDI, Strain Scanner, SANS-Detektoren) sind im Laufe des Jahres gut vorangekommen. Parallel dazu wurden sechs Instrumentprojekte aus vergangenen Jahren erfolgreich abgeschlossen (D4, D16, H113, D17, D20, IN4), die ersten vier innerhalb des vorgesehenen Zeitplans, die beiden letzten erst nach Überwindung unvorhergesehener technischer Schwierigkeiten; alle fertigen Instrumente sind von den Nutzern mit großer Begeisterung aufgenommen worden. Die letzten zwei Instrumente aus dieser Serie (IN5, IN8) werden im Jahr 2001 fristgemäß fertiggestellt.
Für die kommenden Jahre umfaßt das Millennium-Programm nicht nur viele weitere sehr gute Vorschläge zur Instrumenterneuerung, sondern auch Vorschläge zur grundlegenden Erneuerung der Infrastruktur des ILL, einschließlich aller älteren Neutronenleiter. Mit einem fast neuen Reaktor, einer gesunden Infrastruktur, einem rundum erneuerten Instrumentenpark sowie einer stark verjüngten Mannschaft ist das Institut dann bestens für die Zukunft gerüstet.
Nachdem das Millennium-Programm in den Ausschüssen des ILL sowie in verschiedenen nationalen und internationalen wissenschaftlichen Gremien vorgestellt und diskutiert wurde, wird nun die Diskussion auf breiterer Basis mit allen interessierten bisherigen und zukünftigen Neutronennutzern weitergeführt. Unsere Aufgabe ist, das ILL in einem sich schnell ändernden Umfeld bestmöglich zu plazieren. Dazu müssen die Stärken des ILL insbesondere im Bereich kontinuierlicher Neutronenstrahlen in zukunftsträchtigen Gebieten der Forschung optimal zur Geltung gebracht werden. Ferner streben wir eine Diversifizierung der möglichen Neutronenanwendungen an. Gleichzeitig unterstützt das ILL nach Kräften den Vorschlag zum Bau einer gepulsten europäischen Spallationsquelle ESS.
Gegen Ende des Jahres 2000 gab es eine weitere gute Nachricht für das Institut: Der britische Partner hat beschlossen, seine Beteiligung am ILL in den kommenden Jahren stufenweise anzuheben; zusätzlich will Großbritannien gezielt in bereits genehmigte ILL-Projekte investieren. Dies wird es dem ILL erlauben, weitere Teile des umfangreichen Millennium-Programms sofort in Angriff zu nehmen.
Im Jahre 2000 sind zwei der großen Pioniere des ILL, die Professoren Louis Néel und Heinz Maier-Leibnitz für immer von uns gegangen. Wir werden ihr Andenken stets in hohen Ehren halten.
Auch im vergangenen Jahr hat sich das ILL-Direktorium vorrangig mit Fragen der zukünftigen Wissenschaft am ILL befasst, denn die Erfahrung lehrt: Wenn das "Produkt" stimmt, das heißt, wenn die Wissenschaft von höchster Qualität ist, dann folgt alles andere nach. Auf den folgenden Seiten dieses Berichts stellen wir eine kleine Auswahl aus der ILL-Produktion des vergangenen Jahres vor. Wir danken allen, die diese schönen wissenschaftlichen Ergebnisse möglich gemacht haben. Andere wichtige Herausforderungen, wie z.B. die Sicherung des Brennstoffzyklus, die Einführung der 35-Stundenwoche, oder die Lösung finanztechnischer Fragen wurden von den zuständigen Fachleuten des ILL in gewohnt hervorragender Weise gemeistert. Auch ihnen wollen wir an dieser Stelle besonders danken.
Insgesamt befindet sich das ILL in gutem Fahrwasser und alles deutet darauf hin, daß das Institut auch in den kommenden Jahrzehnten seine führende Stellung in den Neutronenwissenschaften wird behaupten können.

*Dirk Dubbers*

Christian Vettier (right), the French director, Head of the Science Division, shows the experimental hall to the Slovakian Ambassador, Vladimir Valach, who visited the ILL in March.

The French Academy of Science held its annual regional meeting in Grenoble, in November 2000. As a part of the three-day event they visited Grenoble's two major scientific facilities, ILL and ESRF. In the photo, Ekkehardt Bauer, Head of the Reactor Division, guides the members of the Academy around the reactor.

A living atom, made of red protons, blue neutrons and yellow electrons, spins around during *Les ateliers des neutrons*, organised by Anne Le Noël, Communication Officer at the ILL.

*La Fête de la Science* – in October 2000 – helps the general public to find out more about scientific research and technology.

# Scientific highlights

The year 2000 has been another highly productive period for the scientific programme of the ILL. The scientific highlights presented in this section of the Annual Report illustrate the tremendous range of high quality science achieved at the ILL. This is reflected in the large number of exciting results being presented, ranging from quantum critical points to orbital ordering and to the role of orbital moments in magnetic fluctuations. Magnetism as a field of research is evolving very rapidly: new materials are discovered and new problems are contemplated such as magnetic excitations in thin films, quantum phase transitions and correlated fermions. ILL users take advantage of other complementary techniques, such as the synchrotron x-rays produced by our neighbour, the ESRF, in order to reach a better understanding of their scientific problems. This is particularly true in the case of electronic properties of solids and chemistry. The unique characteristics of neutrons - to penetrate deeper into materials, to detect the different isotopes of the same element and to probe the dynamics of atoms and molecules over a wide energy range – allow the investigations of concrete problems such as: conformations of hydrogen bonds; diffusive modes in liquids, intermetallic alloys and ionic conductors; and the structure of polymers and micro emulsions. Furthermore, noteworthy developments have been achieved in biology. The neutron methods coupled to the judicious labelling of the macromolecular assembly provide a powerful investigation tool allowing important observations. Examples include the examination of the rearrangement of proteins and the role played by thermal fluctuations in proteins stability. At another extreme end of the length scale probed at ILL, it is recognised that neutrons are an ideal tool to investigate fundamental interactions such as the gravitational field and to induce nuclear reactions giving indications about the structure and the excited states of nuclei.

The activity of the ILL Theory Group has also contributed to the reputation of the ILL and over the years has become a famous centre of attraction thanks to the leadership of Philippe Nozières. Last year, when he decided to retire, the ILL and the ESRF celebrated together the fruitful collaboration with him by hosting a meeting during which his many friends could present the most recent developments in theoretical models for strongly correlated fermions. The ILL wishes to express the deepest thanks to Philippe Nozières for such a productive and rewarding partnership.

The ILL is very grateful to the many collaborators who have eagerly submitted their highlights to the present report. We wish to thank most warmly all of you who have contributed to this year's version and, more especially, those whose contributions could not be included.

# Origin of the 3D ferromagnetic ordering in the free radical Nit(SMe)Ph


- S. Pillet, M. Souhassou, C. Lecomte (Université Nancy I)
- Y. Pontillon (ILL)
- A. Caneschi, D. Gatteschi (University of Florence)
- E. Ressouche, J. Schweizer (CEA, Grenoble)



**A combined study of the magnetic properties of a nitronyl nitroxide free radical exhibiting 3D ferromagnetism, by experimental spin and electron density has been performed using non polarised and polarised neutron and X-ray diffraction. In this family of compounds, the short contacts between radicals are thought to explain the macroscopic magnetic behaviour. Charge transfer from the nitroxide fragments to the methyl-thio group has been evidenced. The role of intermolecular contacts is also highlighted to explain the long range magnetic ordering involving three hydrogen bonds and one nitroxide-nitroxide short contact.**


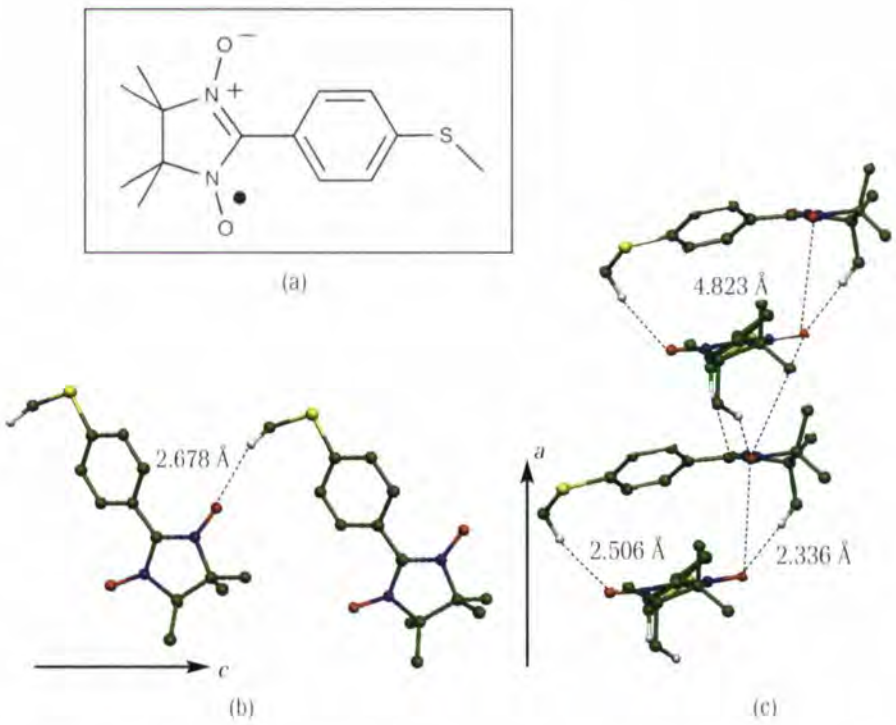


Figure 1: View of the Nit(SMe)Ph radical (a) and short intermolecular contacts (b, c).

Since the discovery of the first purely organic ferromagnet in 1991 [1], the β form of the p-nitrophenyl nitronyl nitroxide Nit(p-$NO_2$)Ph (Tc = 0.6 K), these series of organic free radicals have been extensively studied with the hope to find molecular magnets with high critical temperatures. The long range magnetic ordering observed in this kind of compounds, which requires co-operative effects, is driven principally by the nature of the radical (i.e. subsituents) and the crystal packing (short intermolecular contacts). The techniques used in this context are polarised neutron diffraction which gives direct access to the distribution of unpaired electrons in the solid and X-ray diffraction which gives access to the distribution of the whole electrons of the system. These informations are of utmost importance to understand well the magnetic coupling mechanisms at the microscopic level. In a second step, this should help in designing new molecular systems exhibiting more efficient magnetic interactions (higher Tc), if one could rationalise the length and orientation of the intermolecular contacts in the solid state.

The 2-(4-methylthiophenyl)-4,4,5,5-tetramethyl-imidazoline-1-oxyl-3-oxide [Nit(SMe)Ph] exhibits bulk ferromagnetism with a low Curie temperature (Tc = 0.2 K) [2,3]. This radical carries a single delocalised unpaired electron (S = 1/2) which is the basis for its magnetic properties (Fig. 1a).

The packing of the radicals in the cell involves different intermolecular contacts, as shown on Fig. 1b and 1c. First, a network of intermolecular hydrogen bonds between the two oxygen atoms of the nitroxide groups and methyl fragments, links the radicals in the crystallographic *a* and *c* directions. The O-N-C-N-O groups of each radical are stacked in a nearly perpendicular way in the *a* direction (4.8229(1) Å).

The behaviour of one radical in the crystal, thus showing the effects of the magnetic couplings on this radical, has been investigated in two different ways using the complementarity between polarised neutron diffraction with spin density modelling and high resolution X-ray diffraction with electron density modelling and topological analysis. It must be noted that the models (multipolar model, see for example Coppens 1997, [4]) used to

reconstruct the spin and electron density are similar, enabling a direct comparison of the results. The polarised neutron measurement - done at the diffractometer DN2 (CEA, Grenoble) - demonstrates that the unpaired electron is mainly located in a $\pi^*$ molecular magnetic orbital but also partially delocalised on several parts of the radical. Significant spin density is also observed on the carbon of the methyl-thio group and on one methyl-carbon of the nitronyl ring, involved in the intermolecular contacts (Fig. 1b, 1c); this gives evidence for the intermolecular magnetic interactions.

On the other hand, high resolution X-ray diffraction measurements provide accurate knowledge of the electron density distribution in this compound and therefore give a clear picture of the interatomic links, completing the previous spin density (only unpaired electrons) point of view [7]. The delocalised system spanned to the sulphur atom is demonstrated by the X-ray study : bond lengths and electron density in all bonds involved in the delocalisation scheme are in a medium range between those of a pure single and a pure double bonds. The parameterisation of the multipolar model used to reconstruct the experimental electron density shows small negative net charges (-0.16 e) on each nitroxide fragment which is surprising for such electronegative atoms, whereas the methyl-thio group is highly negative (-0.59 e). This can be interpreted in terms of charge transfer between these two parts of the molecule. The main motivation for studying accurately the intermolecular regions were these observations on the behaviour of one Nit(SMe)Ph radical (spin and charge densities), reflecting the intermolecular interactions.

The intermolecular interactions involve three hydrogen bonds and one short N-O···O-N contact for which the study in the context of magnetic couplings, is of great interest. For this purpose, the electron density distribution was analysed in the hydrogen bond regions using its topoligical properties. In order to obtain the real positions of the hydrogen atoms and the elements of their anisotropic thermal displacement tensor, neutron diffraction measurements were performed on D9 and D15. This point is of major importance to model the electron density in the hydrogen bond regions by the so-called (X-(X+N)) [8] multipolar refinement (a combination of diffraction data collected with classical neutron and X-ray). In the intermolecular regions, an electron density of ~ 0.05 eÅ$^{-3}$ is observed (Fig. 3), only in the hydrogen bond paths. This network of hydrogen bonds in the solid could induce the long range magnetic ordering observed by magnetic measurements [1,2] at much lower temperature.

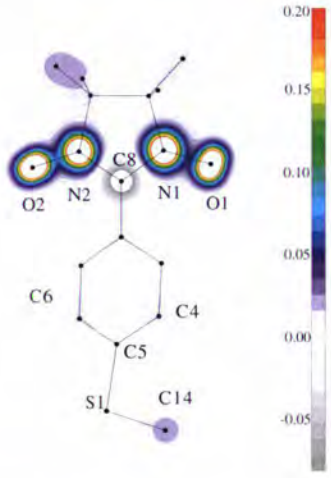


Figure 2: Projection of the spin density, as obtained by wave function modelling and projected into the ONCNO plane (units are $\mu_B$Å$^{-3}$).

This work has confirmed that the combination of neutron diffraction (polarised and non-polarised) and high resolution X-ray diffraction is a perfect technique to study magnetic interactions at the microscopic scale in the field of molecular magnetism including atomic, interatomic and intermolecular behaviours.

Figure 3: Electron density as 3D representation, isocontour at 0.02 eÅ$^{-3}$ level showing one of the intermolecular contacts by accumulation of electron density in the intermolecular region. Only the hydrogen atom involved in the hydrogen bond is represented and only O-N-C-N-O···H-C-S fragment is included in electron density representation for clarity.

## References


[1] P. Turek, K. Nozawa, D. Shiomi, K. Awaga, Y. Maruyama and M. Kinoshita, Chem. Phys. Lett. 180 (1991) 327 • [2] A. Caneschi, F. Ferraro, D. Gatteschi, A. Le Lirzin and E. Rentschler, Inorg Chem. Acta 235 (1995) 159 • [3] A. Caneschi, F. Ferraro, D. Gatteschi, A. Le Lirzin, M. Novak, E. Rentschler and R. Sessoli, Adv. Mater. 7 (1995) 476 • [4] P. Coppens, X-ray Charge Densities and Chemical Bonding, IUCr, Oxford University Press (1997) • [5] Y. Pontillon, A. Caneschi, D. Gatteschi, A. Grand, E. Ressouche, R. Sessoli and J. Schweizer, Chem. Eur. J. 5 (1999) 3616 • [6] Y. Pontillon, A. Caneschi, D. Gatteschi, E. Ressouche, J. Schweizer and R. Sessoli, Physica B (1999) 51 • [7] S. Pillet, M. Souhassou, Y. Pontillon, A. Caneschi, D. Gatteschi and C. Lecomte, New J. Chem. (2001 special issue) in press • [8] E. Espinosa, C. Lecomte, E. Molins, S. Veintemillas, A. Cousson and W. Paulus, Acta Cryst. B52 (1996) 519

# Quantum magnetic phase transition: a top-down approach


- N. Cavadini, W. Henggeler, A. Furrer (LNS, ETH Zürich & PSI Villingen)
- K. Krämer, H.U. Güdel (University of Berne)
- H. Mutka, A. Wildes (ILL)
- P. Vorderwisch (HMI Berlin)



**Quantum magnetism exhibits unique collective features, bearing no classical analogies. The unconventional magnetic excitations realised in S =1/2 copper insulators $KCuCl_3$ and $TlCuCl_3$ were investigated by inelastic neutron scattering. We identify in $TlCuCl_3$ a promising candidate for the microscopic study of a quantum phase transition, driven by zero-point spin fluctuations at the lowest temperature. Such novel studies often remained precluded to neutron scattering due to the lack of suitable samples. Nevertheless, they address some of the most fundamental and debated issues of condensed matter physics.**


Temperature-induced phase transitions are ubiquitous phenomena in condensed matter physics. The crossover from occurrence of disorder to order, dictated by an underlying symmetry breaking, generally reflects the competition between cooperative interactions and thermal fluctuations. Classical magnetic systems, in which well-localised spins interact among themselves on the grounds of exchange couplings, provide a rich variety of ordered phases. Below a characteristic critical temperature $T_c$, collective spin correlations overcome thermally driven fluctuations, and a spontaneous magnetisation sets in. Concepts like order parameters, critical behaviour and universality find ideal realisations in the field of classical magnetism, which has constituted a privileged testing ground for theoretical models of wide application. Comprehensive experimental studies often relied on the detailed microscopic data accessible by neutron scattering.

Recent years have witnessed the growing interest in a different mechanism leading to symmetry breaking: quantum phase transitions occurring at "T=0". At a quantum critical point - controlled by an external parameter like doping, pressure or magnetic field - the ground state changes from order to disorder due to zero-point fluctuations of quantum nature [1]. Statics and dynamics at "T=0" are deeply interconnected, as expressed by the upper critical dimension d<4-z separating non-classical from classical critical behaviour, where z is the model specific dynamic critical exponent [2]. The novel insights to be gained by the study of such unconventional phenomena are by no way of pure academic interest. Quantum critical behaviour, related to the existence of competing ground states in strongly correlated electron systems, is for instance believed to have deep implications for the yet unsolved issue of high-Tc superconducting materials [1,3]. Again, magnetic insulators provide us with appealing model systems, which represent the complexity of true many-body quantum correlations with well-understood spin interactions. It is along these lines that we started the microscopic investigation of the unconventional S=1/2 antiferromagnets $KCuCl_3$ and $TlCuCl_3$. Both compounds share the same monoclinic structure, characterised by the stacking of nearly isolated $Cu_2Cl_6$ plaquettes in double chains along the a axis (Fig.1). Static magnetic measurements reveal a nonmagnetic singlet ground state

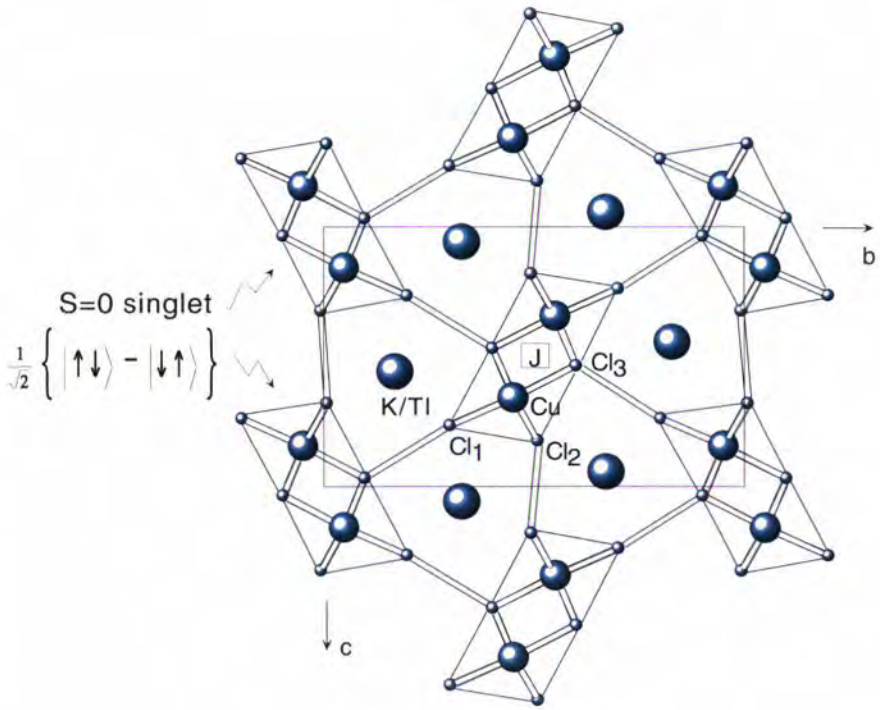


Figure 1: Schematic view of the magnetic interactions in the S=1/2 (K/Tl)$CuCl_3$ family, projected on the bc plane of the unit cell. Centrosymmetric $Cu_2Cl_6$ plaquettes behave as singlet-triplet dimer units, building a 3-D interacting dimer network. Correlations along the a axis are not shown.

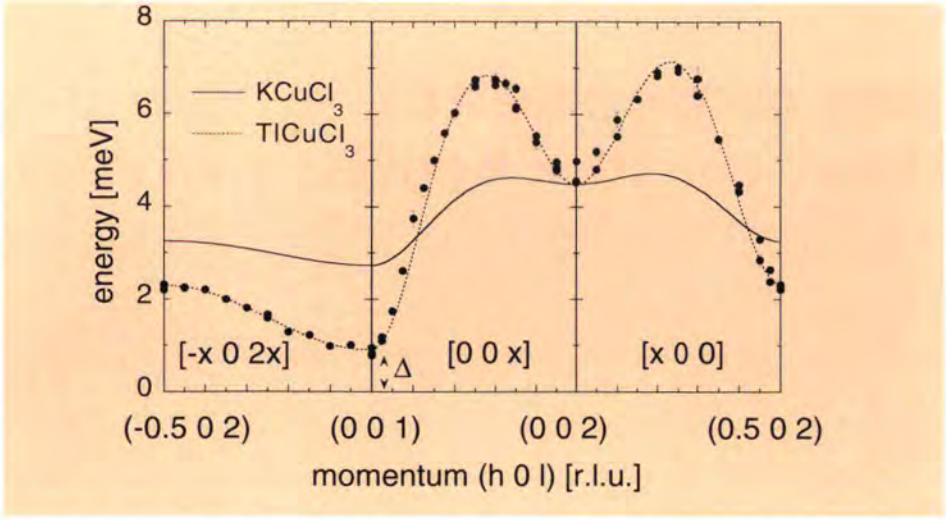


Figure 2: Observed energy dispersion of the magnetic excitations in $TlCuCl_3$ (circles - experimental data; dashed lines - model calculations) and $KCuCl_3$ (continuous line - model calculations; data not shown), compared along selected directions of reciprocal space at T~2K. Calculations reflect the model explained in the text.

with a finite energy gap to excited states [4]. From detailed inelastic neutron scattering studies we have determined that the dominant valence bond J contracts neighbouring $Cu^{2+}$ spins into singlet dimer units, and that elementary excitations result from the breaking of such singlet units into triplets [5]. The triplet modes propagate from one dimer site to the other due to the presence of weaker inter-dimer correlations (Figs. 1 and 2). The minimum of the observed dispersion relation corresponds to the energy excitation gap Δ, a quantity which is accessible by susceptibility or high-field magnetisation measurements. However, only inelastic neutron scattering can determine the low-lying spectrum and the dynamic spin correlations [6]. Due to the weak transition matrix element associated with the S=1/2 dimers, the ILL spectrometers IN8, IN22 and IN14 have been decisive for the successful mapping of reciprocal space.

A surprising result was the observation of the dispersive behaviour of the triplet excitations along each direction, clearly revealing the three-dimensional (3-D) nature of the magnetic interactions within the dimer network. Despite this fact, both $KCuCl_3$ and $TlCuCl_3$ retain a quantum disordered ground state down to the lowest temperature. A direct comparison of the neutron spectra further shows that the network in $TlCuCl_3$ is stronger than in $KCuCl_3$ (Fig. 2), resulting in an appreciable energy bandwidth across the leading parameter J.

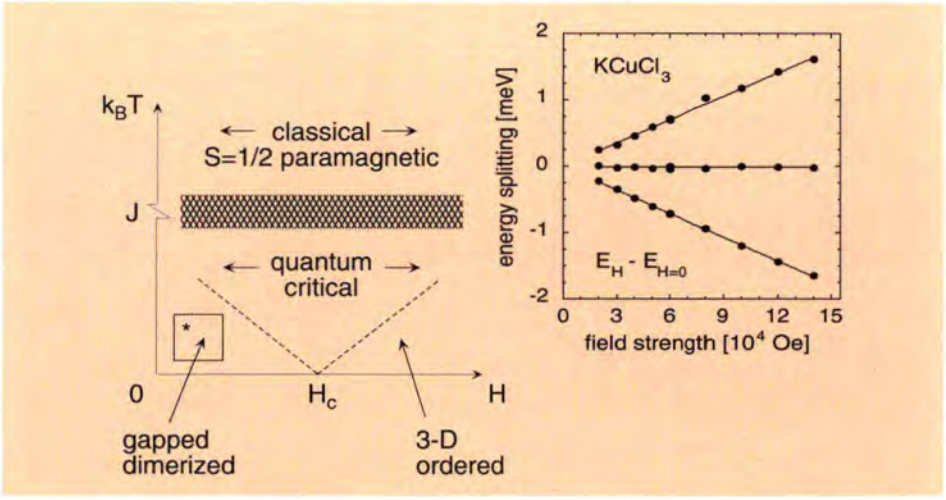


Figure 3: Characteristic (H,T) phase diagram of dimer-like S=1/2 quantum spin systems. Below the typical thermal energy $k_BT$~J (dashed area), fluctuation modes are subject to the quantum effects described in the text. The critical fields for $KCuCl_3$ and $TlCuCl_3$ correspond to $H_c$~$20 \cdot 10^4$ Oe and $H_c$~$6 \cdot 10^4$ Oe, respectively [4]. Inset: observed Zeeman splitting of the triplet modes in $KCuCl_3$ at T~2K as a function of applied field.

In the presence of an external magnetic field H, the excited triplet state undergoes Zeeman splitting, which eventually overcomes the energy gap at the critical field given by $g\mu_B H_c \sim \Delta$ where g denotes the gyromagnetic factor of the $Cu^{2+}$ moment (Fig. 3). For $H>H_c$, zero-point quantum fluctuations are quenched by the cooperative effect of the 3-D exchange interactions, and the gapless spin system recovers an ordered magnetic state [7]. The quantum phase transition separating order at $H>H_c$ from disorder at $H<H_c$ strictly occurs at "T=0". Nevertheless, a broad critical region at finite T is influenced by the interplay between thermal and quantum correlations. The fundamental nature of the transition at $H_c$, and the field-induced 3-D phase are theoretical issues of relevant interest [8,9]. However, the lack of suitable systems in the appropriate parameter range has so far precluded complete neutron investigations. With S=1/2 $TlCuCl_3$, we have fully characterised an excellent candidate for the dynamic study of such open questions at a microscopic level, completing at the same time corresponding macroscopic studies [7]. Our experiments result from the close collaboration between ILL Grenoble, HMI Berlin and SINQ PSI Villigen. In connection with the parent compound $KCuCl_3$, we illustrate a coherent top-down approach towards unconventional quantum critical features.

The clear determination of the elementary triplet spin excitations in the above compounds provides a promising starting point for future neutron investigations, hopefully contributing to elucidate some of the unsolved problems encountered at the forefront of condensed matter physics.

## References


[1] S. Sachdev, Science 288 (2000) 475 • [2] J. Hertz, Phys. Rev. B 14 (1976) 1165 • [3] E. Dagotto and T.M. Rice, Science 271 (1996) 618 • [4]W. Shiramura et al., J. Phys. Soc. Jpn. 66 (1997) 1900 • [5] N. Cavadini et al., Eur. Phys. J. B 7 (1999) 519 • [6] N. Cavadini et al., J. Phys.: Condens. Matter 12 (2000) 5463 • [7] A. Oosawa et al., J. Phys.: Condens. Matter 11 (1999) 265 • [8] S. Wessel and S. Haas, Phys. Rev. B 62 (2000) 316 • [9] T. Nikuni et al., Phys. Rev. Lett. 84 (2000) 5868

# The temperature dependence of the magnetisation in $Fe_{65}Ni_{35}$ invar: evidence contradicting the two state model

P.J. Brown
(ILL and Loughborough University)

K-U. Neumann, K.R.A. Ziebeck
(Loughborough University)

**We have used polarised neutron diffraction measurements on single crystals of the $Fe_{65}Ni_{35}$ invar alloy to determine the magnetisation distribution in the temperature range 100 to 600 K. We find that the shape of the magnetisation distribution remains essentially unchanged throughout the whole temperature range. The fraction of magnetic electrons with $e_g$ symmetry remains constant at ~0.47. This finding is inconsistent with models of the invar effect in which a state, or states, with a configuration different from the ground-state and with slightly higher energy, is thermally populated.**

The invar effect, was discovered more than 100 years ago by Guillame [1].
He found that the face centred cubic (fcc) alloys of iron and nickel containing roughly 35% of nickel ($Fe_{65}Ni_{35}$) have an almost zero thermal expansion coefficient over a broad temperature range. This useful property has been widely exploited in the construction of high precision mechanical instruments, but has as yet received no satisfactory microscopic explanation. In a recent volume of Nature [2,3] it was claimed that the effect had been explained in microscopic detail. This claim was based on improved band structure calculations taking into consideration non-collinear components of the magnetisation. However, Lynn's neutron polarisation analysis experiments [4] show that the only perpendicular components of magnetisation are those associated with the spin waves. This contradiction serves to emphasise that although self-consistent band structure calculations give a reasonable account of the ground state properties of 3d transition metals, the same is not true for the finite temperature properties of which the invar effect is one.

The invar effect disappears above the Curie temperature, which suggests that the magnetic properties must in some way offset the normal lattice expansion and this premise is the foundation of most explanations given for the effect. Most theories are based upon volume instabilities of the magnetic moments which give rise to the magneto elastic coupling. The earliest model of this type was formulated by Weiss [5] who postulated that there are two possible states for fcc iron, the ferromagnetic high volume state and the antiferromagnetic low volume state. Thermally excited transitions between these two states are supposed to compensate for the lattice expansion due to the anharmonic components of the lattice vibrations. Recent spin polarised band structure calculations made by Entel [6] lend support to this model. They predict the existence of at least two stable states in an fcc iron-nickel alloy, which have different moments and atomic volumes. Although the thermodynamic consequences of such a model are difficult to quantify, it has been suggested that the invar effect arises from the thermal population of the low moment, low volume, state which lies at a slightly higher energy than the high moment state. To date there is no direct experimental evidence for the existence of these distinct states. However in Entel's calculations 3d electrons

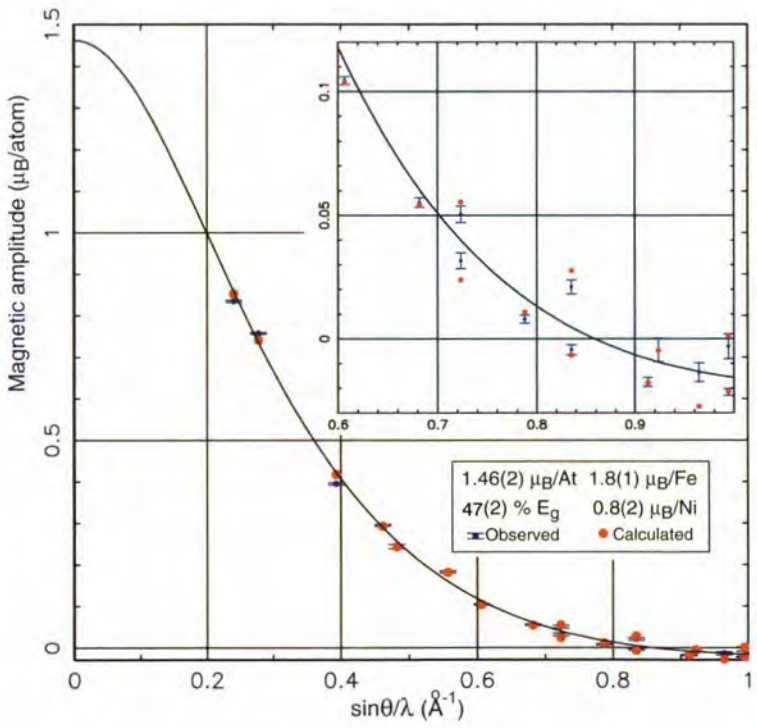


Figure 1: Observed and calculated values of the magnetic scattering per atom in $Fe_{65}Ni_{35}$ at 400 K in 9 T. The inset shows the points with $\sin\theta/\lambda > 0.6$ Å$^{-1}$ on a larger scale.

in the two states are divided differently between the orbitals with $e_g$ and with $t_{2g}$ symmetry. This means that the shape of the associated magnetisation distributions differ. The magnetic moment of the higher energy state is supposed to be mostly due to electrons in $t_{2g}$ orbitals, so the proportion of electrons with this symmetry in the mean distribution should rise with increasing temperature. Neutron scattering provides a unique means of probing this distribution.

In a ferromagnet the spatial distribution of the periodic magnetic moment can be determined from precise measurements of the magnetic neutron scattering in the Bragg reflections. In order to obtain the magnetisation distribution in $Fe_{65}Ni_{35}$ we have carried out a series of polarised neutron diffraction experiments. In these experiments the polarisation dependence of the intensity of Bragg reflections was used to determine the ratio of magnetic to nuclear scattering and hence to obtain the magnetic scattering amplitudes. Measurements were made at temperatures between 100 and 600 K, chosen to cover the region of anomalous thermal expansion and the paramagnetic regime where the thermal expansion has regained its normal lattice behaviour.

We have made measurements on two pillar shaped single crystals of $Fe_{65}Ni_{35}$, elongated parallel to ⟨110⟩ with dimensions ~2.5x2.5x5 mm and 1x1x5 mm; these were cut from a larger crystal grown using the Bridgeman technique. They were mounted with their long axes parallel to the field direction of a cryomagnet on the polarised neutron diffractometer D3. In a first experiment, made whilst the hot source was in place, we measured the polarised neutron flipping ratios of all hhl reflections with $\sin\theta/\lambda < 1.0$ Å$^{-1}$ from both crystals at neutron wavelengths of 0.85, 0.71, 0.61 and 0.48 Å. We measured under this wide range of experimental conditions to allow a reliable model for the extinction in the crystal to be elaborated, since extinction is the biggest source of error in this type of measurement. By comparing the eight sets of data we were able to establish an extinction model which proved reliable up to about 20% of extinction. By using the smaller crystal to measure the strong low angle reflections and the larger one to measure those at higher angle, we were able to keep the corrections to

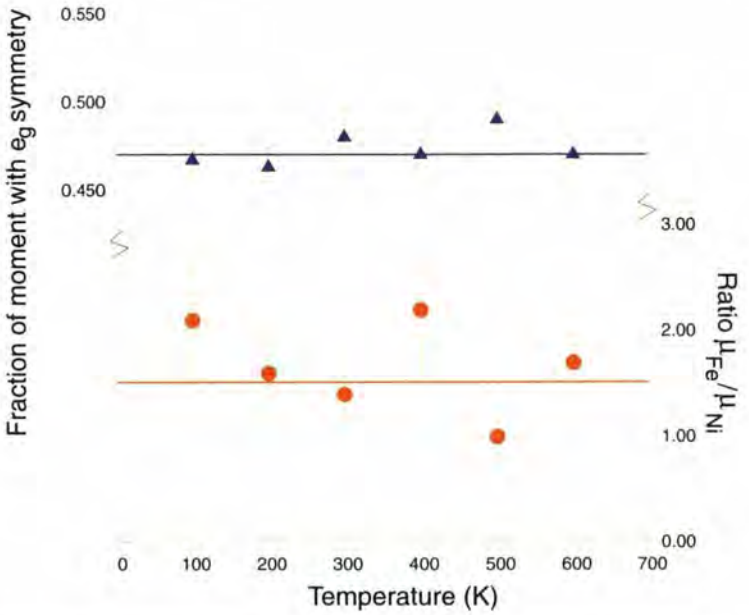


Figure 2: Temperature variation of the parameters describing the shape of the magnetisation distribution in the $Fe_{65}Ni_{35}$ invar alloy. The blue triangles give the fraction of magnetic electrons in $e_g$ orbitals (left hand scale) and the red circles the ratio of the Iron to Nickel moments (right hand scale). The red and blue horizontal lines are drawn through the corresponding mean values.

be applied to later data sets below this limit. In a second experiment made on D3 at 0.84 Å (without the hot source) we measured flipping ratios for the same set of reflections at temperatures of 100, 200, 300, 400, 500 and 600 K in an applied field of 9 T. From these data we were able to determine the temperature dependence of the magnetic moment distribution.

In order to quantify the changes taking place with temperature we used a simple model of the magnetisation distribution. The model consisted of a random arrangement of atoms on a fcc lattice with 65% having a moment $\mu_{Fe}$ and scattering like the 3d electrons of iron and 35% having moments $\mu_{Ni}$ and scattering like the 3d electrons of Nickel. The asphericity of the distribution about the atomic sites was modelled by allowing a fraction $\gamma$ of the 3d electrons to have $e_g$ and the rest $t_{2g}$ symmetry. The parameters $\mu_{Fe}$, $\mu_{Ni}$, and $\gamma$ of this model were fitted to the observed magnetic structure amplitudes at each temperature. Very good fits were obtained as can be seen from the graph of the observed and calculated amplitudes at 400 K shown in Fig. 1.

The variation with temperature of $\gamma$ and the ratio $\mu_{Fe}/\mu_{Ni}$ is shown in Fig. 2. It is clear from this figure that the symmetry of the magnetisation distribution around the atomic sites, which is characterised by $\gamma$, does not change significantly between 100 and 600 K. Furthermore the ratio $\mu_{Fe}/\mu_{Ni}$ is essentially constant, showing that there is little variation in the radial density either. There is therefore no significant change in the shape of the time-averaged magnetic moment distribution between 100 and 600 K. In particular there is no significant thermal population of a low moment, low volume state with a high proportion of electrons in orbitals of $t_{2g}$ symmetry in this temperature range. We conclude therefore that the two-state model of the invar effect based on the static interpretation of band structure calculations can not be valid. Recent neutron inelastic scattering studies of $Fe_{65}Ni_{35}$ [7] suggest that further progress in understanding the invar effect may be obtained by considering the dynamic implications of instabilities in the band structure.

## References

[1] Ch. E. Guillaume, C.R. Acad. Sci 10 (1897) 235 • [2] P. Mohn, Nature 400 (1999) 18 • [3] M.V. Schilfgarde, I. A Abrikosov and B. Johanson, Nature 400 (1999) 46 • [4] J.W. Lynn, N. Rosov, M. Acet and H. Bach, J. Appl. Phys. 75 (1994) 6069 • [5] R.J. Weiss, Proc. Roy. Soc. 82 (1963) 281 • [6] P. Entel, E. Hoffmann, P. Mohn, K. Schwarz V. L. Moruzzi, Phys. Rev. B 47 (1993) 8706 • [7] P. J. Brown, B. Roessli, J.G. Smith, K-U. Neumann and K. R. A. Ziebeck J. Phys. Condens. Matter 8 (1996) 1527

(paper accepted: J.Phys. Condens. Matter 13 1563 (2001) in press)

# Magnetic configurations:
## complementarity of neutrons and synchrotron X-rays

P. Normile, W. G. Stirling (University of Liverpool)

D. Mannix, J. Rebizant, F. Wastin, G. H. Lander (Institute for Transuranium Elements, Karlsruhe)

F. Bourdarot, P. Burlet (CEA-Grenoble)

**To understand the unusual nature of the 5f electrons in actinide systems, we use both neutrons and synchrotron X-rays to characterise their ground-state configurations. The experiments reported here involve single crystals containing plutonium, an element in which the 5f electrons are close to being localised. Despite the considerable knowledge provided by the synchrotron experiments, a key experiment, allowing a clearer interpretation of both the synchrotron and magnetisation results, was performed at the ILL diffractometer D15.**

Neutrons are a powerful probe of microscopic magnetic arrangements in solids. However, in the case of materials with high symmetry and associated magnetic domains, neutron experiments are often unable to distinguish between many possible configurations. A well known example is illustrated in Fig. 1 for the case of materials with the NaCl (fcc) atomic structure, in which magnetic structures of the so-called multiple-$q$ type give rise to identical neutron-diffraction patterns. This is because the neutron intensities are sensitive to the square of the magnetic Fourier components, and, when taking account of domain populations, the measured intensities are identical for the configurations shown in Fig. 1.

The late Rossat-Mignod and his colleagues realised that this degeneracy could be lifted by applying an external perturbation such as a magnetic field or uniaxial stress, and a series of studies [1] in the early 1980's, and subsequent work, has allowed the magnetic structures of many actinide (5$f$) compounds with the NaCl structure, such as UN, UAs, USb, NpAs, PuSb etc. to be determined. Such moment configurations have recently been the subject of theory [2, 3] so that, for example, the 3$q$ structure (Fig. 1) in USb is a consequence of the extended distribution and relativistic nature of the 5$f$ states [3].

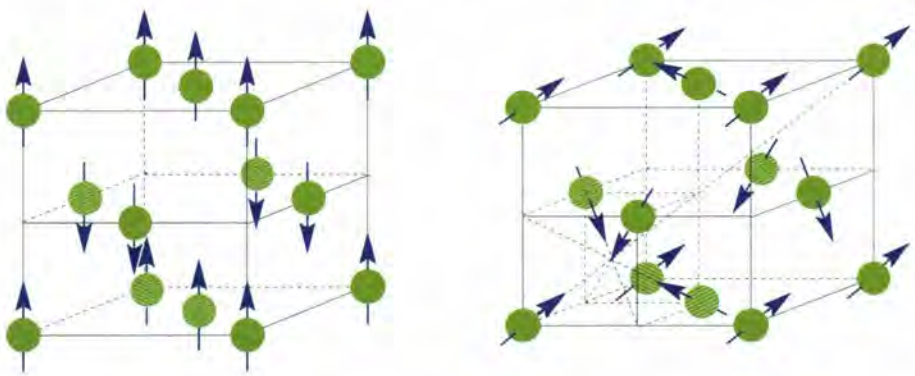

Figure 1: Illustration of left: single-$q$ (1$q$), and right: triple-$q$ (3$q$) magnetic configurations for the series of actinide compounds having the simple fcc NaCl crystal structure. Note that although these appear different, they give identical neutron patterns as long as the domain population of the 1$q$ configuration is random. (For the compound discussed in this article, the wavevector q = 1/4, which implies that there are four layers with moments pointing one way, followed by four layers with moments the other way, rather than the one up, one down (q = 1) sequence shown in Fig. 1. However, the principle of the multi-q arrangements is the same as shown in these two figures.

Our current interest is in probing the stability of the 3$q$ ground state in USb by dilution with both anions, e.g. U(Sb,Te), as well as other actinide cations, e.g. (Pu,U)Sb, as in this example. PuSb has a 1$q$ structure (Fig. 1) and here we concentrate on experiments with both neutrons and synchrotron X-rays on single crystals of $(Pu_{0.75}U_{0.25})Sb$. Magnetisation experiments at ITU (Karlsruhe) showed $T_N \sim 90$ K, and another anomaly around $T' \sim 55$ K. Initial neutron experiments (in zero magnetic field) at Risø National Laboratory in Denmark established the ordering wavevector, $\mathbf{q} = <0, 0, 1/4>$, and found no evidence for a further phase transition at T'.

Resonant X-ray magnetic scattering (RXMS) experiments (performed at the synchrotron at Brookhaven National Laboratory, USA) gave important information on the element-specific magnetism associated with each actinide cation in the solid solution [4], and found anomalies in the intensities around T'. RXMS has the advantage over neutron scattering that there is an extra term in the cross section that gives rise to additional satellites [5] at positions in reciprocal space identified as $2\mathbf{q}$ provided that the magnetic configuration has non-collinear components. An examination of Fig. 1 shows that such non-collinearity is present in the multi-$q$, but not in the case of the 1$q$ configuration. This, therefore, gives a direct method to determine the $q$-state, without adding an external perturbation. On the other hand, other effects, such as changes in the relative phases of the multi-$q$ components, may also influence the intensity of the $2\mathbf{q}$ satellite.

Fig. 2(a) shows the temperature dependence of the $1\mathbf{q}$ and $2\mathbf{q}$ satellites measured in RXMS. Both start to increase below $T_N$, but then unexpectedly the $2\mathbf{q}$ satellite starts to decrease below T'. This decrease below T' was not

understood, nor were some other features of the magnetisation and RXMS studies.

We then turned to neutron experiments on D15. This instrument has the capability of performing experiments with the sample in an applied magnetic field, and with the normal-beam technique we can measure intensities from different components. A key result is shown in Fig. 2(b), in which we show the intensities of the three Fourier $\mathbf{q}_x$, $\mathbf{q}_y$, and $\mathbf{q}_z$ components as a function of temperature with a 1 T field applied parallel to the [1, -1, 0] direction. Just below $T_N$ all intensities are equivalent; this shows that the configuration is $3q$. However, below T' the component with the antiferromagnet moments perpendicular to the field rapidly dominates, which is due to the structure changing from $3q$ to $1q$ at T'.

Fig. 3 shows a schematic (H, T) phase diagram of this material. There are at least two interesting features (1).

The critical field $H_c = 3.5$ T suppresses the $3q$ structure independent of temperature, and (2) there is a sluggish (entropy driven) transition from 3q to $1q$ as the temperature is lowered for all $H < H_c$. Determining the magnetic configurations of actinide materials has been found to be a prerequisite for understanding their electronic structure [2, 3]. Although the RXMS study gives spectral information not covered here, the results of the D15 neutron experiments are fundamental in identifying the ground-state configuration. They allowed a theory of the $3q \rightarrow 1q$ transition, as well other information from the RXMS (and magnetisation) experiments, to be placed on a much firmer base; thus demonstrating, again, the complementarity between the synchrotron and neutron techniques.

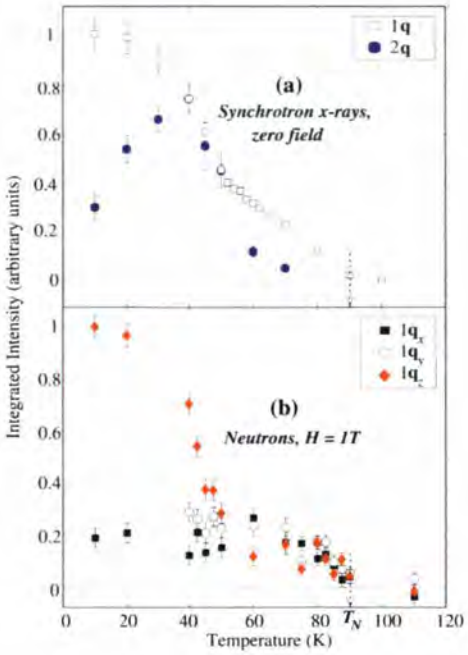


Figure 2: (a) Temperature dependence of the **1q** and **2q** satellite in the RXMS (measured at Brookhaven National Laboratory) experiments on $(Pu_{0.75}U_{0.25})Sb$. The initial growth of the **2q** satellite is due to the presence of the **3q** configuration (see Fig. 1), but at T' there is a sluggish transition to the $1q$ state, in which the **2q** satellite does not exist. There is only a small change at T' in the first-order satellite (1q) in zero field with either neutrons or resonant photons. (At 40 K the 2q satellite is $3{\cdot}10^{-3}$ times weaker than the 1q satellite. To show their relative T-dependence we have normalised their intensities at 40 K) (b) Intensities of the three Fourier $\mathbf{q}_x$, $\mathbf{q}_y$, and $\mathbf{q}_z$ components as a function of temperature with a 1 T field applied parallel to the [1, -1, 0] direction as measured on D15. The sudden change of intensity at T' is interpreted as the magnetic symmetry changing from $3q$ (above T') to $1q$ (below T'). The relatively poor statistics are due to the high absorption of $^{239}$Pu and the resulting small intensity of scattered neutrons.

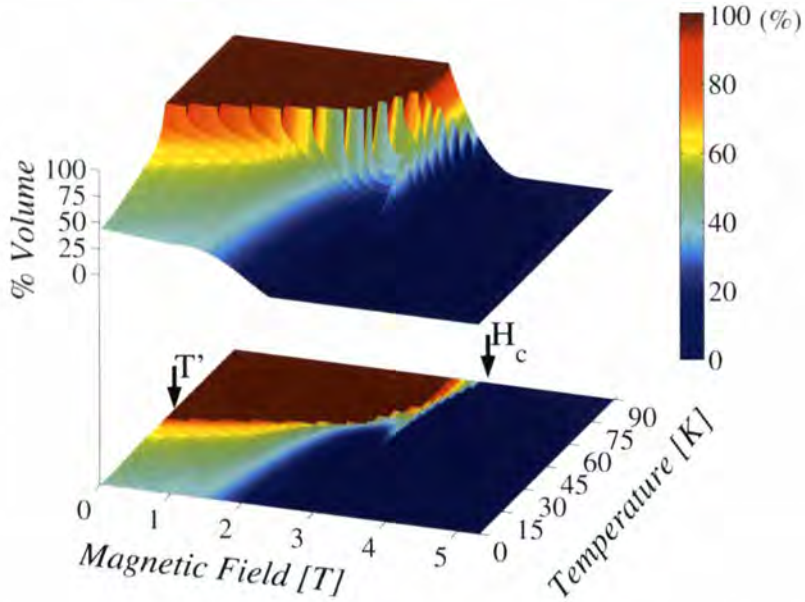


Figure 3: Schematic phase diagram for the $(Pu_{0.75}U_{0.25})Sb$ sample as a function of field (H) and temperature (T). Note that $T_N$ (as shown in Fig. 2(b)) is ~ 90 K, and is independent of magnetic field. The plot has been made to show the percentage of the crystal in the $3q$ magnetic configuration at any H and T. Zero $3q$ implies that the entire sample is in the is $1q$ state - see Fig. 1 for the difference between these.


REFERENCES

[1] J. Rossat-Mignod et al., Physica B 102 (1980) 237

[2] L. M. Sandratski, Adv. in Physics 47 (1998) 91

[3] H. Yamagami, Phys. Rev. B 61 (2000) 6246

[4] See, for example, E. Lidström et al., Phys. Rev B 61 (2000) 1375; P. Normile et al., to be published

[5] C. Vettier et al., SPIE Conf. Proc. 3773 (1999) 351

# **Incommensurate antiferromagnetic fluctuations** in superconducting $YBa_2Cu_3O_{6.85}$


- H. M. Rønnow, L.-P. Regnault (CEA, Grenoble)
- C. Ulrich, B. Keimer (Max-Planck Institut, Stuttgart)
- M. Ohl (FZ, Jülich)
- P. Bourges, Y. Sidis (LLB, Saclay)



**Among the tremendous efforts devoted to understand high-$T_c$ superconductivity, a special position is held by inelastic neutron scattering studies of antiferromagnetic fluctuations within the superconducting state. If not directly responsible for the coupling mechanism, these magnetic fluctuations at least provide an important probe to the nature of the phenomena. The main feature of the magnetic excitation spectrum in superconducting $YBa_2Cu_3O_{6+x}$ is the presence of a resonance at a characteristic energy around 41 meV and a wave vector $(\pi,\pi)$ corresponding to the antiferromagnetic zone center. Recently it was found by unpolarised neutron scattering technique that below the resonance energy the magnetic signal splits into incommensurate positions $(\pi\pm\delta,\pi)$ and $(\pi,\pi\pm\delta)$. We have applied neutron polarisation analysis to obtain state of the art data on the incommensurability of the resonance, from which a precise model for the excitation spectrum can be built.**


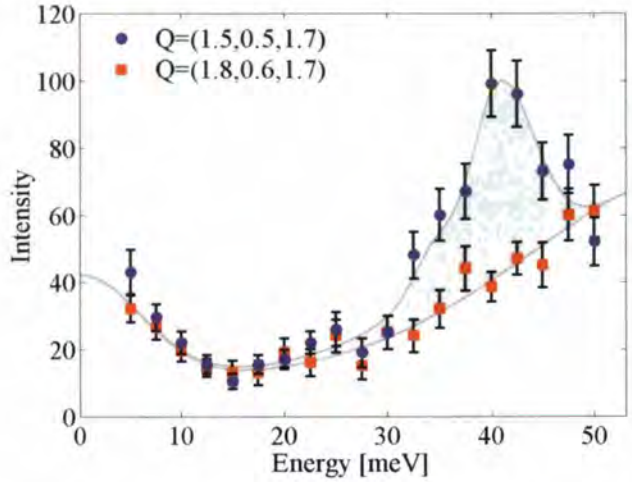


Figure 1: Energy scan through the antiferromagnetic zone center at $\mathbf{Q}$=(1.5,0.5,1.7) (circles) and at a background position $\mathbf{Q}$=(1.8,0.6,1.7) (squares) for an incident polarisation parallel to $\mathbf{Q}$ (spin-flip channel). The energy dependence of the background is due to the increased counting time at higher incident energies. The shaded area illustrates the magnetic signal peaking at the resonance position of 41 meV.

One of the most important outstanding problems in condensed matter physics is that of high temperature superconductivity. In addition to the potential technological applications, it represents a novel quantum state of coupled electron systems. In conventional superconductors the lattice fluctuations mediate a coupling between the electrons, which form quantum mechanically coherent pairs. It has been established that also high-Tc superconductivity is due to pairing of the charge carriers, but that the coupling mechanism is not the standard phonon mediated coupling. The main problem in understanding the phenomena is therefore to find the fluctuations that are responsible for the coupling mechanism. One generic feature of the high-$T_c$ superconductors is that they all contain $CuO_2$ layers, which in the undoped parent compounds form antiferromagnetic insulators [1]. This could indicate that the coupling mechanism is mediated by magnetic fluctuations, which indeed have been found to undergo profound changes as the materials are doped from antiferromagnetic insulators to superconducting metals [2].

Inelastic neutron scattering measures directly the magnetic excitation spectrum with the one drawback that the relative weakness of the neutron scattering signal makes the availability of large single crystals a prerequisite for such studies. For this reason, experimental investigations have mainly been limited to $YBa_2Cu_3O_{6+x}$ and $La_{2-x}Sr_xCuO_4$. In $YBa_2Cu_3O_{6+x}$ the most prominent feature is a resonance around 41 meV at the wave vector $(\pi,\pi)$ of the antiferromagnetic zone center [2]. Also in $La_{2-x}Sr_xCuO_4$ is there a signal around $(\pi,\pi)$, but no sharp resonance has been observed. Instead it was discovered that the intensity is constituted of four incommensurate contributions at $(\pi\pm\delta,\pi)$ and $(\pi,\pi\pm\delta)$ [3,4], which has been associated to the existence of charge stripes [5]. These results were encouraging in the sense that the magnetic excitation spectrum in the superconducting state shows interesting anomalous behavior, but at the same time the apparent differences between the two systems could indicate that the behavior are peculiarities for each material and not universal to high-$T_c$ superconductivity.

Recently, a unified picture emerged from the discovery using unpolarised neutron scattering that also $YBa_2Cu_3O_{6.6}$ develops an incommensurability below the resonance energy, where the signal contains four contributions at $(\pi\pm\delta,\pi)$ and $(\pi,\pi\pm\delta)$ [6]. In more elaborate investigations on $YBa_2Cu_3O_{6.85}$ the incommensurate signal has been tracked down to 35 meV [7]. Quite interestingly and novel, the incommensurate fluctuations,

well-defined below $T_c$, were found to almost vanish in the normal state, contrary to LSCO where the incommensurate peaks persist well above $T_c$. The unpolarised data could be interpreted in terms of a downward dispersion relation connecting the resonant mode and the incommensurate fluctuations.

In order to confirm these puzzling results, we have undertaken a polarized neutron scattering study of $YBa_2Cu_3O_{6.85}$. By separating the magnetic and structural (phononic) scatterring into respectively the spin flip and the non spin flip channels, polarised neutron scattering has repeatedly demonstrated its power to confirm the detailed behavior of complex scattering signal. The experiment was performed on the thermal three axis spectrometer IN22 (CRG) at the ILL using focusing Heusler monochromator and analyser to obtain a flipping ratio of 17 at a fixed final neutron wave vector of 4.1 $Å^{-1}$. A 4 $cm^3$ sample was mounted with the reciprocal space directions [3,1,0] and [0,0,1] in the horizontal scattering plane, such that scans could be performed around the (1.5,0.5,1.7) position.

Figure 1 depicts an energy scan at the antiferromagnetic zone center **Q**=(1.5,0.5,1.7) and at a background position **Q**=(1.8,0.5,1.7)

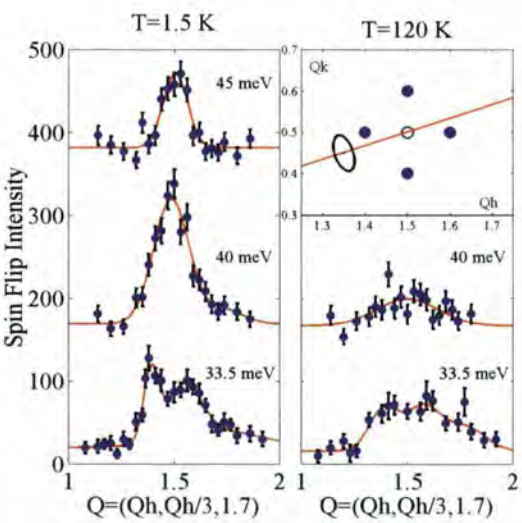


Figure 2: Constant energy scans through **Q**=(1.5,0.5,1.7) as sketched in the upper right corner, which also illustrates the FWHM of the resolution ellipse. Three energies respectively below, at and above the resonance are shown for T=1.5 K (left) and the two lower energies are also shown for T=120 K (right). The scans have been displaced vertically and the solid lines are guides to the eye.

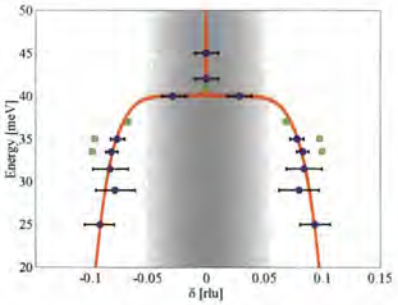


Figure 3: The peak locations as a function of energy for respectively the unpolarised (squares) and the polarised (circles) neutron scattering data. As described in the text, the observed signal may be constituted of a sharp signal illustrated by the solid line and a broad commensurate contribution as sketched by the shaded area.

respectively. Scans through (1.5,0.5,1.7) at three energies respectively above, at and below the resonance energy are shown in Fig. 2, which unambiguously confirm the incommensurate splitting below the resonance energy, while on the other hand the signal remains commensurate and resolution limited at higher energies. With these data at hand, it is now possible to conclude several definitive facts about the spin fluctuations in $YBa_2Cu_3O_{6.85}$

1) Below the resonance energy, an incommensurate signal exists down to 25 meV, below which the intensity became untractable.
2) Above the resonance energy the signal stays commensurate and resolution limited up to at least 45 meV.
3) Above $T_c$ (at 120 K) the signal at 40 meV almost disappears, while the signal at 33.5 meV is only reduced by a factor of 1.6.
4) Based on fits with resolution convoluted models for the scattering, we can add that after a rapid development just below the resonance energy, the incommensurability saturates around $\delta$=0.09x2$\pi$ (see Fig. 3).

It is difficult to imagine how the dispersion like feature observed at 1.5 K can loose its intensity at 40 meV but not at 33.5 meV when temperature is increased to 120 K. This behavior can more naturally be understood if one assumes the presence of two signals. The sharp dispersion of the resonance, whose intensity almost vanishes above Tc, and a broad commensurate signal, which is less energy and temperature dependent. These signals are sketched in figure 3, which also shows the commensurability at 1.5 K as extracted from fits with the resolution convoluted model.

In summary, we have presented a state of the art polarised inelastic neutron scattering experiment to characterise the incommensurability around the resonance feature in the magnetic excitation spectrum of the high-$T_c$ superconductor $YBa_2Cu_3O_{6+x}$. There are two main theoretical approaches to describe this incommensurability. One is based on the formation of static or slowly fluctuating charge stripes [5] and the other builds on Fermi-surface effects [8,9]. We believe that the selection of the most probable model will be based on its ability to reproduce the emerging experimental picture of the incommensurate to commensurate crossover as a function of energy and temperature. Even if the magnetic fluctuations should turn out not to be directly responsible the coupling mechanism in high-$T_c$ superconductivity, it is a strong fingerprint of the electron correlations within the system. And any theory aiming to explain the coupling mechanism should be consistent with the detailed experimental picture that is currently being established for the magnetic excitations spectrum.

## References


[1] D. Vaknin, S. K. Sinha et al., Phys. Rev. Lett. 58 (1987) 2802 • [2] J. Rossat-Mignot, L.-P. Regnault et al., Physica C 185-189 (1991) 86 • [3] J. M. Tranquada et al., Nature 375 (1995) 561 • [4] B. Lake, G. Aeppli et al., Nature 4000 (1999) 43 • [5] V. J. Emery, S. A. Kivelson and O. Zachar, Phys. Rev. B 56 (1997) 6120 • [6] H. A. Mook, P. Dai et al., Nature 395 (1998) 580 • [7] P. Bourges, Y. Sidis et al., Science 288 (2000) 1234 • [8] F. Onufrieva and P. Pfeuty, cond-mat/9903097 • [9] Y.J. Kao and Q. Si and K. Levin, Phys. Rev. B 61 (2000) 11898

# Weak antiferromagnetic order of $UPt_3$ studied under extreme conditions


- N.H. VAN DIJK (IRI DELFT)
- B. FÅK (ISIS, CEA GRENOBLE)
- P. RODIÈRE, A. HUXLEY, L.P. REGNAULT, J. FLOUQUET (CEA GRENOBLE)
- F. YAKHOU (ESRF)
- M.-T. FERNÁNDEZ-DÍAZ (ILL)



**The antiferromagnetic order of the heavy-fermion compound $UPt_3$ shows a remarkably small ordered moment of only 0.02 $\mu_B$ below $T_N$ = 6 K, which is believed to play a crucial role in the unconventional superconducting behaviour at low temperatures ($T_c$ = 0.55 K). In order to gain more insight in the nature of the antiferromagnetic order, we have performed low-temperature elastic neutron-scattering measurements under uniaxial pressures up to 6 kbar and in magnetic fields up to 12 T. The uniaxial pressure dependence is found to be strongly anisotropic with a suppression of the ordered moment for pressure along the hexagonal c axis and a domain repopulation for pressure in the hexagonal plane. Both the size of the ordered moment and the domain population are however hardly affected by applied magnetic field up to 12 T along and perpendicular to the hexagonal axis.**


For the heavy-fermion superconductor $UPt_3$, early elastic neutron-scattering measurements [1] revealed the onset of antiferromagnetic order below $T_N$ = 6 K with an unusually small ordered moment of $m$ = 0.02 $\mu_B$ /(U atom). The antiferromagnetic order has a propagation vector of **k** = (1/2,0,0) with the ordered moment along the propagation vector in the basal plane of the hexagonal close-packed crystal structure.

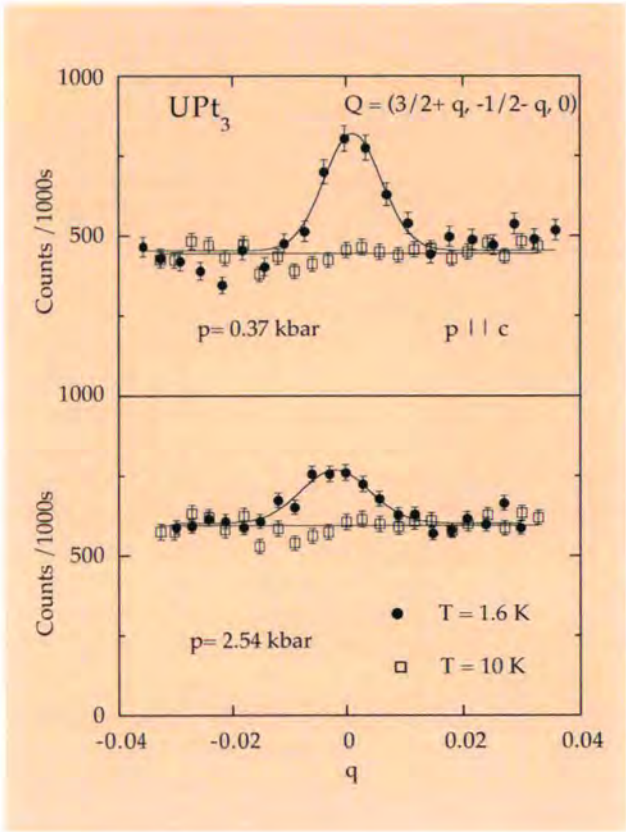


Figure 1: Magnetic Bragg peak intensity of $UPt_3$ at Q = (3/2+$q$,-1/2,0) as a function of $q$ under an applied pressure of p = 0.37 and 2.54 kbar for $p \perp c$ at $T$ = 1.6 K. For comparison, the high temperature scans ($T > T_N$) are included.

The magnetic Bragg peaks are not resolution limited but show a Lorentzian broadening that corresponds to a finite correlation length of the order of $\xi \approx$ 250-500 Å.

At low temperatures, $UPt_3$ shows unique unconventional superconducting properties. The superconducting transition at $T_c^+$ = 0.55 K is followed by a second superconducting transition at $T_c^-$ = 0.47 K. As a function of magnetic field and temperature, an exotic superconducting phase diagram [2] is observed with three different superconducting phases that meet at a tetracritical point. Combined elastic neutron-scattering and specific-heat measurements under hydrostatic pressure [3] showed a direct relation between the size of the weak ordered moment and the splitting of the superconducting transition temperatures $\Delta T_c = T_c^+ - T_c^-$.

By applying a pressure of 3-4 kbar, the antiferromagnetic order is fully suppressed and the two superconducting transition temperatures merge. As a consequence, the weak antiferromagnetic order is generally considered to act as a symmetry-breaking field for the superconductivity. Recent small-angle neutron-scattering measurements [4] of the superconducting flux-line lattice in an applied magnetic field along the $c$ axis demonstrated the unconventional nature of the superconductivity and uniquely assigned the symmetry of the superconducting gap.

We studied the weak antiferromagnetic order in $UPt_3$ by elastic neutron-scattering measurements under applied pressures up to 6 kbar ($p \| a$ and $p \| c$) and magnetic fields up to 12 T ($B \| a$ and $B \| c$) on the cold triple-axis spectrometer IN14. Pyrolytic graphite (002) planes were used as both monochromator and analyzer and a beryllium filter was placed before the sample.

The uniaxial stress was applied with a hydraulic press via a stainless steel rod and a knee-joint placed at low temperature to the faces of the sample. This system designed by the pressure group of the ILL allows for changing the pressure without heating the pressure cell. The magnetic field was applied by the 12 T vertical cryomagnet from the CEA Grenoble.

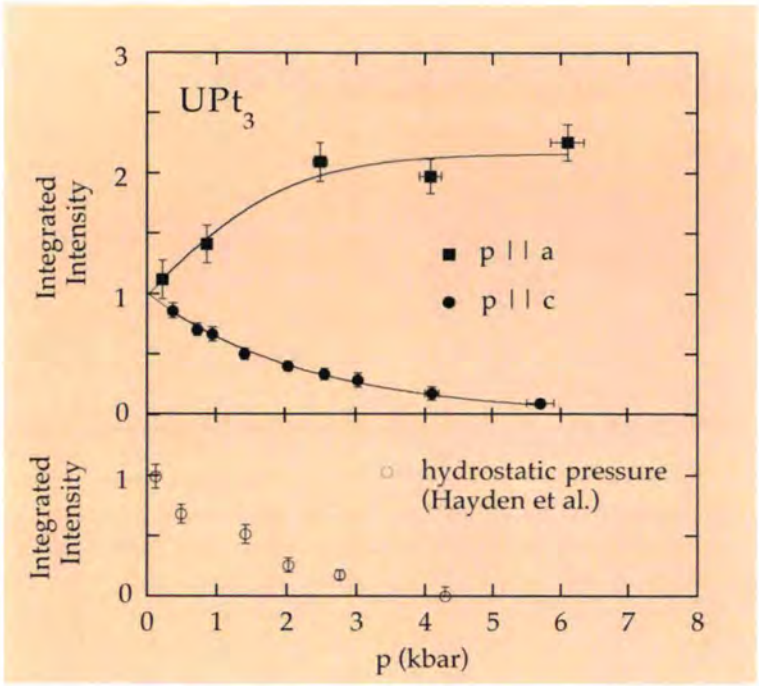


Figure 2: Relative integrated intensity of the magnetic Bragg peaks at Q = (3/2,-1/2,0) and Q = (0,1/2,2) as a function of the applied pressure for $p\|c$ and $p\|a$, respectively. The data points for $p\|a$ (solid squares) and p||c (solid circles) are normalised to the extrapolated zero-pressure value and compared with the earlier measurements under hydrostatic pressure (open circles) [3].

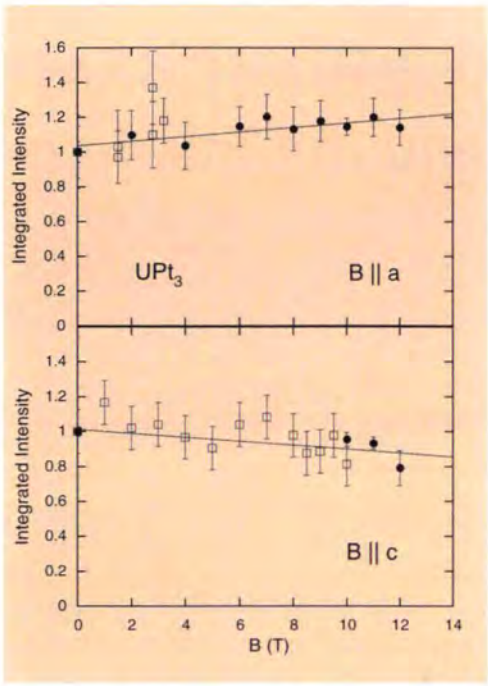


Figure 3: Relative integrated intensity of the magnetic Bragg peak as a function of applied magnetic fields up to 12 T ($B\|a$ and $B\|c$). The measured data points (solid spheres) are normalised to the zero-field value and compared with earlier low-field measurements (open squares)[6].

In Fig. 1, scans through the magnetic Bragg peak at Q = (3/2,-1/2,0) along **k** = (1/2,-1/2,0) are shown for applied pressures along the $c$ axis of $p$ = 0.37 and 2.54 kbar in antiferromagnetic state ($T > T_N$) and the paramagnetic state ($T > T_N$). Under a pressure of 2.54 kbar the Bragg peak intensity, which is proportional to the square of the ordered moment, is strongly suppressed.

The relative pressure dependence of the integrated intensity of the magnetic Bragg peak is shown in Fig. 2 for $p\|a$ and $p\|c$ [5]. For applied pressures along the $c$ axis the magnetic Bragg peak intensity shows a non-linear decrease for increasing pressure, while for applied pressures along the $a$ axis a significant non-linear increase in the relative integrated intensity is observed. The uniaxial pressure dependence for $p\|c$ strongly resembles the data from earlier elastic neutron-scattering measurements under hydrostatic pressure [3] as shown in Fig. 2. The strong increase in Bragg peak intensity observed for $p\|a$ therefore suggests a repopulation of the three **k** domains with a constant moment. These results are in good agreement with specific heat measurements under uniaxial pressure [5] which show that the splitting in $T_c$ decreases for p||c and is constant for $p\|a$. This confirms the existence of a direct relation between the size of the ordered moment and the splitting of the superconducting transition temperatures $T_c^+$ and $T_c^-$.

Similar scans as shown in Fig. 1 have been performed in magnetic fields up to 12 T for $B\|a$ and $B\|c$ [6]. The relative integrated intensity of the antiferromagnetic Bragg peaks is shown in Fig. 3. The observed field dependence closely corresponds to earlier low-field measurements and is very weak in magnetic fields up to 12 T. For $B\|a$ no significant domain repopulation is observed.
Additional temperature-dependent measurements of the antiferromagnetic Bragg peak intensity have shown that the ordering temperature of $T_N$ = 6 K is insensitive to applied pressures up to 6 kbar and magnetic fields up to 12 T. In combination with the finite correlation length of $\xi \approx$ 250-500 Å, this supports a scenario of slowly fluctuating moments which appear static on the time scale of cold neutrons.


**References**

[1] G. Aeppli, E. Bucher, C. Broholm, J.K. Kjems, J. Baumann, and J. Hufnagl, Phys. Rev. Lett. 60 (1988) 615 • [2] S. Adenwalla, S.W. Lin, Q.Z. Ran, Z. Zhao, J.B. Ketterson, J.A. Sauls, L. Taillefer, D.G. Hinks, M. Levy, and B.K. Sarma, Phys. Rev. Lett. 65 (1990) 2298 • [3] S.M. Hayden, L. Taillefer, C. Vettier, and J. Flouquet, Phys. Rev. B 46 (1992) 8675 • [4] A. Huxley, P. Rodière, D. McK. Paul, N. van Dijk, R. Cubitt, and J. Flouquet, Nature 406 (2000)160-164 • [5] N.H. van Dijk, P. Rodière, F. Yakhou, M.-T. Fernández-Díaz, B. Fåk, A. Huxley, and J. Flouquet, Phys.Rev. B63 (2001) 104426 • [6] N.H. van Dijk, B. Fåk, L.P. Regnault, A. Huxley, and M.-T. Fernández-Díaz, Phys. Rev. B 58 (1998) 3186

# Unconventional superconductivity and the flux-line lattice

A. Huxley, P. Rodière, J. Flouquet (CEA-Grenoble)
D. McK. Paul (University of Warwick)
N. van Dijk (DUT, Delft)
R. Cubitt (ILL)

**When a magnetic field is applied to a superconductor the magnetic field can penetrate as an array of flux lines. These lines are often ordered to form a lattice, the orientation and geometry of which reflects the anisotropy of the underlying interactions between the lines. Our experiments show that these interactions can be strongly modified in an unconventional superconductor, which in the case of $UPt_3$ gives rise to preferred orientations of the flux-line lattice. The unusual lattice orientations we observe in the superconducting A-phase help identify a particular symmetry for the unconventional superconductivity in this enigmatic material.**

In a superconductor the phases of individual electron wave functions become locked together. This rigidity underlies the frictionless passage of currents synonymous with a complete loss of electrical resistivity. Although a magnetic field induces angular momentum into the electron fluid, the phase rigidity can be conserved if the resulting motion is quantized and the magnetic field is bunched to thread the sample as an array of flux lines.
In general, repulsive forces between the flux lines favour the formation of a hexagonal flux-line lattice (FLL) to maximise the separation between the lines. However the screening currents surrounding an isolated flux line need not be exactly cylindrical, and this can lead to deviations from this geometry and a preferred orientation of the FLL. Even in a conventional superconductor small deviations from perfectly cylindrical screening currents can occur due to the anisotropy of the underlying fermi-surface. For a field applied along a four fold axis this anisotropy can lead to deformed hexagonal lattices and changes of their alignment [1]. However for the special case we will consider when the field is applied along a hexagonal crystal direction the fermi-surface re-enforces the hexagonal structure with a preferred orientation. Another potential source of anisotropy in the screening currents comes from the angular dependence of the superconducting gap. This effect is expected to be particularly significant for an unconventional superconductor where the locking of the electron phases has an angular dependence. In real materials it is also important to consider the complicating effect of crystal defects. Flux lines trapped in extended defects can locally perturb the orientation of the lattice (FLL). This effect can however be substantially reduced if all the flux lines are made to move, since the defect potentials seen by the moving flux lines are then averaged out.
The measurements we report have been made on one of the best known heavy-fermion superconductors, $UPt_3$. Since the magnetic contrast from the FLL that gives rise to neutron scattering is inversely proportional to the square of the electronic mass enhancement, the diffracted signal from the FLL in $UPt_3$ is very weak. It is then essential to have a combination of a high neutron flux, highly stable apparatus and a high quality crystal to detect the scattering. However the superconductivity in $UPt_3$ is highly unusual. The distinguishing feature is that the superconducting gap and not just the phase of the order parameter is believed to have a

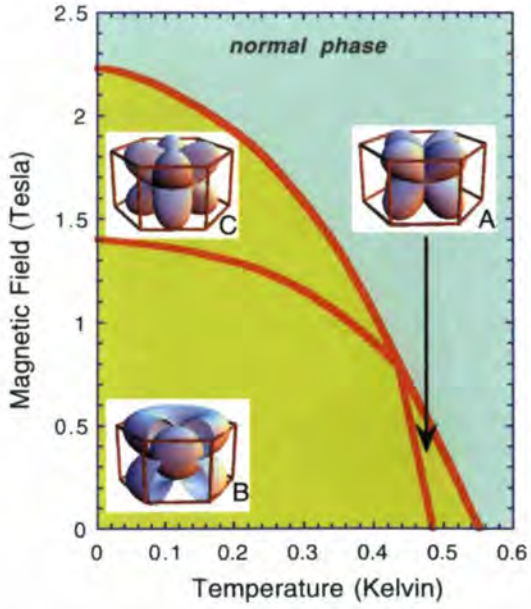


Figure 1: The low temperature phase diagram of $UPt_3$. Three different superconducting phases exist as a function of temperature and field denoted by A,B and C. The geometric figures show schematically the gap structure in each phase, relative to the hexagonal crystal axis depicted by the frames.

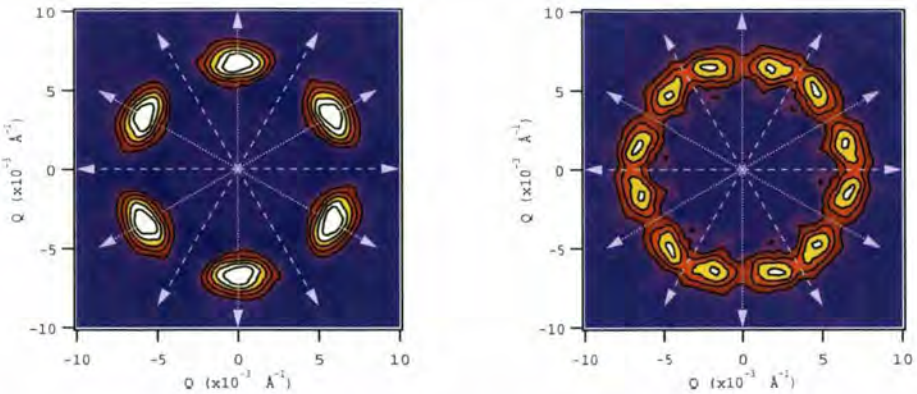


Figure 2: Symmetrized images of the small angle scattering from the flux-line lattice measured on D22. Panel (I) shows the image when the lattice was formed at 100mK in the B phase. In (II) the lattice was grown at 500mK in the A-phase. The second image is consistent with two domains of differently oriented nearly hexagonal lattices inclined at ±15° to the crystal symmetry axis shown by the solid and dashed lines (the a axis is vertical and an a* axis is horizontal).

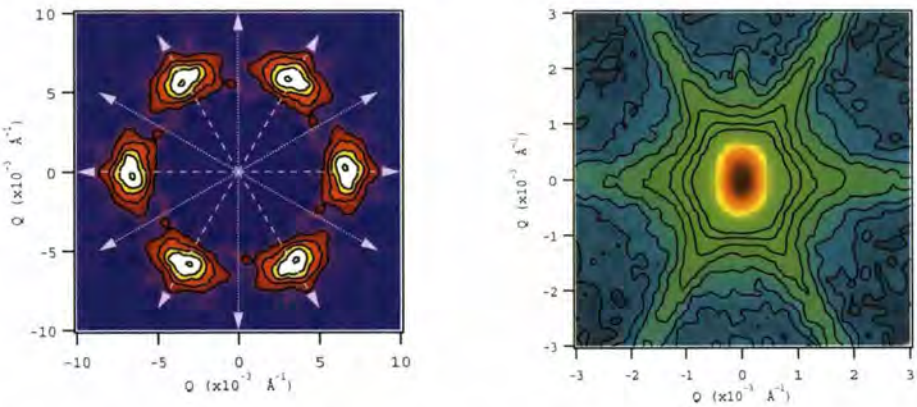


Figure 3: The image of the small angle scattering from a flux-line lattice grown at $T_c$ (field cooled). The image, measured on D22 represents integrated diffracted intensities as in figure 2. The range of rocking angles over which the spots were illuminated is however much larger in this case. The FLL is aligned to extended metallurgical defects which themselves give rise to small-angle scattering that was measured on D11 and is shown in panel II.

lower rotational symmetry than the crystal structure (see Fig. 1) and further, this symmetry changes with field and temperature, defining three distinct superconducting phases denoted A,B and C.

We have used D22 to measure the orientation and geometry of the FLL with a magnetic field along the hexagonal crystal axis for an applied field of 0.2 Tesla to explore any evolution in the FLL between the B and A superconducting phases [2]. As the temperature at which the FLL was formed was increased, we observed a change from an hexagonal lattice aligned along crystal symmetry directions, to two equally populated domains of approximately hexagonal lattices aligned at +15° and -15° to the symmetry axes (see Fig. 2). These new alignments were stable over a range of formation temperatures that span the A-phase. The natural explanation for the appearance of these new orientations is that they reflect the underlying symmetry of the superconducting gap. In the B-phase the gap appears isotropic about the hexagonal axis and the diffraction spots are aligned with the directions of maximum projected fermi-velocity. As the A-phase is approached however the gap becomes highly anisotropic about the hexagonal axis and the diffraction spots align with the directions of the maximum gap. The observed alignment therefore points to a maximum gap in the A-phase pointing along directions in between the symmetry axis of the crystal structure. The possible gap symmetries have previously been classified by symmetry analysis and only two possibilities appear compatible with the above observation, one of which can be eliminated by other measurements.

The above experiment thus provides evidence in favour of a particular gap symmetry shown in Fig. 1. Finally if the lattice is formed at $T_c$ by cooling in a constant field we observe a third FLL orientation that is aligned with extended crystal defects (Fig. 3). In this case the flux lattice shows considerable longitudinal disorder, characterised by wide rocking curves compared to the resolution limited curves recorded in the other two cases.


**References**

- [1] D. McK. Paul, C. V. Tomy, C. M. Aegerter, R. Cubitt, S. H. Lloyd, E. M. Forgan, S. L.Lee and M. Yethiraj, Phys. Rev. Lett. 80 (1998) 1517
- [2] A. Huxley, P. Rodière, N. H. van Dijk, M. D. Paul, R. Cubitt and J. Flouquet, Nature 406 (2000) 160

# Dynamics of an itinerant magnet with orbital moments


- A. Hiess (ILL)
- N. Bernhoeft (CEA-Grenoble)
- S. Coad (ILL and Inst. Transuranium Elements, Karlsruhe)
- G.H. Lander (Inst. Transuranium Elements, Karlsruhe)
- L. Paolasini (ESRF)
- D. Kaczorowski, A. Czopnik, R. Troc (W. Trzebiatowski Institute, Wroclaw)



**$UGa_3$, which has the simple cubic $AuCu_3$ structure and orders at $T_{Néel}$ = 67 K, is an itinerant 5*f* antiferromagnet with an orbital moment. We have examined the dynamical magnetic response with single crystals on both IN8 and IN14. Two interesting features are present. First, there are two parts to this response, one quasielastic and the other inelastic. Second, all the scattering is localised around the magnetic zone centre. The implications for our understanding of the magnetic response of itinerant *f* electrons are discussed.**


The challenge to understand the magnetic excitation spectra in actinide materials arises since the dominant 5*f* states are considerably extended in real space and hybridise strongly with band levels involving both on site and neighbouring ligand wavefunctions. In addition to their hybrid nature the 5*f* states experience strong spin-orbit coupling leading to anisotropic response functions and the possibility of a significant orbital moment. One manner to handle these complexities is to make a conceptual separation of the fast and slow degrees of freedom of the 5*f* levels whilst recognising that the measured cross section is the total response function of these two interacting fields. In general, the fast, high frequency aspect may be associated with a propagating component whilst the slow, low frequency part has the characteristics of an overdamped mode [1, 2]. $UGa_3$ is a prototypical example of this class of materials for which the results of bulk thermodynamic [3] and microscopic de Haas van Alphen [4] experiments yield unambiguous evidence for the itinerant nature of the 5*f* electron states. We have extended these investigations by neutron spectroscopic studies which give us detailed information on the dynamical magnetic response spectrum.

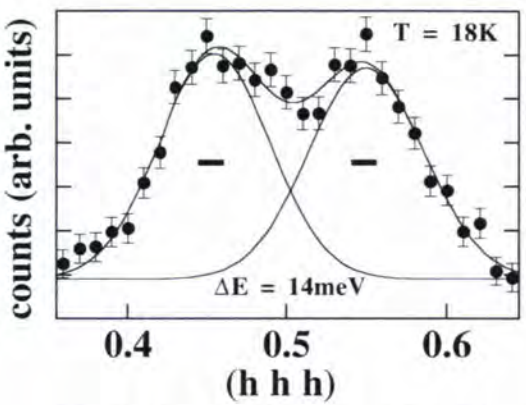


Figure 1: Typical constant-E scan with energy transfer of 14 meV. Data taken at T = 18 K with IN8. The two shoulders represent a propagating mode symmetric about $\mathbf{Q_0}$. This mode becomes difficult to observe above ~ 16 meV. The solid lines are Gaussian fits to the data. The Q-width (FWHM) of the (1 1 1) nuclear reflection is marked as black bars.

Initial experiments were performed with single crystals on the thermal triple-axis spectrometer 1T1 at LLB, Saclay, and were then continued on IN8 at ILL, Grenoble. These experiments, reported in Fig. 1 and 2, established an inelastic response at low temperature in the antiferromagnetic phase around the magnetic zone centre, $\mathbf{Q_0} = (\frac{1}{2}, \frac{1}{2}, \frac{1}{2})$, with a gap of about 5 meV. Interestingly this spin wave like excitation propagates only over a limited part (~25%) of the Brillouin zone in any of the high symmetry directions before the intensity dies away; previously, in ferromagnetic metals similar effects have been attributed to Landau damping on approaching the Stoner continuum [5].

To explore the slow, Fermi liquid like contribution anticipated from the 5*f* states we have extended our investigations with the cold-source triple axis spectrometer IN14.

At low frequencies, within the spin wave gap, we have been able to characterise a response around $\mathbf{Q_0}$. Figure 3*(a)* gives the thermal evolution of the spectra and 3*(b)* the wave vector dependence at 15 K, the solid lines have been calculated on the basis of a phenomenological model developed previously [2]. This consists of two modes, one slow and overdamped, the other having a pole at finite frequency with the interaction between the two components being taken into account in a mean-field approximation to yield the measured cross section. As with the inelastic scattering the quasielastic contribution dies rapidly as $q$ increases from the zone centre, this is evidenced by the decrease in intensity around $\Delta E = 0$ in Fig. 3*(b)*. If one takes the low frequency spectral weight to be associated with the propagation of quasiparticles at the Fermi

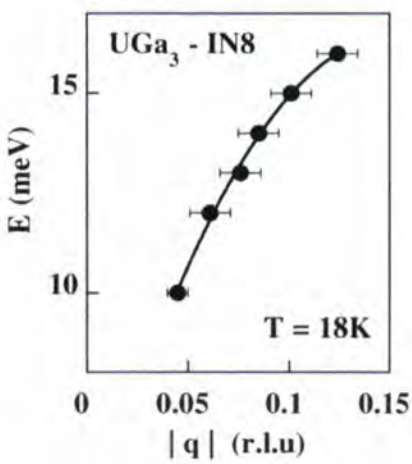


Figure 2: Peak positions (deduced from Gaussian fits, see Fig. 1) versus $|q|$ away from the magnetic zone centre $\mathbf{Q_0} = (\frac{1}{2}, \frac{1}{2}, \frac{1}{2})$ derived from constant-E scans in all three high-symmetry directions. Data taken at T = 18 K with IN8. The solid line is a guide to the eye.

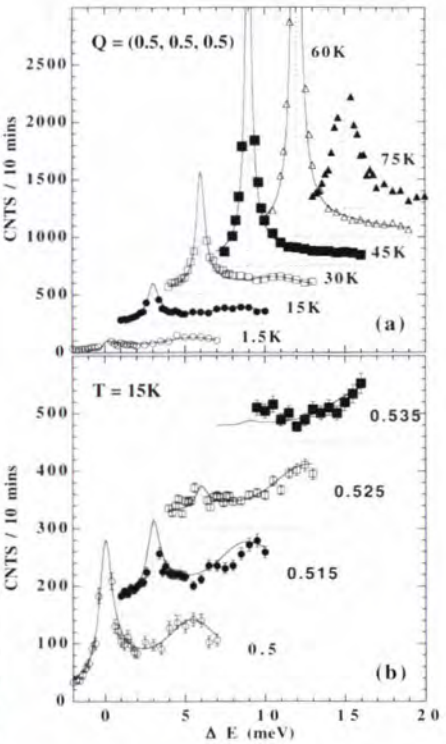


Figure 3: (a) Temperature dependence of the scattering at $\mathbf{Q_0}$ versus energy transfer. (b) **Q**-dependence of the scattering along the [h h h] direction at T = 15 K. Note the displaced axes in both panels. The solid lines are fits to the interacting two component model as described in the text, and more fully in Ref. [2].(Data taken with IN14).

surface, the topology of one particle calculations [4] suggests a dominant contribution of states derived from the «rugby ball» part of the Fermi surface- the strong curvature implying a small amplitude for low-energy excitations having wave vectors substantially different from $\mathbf{Q_0}$. Further detailed numerical analysis is required to confirm this conjecture.

Figure 4 gives a colour contour map of the temperature and energy dependence at $\mathbf{Q_0}$. This plot emphasises the merging, for T > 35 K, of the fast and slow contributions to the total response. The energy gap associated with the propagating part of the response, which in part may arise from the spin-orbit interaction, decreases together with the staggered spin polarisation on approaching $T_{Néel}$ (67 K). In contrast, the strong quasielastic correlations in the dynamic magnetic response around $\mathbf{Q_0}$ persist up to at least $2T_{Néel}$.

In concluding we note that, whilst a self-consistent RPA [6] is able to provide a framework for understanding the antiferromagnetic response of itinerant $3d$ compounds, as recently discussed both in the lanthanum cuprates and $V_2O_3$ [7], it is insufficient for the interpretation of the more complex $5f$ spectra evidenced in this work. One major feature of the work on $UGa_3$ reported here is to demonstrate unambiguously the presence of a two component lineshape in the antiferromagnetic phase. The coupled mode phenomenology used in our analysis is a flexible generalisation of the theory of the Néel state and finds support in more formal theories based on, for example, the functional integral decoupling of fast and slow quasiparticle excitations [1]. We hope that these results will stimulate new activity on the magnetic response of metals in the presence of a large spin-orbit interaction.

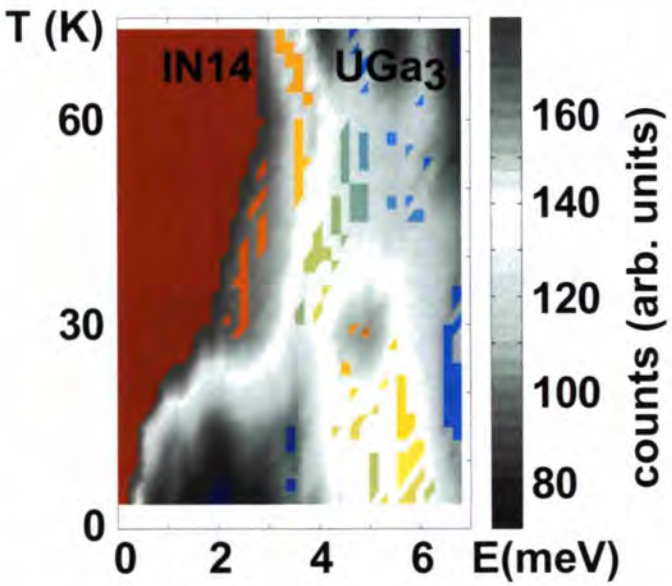


Figure 4: Colour contour map of the temperature and energy dependence at $\mathbf{Q_0}$ as measured on IN14. Once the distinct inelastic feature disappears above 40 K the response is dominated by the quasielastic component ($T_{Néel}$ = 67 K.).


REFERENCES

[1] C. Pepin and M. Lavagna, Phys. Rev. B 59 (1999) 2591 • [2] N. Bernhoeft et al., Phys. Rev. Letters 81 (1998) 4244; Physica B 259-261 (1999) 614 • [3] D. Kaczorowski et al., Phys. Rev. B 48 (1993) 16425 • [4] A.L. Cornelius et al., Phys. Rev. B 59 (1999) 14473 • [5] Y. Ishikawa et al. Phys. Rev. B 25 (1982) 25 • [6] H. Hasegawa and T. Moriya, J. Phys. Soc. Japan 36 (1974) 1542 • [7] T.E. Mason et al., Phys. Rev. Letters 68 (1992) 1414; W. Bao et al., Phys. Rev. B 58 (1998) 12727

# Spin excitations in a magnetic superlattice: the first inelastic neutron scattering measurements


- A. SCHREYER (RUHR–UNIV. BOCHUM AND ILL)
- A. WILDES, W. SCHMIDT (ILL)
- C.F. MAJKRZAK, R.W. ERWIN, S. H. LEE (NIST)
- M. HONG, R. KWO (BELL LABORATORIES, MURRAY HILL)


**The observation of magnetic excitations in artificial systems with inelastic neutron scattering methods represents a major challenge owing to the weak scattered signals. In this report we present measurements of spin waves in a Dy/Y superlattice using inelastic neutron scattering. The ingredients of our success have been the growth of a sample with a large number of layers and a large magnetic moment and the use of modern high flux neutron instrumentation. Our data indicates a folding of the Brillouin zone due to the superlattice periodicity.**

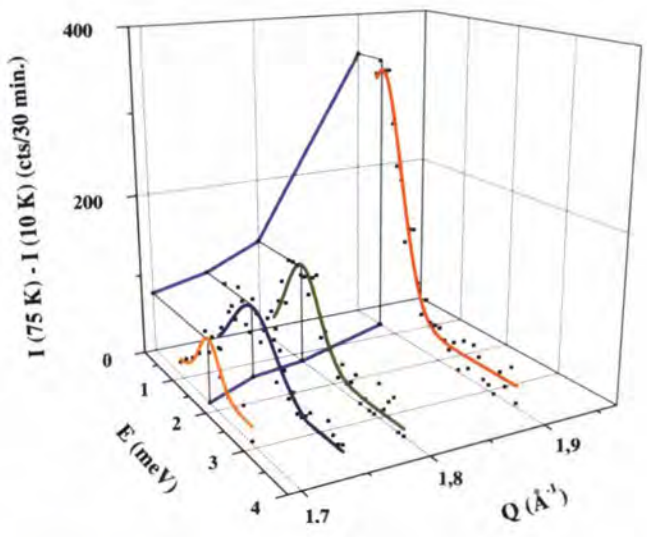


Figure 1: Difference of inelastic constant Q scans at T = 75 K and 10 K with fitted Gaussians. The projection onto the Q-E plane yields the dispersion curve. Q is parallel to the Dy c-axis and the superlattice growth direction.

Up to now, information on magnetic excitations in magnetic thin films and superlattices has come from inelastic light scattering (Brillouin scattering, BS) [1,2] and ferromagnetic resonance (FMR) experiments [3]. FMR can probe spin waves at the centre of the Brillouin zone (BZ), and at magnon wave vectors q inversely proportional to the film thickness. With Brillouin scattering, wave vectors on the order of the wave vector of light are accessible, i.e. also close to the BZ centre. Thus, it has not been possible to determine the dispersion of spin waves in magnetic thin film systems in the whole BZ. With inelastic neutron scattering (INS), on the other hand, the dispersion of spin waves in much larger portions of the BZ is in principle accessible. Smaller wavelength (higher Q) spin waves on the order of the superlattice periodicity would become accessible which can be dominated by the magnetic exchange coupling between the magnetic layers. Thus, INS would open up the opportunity to study the dynamic behaviour and the exchange coupling in magnetic superlattices in more detail than was possible so far.

Thin film samples made from Rare Earth materials are the prime candidates for a study of magnetic excitations with inelastic neutron scattering, since the Rare Earths exhibit the largest magnetic moments of all elements, causing the largest possible cross-section for magnetic neutron scattering. Rare earth superlattices have been studied intensely over the last decade using elastic neutron scattering to determine their magnetic structures [4].

The inelastic measurements were performed on a superlattice of the layer sequence $Y_{500Å}[Dy_{43Å}/Y_{28Å}]_{350}/Y_{2340Å}/Nb_{2000Å}/Al_2O_3$(substrate), which was grown by MBE methods [5] along the c-axis of the hcp structure of Dy and Y. The amount of Dy in the sample was maximised by growing 350 bilayers and using a rather large 2.5 · 1.25 cm² substrate. Nevertheless, the Dy in the sample amounts to only 10 mg. Below its bulk Néel temperature of 179 K, Dy exhibits a helical phase along the Dy c-axis which transforms into a ferromagnetic structure below 89 K. In Dy/Y superlattices a coherent helical phase occurs which extends over many bilayers whereas the ferromagnetic phase is suppressed due to magnetoelastic effects [6]. The coherent helical phase is mediated by the diamagnetic Y interlayers via RKKY exchange coupling. Elastic neutron scattering experiments have confirmed that the present Dy/Y sample exhibits the same long-range helical order observed previously.

After initial work at the NIST Center for Neutron Research on the cold neutron spectrometer NG-5 the measurements were continued at ILL on IN14 and IN12. The inelastic scans were performed at 75 K where the Bose factor increases the spin-wave signal to a sufficient level that it may be measured [7]. Equivalent scans at 4 K, where the inelastic scattering is much wea-

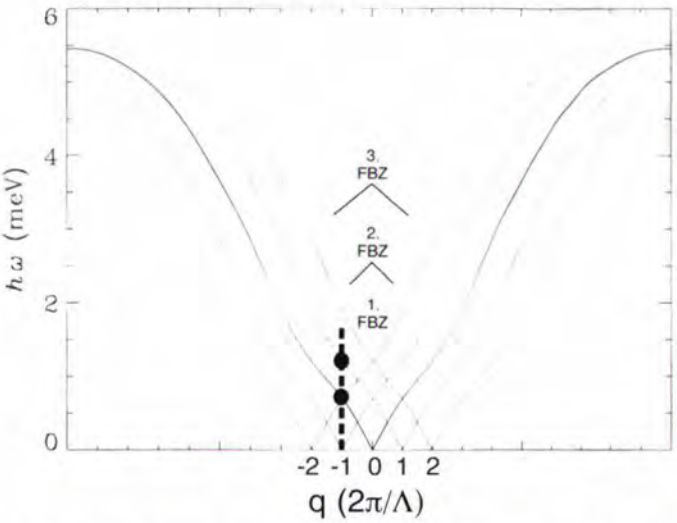


Figure 2: Schematic visualisation of the folding of the Brillouin zone in a superlattice on the spin wave dispersion curves. The resulting 1., 2. and 3. folded Brillouin zones (FBZ's) are marked. The dashed line indicates the scan of Fig. 3, the dots mark the expected peak positions.

ker, serve as a quasi-background. The intensity difference of these scans then is a good measure of the spin-wave cross section. In Fig. 1 the difference between a few 75 K and 10 K data sets is plotted together with Gaussian fits and the projections of the peaks onto the Q-I and Q-E planes [8].

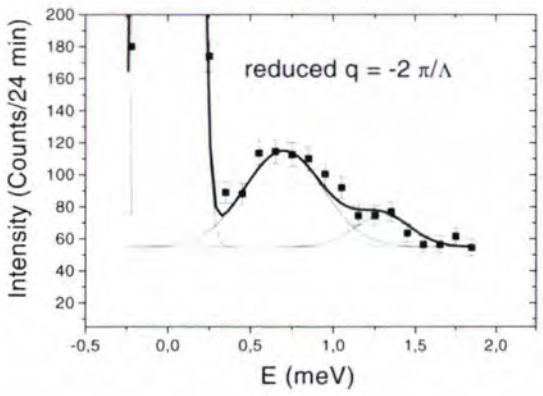


Figure 3: High resolution scan along the dashed line of Fig. 2 yielding the two expected peaks.

We find a spin-wave excitation, which is well-localised in energy. The resulting dispersion curve is shown in the Q-E plane. Its extrapolation to higher Q yields an elastic peak at $Q_{heli}$ = 1.97 Å$^{-1}$ as its origin. This peak is caused by the helical long-range magnetic order in the superlattice which propagates through the superlattice stack due to the exchange coupling by the Y layers. The wave vector q of the spin wave is then obtained from the relation $q = Q - Q_{heli}$. Comparison with the data of bulk Dy [9] shows that the dispersion curve observed here is essentially consistent with the bulk curve. In bulk the Brillouin zone is determined by the periodicity of the lattice, i.e. by the lattice constant $a_0$. However, an additional period is present in a superlattice along the growth axis. This superlattice period L, which is the sum of the individual Dy and Y layer thicknesses, is expected to induce a folding of the Brillouin zone like in the case of phonons in superlattices [10] or graphite intercalated compounds [11]. This effect is visualised schematically in Fig. 2. The superlattice period $\Lambda$ causes satellite peaks in the elastic scattering (at E = 0) at positions $q = \pm n \cdot 2\pi/\Lambda$ (n = 1,2,3...) around the helimagnetic peak at $Q_{heli}$ (i.e. q = 0). In principle, each of these satellite peaks is the source of a dispersion curve, which, consistent with the experiment, we have assumed to be bulk-like in Fig. 2. The resulting folded Brillouin zone (FBZ) is only $2\pi/\Lambda$ wide in q (instead of $2\pi/a_0$ in bulk) and contains all the information about the dispersion curve. The obvious question at this point is if we can see a sign of this folding effect with neutrons. For example, instead of a single peak, we would expect a series of equidistant peaks in an energy scan at fixed $q = n \cdot 2\pi/\Lambda$. Such a scan at $q = -2\pi/\Lambda$ performed with a higher instrumental resolution on IN14 compared to the ones of Fig. 1 is shown in Fig. 3. Two peaks are now clearly visible. The energies roughly correspond to those which we expect assuming bulk-like dispersion curves (see Fig. 2). In conclusion these results demonstrate the feasibility of inelastic neutron scattering studies on spin waves in a rare earth superlattice for the first time. We find a bulk-like dispersion curve and clear evidence of Brillouin zone folding effects. These results may open up a new field of research for inelastic neutron scattering providing access to much wider regions of the Brillouin zone of magnetic superlattice structures than were accessible with other methods so far. Details and additional results will be published shortly [12].

## References


[1] P. Grünberg, in "Light scattering in Solids V", edited by M. Cardona and G. Güntherodt, Springer Verlag, Berlin, Heidelberg, New York (1989) [2] B. Hillebrands and G. Güntherodt, in "Ultrathin Magnetic Structures", edited by B. Heinrich and J. A. C. Bland, Springer Verlag Berlin, Heidelberg, 1994, Vol. II, p. 258-277 [3] B. Heinrich, in Ref. 2, p. 195-257 [4] C.F. Majkrzak et al., Adv. in Phys. 40 (1991) 99; D.F. McMorrow et al., Physica B 192 (1993) 150 [5] J. Kwo, in "Thin Film Techniques for Low Dimensional Structures", edited by R.F.C. Farrow, S.S.S. Parkin, P.J. Dobson, N.H. Neaves and A.S. Arrott, NATO ASI series B, Physics V13, Plenum Publisher Corporation (1988) p. 337; M. Hong, R.M. Fleming, J. Kwo, L.F. Schneemeyer, J.V. Waszczak, J.P. Mannaerts, C.F. Majkrzak, D. Gibbs, and J. Bohr, J. Appl. Phys. 61 (1987) 4052 [6] M.B. Salomon et al., Phys. Rev. Lett. 56 (1986) 259 [7] See for example: G.L. Squires, "Introduction to Thermal Neutron Scattering", Cambridge University Press, Cambridge, New York, 1978 [8] A. Schreyer et al., J. Appl. Phys. 87 (2000) 5443 [9] R.M. Nicklow et al., Phys. Rev. Lett, 26 (1971) 140 [10] J. Sapriel and B. Djafari Rouhani, Surface Science Reports 10 (1989) 189 [11] A. Magerl and H. Zabel, Phys. Rev. Lett. 46 (1981) 444; G. Dresselhaus et al., Sol. State Comm. 40 (1981) 229 [12] A. Schreyer et al., in preparation

# Magnetic solitons in $CuB_2O_4$


- M. Böhm (ILL and LNS, ETHZ & PSI, Villigen)
- B. Ouladdiaf, J. Kulda (ILL)
- B. Roessli, J. Schefer (LNS, ETHZ & PSI, Villigen)
- U. Staub (Swiss Light Source, PSI, Villigen)
- G. Petrakovskii (Institute of Physics, Krasnoyarsk)



**Elastic and inelastic neutron scattering measurements on single crystal have been performed to investigate the magnetic ground-state of copper metaborate $CuB_2O_4$.**
**The compound exhibits a second order phase transition from a paramagnetic to a commensurate antiferromagnetic phase (CP) with $\vec{k}=0$, followed by another second order transition to an incommensurate one (ICP) at T*=10K. The association of the Dzyaloshinskii-Moriya(DM)-interaction, lattice symmetry and tetragonal anisotropy leads to the formation of a magnetic soliton lattice.**


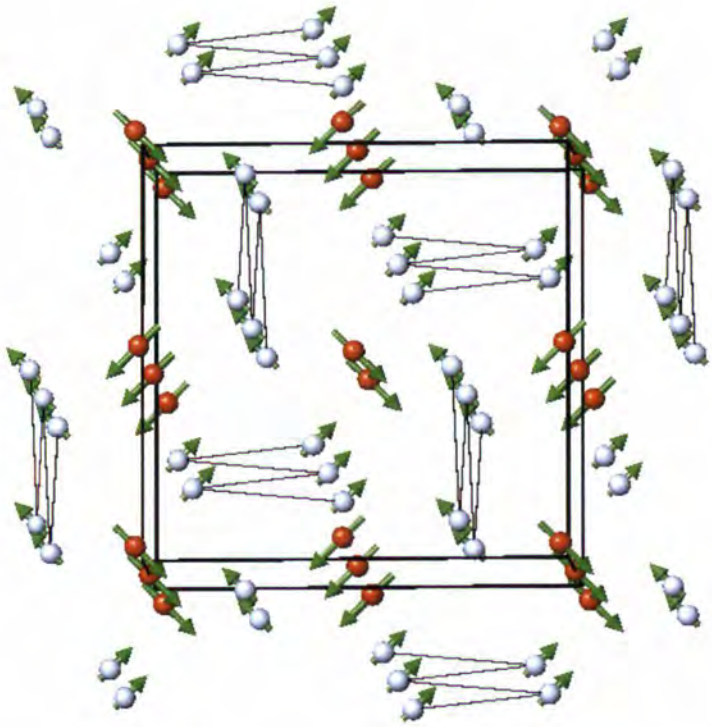

Figure 1: Antiferromagnetic structure of $CuB_2O_4$ in the commensurate phase.

Magnetostatic measurements such as specific heat and susceptibility have revealed two phases transitions in $CuB_2O_4$ at $T_N$=21K and T*=10K. The magnetisation data show a very weak ferromagnetic component in the basal plane [1]. $CuB_2O_4$ crystallises in space group $I\bar{4}2d$ ($D_{2d}^{12}$). The chemical contains 12 formula units. The $Cu^{2+}$ ions occupy two non-equivalent sites namely Cu(A) at 4b site (local symmetry) and Cu(B) at 8d site (local symmetry $\bar{4}$) [2]. The neutron diffraction on single crystal measurements were carried out using the four-circle diffractometer D10 with $\lambda$=2.36Å. Below $T_N$ =21K, the intensity of some nuclear Bragg peaks and specially the forbidden reflections (110) and (0 0 2) increase with decreasing the temperature, which indicates that $CuB_2O_4$ orders antiferromagnetically with a propagation vector $\vec{k}$=0. The magnetic structure for this commensurate phase was determined with the help of group theory. The relevant irreducible representations of the magnetic structure ($\vec{k}$=0) are those of the point group $\bar{4}2n$. There are five irreducible representations. Four of them are one-dimensional ($\Gamma_1$, $\Gamma_2$, $\Gamma_3$, $\Gamma_4$) and one labelled $\Gamma_5$ is two-dimensional. The reduction of the induction representation

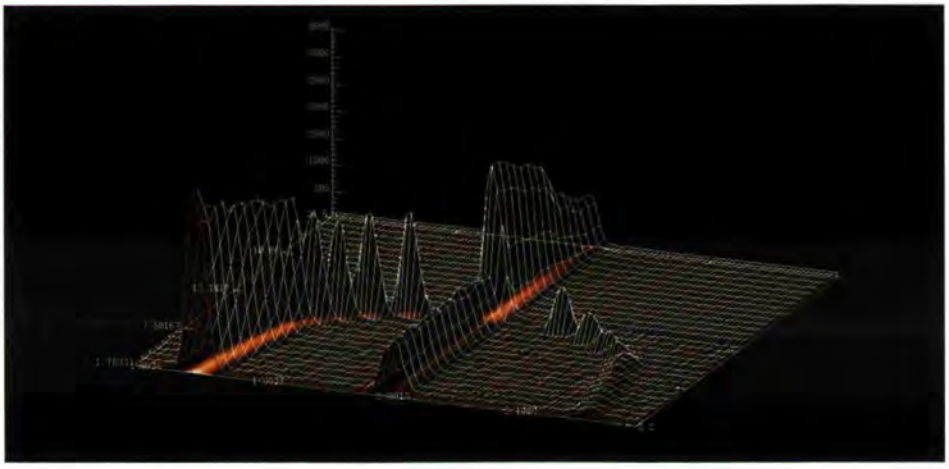

Figure 2: Thermal dependence of the (0 0 2) reflection and the corresponding satellites.

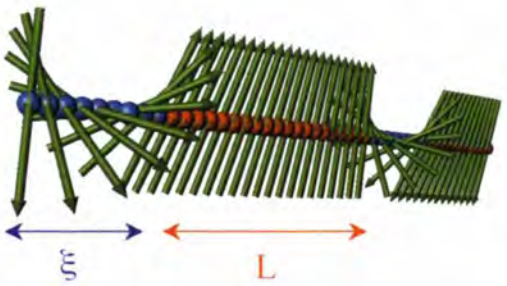


Figure 3: Evolution of the spin arrangement in a soliton lattice.

gives $\Gamma_{4b} = \Gamma_3 + \Gamma_4 + 2\Gamma_5$ and $\Gamma_{8d} = \Gamma_1 + 2\Gamma_2 + \Gamma_5 + 2\Gamma_4 + 3\Gamma_5$ for Cu at site 4b and 8d respectively. The magnetic modes of $\Gamma_3$ and $\Gamma_4$ of the 4b site correspond to a collinear ferromagnetic and antiferromagnetic ordering along the z-axis respectively. The modes associated with $\Gamma_5$ describe a 90° configuration in the basal plane. Similar magnetic modes for 8d site can be deduced. A set of 25 pure magnetic reflections was used in the refinement at T=12K. The magnetic structure, which is obtained from these calculations, can be described as a non-collinear arrangement of both the Cu(A) and Cu(B) spins along the diagonals of the tetragonal plane (Fig. 1). The value of the magnetic moment is $\approx 1\mu_B$ for the Cu(A) with a small component along the c-axis $\mu=0.25\mu_B$. The Cu(B) spins are confined within the ab-plane and have a small magnetic moment $\mu\approx0.25\mu_B$. The magnetic moments do not compensate and therefore a small spontaneous ferromagnetic component arises in the basal plane.

The magnetic structure belongs to two different irreducible representations $\Gamma_5$ and $\Gamma_3$, the spin Hamiltonian describing the system should be higher than order two [3]. On the other hand, the transition at $T_N$ being second order, the transition temperature should be considered as a bicritical point [4].

Below T*, new magnetic satellites appear at symmetrical points with respect to the commensurate reciprocal lattice points. The corresponding propagation vector is $\vec{k}$=(0,0,0.15) at T=1.8K. This indicates that the magnetic structure becomes incommensurate along the c-axis. Fig. 2 shows the thermal dependence of the 0 0 2 reflection and the corresponding satellites. The refinement of the neutron data shows that the magnetic structure of $CuB_2O_4$ below T*=10K consist of an helix with a constant amplitude and phase shifts between different spins in the unit cell. At the incommensurate-commensurate transition, the propagation vector $\vec{k}$ (T) goes smoothly to zero. The transition is of second order. Therefore it is not likely that competing interactions are at the origin of the helical structure. In such case a first order phase transition and a jump in the wave vector is produced [5].

On the basis of the Landau theory of phase transitions Dzyaloshinskii showed that incommensurate structures can arise due to the Dzyalloshinskii-Moriya (DM) interaction in chemical structures belonging to the following eleven point groups: $D_2$, $D_{2d}$, $C_{3h}$, $D_3$, $D_{3h}$, $S_4$, $D_4$, $D_6$, T, $T_d$, O [6]. Symmetry analysis of the chemical structure of $CuB_2O_4$ shows that the DM-interaction is allowed between two Cu(A)- nearest-neighbour spins, with a DM-vector parallel to the tetragonal c-axes. The role of this interaction in forming the magnetic ground state in copper metaborate is confirmed by the 90° configuration of the magnetic moments in the commensurate phase as the DM- interaction favours a non-collinear spin arrangement. According to Dzyalloshinskii's theory the presence of an additional crystal anisotropy distorts the regular helical arrangement of the spins along the helical axis. In order to minimise the free energy, the spins acquire a phase dependence $\varphi(z)$ of the helix which is given by a solution of the non-linear sine-Gordon differential-equation [6]. The solution of this equation describes a situation where the phase of the spins along z will stay almost constant over a given length L but changes abruptly over a short period ξ (Fig. 3). Changing the temperature changes the anisotropy term, which causes on the other hand an increase of L. Close to the phase transition T*, the magnetic structure can be represented as a periodic structure of domains which are separated by domain walls or equivalently solitons [5]. In such a case, higher order harmonics are expected to be observed in neutron diffraction pattern at positions (n±1)k, (2n±1)k,..., where n gives the order of anisotropy [5]. Fig. 4 shows a scan along the crystallographic c*-axis around the magnetic zone-centre (110) at T=9.5K. As the anisotropy in the basal plane is of the order of 4 [1], higher harmonics appear at the positions 3k, 5k,.. The soliton lattice is further confirmed by the appearance of considerable diffuse scattering near the central peaks in agreement with the calculation of Izyumov [5]. The intensity of the diffuse scattering increases with increasing temperature and exhibits a critical divergence close to T*, in accordance with the observation of susceptibility and specific heat peaks at this temperature [1].

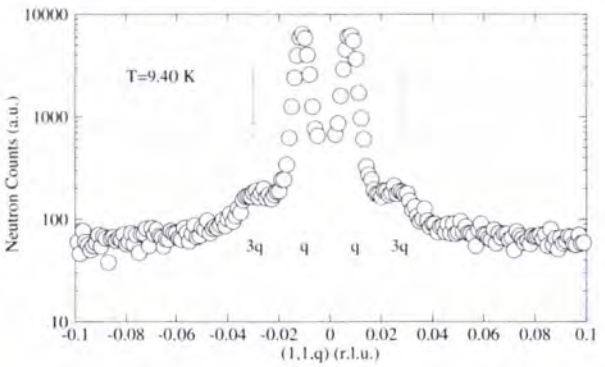


Figure 4: Neutron elastic scan along the [1 1 q] direction at T=9.4K showing the presence of higher order harmonics in addition to the principal magnetic satellites.


**References**

[1] G. Petrakovskii et al., J. Mag. Mag. Mat. 205 (1999) 105-109 [2] M. Martinez-Ripoli et al., Acta Crystallogr. B 27 (1971) 677-681 [3] E. F. Bertaut, Acta. Cryst., A24 (1968) 217 [4] B. Barbara, D. Gignoux and C. Vettier , Lecture on Modern Magnetism, published by Science Press Beijing, Springer-Verlag, Berlin Heidelberg 1988. P221 [5] Yu.A. Izyumov, Sov. Phys. Usp. 27(11) (1984) 845 [6] I.E. Dzyaloshinskii, Sov. Phys. JETP 20 (1965) 665-671 [7] Yu.A. Izyumov, Physica B 174 (1991) 9-17

# Clusters or 'combed hair' in Fe-Zr metallic glasses?

A. R. Wildes (ILL)

N. Cowlam (University of Sheffield)

S. Al-Heniti (ILL and University of Sheffield)

**Iron, with a small percentage of impurity, may be quench-cooled into an amorphous, or 'glassy', state. While these materials have been extensively researched – indeed, they are used for a wide variety of commercial purposes today – their magnetic properties are still not fully understood. Many models have been proposed to explain the behaviour of these materials, including magnetic cluster and wandering axis models. We have applied the techniques of polarised neutron scattering to measure the ferromagnetic structure of Fe-Zr, an example of a metallic glass, and are able to determine which of the many proposed models is closest to the truth.**

Ferromagnetic materials that readily align with an externally applied magnetic field – so-called 'soft' magnets – have a wide variety of applications, from magnetic recording heads to transformers for power grids. Iron-based metallic glasses are extremely soft and are currently commercially produced in large quantities to satisfy the demand for these important materials. They are commonly made by pouring a liquid melt of the constituents onto a cooled, spinning wheel. The melt is quench-cooled and flies off the wheel in the form of a ribbon. The atoms in the ribbon have no long-range order and therefore the atomic structure is amorphous.

Besides being commercially important, these metallic glasses provide a test bed for the understanding of magnetism. An amorphous structure is free of crystal symmetry, invalidating many approximations, and is subject to magnetic frustration and short-range order. As a result, many metallic glasses show anomalous magnetic behaviour, frequently interpreted as being due to 'non-collinear' ferromagnetism. Such structures may take many forms, and the exact nature of the ferromagnetic structure of metallic glasses is still being debated. Postulated examples are shown in Fig. 1.

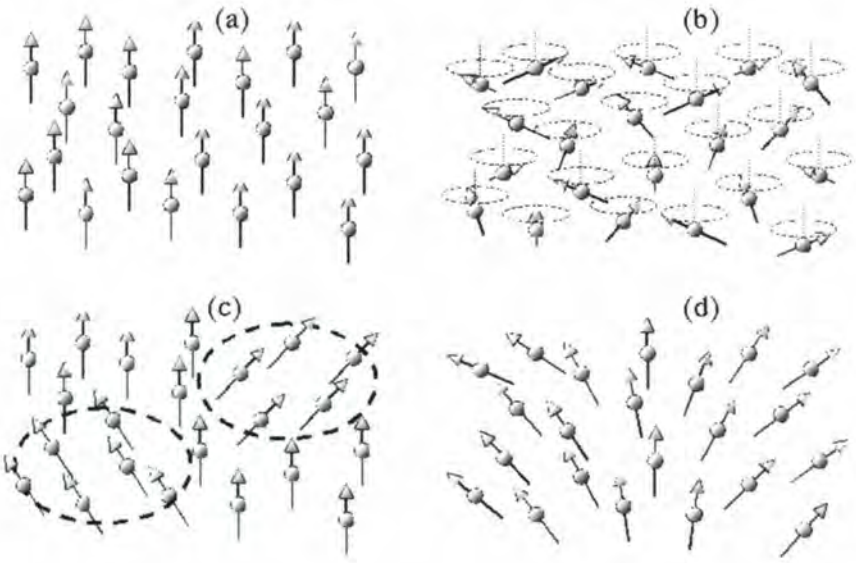


Figure 1: Previously proposed models for the ferromagnetic structure of metallic glasses. 1(a) shows a collinear ferromagnet. 1(b) shows a structure where the moments are randomly oriented on a cone. 1(c) shows a 'canted cluster' model. The moments in certain regions are ferromagnetically aligned, but the local axis is inclined with respect to the mean ferromagnetic direction. 1(d) shows a 'combed hair' model, where the moments are ferromagnetically coupled, but the axis wanders about the mean direction.

Figure 1(a) shows a conventional collinear ferromagnet, the magnetic moments all collinear with a common direction. Of the proposed non-collinear models, the simplest has the moments randomly oriented on a cone, as shown in Fig. 1(b) [1, 2]. More complicated models involve correlations between the non-collinear components of the moments. One model proposes that the sample has within it regions, or 'clusters'. All the moments in each cluster are ferromagnetically aligned, but at an angle to the collinear direction, as shown in Fig. 1(c) [3,4]. In an alternative model, shown in Fig 1(d), the moments are ferromagnetically aligned, but the axis fluctuates around the mean collinear direction. This type of model is called a 'wandering axis' or 'combed hair' model [1].

All of these models have been used to describe the metallic glass system $Fe_{100-x}Zr_x$, $7 \leq x \leq 12$. It is not agreed which model best describes the magnetic structure. We have therefore looked at $Fe_{90}Zr_{10}$ and $Fe_{92}Zr_8$ to attempt to resolve whether non-collinear ferromagnetism exists and, if so, which form

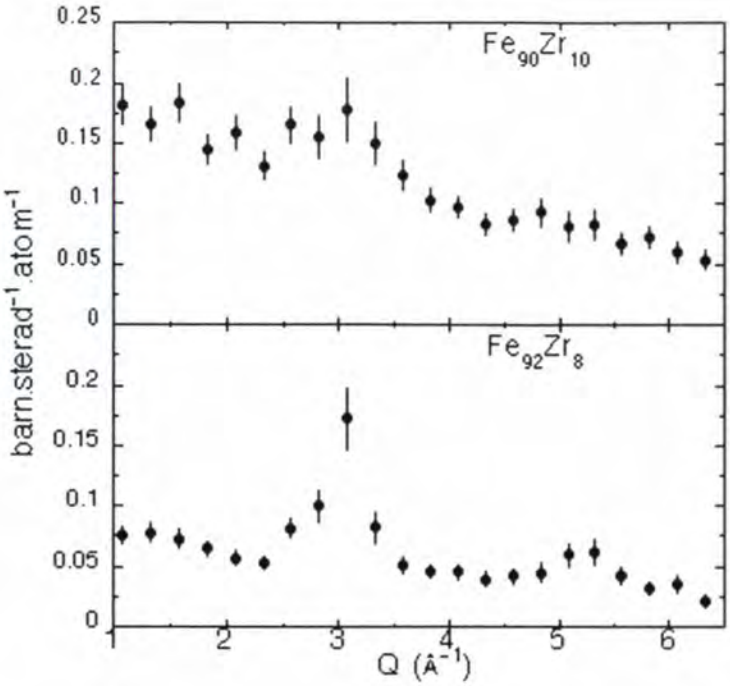


Figure 2: The spin-flip cross-sections of $Fe_{90}Zr_{10}$ and $Fe_{92}Zr_8$ at 135 K in 2T. This cross-section is directly proportional to the correlations between any non-collinear magnetism. The cross-section of $Fe_{90}Zr_{10}$ is finite, but essentially featureless, suggesting it has a structure similar to 1(b). $Fe_{92}Zr_8$ has peaks in the cross-section at the first two maxima of the atomic S(Q). Comparison of calculation with the data suggests that it has a 'combed hair' structure with some random disorder.

does it take. We have used the technique of neutron diffraction with polarisation analysis on the IN20 spectrometer. This is the *only* technique capable of unambiguously detecting non-collinear magnetic structures. The samples were subjected to a vertical magnetic field of 20 kOe to saturate the magnetic domains. In this configuration, any spin-flip cross-section is directly proportional to the structure factor of the non-collinear components of the moments. A collinear ferromagnet, therefore, will have no spin-flip cross-section. Figure 2 shows the spin-flip cross-section for the two samples at 135 K, where they are ferromagnetic.

The spin-flip cross-section of $Fe_{90}Zr_{10}$ (Fig 2(a)) is finite and diffuse, decreasing smoothly with increasing Q. Such a cross-section has been seen before [2,5] and is representative of a non-collinear system with no correlations between the non-collinear components. This sample therefore has a magnetic structure similar to Fig. 1(b).

The spin-flip cross-section of $Fe_{92}Zr_8$ (Fig. 2(b)) has, in addition to a diffuse feature, distinct peaks at Q ≈ 3.1 Å$^{-1}$ and ≈ 5.25 Å$^{-1}$, matching the first two maxima in the atomic S(Q). Such features have never been seen before and are representative of a correlated non-collinear ferromagnetic structure, such as those of Figs. 1(c-d).

We have made detailed calculations of the model structures to see which will reproduce the features in Fig 2(b). Two possibilities exist: the magnetic structure has either a 'combed hair' component with some random disorder; or it is a 'cluster canted' structure with virtually every moment in a cluster and very few collinear with the mean ferromagnetic direction. Looking carefully at the proposed models and how they compare with our conclusions, we believe that the former structure is the closest to the truth. Our results can now be used to refine extremely detailed theoretical calculations [6], providing vital evidence to understand the complex magnetic behaviour of metallic glasses.

## References


[1] D. H. Ryan et al., Phys. Rev. B 35 (1987) 8630 [2] R A Cowley et al., J. Phys.: Condens. Matter 3 (1991) 9521 [3] S. N. Kaul, J. Phys. F: Met. Phys. 18 (1988) 2089 [4] L. F. Kiss et al., J. Mag. Mag. Mat. 135 (1994) 161 [5] A R Wildes et al., J. Phys.: Condens. Matter 10 (1998) 2617 [6] R. Lorenz and J. Hafner, J. Mag. Mag. Mat. 139 (1995) 209

# Very short C-H···O hydrogen bonds in phosphonium aryloxides


- M.G. Davidson (University of Bath)
- C.K. Broder, A.E. Goeta and J. A. K Howard (University of Durham)
- V. T. Forsyth and S.A. Mason (ILL)


**We have characterised a series of three phosphonium aryloxides by single crystal neutron diffraction on D19. Definitive location of the hydrogen atoms reveals uniquely short C-H···O hydrogen bonds. Using neutron diffraction we have been able to address fundamental questions concerning the bonding in these interactions. The three structures can be rationalised in terms of a common supramolecular synthon which may have significance for future crystal engineering applications.**

Conventional 'strong' hydrogen bonds (e.g., O-H···O, N-H···O, etc.) are recognised to be of fundamental importance in determining the supramolecular structure of organic solids [1]. Among the many roles played by strong hydrogen bonds in structural chemistry and biology, one area of intensive research is their use to control supramolecular structure in crystal engineering [2]. In contrast, 'weak' hydrogen bonds (e.g., C-H···O and C-H···π, etc.) have not been exploited in crystal engineering to the same extent even though they have been shown to be capable of exerting a profound influence on supramolecular structure [2]. Indeed, until relatively recently, even their existence was still being seriously questioned [3]. In this contribution we investigate the nature of very short C-H···O hydrogen bonds and consider whether they are useful as tools for crystal engineering.

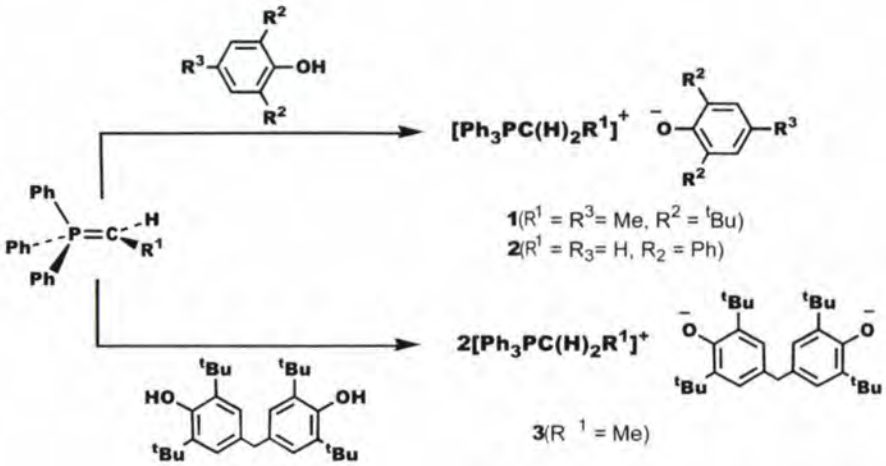


Figure 1: The Synthesis of 1-3.

We have recently described the synthesis of a range of organic phosphonium salts which contain extensive C-H···X interactions (where X = O, N, P or π) in the solid state [4]. In order to gain insight into both the fundamental nature of C-H···O hydrogen bonds themselves and their potential utility in crystal engineering we have now undertaken single crystal neutron diffraction studies of three phosphonium aryloxides (**1-3**, Fig. 1) using the D19 single-crystal diffractometer at the ILL. Due to their sensitivity to air and moisture, all crystals were mounted under an inert argon atmosphere which was maintained using thin-walled quartz domes during data collection at 20 K.

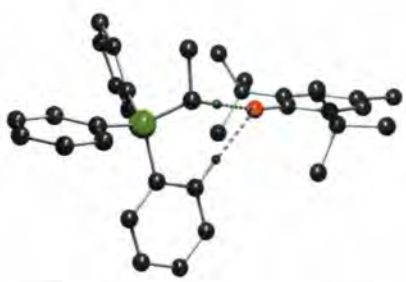

Figure 2: Single crystal neutron structure of **1** (carbon, hydrogen, oxygen and phosphorus shown in grey, dark green, red and green, respectively).

The structure of **1** [5] (Figs. 2 and 3(a)) is monomeric with interactions between cations and anion mediated via two C-H···O interactions, one from an alkyl C-H group and the other from an aryl C-H group. The structural parameters of the C-H···O interactions in **1** have all been accurately determined and the distances are at the lower limit of those found previously for C-H···O hydrogen bonds.

By reducing the steric bulk of both the cation and anion we were able to obtain the dimeric structure found in **2** [5] (Figs. 4 and 3(b)). Here, each phosphonium cation partakes in the same alkyl/aryl chelation as was seen in **1** but also hydrogen bonds to a second anion via an alkyl C-H donor. This generates the puckered eight-membered $(\cdots H\text{-}C\text{-}H\cdots O)_2$ ring shown in Fig. 5. The C-H···O hydrogen bonds within this ring are to our knowledge the shortest yet determined by neutron diffraction, being up to 5% shorter than any others found in the Cambridge Structural Database.

Accurate location and refinement of the hydrogen atoms has allowed us to address fundamental questions concerning the nature of the bonding in these very short interactions. Firstly, unlike strong hydrogen bonds which can be partially covalent, even these very short C-H···O interactions appear to be purely electrostatic in nature. There is no significant increase in the C-H bond lengths nor is there any distortion of the hydrogen atom

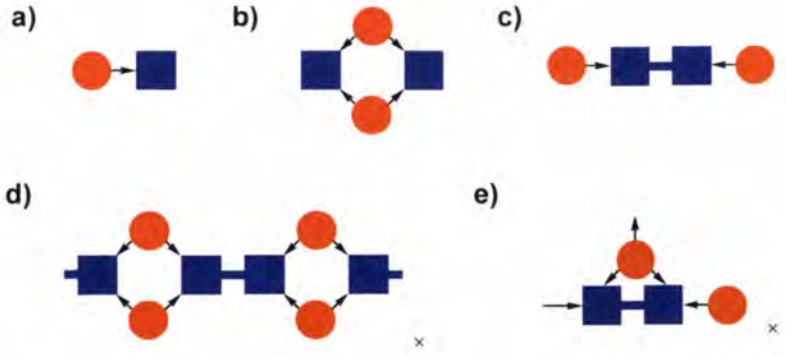


Figure 3: Cartoons of C–H···O hydrogen bonded phosphonium salts (cations, anions and hydrogen bonds shown as red circles, blue squares and arrows, respectively).

anisotropic displacement parameters along the C–H bond vectors (Fig. 5). Any covalent contribution to the bonding would be manifested in one or both of these effects. Secondly, the neutron data provides unequivocal evidence that there is no disorder of the hydrogen atom position between the two possible forms (C–H···O, ionic, or C···H–O, neutral) which might be expected by analogy with very short O–H···O systems.

Because the structures of **1** and **2** contain the same structural feature of alkyl/aryl C–H chelation of an O atom (Figs. 3(a) and (b)) we were interested in the possibility of utilising this motif as a so-called supramolecular synthon [2] in the design of more complex supramolecular structures. By analogy with compounds **1** and **2** we expected that the structure of a bisaryloxide salt would conform to one of two structures depicted in Figs. 3(c) and 3(d). In fact, the actual structure of **3** (Fig. 6) is not so simple [6]. The synthon found in **1** and **2** is reproduced but only for one of the cation-anion interactions. The second cation

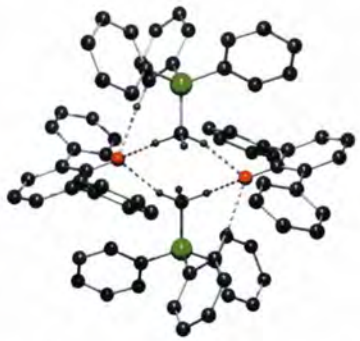

Figure 4: Single crystal neutron structure of **2** (carbon, hydrogen, oxygen and phosphorus shown in grey, dark green, red and green, respectively).

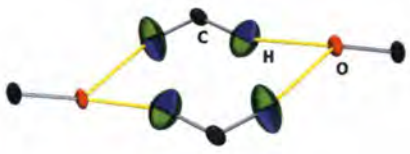


Figure 5: Detail of the $(H{-}C{\cdots}H{\cdots}O)_2$ ring in **2** (all anisotropic displacement parameters drawn at the 80% probability level; hydrogen bonds shown in yellow).

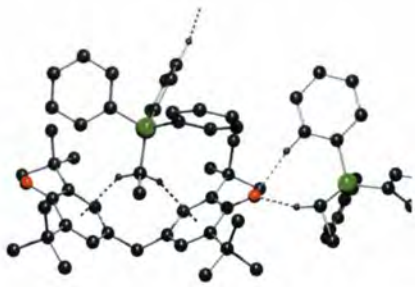

Figure 6: Single crystal neutron structure of **3** (carbon, hydrogen, oxygen and phosphorus shown in grey, dark green, red and green, respectively).

interacts with two dianions in a previously unobserved manner via two C-H···π and one C-H···O interactions thus generating the unpredicted polymeric supramolecular structure shown in Figs. 6 and 3(e).

In conclusion, we have been able to fully characterise a series of three C-H···O and C-H···π hydrogen bonded phosphonium aryloxides by single crystal neutron diffraction including the shortest interaction known to date. By accurate location and anisotropic refinement of the hydrogen atoms we have shown that these uniquely short interactions are consistent with a 'normal' electrostatic bonding model for weak hydrogen bonds. All three supramolecular structures possess the same supramolecular synthon which may be applicable for use in crystal engineering although, consistent with the relative weakness of the interactions, precise control of structure may be problematic.

## References


● [1] G.A. Jeffrey, An Introduction to Hydrogen Bonding, Oxford University Press Inc, USA (1997) ● [2] G.R. Desiraju, Angew. Chem. Int. Ed. Engl., 34 (1995) 2311 ● [3] G.R. Desiraju and T. Steiner, The Weak Hydrogen Bond: In Structural Chemistry and Biology, Oxford University Press, Oxford (1999) ● [4] M.G. Davidson, K.B. Dillon, J.A.K. Howard, S. Lamb and M.D. Roden, J. Organomet. Chem., 550 (1998) 481; M.G. Davidson and S. Lamb, Polyhedron, 16 (1997) 4393; M.G. Davidson, Chem. Commun. (1995) 919 ● [5] M.G. Davidson, A.E. Goeta, J.A.K. Howard, S. Lamb, S.A. Mason, New J. Chem 24, 477-479 (2000). ● [6] C.K. Broder, M.G. Davidson, V.T. Forsyth, J.A.K. Howard, S. Lamb and S.A. Mason, J. Am. Chem. soc. (submitted for publication)

# **Hydrogen fluoride:** a model system for the understanding of the hydrogen bond


- T. Pfleiderer, I. Waldner, H.Bertagnolli (University of Stuttgart)
- K. Tödheide (University of Karlsruhe)
- H. E. Fischer (ILL & Université Paris-Sud, Orsay)


**In view of its high importance as a model system for hydrogen bonds, we performed high pressure neutron diffraction experiments on the very corrosive and toxic hydrogen fluoride. Using neutrons from the hot source at D4B we were able to determine its microscopic structure and thereby the temperature dependence as well as density dependence of hydrogen bonds over a broad range of thermodynamic states [1].**

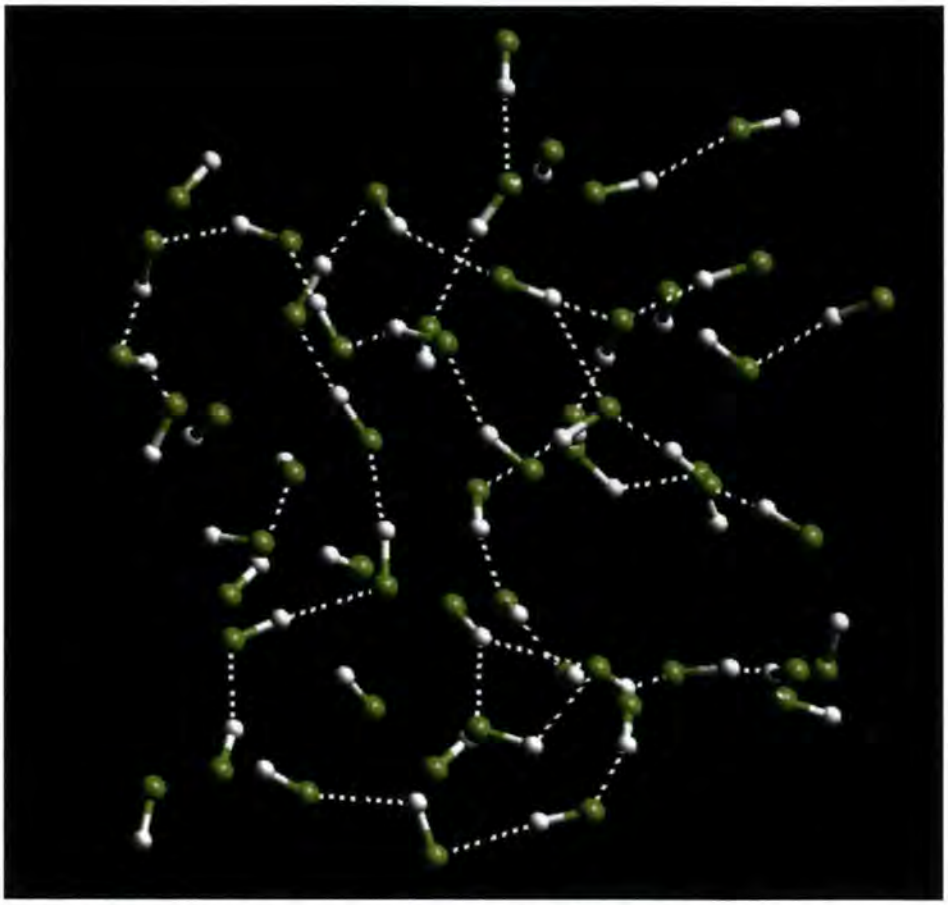

Figure 1: Snapshot of the ab initio molecular dynamic simulation of hydrogen fluoride at ambient conditions.

During the past decades the importance of hydrogen bonds with respect to the structure, intra- as well as intermolecular, has become more and more obvious. These bonds determine the structure of water, alcohols and also the conformation of macromolecules, e.g. bio-organic molecules. Therefore, investigations on hydrogen bonds are of great interest for many physical and chemical disciplines. Hydrogen fluoride has become a popular model system for hydrogen bonds because of the strong influence of hydrogen bonds on its properties - in fact hydrogen fluoride forms the strongest hydrogen bonds known - and because of its low complexity in comparison to alternative systems, e. g. water with two hydrogen bonds per molecule.

Structural data of hydrogen fluoride are the ideal experimental reference for theoretical investigations and computer simulations, but surprisingly little is known about the structure of liquid and gaseous hydrogen fluoride. In the solid state, hydrogen fluoride forms (HF)n chains, as determined by x-ray [2] and neutron diffraction [3] studies. A great number of investigations clearly reveal the presence of $(HF)_n$ chains in the liquid, too. This is also supported by the only elastic diffraction study on liquid hydrogen fluoride. In 1985, Deraman et al. [4] determined the structure factor of liquid deuterated hydrogen fluoride (deuterium fluoride) at ambient conditions using the diffractometer D4B at ILL. Undoubtedly, the liquid hydrogen fluoride consists of a network of winding chains. But a more detailed description was not accessible by these experimental studies.

The knowledge of the structure of gaseous hydrogen fluoride is also restricted. Some progress was provided by IR spectroscopy in synchronised pulse supersonic jet expansions by Suhm [5]. Indications of $(HF)_{4-7}$ clusters were found together with a great amount of monomers and dimers. But the reliability of the structural data for these clusters, and for their temperature and density dependencies, is debated.

In addition, many theoretical investigations and computer simulations have been carried out to depict the properties of hydrogen fluoride. In general, good agreement with thermodynamic results has been obtained by classical simulations using different potential models for the description of the hydrogen bonds. But for all these models the structure turns out to be rather different. The situation

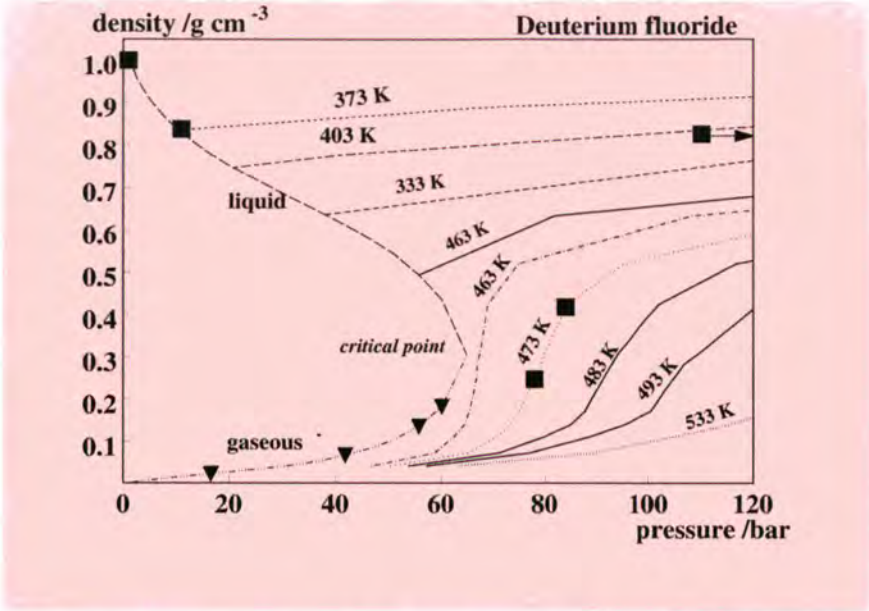


Figure 2: Density as a function of pressure for deuterium fluoride: (■) performed, (▼) planned experiments.

was aggravated by the fact that the question as to which model describes the structural properties of liquid hydrogen fluoride best, relied on the comparison with the structural data of Deraman et al. [4] at only *one* thermodynamic state. A step forward was made by ab initio molecular dynamic simulations on liquid hydrogen fluoride at ambient conditions [6]. In Fig. 1 a snapshot of the liquid structure during a repetition of this simulation is depicted. The winding chains are clearly visible. The results of the simulation are supported by the good agreement between the total atom pair correlation function G(r) deduced from the simulation and the one determined by Deraman et al. [4]. Further theoretical investigations and computer simulations on the structure at other thermodynamic states are still missing because of the lack of experimental structural data.

In order to extend the thermodynamic range of available data, we have undertaken high pressure neutron diffraction experiments on hydrogen fluoride. Using the diffractometer D4B, we were able to determine the total atom pair correlation functions G(r) of deuterated hydrogen fluoride (deuterium fluoride) at two liquid and four supercritical states in the temperature range of 300 – 473 K and for pressures up to 320 bar [1]. The investigated (■) states are marked in Fig. 2. The sample density is changing by a factor of 4 from liquid-like to gas-like densities.

In Fig. 3 we present the total atom pair correlation functions G(r) weighted with the number density C and the factor $4\pi r^2$, i.e. radial distribution functions. As the area under the first maximum is directly related to the average number of hydrogen bonds per deuterium fluoride (DF) molecule, these function give a quantitative impression of the changes in the hydrogen bonds. The left part of figure 3 illustrates the temperature dependence in the range from 300 - 473 K and the right part the density dependence in the supercritical region at 473 K. Both dependencies are mainly described by a strong decrease of hydrogen bonds per molecule, whereas only the variation of temperature affects the shape of the functions in the depicted distance range.

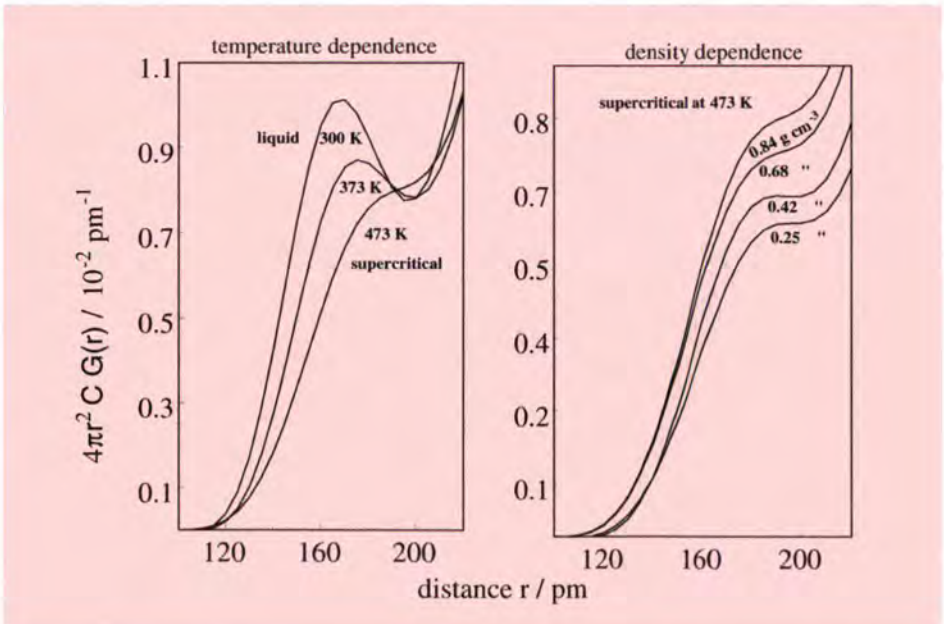


Figure 3: The weighted atom pair correlation functions of deuterium fluoride in the distances range of the hydrogen bonds.

Together with the planned experiments on the saturated vapour at D4C, which are marked in Fig. 2 as (▼), these measurements represent the first comprehensive study of the structure of hydrogen fluoride from the liquid through the supercritical region to the vapour phase and thereby provide detailed information on how the structure changes from a chain-like arrangement in the liquid phase to small clusters in the vapour phase. It is hoped that these structural data will help to develop improved models for hydrogen bond potentials and to verify the results of theoretical investigations and computer simulations.

## References


● [1] T. Pfleiderer, I. Waldner, H. Bertagnolli, K. Tödheide and H. Fischer, J. Chem. Phys. 113 (2000) 3690 ● [2] M. Atoji and W. N. Lipscomb, Acta Crystallogr. 7 (1954) 173 ● [3] M. W. Johnson, E. Sandor and E. Arzi, Acta Crystallogr., Sect. B: Struct. Crystallogr. Cryst. Chem. 31 (1975) 1998 ● [4] M. Deraman, J. C. Dore, J. G. Powles, J. H. Holloway, and P. Chieux, Mol. Phys. 55 (1985) 1351 ● [5] M. A. Suhm, Ber. Bunsenges. Pys. Chem. 99 (1995) 1159 ● [6] U. Röthlingsberger and M. Parrinello, J. Chem. Phys. 106 (1997) 4658

# Anomalously high temperature charge ordering in $Bi_{1/2}Sr_{1/2}MnO_3$: the role of the Bi lone pair


- J.L GARCIA-MUNOZ, C. FRONTERA, A. LLOBET (ICMAB-CSIC, BELLATERRA)
- M.A.G. ARANDA, (UNIVERSITY OF MALAGA)
- C. RITTER (ILL)



**The discovery of 'colossal' magnetoresistance, CMR, in $Ln_{1-x}M_xMnO_3$ manganites (Ln = trivalent lanthanide, M = Ca, Sr, Ba) has led to an explosion of interest in the tendency displayed by many of these compounds to form nanoscopic inhomogeneous states: electronic phase separation and charge-ordering (CO) phenomena. CO is a fascinating phenomenon in metal oxides with important implications in the CMR of manganese perovskites and in the high-temperature superconductivity of copper oxides [1,2]. Using temperature dependent neutron and synchrotron diffraction a spectacular high orbital/charge ordering temperature, $T_{CO}$ = 475 K, was found in $Bi_{1/2}Sr_{1/2}MnO_3$. The charges order approximately 325 K above the temperature predicted by the bandwidth tuning mechanism for the $Ln_{1/2}(Ca; Sr)_{1/2}$ $MnO_3$ family. The results point to the conclusion that a $6s^2$ character of the $Bi^{3+}$ lone pair favours markedly a charge ordering.**


The stability of charge-ordered states is determined by the Coulomb repulsion between charges and the elastic energy from the lattice deformations associated with the orbital ordering (Jahn-Teller distortion of the octahedra occupied by $e_g$ electrons) [3]. The bandwidth tuning mechanism has been widely used to quantitatively justify the $T_{CO}$ variation in the $Ln_{1/2}M_{1/2}MnO_3$ family of compounds [4]. Wide $e_g$ bandwidths and large mean size of the A-site cations $<R_A>$ favor the mobility of the itinerant electrons through the lattice decreasing thereby $T_{CO}$, while narrow bandwidths reduce this mobility, increasing $T_{CO}$. The bandwidth itself can be approximately determined from the tilting of the $MnO_6$ octahedra which is reflected in the average bonding angle <Mn –O –Mn>.

First strong indications for the presence of CO in $Bi_{1/2}Sr_{1/2}MnO_3$ at high temperatures were seen in susceptibility data, which revealed a transition at 475 K. High resolution neutron powder diffraction were performed at the ILL on D2B at 1.5 K and 300 K on $Bi_{1/2}Sr_{1/2}MnO_3$ and $Bi_{1/2}Ca_{1/2}MnO_3$ [5].

The Sr compound was as well measured between 400 K and 560 K with high resolution on D1A. Three different signatures seen in diffraction studies are typical for the evolution of a charge-ordered state: 1) a lattice deformation comprising the expansion of the *a* and *b* cell parameters and the contraction of the c cell parameter using the normal *Pbnm* space group setting, 2) the formation of small superlattice peaks originating from the larger unit cell necessary to describe the structural modulation induced by CO 3) the formation of a CE-type magnetic ordering at low temperatures.

The lattice deformation and the formation of the CE magnetic order were clearly seen in neutron diffraction data. In order to check for the presence of superlattice reflections we benefited from the complementarity of synchrotron powder x-ray diffraction available at the ESRF: Fig. 1 shows these extremely small extra peaks as measured on BM16; they can be indexed by doubling the cell along b. The temperature dependence of the superlattice peaks as well as the evolution of the cell parameters indicated $T_{CO}$ to be at about 480 K. The high resolution diffraction data also showed that the sample actually splits into 2 macroscopic phases with slightly different lattice parameters when cooled below $T_{CO}$. The neutron data have confirmed that the two phases present different magnetic structures at low temperatures. The q = 2b* modulated mainphase (70%) orders antiferromagnetically with the CE type magnetic structure while the minority phase (30%) adopts the antiferromagnetic A-type structure.

Macroscopic phase separation is commonly observed in samples with even very small compositional fluctuations as the CE and A type phases have very similar energies [6].

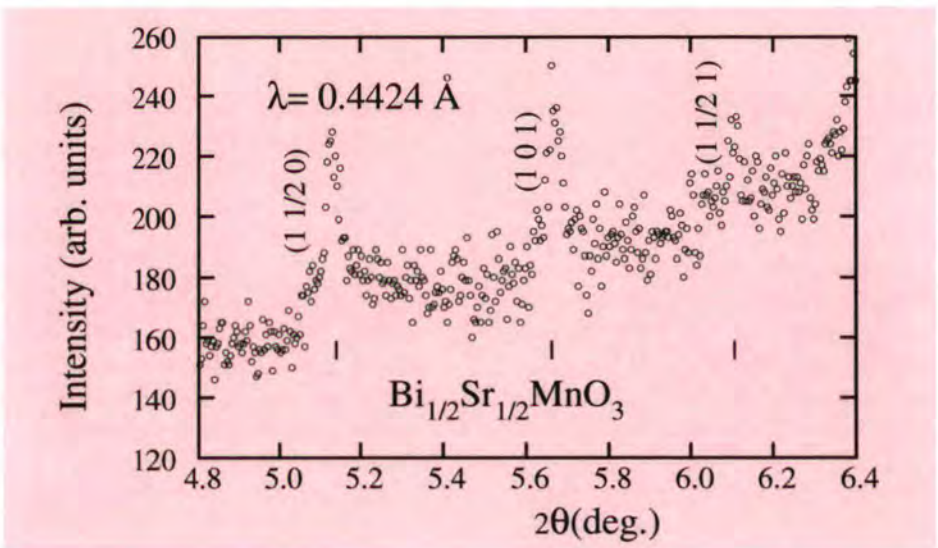


Figure 1: (1 1/2 0) and (1 1/2 1) superlattice peaks of $Bi_{1/2}Sr_{1/2}MnO_3$.

Although $Bi^{3+}$ and $La^{3+}$ have similar radii in many oxides, replacement of La by Bi leads to an increase of the average Mn-O-Mn distortion. The striking behavior of the $Bi_{1/2}Sr_{1/2}$ compound becomes clear comparing it to the $Bi_{1/2}Ca_{1/2}$ compound: As expected the average Mn-O-Mn distortion is more pronounced in the Ca-compound, however, $T_{CO}(Bi_{1/2}Sr_{1/2}) >> T_{CO}(Bi_{1/2}Ca_{1/2})$. According to the classical bandwidth tuning approach for the evolution of $T_{CO}$ as a function of the tilting of the octahedra in the $Ln_{1/2}M_{1/2}MnO_3$ series, $T_{CO}$ for $Bi_{1/2}Sr_{1/2}MnO_3$ is expected at about 150 K, more than three times lower than the measured value (Fig. 2). It is clear that the extraordinarily high CO transition temperature of 475 K observed in $Bi_{1/2}Sr_{1/2}$, which is unprecedented in Ln-Mn-O manganites, cannot be explained by considering only the average buckling of the Mn-O-Mn bonds. Obviously, an A-site mismatch effect cannot explain such a high $T_{CO}$ as the A-size variance is larger for $Bi_{1/2}Sr_{1/2}$ than for $Bi_{1/2}Ca_{1/2}$ which should lead to even a lower $T_{CO}$ for $Bi_{1/2}Sr_{1/2}$. So why do the Sr and the Ca oxides behave so differently?

Indeed, our data suggest that the lone pair of $Bi^{3+}$ plays a role in these apparently contradictory observations. In Fig. 3 the unit cell volumes of $Ln_{1/2}M_{1/2}MnO_3$ (M = Ca, Sr) compounds at RT are plotted versus the ionic radii $\langle R_{(Ln,M)}\rangle = 1/2(\langle R_{Ln}\rangle + \langle R_M\rangle)$.

Here we have to recall that the effective ionic radius of $Bi^{3+}$ depends on the character of the $6s^2$ lone pair. In most Bi oxides $\langle R_{Bi}\rangle$ = 1.24 Å when the lone pair character is dominant or $\langle R_{Bi}\rangle$ = 1.16 Å when the lone pair character is constrained. Both possibilities have been considered in Fig. 3 for $Bi_{1/2}Sr_{1/2}$ and $Bi_{1/2}Ca_{1/2}$. It is apparent from this figure that the two compounds behave differently: the volume of $Bi_{1/2}Sr_{1/2}$ matches well the dependence of Sr half-doped manganites assuming dominant $6s^2$ character ($\langle R_{Bi}\rangle$ = 1.24 Å). However, the volume of $Bi_{1/2}Sr_{1/2}$ follows the linear trend of the $Ln_{1/2}Ca_{1/2}$ series only if the $6s^2$ character is constrained ($\langle R_{Bi}\rangle$ = 1.16 Å).

The average interatomic distances, found to be (Bi,Sr)-O = 2.67 Å (expected for $\langle R_{Bi}\rangle$ = 1.24 Å: 2.675 Å) and (Bi,Ca)-O = 2.57 Å (expected for $\langle R_{Bi}\rangle$ = 1.16 Å: 2.57 Å), also point to the same interpretation. Hence, diffraction data suggest that the $Bi^{3+}$ lone pair is strongly screened in $Bi_{1/2}Ca_{1/2}$ (marked p-character at the A site) with a preferred orientation far from the Bi-O bonds. Conversely, the $6s^2$ lone pair character is dominant in $Bi_{1/2}Sr_{1/2}$ increasing the electron density along some Bi-O bonds resulting in an effective bigger $Bi^{3+}$ ionic size. Assuming a partial hybridisation of the lone pair electrons with some O:2p orbitals participating in the $e_g(Mn)$ - $2p^*\sigma O$) - $e_g(Mn)$ chemical bond, an important reduction of the mobility of the carriers would take place leading to the charge ordering at extraordinarily high temperatures. It is notable that this new mechanism is strongly inhibited in $Bi_{1/2}Ca_{1/2}$, suggesting the possibility that it can be sterically controlled/activated by pressure in selected oxides (e.g. the $Bi_{1/2}(Ca;Sr)_{1/2}MnO_{1/3}$ series).

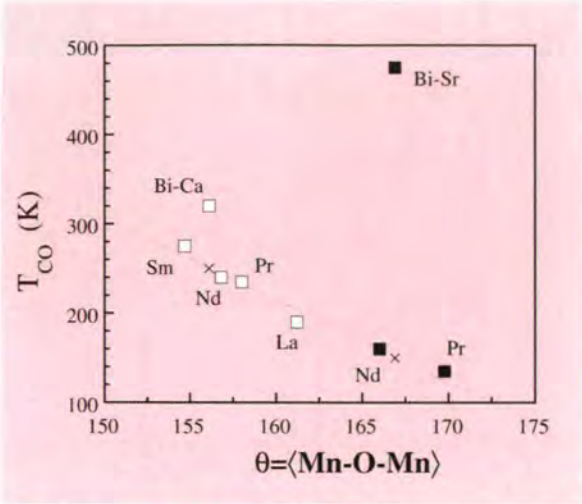


Figure 2: Dependence of $T_{CO}$ for $Ln_{1/2}M_{1/2}MnO_3$ (M = Ca, open squares, and Sr, solid squares) on the average Mn – O – Mn bending angle. Crosses indicate the values of $T_{CO}$ for $Bi_{1/2}Ca_{1/2}MnO_3$ and $Bi_{1/2}Sr_{1/2}MnO_3$ estimated from the bandwidth tuning mechanism.

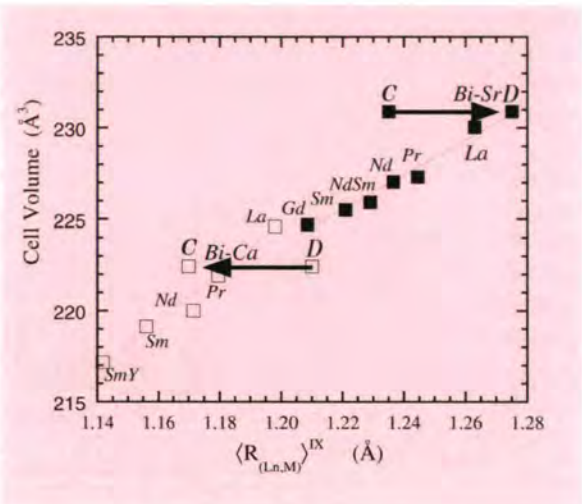


Figure 3: Unit cell volume of $Ln_{1/2}M_{1/2}MnO_3$ compounds (M = Ca, open squares, and Sr, solid squares) at RT versus the A-site radius. As explained in the text, the two possible ionic radii for $Bi^{3+}$ are considered corresponding to dominant (**D**) and constrained (**C**) lone-pair character.


**References**

● [1] C.N. R. Rao and A.K. Cheetham, Adv. Mater. 9 (1997) 1009 ● [2] J.M. Tranquada, B.J. Sternlieb, J.D. Axe, Y. Nakamura and S. Uchida, Nature 375 (1995) 561 ● [3] J.P. Attfield, A.M.T. Bell, L.M. Rodriguez-Martinez, L.M. Greneche, R.J. Cerniks, J.F. Clarke and D.A. Perkins, Nature 396 (1998) 655 ● [4] J. Fontcuberta, B. Martinez, A. Seffar, S. Pinol, J.L. Garcia-Munoz and X. Obradors, Phys. Rev. Lett. 76 (1996) 1122 ● [5] J.L. Garcia-Munoz, C. Frontera, M.A.G. Aranda, A. Llobet and C. Ritter, Phys. Rev. B 63 (2001) 064415 ● [6] C. Ritter, R. Mahendiran, M.R. Ibarra, L. Morellon, A. Maignan, B. Raveau and C.N.R. Rao, Phys. Rev. B 61 (2000) R9229

# Crystal structure of new fast oxide-ion conductor $La_2Mo_2O_9$ leads to novel design concept


- P. Lacorre, F. Goutenoire (University of Le Mans)
- O. Isnard (CNRS Grenoble)
- E. Suard (ILL)



**We have used neutron powder diffraction to study the structural arrangement of a recently discovered new family of fast oxide-ion conductors. The parent compound of this family is lanthanum molybdate $La_2Mo_2O_9$, whose oxide-ion conduction above 600°C is comparable to or slightly higher than that of stabilised zirconia. The structural arrangement of $La_2Mo_2O_9$ is close to that of $\beta SnWO_4$, where divalent tin has an electronic lone pair. This structural similarity enabled us to explain the origin of anion conduction in $La_2Mo_2O_9$, and to propose an original concept to design new families of fast oxide-ion conductors, based on lone pair substitution.**


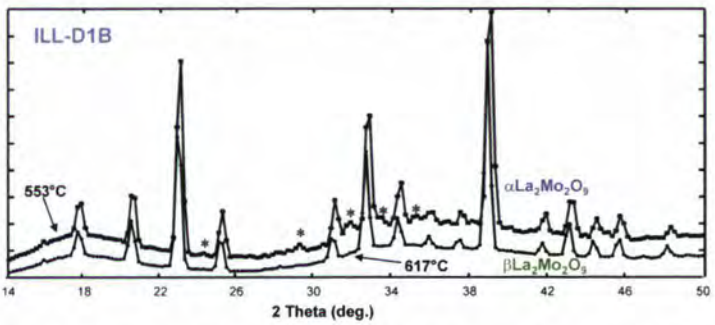


Figure 1: Neutron diffraction patterns of $La_2Mo_2O_9$ collected below (533°C) and above (617°C) the phase transition (D1B, $\lambda$=1.28Å). The stars point out the small superstructure peaks of $\alpha$ $La_2Mo_2O_9$.

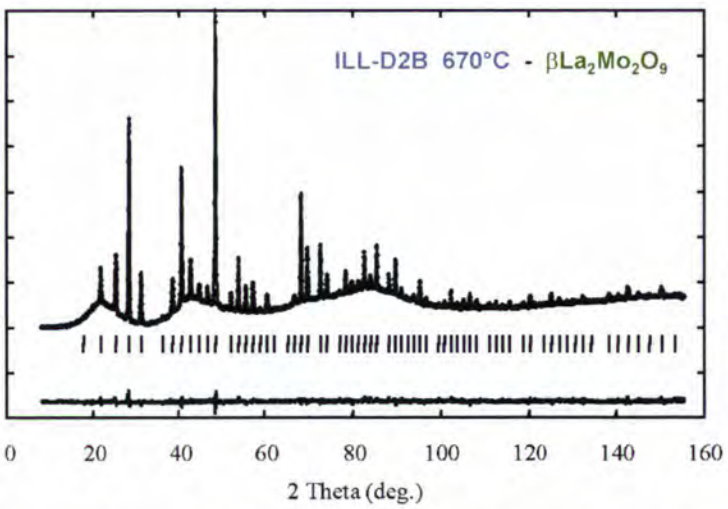


Figure 2: D2B neutron diffraction pattern fit of the crystal structure of $\beta$ $La_2Mo_2O_9$ at 670°C. Note the strong decrease of diffracted intensities with the diffraction angle, due to large oxygen thermal factors (the modulated background is in this case due to the diffusion from the glass container).

Fast oxide-ion conductors form a class of materials which are widely sought for and studied since they can be used in many different applications. They include Solid Oxide Fuel Cells (SOFC) as low-polluting power generation systems, oxygen sensors for electronic fuel injection systems in car motors, or oxygen pumping devices to separate nitrogen from oxygen in air, for instance [1]. The most famous and widely used material of that kind is probably stabilised zirconia, with an oxygen-deficient fluorine-type structure. Other oxide-ion conductors belong to different, scarce, structural types, such as deficient-perovskites, intergrowth perovskite/$Bi_2O_2$ Aurivilius type phases, or pyrochlores. Research directions in the field have focussed on improving the properties of already known compounds or on finding new families with the main goal to lower the temperature range within which such materials can be efficiently used (usually above 700-800°C).

Recently, some of us have investigated a new family of fast oxide-ion conductors based on parent compound $La_2Mo_2O_9$ [2]. This compound has been known for thirty years, but neither its structure nor its conducting properties. We have shown that it undergoes a reversible phase transition around 580°C from a slightly distorted low temperature $\alpha$ phase to a cubic high temperature $\beta$ phase. There is an abrupt jump in conductivity of almost two orders of magnitude at the transition toward the high T phase, the oxide-ion conduction being around 6 $10^{-2}$ $S.cm^{-1}$ at 800°C, slightly higher than that of usual stabilised zirconia. Electron and neutron diffraction show superstructure reflections in the low temperature phase, most probably due to an oxygen/vacancy ordering (see Fig. 1), as usually encountered in this type of materials. Neutron diffraction experiments were conducted on D2B and D1B at the ILL. The neutron diffraction patterns show an important decrease of the diffracted intensities with

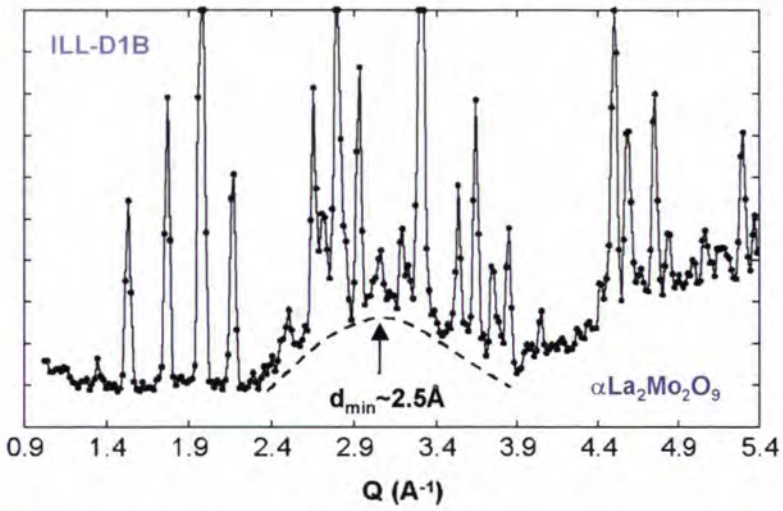


Figure 3: Detail of the neutron diffraction pattern of $La_2Mo_2O_9$ at room temperature versus $Q=4\pi \sin\theta/\lambda$, showing a large diffusion peak around 2.31 $Å^{-1}$ (due to short range order with pair distances around 2.5 Å). Note that here, the container contribution to the background is negligible (vanadium container).

the diffraction angle (Fig. 2), an indication of the large thermal factors of oxygen atoms due to delocalisation. Another signature of oxygen diffusion can be found in the modulation of the neutron diffraction background, with a first maximum around Q = 3.1 $Å^{-1}$ (see Fig. 3). According to the Debye formula, which can be used to express the contribution of static structural disorder in diffuse elastic scattering, the first marked maximum appears at $Q_{max}=(2\pi x1.23)/d_m$, where $d_m$ is a preferred atomic pair distance [3]. When applied to our data, such a formula gives a preferred pair distance around 2.5 Å, which is characteristic of minimal oxygen-oxygen distances. This is a good confirmation of some oxygen short range order in this compound.

Neutron diffraction allowed us to determine the crystal structure of $\beta La_2Mo_2O_9$ [4]. The cationic arrangement is close to that found in $\beta SnWO_4$ [5], as well as the location of two over the three oxygen sites (see Fig. 4). All the oxygen atoms have large anisotropic thermal factors, and three forth of them are located on sites which are 50% occupied on average. This leads to short distances between such sites, characteristic of short oxygen-vacancy distances, and thus of the most probable conduction path in the structure, which appears to be tridimensional. The most interesting and suggestive way to understand the origin of anion conduction in $\beta La_2Mo_2O_9$ is

necessary to fulfil the lanthanum valence. The lanthanum molybdate formula can thus be rewritten $La_2Mo_2O_{8+1}$, with the extra oxygen atom allowed to migrate through the vacancy [2]. Such an approach [7], called the LPS (for Lone Pair Substitution) concept can be applied to a variety of already known oxides of lone-pair elements (such as $In^+$, $Ge^{2+}$, $Sb^{3+}$, $Se^{4+}$, $I^{5+}$, among others). Substituting such elements by appropriate none-lone pair elements of similar size and identical or +1 extra charge is likely, if the structure is kept, to turn the insulating compounds into oxide-ion conductors. The large number of already known oxides of lone-pair elements ensures a significant source of parent compounds for future tests of the LPS concept. It is expected that such tests will be fruitful and will lead to new families of fast-oxide ion conductors, in order to improve the knowledge of such materials as well as their efficiency in applications such as solid oxide fuel cells.

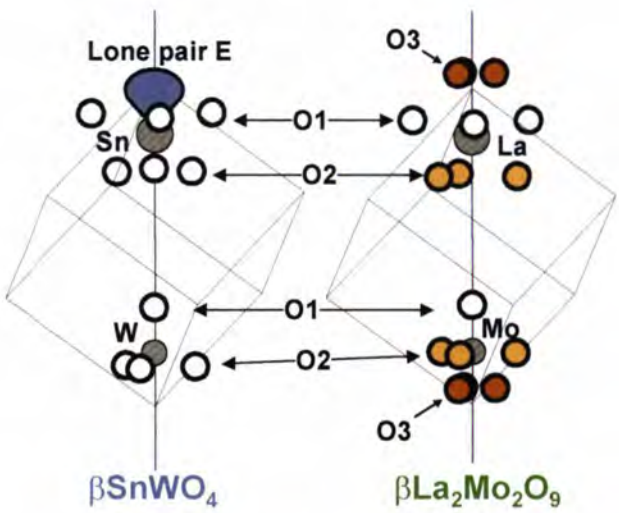


Figure 4: Cationic environments in $\beta SnWO_4$ and $\beta La_2Mo_2O_9$. For comparison purpose, the environment of La is limited to the nearest neighbours. Coloured circles indicate oxygen sites which are partially occupied.

through its structural relationship with $\beta SnWO_4$. In this last compound, divalent tin is a cation with an electronic lone pair. It is well known and documented that electronic lone pairs, whatever the electronic shell, have a spatial extension close to that of an oxide ion, thus distorting the ligands environment of the cation [6]. Taking into account the presence of a lone pair E in the formula of the tin tungstate leads to the formulation $SnWO_4E$, or $Sn_2W_2O_8E_2$. Substituting $2Sn^{2+}$ with lone pairs by $2La^{3+}$ without any lone pair creates two vacancies in place of the lone pairs, half of which being occupied by the extra oxygen atom


**References**

● [1] J.C. Boivin and G. Mairesse, Chem. Mater. 10 (1998) 2870 ● [2] P. Lacorre, F. Goutenoire, O. Bohnke, R. Retoux and Y. Laligant, Nature 404 (2000) 856 ● [3] R. N. Vannier, F. Abraham, G. Nowogrocki and G. Mairesse, J. Solid State Chem. 142 (1999) 294 ● [4] F. Goutenoire, O. Isnard, R. Retoux, and P. Lacorre, Chem. Mater. (2000), in press ● [5] W. Jeitschko and A.W. Sleight, Acta Cryst. B 28 (1972) 3174 ● [6] J. Galy, G. Meunier, S. Andersson, and A. Åström, J. Solid State Chem. 13 (1975) 142 ● [7] P. Lacorre, Solid State Sci. 2 (2000) 755

# Collective excitations in liquid metal alloys K-Cs: the role of the electron density

L.E. Bove, C. Petrillo, F. Sacchetti (Istituto Nazionale per la Fisica della Materia - INFM)

B. Dorner (ILL)

**We have investigated the ion dynamics of the liquid alloy $K_{52}Cs_{48}$ by measuring the dynamic structure factor of the system. Well defined collective excitations were observed up to the maximum value of wave-vector transfer of the experiment, 0.7 Å$^{-1}$.**
**We carried out a comparative analysis of the present data with those measured in liquid Rubidium and Cesium and we found that a scaling relation holds for the dispersion curves measured in all these systems.**
**The derived scaling reveals the key role of the conduction electron density in the collective dynamics of alkali metals.**

Alkali metals can be regarded as prototype systems of *simple liquid metals* and they can be described as a two-component mixture of interacting electrons and ions. Such systems have focussed interest because they offer the opportunity to address the fundamental field of static and dynamic screening phenomena in the interacting electron gas. Furthermore, the interplay between the electronic and the ionic components of the liquid metal affects the dynamic behaviour of the system. Since the pioneering experiment of Copley and Rowe on Rb[1], liquid Cs[2] and Li[3,4] have also been investigated. Collective excitations, i.e. propagating longitudinal ion density fluctuations, extending to relatively large momentum transfers, have been reported for all these systems. Evidence for a so-called *positive dispersion*, that is an enhanced group velocity of the ion density fluctuations against the sound velocity, was found by the low-$Q$ extrapolation of the measured dispersion relation in Rb[1] and Cs[2].

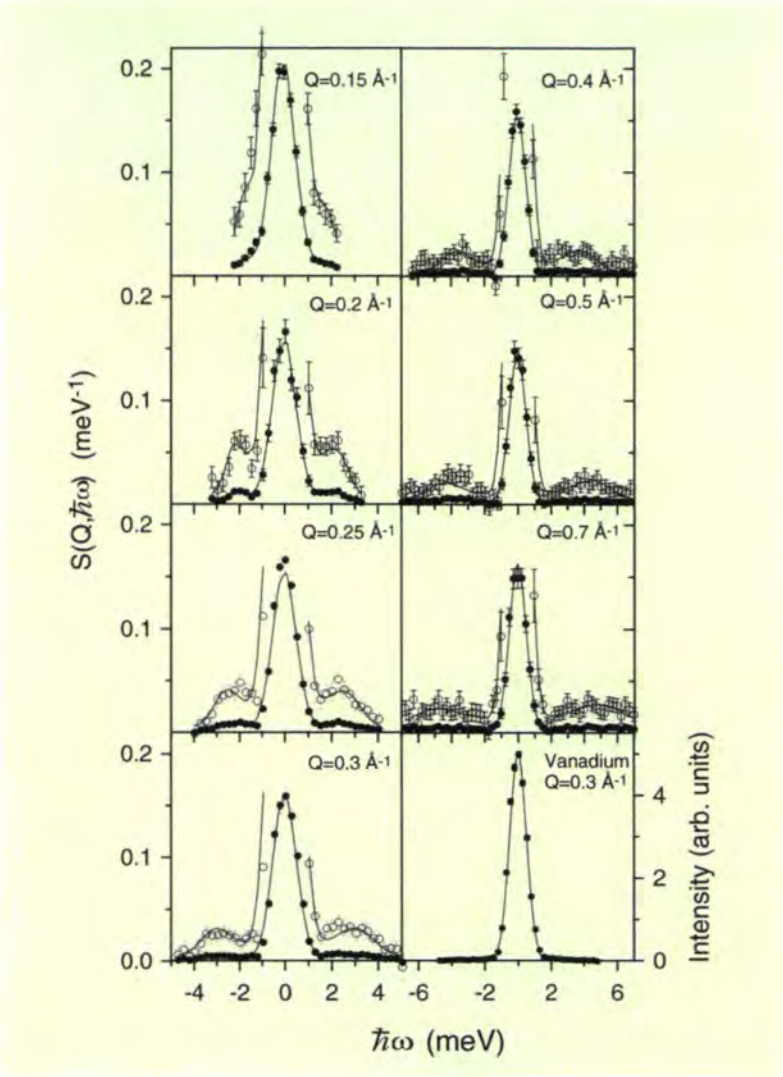


Figure 1: Coherent dynamic structure factor of $K_{52}Cs_{48}$ versus energy transfer and at the wavevector transfer values of the measurements, namely at $Q = 0.15, 0.2, 0.25, 0.3, 0.4, 0.5$ and $0.7$ Å$^{-1}$. The experimental data (dots) are also shown on a scale expanded by a factor five (circles) to emphasise the inelastic structures. The full lines are the curves calculated according to the fitted model described in the text. The intensity measured on the Vanadium standard at $Q = 0.3$ Å$^{-1}$ (dots) is compared with the calculated instrument resolution function (full line) in the bottom panel on the right.

In liquid alkali metals, experimental observations reveal that systems with different atomic mass and density, all sustain density fluctuation modes characterised by an extended dispersion relation and a rather long lifetime. Therefore, it is very tempting to interpret the characteristics of the dispersion curves and the decay of the collective density fluctuations with a model common to all the alkali metals which is based on the picture of ions mostly interacting through the Coulomb potential screened by the electron gas. An unified description where the *electron density* parameter plays a fundamental role for the

dynamic properties of the alkali metals would be quite attractive. The significance of such an approach can be established on experimental ground by studying the dynamics of liquid binary alloys of alkali metals with a composition chosen to match the electron densities appropriate to the pure metals. The alloy would then resemble the pure metal in terms of electronic density, although the mass differences, possibly present, could give rise to some dynamic features typical of an alloy.

Following this idea, we investigated the ion dynamics of the binary liquid alloy $K_{52}Cs_{48}$ which has a melting temperature of 236 K, an electron density matching that of pure Rb and an average atomic weight comparable with that of Rb within 1%. We carried out room temperature measurements at the three-axis spectrometer IN8 operated at constant analyser energy (4.1 Å$^{-1}$ final neutron wave-vector). An evacuated flight path around the sample, made it possible to collect high quality data down to 1° scattering angle.

The experimental data were reduced following the procedure described in [5]. The resulting coherent dynamic structure factors $S(Q, \omega)$ are shown in Fig. 1 as a function of the energy transfer and at the different wave-vectors. Side peaks originating from inelastic (Brillouin) scattering can be observed up to the maximum momentum transfer, thus indicating the rather slow decay of these collective density fluctuations. Moreover, the presence of an associated dispersion is evident from the low-$Q$ spectra. We analysed the spectra of Fig. 1 by decomposing $S(Q, \omega)$ into the sum of three lines, the central quasi-elastic Rayleigh line and the two inelastic Brillouin lines. The inelastic contribution was represented by means of the Random Phase Approximation to the dynamic structure factor of a simple liquid metal [6]. Further details can be found in [7]. The dispersion $\hbar\omega(Q)$ of the inelastic propagating modes, obtained from the fit to the experimental data, is shown in Fig. 2 in comparison with the data measured in liquid Rb [1].

Even though $K_{52}Cs_{48}$ and pure Rb have the same electron density and a very similar average mass, the presence of two quite different ionic masses in the alloy can have an effect on the dispersion relations. In order to understand the role of the masses, we referred to the simplified model where the liquid metal or the alloy is described by a gas of point-like ions interacting through the Coulomb potential screened by the electron gas. In a pure metal, this model results in the well known long-wavelength limit for the energy of the longitudinal collective excitations, as given by the Bohm-Staver formula [6], that is $\omega_{BS}^2(Q) = \Omega_p^2/\varepsilon(Q)$. Where $\Omega_p^2$ is the plasma frequency of the ionic gas and $\varepsilon(Q)$ is the (static) dielectric function of the homogeneous electron gas. We extended this approximation to the alloy system and found that a relationship similar to the Bohm-Staver result holds if the plasma frequency $\Omega_p$ is replaced by that of a gas of ions with the same average density as the alloy and an effective mass given by $1/M_{eff} = x_1/M_1 + x_2/M_2$ ($x_i$ being the concentration of the i-th component in the alloy). This result can be understood on intuitive grounds reminding that the frequency squared is proportional to the inverse of the mass. In the present sample the average atomic mass is 84.1 a.u., that is nearly the same as Rb (85.5 a.u.), whereas $M_{eff}$ is 59.1 a.u., that is 1.45 times smaller than that of Rb. We found that multiplying the energy of the collective excitations in pure Rb by $(1.45)^{1/2}$, the dispersion relation of Rb scales to that of the alloy. The scaled dispersion relation is also shown in Fig. 2 where the good agreement with the alloy curve is apparent.

This result shows that the interaction governing the propagation of collective modes is the (additive) Coulomb potential screened by the electron gas, with the repulsive core potential confined to a secondary role. The validity of this hypothesis can be further checked by applying the scaling procedure to the energy of the collective excitations in Rb[1], $K_{52}Cs_{48}$ and Cs[2]. Since the electron density, and hence the dielectric function, of Cs is now different from that of the two other systems, the data were scaled according to the following relationship

$$\omega(Q)_{scaled} = Q\,\omega\,(Q)\,[\varepsilon(Q)/\,\Omega^2_p]^{1/2}$$

Using the Lindhard dielectric function, evaluated in the static limit, we obtained the scaled dispersion relations that are plotted as a function of $Q/Q_0$ in Fig. 3 ($Q_0$ is the position of the first maximum of the static structure factor). A remarkable agreement is observed for the three systems including Cs with a quite different electron density. Note, that the result of a single scan on $K_{32}Cs_{68}$, scaled as explained above, coincides with the other data. We believe that the present experiments give a clear indication of the role of the electron gas in liquid alkali metals and an extended investigation of the collective excitations in these systems could help in deriving new information on the interacting electron gas [7].

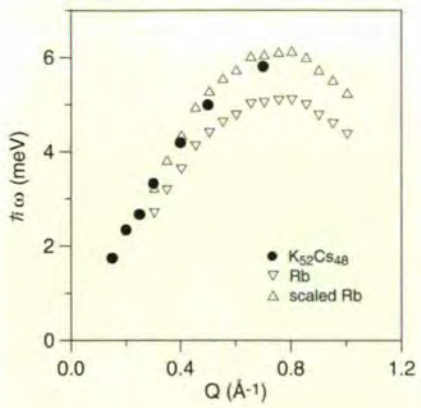


Figure 2: Dispersion relation of the collective excitations in $K_{52}Cs_{48}$ in comparison with the results of the neutron scattering experiment in pure Rb. The data of pure Rb after scaling by $\sqrt{(1.45)}$ are also shown.

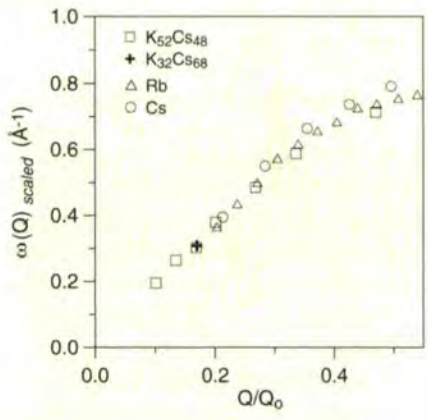


Figure 3: Dispersion relation of the collective excitations in $K_{52}Cs_{48}$, $K_{32}Cs_{68}$, pure Rb and pure Cs as scaled according to the relation described in the text and versus $Q/Q_0$.


**References**

● [1] J.R.D. Copley and J.M. Rowe, Phys. Rev. Lett. 32 (1974) 49; J.R.D. Copley and J.M. Rowe, Phys. Rev. A9 (1974) 1656 ● [2] T. Bodensteiner, Chr. Morkel, W. Glaser and B. Dorner, Phys. Rev. A45 (1992) 5709 ● [3] P.H.K. de Jong, P. Verkerk and L.A. de Graaf, J. Non-Cryst. Solids 156-158 ● [4] H. Sinn et al., Phys. Rev. Lett. 78 (1997) 1715; T. Scopigno et al., J. Phys.: Condens. Matter 12 (2000) 8009 ● [5] C. Petrillo, F. Sacchetti, B. Dorner and J.-B. Suck, Phys. Rev. E62 (2000) 3611 ● [6] N.H. March, Liquid Metals (Cambridge University Press, 1990) ● [7] L.E. Bove, F. Sacchetti, C. Petrillo and B. Dorner, Phys. Rev. Lett. 85 (2000) 5352

# Diffusion in a simple liquid
## beyond Brownian motion

W.-C. Pilgrim (University of Marburg)
C. Morkel (TU München)

**The single particle motion in liquid sodium was studied by quasi-elastic neutron scattering over a wide density range along the liquid-vapour coexistence curve. The results are in excellent agreement with mode coupling theory (MCT) and with computer simulations. They all reveal a distinct universal deviation for the density dependence of the diffusion constant *D* from the expectations of simple hard sphere theory.**

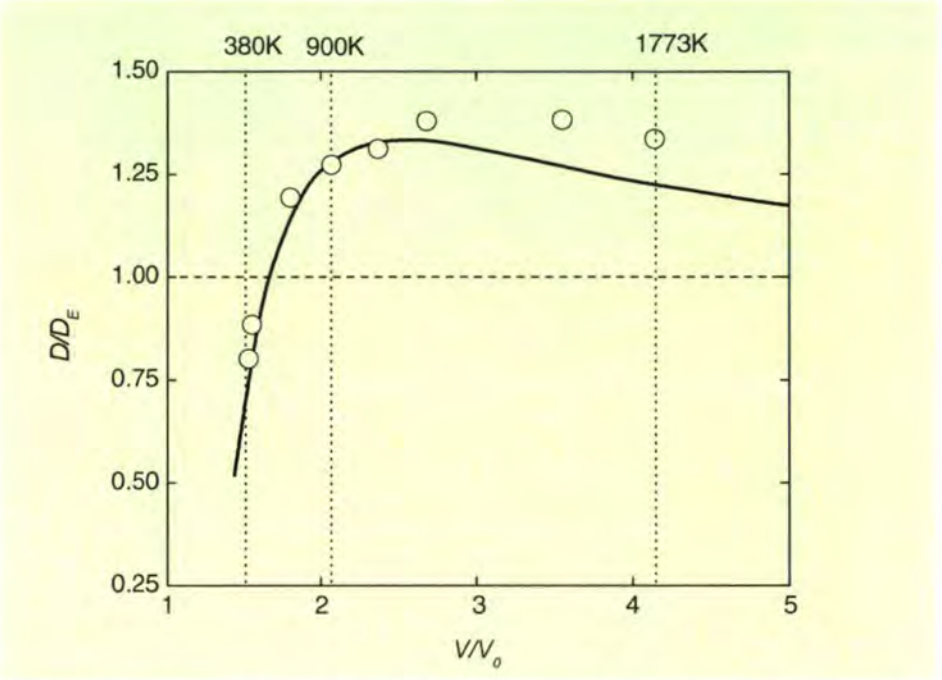


Figure 1: Reduced diffusion constant $D/D_E$ versus reduced volume $V/V_0$ ($D_E$: Enskog diffusion constant, $V_0$: volume at close packing). Circles: experimental results; solid line: computer simulations (based on hard spheres).

Since the earliest studies on diffusion by R. Brown in 1827, single particle motion in liquids has always been of particular interest as the knowledge on the behaviour of single particles has always been viewed to provide a link between the macroscopic and microscopic properties of condensed matter.

Still today, most of the experimental results are interpreted in terms of rather phenomenological models. Among these, the Enskog theory [1] describes the dynamics of a single particle in an assembly of hard spheres by means of two particle collisions. However, computer simulations [2], carried out already more than 30 years ago, showed that the density dependence of the diffusion constant for a system of hard spheres deviates considerably from the predictions of the simple Enskog picture. This is illustrated by the solid line in Fig. 1 [3] where the ratio $D/D_E$ of the actual diffusion constant to the expected Enskog value is shown as a function of volume, normalized to closed packing ($V/V_0 = \sqrt{2}/n.\sigma^3$). If the simple Enskog theory would apply, $D/D_E$ should be equal to one for all volumes (dashed line). However, Fig. 1 shows that even in a simple hard sphere system, mechanisms exist which suppress the forward motion of the particles at high densities but support it at lower densities. During the last 20 years, progress has been made towards a more quantitative understanding of the underlying processes [4,5] by introducing a coupling between diffusive motion and collective density fluctuations. Our experimental results support this view and allow to draw a comprehensive picture of the single particle motion along the whole density range of the liquid.

Since the behaviour of liquid alkali metals was often approximated by employing hard sphere models the choice of liquid sodium as the object of investigation appeared to be near at hand. Additionally, the diffusion constant can be determined in an inelastic scattering experiment from the incoherent contribution to $S(Q,\omega)$ and sodium has the largest incoherent scattering cross section among the alkalis ($\sigma_i$=1.62 barn). It can be easily shown (see e.g. [6]) that in the limit $q \rightarrow 0$ the incoherent scattering law $S_s(Q,\omega)$ is a Lorentzian with halfwidth, $\omega_{1/2} = D \cdot Q^2$, indicating classical Brownian diffusion. However, with increasing $q$, the line shape changes and the classical description no longer holds. A useful quantity which describes this departure is the reduced halfwidth $\gamma(Q) = \omega_{1/2}^{exp} / D.Q^2$ given by the ratio of the experimental halfwidth to the classical value.

Thus $\gamma(Q) \neq 1$ indicates deviations from ordinary Brownian motion which must set in with increasing $q$ where the quasielastically scattered intensity probes the particle motion on a microscopic length scale.

In our experiments, liquid sodium was studied over nearly the entire liquid range from melting ($T_m$=371 K, $\rho_m$=0.98 g/cm³) up to temperatures as high as 1773 K ($\rho$ = 0.58 g/cm³). All experiments were performed at the best cold neutron spectrometer for the study of

quasielastic dynamics, the time-of-flight instrument IN5. For each thermodynamic state, the diffusion constant was determined from the $S_S(Q,\omega)$ spectra at low momentum transfer and an appropriate extrapolation to $Q = 0$. The experimental results are given in Fig. 1 as circles. They agree well with the computer simulation.

In Fig. 2, the deviation from classical behaviour is shown in terms of $\gamma(Q)$ for melting point conditions (*380 K*, closed circles) and for an experiment carried out close to the boiling point (*900 K*, open circles).

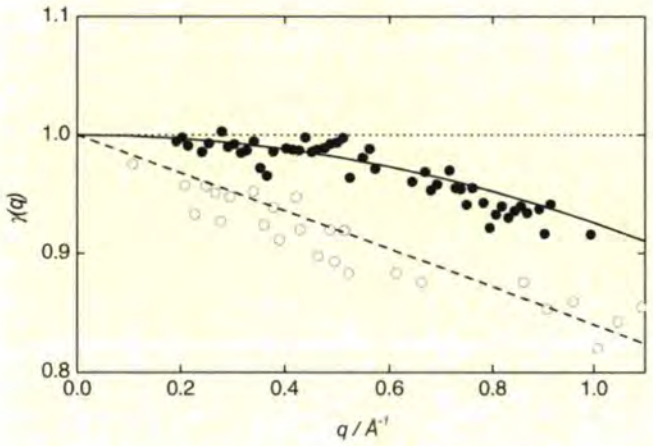


**Figure 2: Reduced halfwidth $\gamma(Q) = \omega_{1/2}^{exp}/\ D_L Q^2$ for sodium at 380 K (filled circles) and at 900 K (open circles). Solid and dashed lines represent the corresponding mode-coupling results.**

The corresponding $\gamma(Q)$s obtained from MCT (solid and dashed line) are also shown. At lower temperature, coupling between diffusive motion and longitudinal density fluctuation was considered [4] which leads to a quadratic deviation from unity for $\gamma(Q)$ (solid line in Fig. 2). This is in excellent agreement with the experimental finding. In addition, the diffusion constant obtained from the calculations is also in perfect conformity with experiment ($D_{th}$=*0.426.10⁻⁴ cm²/s*; $D_{exp}$=*0.423.10⁻⁴ cm²/s*). The agreement between experiment and theory allows to draw a clear physical picture from the MCT ansatz. The $Q$-dependence of $\gamma(Q)$ arises from slowly decaying density correlations on a next neighbouring length scale. The particle under consideration oscillates in a stable cage built by its own coordination sphere. This motion does not contribute to the forward motion. Single particle diffusion is only accomplished through a longitudinal density mode which carries the particle collectively with its immediate neighbourhood from one point to another. This mechanism hinders the diffusion process compared to the simple Enskog dynamics.

While single particle motion is hampered at high density, it is supported at lower density (see Fig.1). In this case, the corresponding MCT-ansatz combines the diffusive motion with a transverse density fluctuation [5]. Again, experimental and theoretical diffusion constants are in excellent agreement ($D_{th}$=*2.98.10⁻⁴ cm²/s*; $D_{exp}$=*2.95.10⁻⁴ cm²/s*).

The predicted Q-dependence of $\gamma(Q)$, a linear deviation from 1, is also perfectly confirmed by experiment (see dashed line in Fig. 2). The underlying physical picture can be clarified with the aid of computer simulation results [2]. Coupling to a transverse mode generates a specific velocity field around the propagating particle which enhances its forward motion, hence an increase in the diffusion constant compared to the Enskog value.

At even higher temperatures and corresponding lower density, the mode coupling effects die out and the particle dynamics becomes Enskog like. In Fig. 1 this is indicated by the asymptotic decrease of $D/D_E$ to unity with increasing volume. At very low density and high temperature the particle dynamics is controlled by repulsive interactions resulting in a simple two particle collision dynamics. However, the experiments confirm qualitatively the return to Enskog dynamics at large volumes (see Fig. 1) although this process sets in later than predicted by computer simulations.

The MCT results together with the experimental data presented here demonstrate that in a simple liquid the diffusion constant is determined by a coupling between single particle motion and collective modes. The interplay of the underlying mechanisms which are governed by a density dependent competition of mode coupling effects leads to a new understanding of single particle dynamics in simple liquids on a purely microscopic basis.


**References**

● [1] S. Chapman, T. Cowling, in "The mathematical theory of non-uniform gases", Cambridge University Press, Cambridge 1952 ● [2] B. Alder, T.E. Wainwright, Phys. Rev. A 1 (1970) 184 ● [3] J. Erpenbeck, W. Wood, Phys. Rev. A 43 (1991) 4254 ● [4] G. Wahnström, L. Sjögren, J. Phys. C 15 (1982) 401 ● [5] I.M. de Schepper, M.H. Ernst, Physica A 98 (1979) 189 ● [6] P. Egelstaff, "An introduction to the liquid state", Clarendon Press, Oxford 1994

# Origin of negative thermal expansion in cubic $ZrW_2O_8$: a high pressure neutron inelastic scattering study


- R. Mittal, S. L. Chaplot, (Bhabha Atomic Research Center, India)
- H. Schober (ILL)
- T. A. Mary (Indira Gandhi Center for Atomic Research, India)



**Isotropic negative thermal expansion (NTE) has been reported in cubic $ZrW_2O_8$ over a wide range of temperature T=0.3-1050 K. Our calculations of phonon spectra predicted a softening at P=1.5 Kbar compared to that at ambient pressure, by about 100-200 μeV for phonons of energy below 8 meV. This unusual phonon softening corresponding to negative Grüneisen parameters is able to account for the anomalous thermal expansion. We report here our recent high pressure inelastic neutron scattering experiment performed at the IN6 time-of-flight spectrometer on the cubic phase of $ZrW_2O_8$ at 160 K and pressures up to 1.7 Kbar. Excellent agreement is found with the phonon softening predicted by lattice dynamical calculations.**


An isotropic negative thermal expansion (NTE) has been reported in cubic $ZrW_2O_8$ over a wide temperature range from 0.3 to 1050 K [1]. The structure of $ZrW_2O_8$ consists of a framework of corner linked $ZrO_6$ octahedral and $WO_4$ tetrahedral units [1]. The NTE has been associated with the presence of Zr-O-W transverse vibrational modes [1] and rigid unit modes [2]. The material finds applications as a component in composites in order to reduce the overall thermal expansion near to zero. Specific heat [3] and neutron inelastic scattering measurements [4] have been reported for cubic $ZrW_2O_8$.

The neutron diffraction data show a cubic to orthorhombic phase transition at pressure around 2.1 Kbar [5]. An anomalous thermal expansion is also observed in the orthorhombic phase [5]. The Grüneisen parameters of the zone center Raman modes above 5 meV have been determined for the cubic and orthorhombic phases of $ZrW_2O_8$ [6]. We have reported earlier lattice dynamical calculations for $ZrW_2O_8$ [7] which reproduce the anomalous thermal expansion in both the cubic and the orthorhombic phases (Fig. 1). The small sharp drop in volume at about 400 K is associated with a disordering phase transition. Our calculations single out the unusually dominant contributions from the transverse acoustic, and librational and translational optic modes below 8 meV in leading to a large NTE in the cubic and orthorhombic phases. The calculations predicted that large softening of the phonon spectrum at low energies would be responsible for NTE in $ZrW_2O_8$ (Fig. 2).

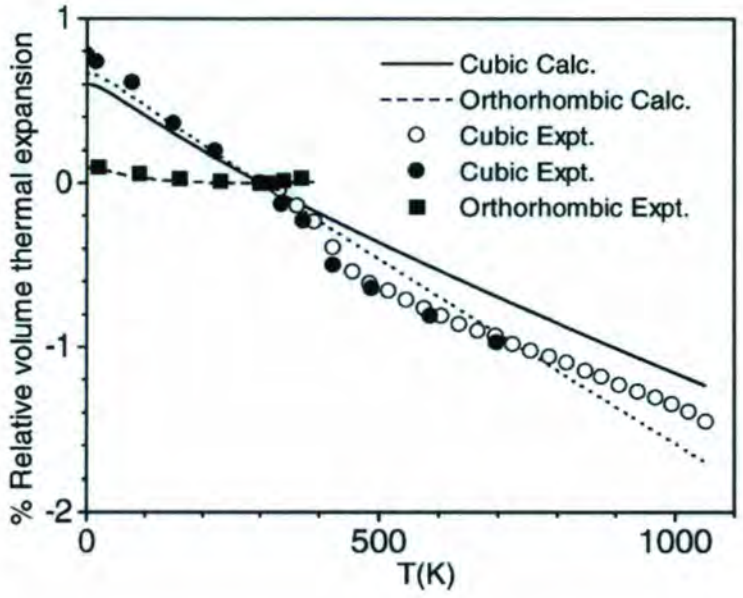


Figure 1: The comparison between the experimental and calculated percentage relative thermal expansion in the two phases, $(V_T/V_{300}-1) \times 100\%$. $V_T$ and $V_{300}$ being the cell volumes at temperature T and 300 K respectively. Experimental data: cubic [1] (solid and open circles are neutron scattering and dilatometer data respectively), orthorhombic [5] (solid squares are neutron scattering data).

In order to check our predictions of softening of phonon mode at low energies we carried out inelastic neutron scattering experiment on a polycrystalline sample of $ZrW_2O_8$ in the energy transfer range 0-10 meV at 160 K and 280 K, and pressures at 0.3 Kbar, 1.0 Kbar and 1.7 Kbar. The used incident energy at IN6 was 3.14 meV, therefore the measurements were performed in the energy gain mode. The sample was compressed using argon gas in a pressure cell available at ILL. The inelastic neutron scattering signal from argon at each pressure and temperature, and the empty cell background were also measured for correcting the signal from the sample.

The compressed argon gas and the pressure walls introduce background scattering. The corrected inelastic spectra for $ZrW_2O_8$ at ambient pressure and 1.7 Kbar are shown in Fig. 2. The spectra at high pressures show an unusual large softening. In conformity with the predic-

tions, the phonon modes of energy below about 5 meV soften by about 0.15 meV. For example, at 3 meV, the softening of 0.15 meV corresponds to a Grüneisen parameter of about -20. At energies above 6 meV, the shift of the spectrum is much less than that at lower energies.

This phonon softening on compression of the crystal is large and unusual since in normal materials the spectrum shifts only slightly to higher energies. The experimental observation of phonon softening is in good agreement with our calculations (Fig. 2), which also shows similar behavior. The experiment validates our lattice dynamical calculation which showed that the NTE behaviour in $ZrW_2O_8$ is due to large negative Grüneisen parameter of low energy phonon modes.

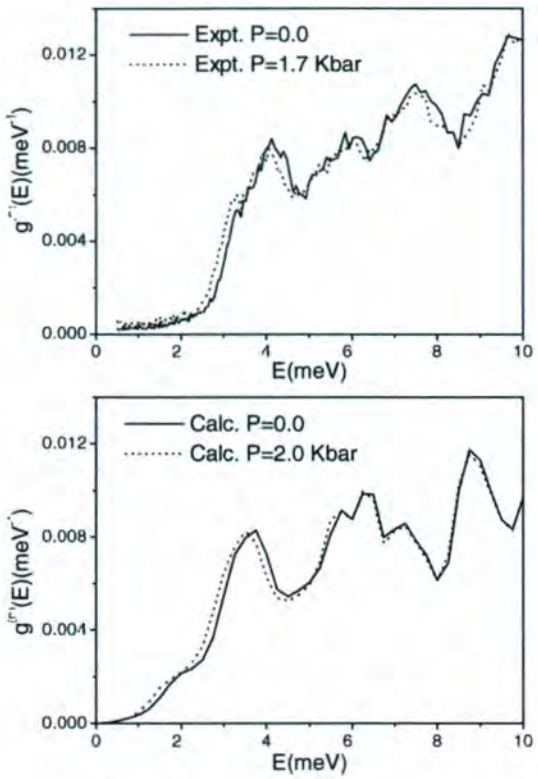


Figure 2: The comparison between the calculated and experimental inelastic neutron scattering spectra for cubic $ZrW_2O_8$. The experimental spectra at p = 0.3 and 1.0 Kbar fall in between those of p = 0 and 1.7 Kbar, and have not been shown here for clarity.


**REFERENCES**

● [1] T.A. Mary, J.S.O. Evans, T. Vogt and A.W. Sleight Science, 272 (1996) 90 ● [2] A.K.A. Pyrde, K.D. Hammonds, M.T. Dove, V. Heine, J.D. Gale and M.C. Warren, J. Phys. Condens. Matter, 8 (1996) 10973 ● [3] A.P. Ramirez and C.R. Kowach, Phys. Rev.Lett, 80 (1998) 4903 ● [4] G. Ernst, C. Broholm, G.R. Kowach and A.P. Ramirez, Nature 396 (1998) 147 ● [5] J.D. Jorgensen, Z. Hu, S. Teslic, D.N. Argyriou, S. Short, J.S.O. Evans, and A.W. Sleight, Phys. Rev B59, (1999) 215 ● [6] T.R. Ravindran, A.K. Arora and T.A. Mary, Phys. Rev. Lett.84 (2000) 3879 ● [7] R. Mittal and S.L. Chaplot, Phys. Rev B 60 (1999) 7234 ; Solid State Commun. 115 (2000) 319

# The elementary jump in intermetallic alloys with CsCl-structure

J. COMBET (ILL & UNIVERSITÉ STRASBOURG)

B. FRICK (ILL)

**The outstanding high temperature properties of intermetallic alloys of CsOl-structure are related to the self diffusion of atoms. A detailed understanding of the elementary jumps is essential. Recent neutron backscattering experiments have shed light on the diffusion process through the crystal lattice and give support to a new model for diffusion.**

Intermetallic alloys are increasingly used for high temperature applications, e. g. in the aerospace industry, due to their corrosion stability and strength. Their extraordinary properties at elevated temperatures are strongly connected to self diffusion, i.e. diffusion of the constituents themselves. The knowledge of the kinetics on the atomic scale in these systems permits the control of crucial processes, e.g. different stages of precipitation, and the optimisation of macroscopic characteristics of these materials. However, even in intermetallics with structures as simple as the CsCl structure, the mechanism of self diffusion is not yet fully understood. While it is generally believed that diffusion in these alloys happens via jumps to vacant sites in the lattice, the nature of the jumps is not yet understood. There exist two possibilities which are illustrated in Fig. 1:

a) An atom *A* may perform a short jump to a nearest neighbour site (NN). This jump is energetically expensive insofar as a nearest neighbour site in the CsCl structure is a so called antistructure site, i.e. 'belonging' to the other element *B*.

b) The *A*-atom may prefer to stay on its own sublattice (*A*-sites). In this case the jump

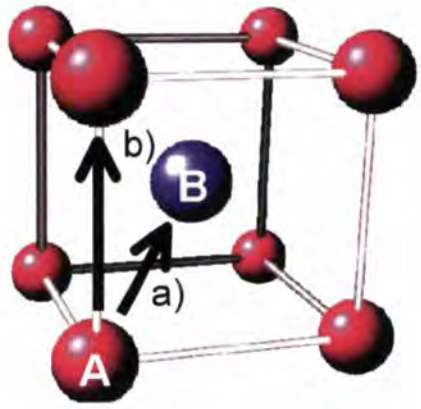


Figure 1: Unit cell of the CsCl structure. The red spheres represent A atoms (nickel or cobalt in the present case), the blue sphere a B atoms (gallium). The two possible jumps for an A atom are jumps to NN sites (a) which belongs to the 'foreign' B sublattice or jumps to more distant but regular NNN sites (b). Please note that there has to be a vacancy on the target site in order to allow a jump.

distance is considerably longer, the corresponding jump being a jump to a next-nearest neighbour site (NNN).

It is obvious that the preference for one or the other jump will be principally governed by the ordering energy of the alloy. While intermetallic alloys with low ordering energies like FeAl [1] favour NN jumps, diffusion in compounds with high ordering energies like NiAl [2] is likely to happen via NNN jumps. However, an open question remains: What happens in intermetallic alloys with intermediate ordering energies like NiGa and CoGa?

These alloys have been subject of extensive studies by tracer diffusion [3] which yield very precise values for the *long range* diffusivities at various compositions and temperatures. However, the conclusions drawn from these data on the microscopic diffusion mechanism are rather indirect and sometimes contradictory.

In contrast, quasielastic neutron scattering (QNS) allows to measure directly the *elementary jump vector* on single crystals, i.e. to observe *direction, length and frequency* of the diffusive jump in these alloys. Ni diffusion in NiGa and Co diffusion in CoGa are ideal for quasielastic neutron scattering studies in terms of scattering cross sections. However, the rather slow diffusion in these alloys ($10^{-13}$ to $10^{-12}$ m²/s) represents an experimental challenge because it corresponds to a quasielastic broadening of at best 0.1 μeV.

Nevertheless, experiments on NiGa and CoGa single crystals could be successfully performed at the backscattering spectrometer IN16. The problem of slow diffusion could be overcome quite successfully by
i) carrying out the experiments close to the melting point (~1450 K) and combining measurements of at least 20h per temperature and sample orientation with an optimised resolution function. A typical spectrum is shown in Fig. 2.
ii) refining models simultaneously at all single crystal orientations for one temperature and composition which reduces considerably the number of free parameters and compensates the weakness of the signal.

In both alloys a diffusion process which involves two distinct time scales was detected: besides the principal quasielastic line, a second much broader line is present in the signal (Fig. 2). These two time scales can be attributed to long residence times on the regular sublattice and short residence times on the 'forbidden' antistructure sites [4]. Fig. 3 shows the measured line widths if the fast process is taken into account (red) or not (green). A comparison with calculations (line) shows clearly that diffusion happens via jumps to antistructure sites *B* and that NNN jumps (to *A* - sites directly) can be excluded.

Further information on the residence time of the diffusing atoms on the antistructure sites is provided by the intensities and widths of the two components. These residence times

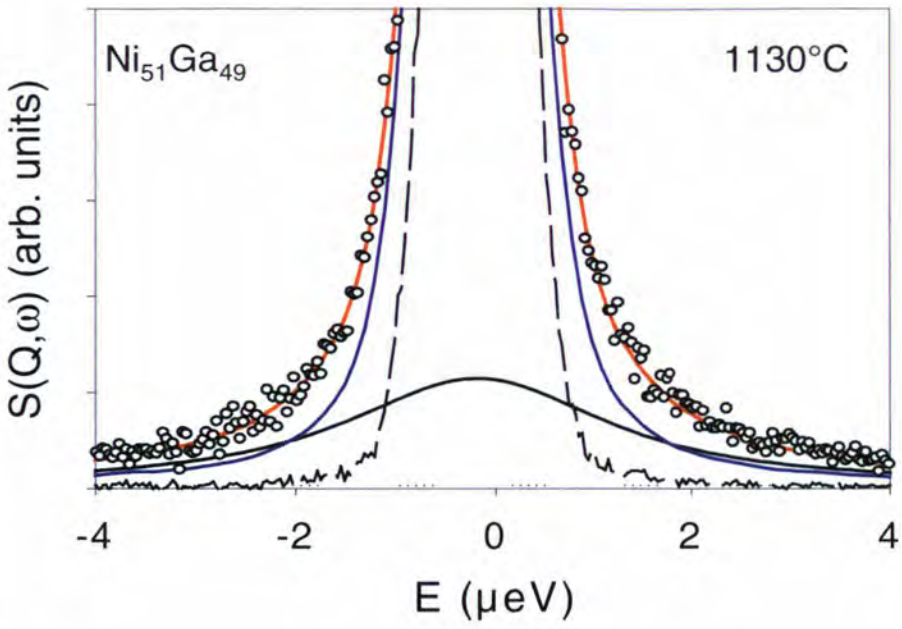


Figure 2: Quasielastic spectrum of $Ni_{51}Ga_{49}$ taken at 1400 K and Q = 1.6 Å$^{-1}$ fitted with the sum (red) of a narrow (blue) and broad (black) Lorentzian, both folded with the resolution (dashed). The broadening is 0.3 μeV for the narrow line and 3 μeV for the broad line (FWHM).

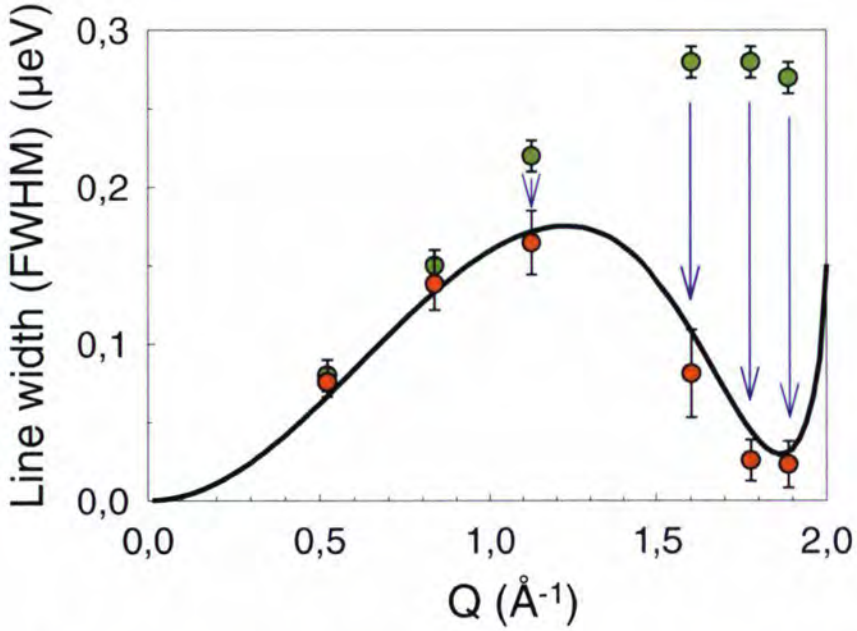


Figure 3: The maximum of the line width at Q = 1.8 Å$^{-1}$ near a reciprocal <100> lattice point which is obtained from a fit with a single Lorentzian (green circles) can not be explained by a model assuming jumps on the regular sublattice. Jumps to antistructure sites, however, produce an additional broad line. If this line is subtracted from the spectra the resulting narrow line (red) shows a minimum at Q ≈ 1.9 Å$^{-1}$ as expected for the NN jump model (solid line). $Co_{64}Ga_{36}$, 1400 K.

are very long, which indicates unusually high concentrations of thermal antistructure atoms - up to several percent. These antistructure atoms in turn influence the diffusion process by decreasing the degree of order in the system. With these neutron scattering data we are able to propose a new model for self diffusion in these alloys. From a comparison of jump frequencies from QNS and long range diffusivities from tracer experiments, one can conclude an unexpectedly weak correlation of subsequent jumps. This indicates that traditional models based on cycles of strongly correlated jumps cannot explain diffusion in the investigated systems NiGa and CoGa.

The neutron results on both alloys, NiGa [5] and CoGa [6], point instead towards a diffusion process which involves more than one defect and which leads to a practically unlimited set of possible jump sequences. An analytical treatment of this scenario is naturally not possible. Monte Carlo simulations, however, taking into account such high defect concentrations, can explain the observed data in alloys which are as different as FeAl or NiGa, solely by varying the interaction energies. Therefore we believe that the self diffusion at high temperatures in most intermetallic alloys with CsCl-structure can be explained within a single and surprisingly simple model.

## References


● [1] R. Weinkamer, P. Fratzl, B. Sepiol, G. Vogl, Phys. Rev. B 59 (1999) 8622 ● [2] Y. Mishin and D. Farkas, Scr. Mater. 39 (1998) 625 ● [3] For an overview see: H. Mehrer, Mater. Trans., JIM 37 (1996) 1259 ● [4] O.G. Randl, B. Sepiol, G. Vogl, R. Feldwisch, K. Schroeder, Phys. Rev. B 49 (1994) 8768 ● [5] M. Kaisermayr, J. Combet, H. Ipser, H. Schicketanz, B. Sepiol, G. Vogl, Phys. Rev. B 61 (2000) 12038 ● [6] M. Kaisermayr, J. Combet, H. Ipser, H. Schicketanz, B. Sepiol, G. Vogl, Phys. Rev. B 63 (2001) 054303

# The nature of ferroelectric transitions in Rochelle salt

J. KULDA (ILL)

J. HLINKA, S. KAMBA, J. PETZELT (INSTITUTE OF PHYSICS CAS, PRAGUE)

**Inelastic neutron scattering study of a deuterated crystal of Rochelle salt confirms the existence of a resonant mode about 2.9 meV at 50 K which softens with increasing temperature and becomes overdamped on approaching the phase transition to the ferroelectric phase. The analysis of the inelastic neutron scattering structure factors allows us to conclude that this mode's eigenvector involves mainly displacements of the same three molecules of crystal water that were found in recent structural studies to show the largest static displacements in the ferroelectric distorsion. We claim that this resonant mode plays a central role in the ferroelectric phase transition.**

Rochelle salt (RS), sel de Seignette(1675) or the sodium potasium tartrate ($NaKC_4H_4O_6 \cdot 4H_2O$), is the substance in which ferroelectricity was discovered for the first time [1]. Moreover, it remains the only system with a re-entrant paraelectric phase. The $C_2^2$ ($P2_111$, Z=4) ferroelectric phase is surrounded by the $D_2^3$ ($P2_12_12$, Z=4) paraelectric phase, so that there are two Curie points, $T_{C1}$ = 255 K and $T_{C2}$ = 297 K. A phenomenological explanation of this curiosity has been proposed in terms of two interpenetrating lattices [2,3]. However, an exact knowledge of the structure of the individual phases and a microscopic understanding of the transition mechanism remained an open problem up to recently.

Although the structure of RS in its high temperature paraelectric phase has been known since the 1940's, the structure of the ferroelectric phase followed more than 30 years after and, even then, the limited accuracy of the results did not permit more than to speculate on the possible structural changes. Only in the last decade high precision X-ray data [4,5] converged to a more or less consistent picture (Fig. 1) according to which

- the structures of the high-temperature (HT) and low-temperature (LT) paraelectric phases are different, mainly because of the positions of three crystal water molecules $O_8$, $O_9$ and $O_{10}$

- the ferroelectric phase is an ordered solid solution in which layers of the HT and LT phases alternate along the **b**-axis.

At the same time dielectric measurements, far infrared and Raman spectroscopy [6,7] have proved the existence of a mode with a frequency of about 22 $cm^{-1}$ (2.7 meV) at low temperatures, becoming soft and overdamped when approaching $T_1$. A relaxational mode in the GHz range has been found to complement the soft mode – a feature typical for systems on the crossover between order-disorder and displacive nature of the phase transition.

In an attempt to elucidate the relationship between the structural and spectroscopic results we have used the IN3 and IN12 triple-axis spectrometers at the ILL to perform neutron inelastic scattering experiments on a partially deuterated single crystal of RS [8].

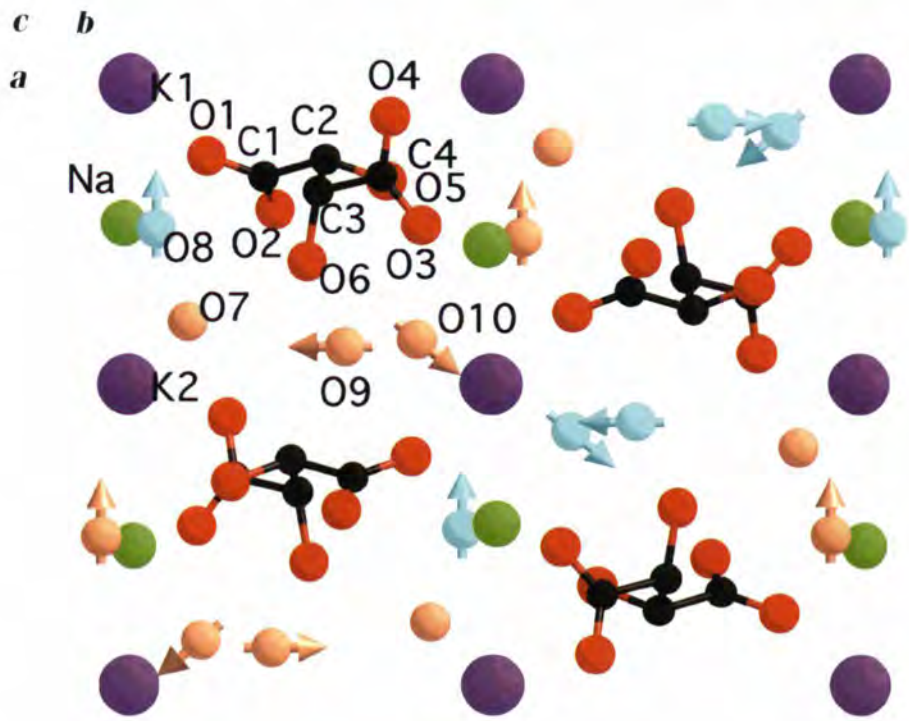


Figure 1: The crystal structure of Rochelle salt. The arrows indicate the main displacements of crystal water molecules in the soft mode of 2.9 meV. On entering the ferroelectric phase at $T_{C1}$ the orange oxygen atoms start to occupy progressively the HT positions (displaced along their orange arrows), while the other half (the turquoise ones) rests in the LT positions. Their displacements (opposite to the turquoise arrows!) follow only when all the "orange" positions are occupied.

Indeed a flat optical dispersion branch is readily observed at 2.9 meV with an anomalous shift due to deuteration observed previously. As seen by comparing both parts of Fig. 2, its evolution with temperature closely follows the behaviour expected on the basis of previous dielectric experiments [6]. The most important consequence of this observation is that the eigenvector of the phonon does not change significantly with temperature.

One of the essential advantages of coherent inelastic neutron scattering is that, in analogy to conventional crystallography, the inelastic structure factor provides information about the phonon displacement pattern (eigenvector). We have therefore collected intensity data for the soft mode in a number of Brillouin zones in order to identify the atoms that play a prominent role in the ferroelectric phase transitions. This part of the experiment was carried out on the IN3 thermal beam TAS, providing access to a more extended range of momentum transfers.

Among the data from about 40 Brillouin zones the strongest signal is observed in the [050] and [800] zones. The [050] Bragg reflection in the paralelectric phase is forbidden by the $2_1$ screw axis. The 2.9 meV mode, breaking this symmetry, softens and gets overdamped at $T_{C1}$, where the family of [0$k$0] ($k$ odd) reflections, recognised as the fingerprint of the ferroelectric phase, appears. The Bragg intensity of the [050], the strongest one of the family, has been found by Shiozaki [9] to be exactly proportional to the square of the electric polarisation $P^2$ - the order parameter of the ferroelectric phase, an intriguing finding because the electric polarisation is parallel to the ***a-axis***. Our detailed analysis of the contributions of the different atoms to the crystallographic structure factor reveals that the [050] Bragg intensity is essentially due to the oxygens of the crystal water molecules $O_9$ and $O_{10}$. A similar analysis of the structure factor in the 800 Brillouin zone reveals an antiphase movement of the $O_8$ and $O_{10}$ water molecules (Fig.1). It is important to note that all the $O_8$ molecules move in phase so that their displacement can modify the electric polarisation of the corresponding layer. From the fact that the soft mode eigenvector does not vary with temperature, we may conclude that the three water molecules $O_8$, $O_9$ and $O_{10}$ play the most important role both in the soft mode displacement pattern below $TC_1$ and in the ferroelectric distortion. Moreover the fact that Shiozaki's result [9] has been obtained with X-rays practically excludes any contribution of hydrogen atoms and confirms the displacive character of their movement (no water molecule reorientation).

The information on the eigenvector of the resonant mode, which we have obtained from the above analysis of the inelastic scattering intensities, provides a link between the previous spectroscopic and crystallographic results and leads to the following scenario for the phase transition at $T_{C1}$. The water molecules $O_9$ and $O_{10}$, involved together with $O_8$ in the 2.9 meV lattice mode, vibrate in a double well potential. With increasing temperature this mode becomes progressively damped by their excursions into the shallow well. $T_{C1}$ corresponds to the temperature at which some of the new positions start to be occupied permanently. It appears that an alternating occupation of HT and LT positions in layers perpendicular to the ***b*** axis is energetically favourable. This ordering breaks the screw axis symmetry along ***b*** and is responsible for the difference in the electric dipole moments in the two halves of the unit cell arising due to different $O_8$ positions. As a result, the crystal exhibits spontaneous electric polarisation in the temperature range up to $T_{C2}$, where also the second half of the water molecules (turquoise in Fig. 1) has passed into the high temperature positions and the $2_1$ screw axis symmetry along ***b*** is re-established.

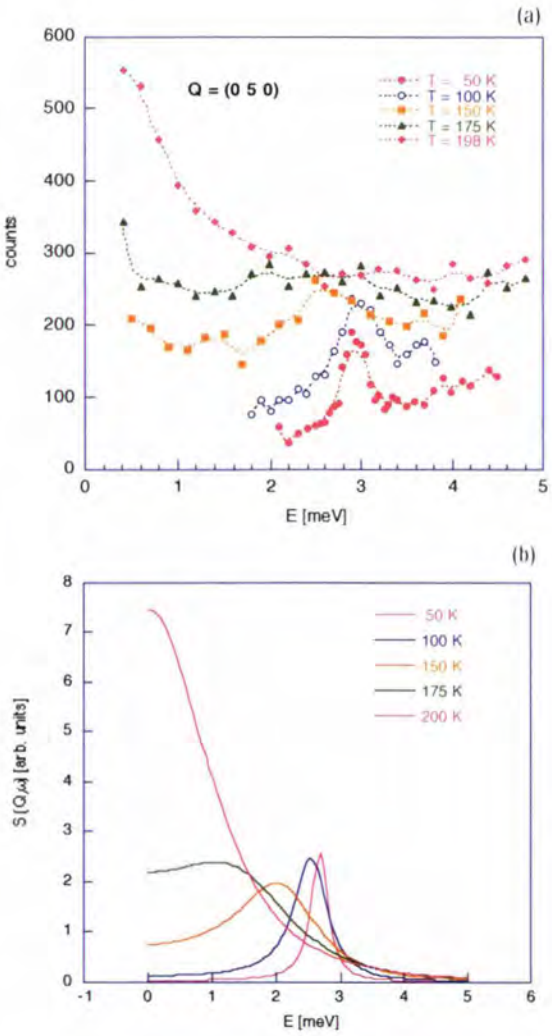


Figure 2: The soft phonon of the ferroelectric transition: inelastic scattering results from IN12 (a) and their expected form (b) calculated on the basis of the results of dielectric measurements [6].


**References**

● [1] J. Valasek, Phys. Rev. 17 (1921) 475 ● [2] T. Mitsui, Phys. Rev. 111 (1958) 1259 ● [3] B. Zeks, G.C. Shukla, R. Blinc, Phys. Rev. B3 (1971) 2306 ● [4] E. Suzuki, Y. Shiozaki, Phys. Rev. B53 (1996) 5212 ● [5] X. Solans, G. Gonzalez-Silgo, C. Ruiz-Perez, J. Sol. St. Chemistry 131 (1997) 350 ● [6] A.A. Volkov, G.V. Kozlov, E.B. Kryukova, J. Petzelt, Sov. Phys. JETP. 63 (1986) 110 ● [7] S. Kamba, G. Schaack, J. Petzelt, Phys. Rev. B51 (1995) 14998 ● [8] J. Hlinka, J. Kulda, S. Kamba, J. Petzelt, Phys. Rev. B 63(2001) 052102 ● [9] Y. Shiozaki, J. Phys. Chem. Sol. 28 (1967) 2381

# Thermostability of proteins:
## How thermal equilibrium fluctuations contribute to protein stability

J. Fitter (FZ Jülich)

R. Herrmann, N.A. Dencher (TU Darmstadt)

**Thermozymes, which are stable and optimally active at elevated temperatures (60°C - 125°C), play a significant role in many biotechnological applications like diagnostics, waste treatment and paper industry as well as starch-processing industry. A key to elucidate the molecular mechanisms of this remarkable thermostability is to understand the role of structural fluctuations for protein stability. The time-of-flight spectrometer IN6 offers a powerful tool to monitor these local conformational picosecond fluctuations of protein structures in solution.**

Biological polymers like proteins are characterised by complex and hierarchically organised structures. One of the most remarkable properties of these molecules is the fact that a protein polypeptide chain (in aqueous solvent) generally folds only into a sole three dimensional conformation. Only this unique fold ensures that the protein will operate. On the other hand, this conformation exhibits a marginal stability, equivalent to the energy of a few hydrogen bonds. The conformational stability, defined as a free energy change $\Delta G_{unf}$ for the transition folded state ↔ unfolded state, is in the order of 30-60 kJ/mol at room temperature [1]. The biological significance of the relatively low $\Delta G_{unf}$ is the requirement for a well balanced compromise between rigidity as a prerequisite of specificity and flexibility ensuring a proper function of the protein. The details about the physical nature of this balance and how proteins achieve this balance even under very different environmental conditions, like extreme temperatures, still are unclear.

Figure 1: Crystal structure of the thermostable α-amylase from *Bac. licheniformis* (PDB-entry: 1BLI).

### Conformational flexibility can stabilise the folded state

A promising approach to investigate the underlying mechanisms of protein stability by concurrent functionality, is to compare proteins which are adapted to very different temperatures. Proteins adapted to extremely high temperatures, known as thermozymes, are produced by thermophilic or hyperthermophilic organisms (living at temperatures ranging from 70 °C to far above 100 °C). They remain folded and functional at elevated temperatures, and they are often less active at lower temperatures. In contrast to this, their mesophilic homologues (adapted to moderate temperatures) keep their specific conformation and their functionality only up to approximately 60 °C. Besides some structural properties which have been related to increased thermostability (e.g., additional hydrogen bonds and salt bridges, shorter loop regions, increased internal hydrophobicity), dynamic features play also a crucial role for thermal adaptation. Therefore, we have studied thermal equilibrium fluctuations of a mesophilic and a thermostable α-amylase [2]. This enzyme catalyses the cleavage of glycosidic bonds in starch and related carbohydrates (see Fig. 1). Since starch is best soluble at high temperatures, thermostable α-amylases play a key role in industrial hydrolysis. In a first comparative analysis of conformational fluctuations, we have applied neutron spectroscopy to highly concentrated protein solutions at room temperature. Incoherent neutron scattering from about 3,400 non-exchanged hydrogen atoms (enzymes were dissolved in $D_2O$), distributed quasi-homogenouses over the whole structure of each α-amylase molecule, gives valuable information about structural fluctuations with amplitudes in the range of 0.1 nm and on the picosecond time scale (see Fig. 2). To our surprise the comparison of conformational fluctuations in both enzymes revealed a higher conformational flexibility of the thermostable enzyme as compared to the mesophilic counterpart (see Fig. 3). Most of the previous studies analysing protein thermostability indicate that thermoenzymes are less flexible as compared to their mesophilic analogues. It is assumed, that one of the main effects of these stabilisation features is to increase the rigidity of the protein structure. The reduced conformational flexibility of loop regions, of secondary structure elements, or of the core region is supposed to make the protein structure less susceptible to thermal unfolding [3,4]. On the other hand, structural flexibility observed through equilibrium fluctuations contributes to the entropy change $\Delta S$ during unfolding and may have a profound influence on the free energy change ($\Delta G_{unf} = \Delta H - T\Delta S$). Generally, the unfolded state exhibits a higher conformational entropy as compared to the folded state.

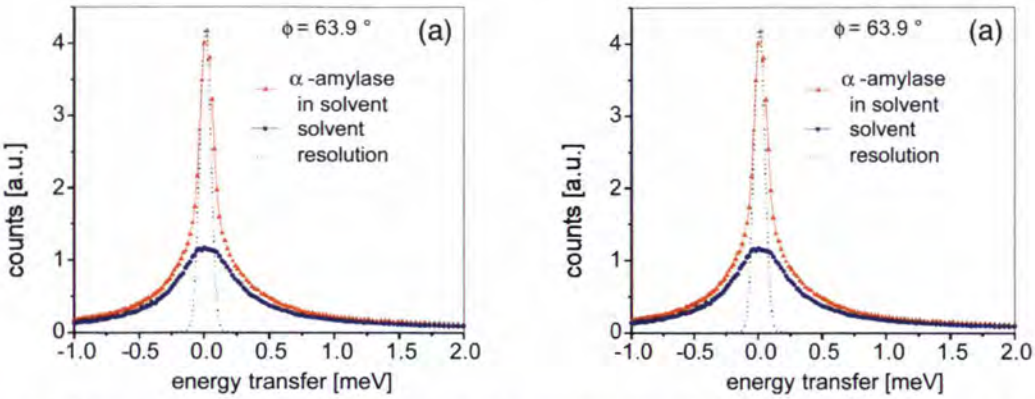


Figure 2: Steps in the data analysis of α-amylase in $D_2O$ solution. (a): Comparison of spectra as measured with enzyme solution (triangles) and with pure buffer only (circles). At the given scattering angle the solvent scattering is about two third of the total scattering observed for enzyme solutions. (b): The difference spectrum (enzyme solution minus solvent as shown in (a)) at the given scattering angle ϕ has been fitted with an elastic contribution, a single Lorentzian, and a linear background.

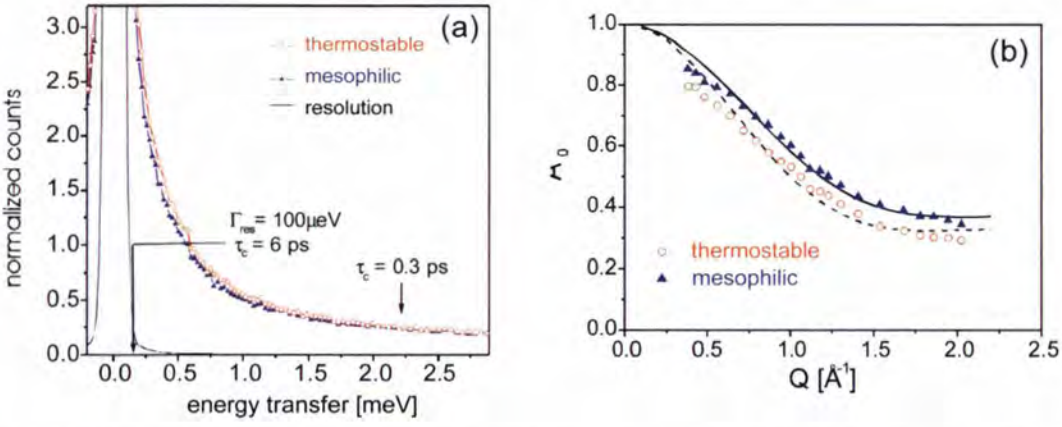


Figure 3 (a): Incoherent neutron scattering spectra as measured for both α-amylases at 30 °C (solvent scattering subtracted). The figure represents an enlargement of the quasielastic scattering due to stochastic motions in α-amylase. In this window the quasielastic scattering is about 10% larger for the thermostable enzyme as compared to the mesophilic analogue. (b): The modelfit of elastic incoherent structure factors $A_0$ as a function of momentum transfer Q also indicates a higher conformational flexibility of the thermostable enzyme.

Therefore, our results indicate that the higher conformational flexibility of the folded state as observed for the thermostable enzyme is related to the smaller entropy change ΔS, which favours the folded state. Very recently, we have obtained results measured which α-amylase at higher temperatures and enzymes in the unfolded state which support the idea that the mechanism of entropic stabilisation plays an important role for thermostability in the case of α-amylase [5].

This work demonstrates how neutron spectroscopy, in particular with enzymes in solution, can contribute significantly to solve major problems in the field of molecular biophysics and biochemistry. Neutron scattering has already provided some hints to questions about the role of protein dynamics in the functionality of these molecules. We have shown that in addition neutron spectroscopy offers a promising approach to answer another important question: how do proteins achieve their stability under very different or extreme environmental conditions? This question is of enormous importance for many biotechnological applications.


**References**

- [1] P.L. Privalov, Adv. Protein Chem. 33 (1979) 167
- [2] J. Fitter & J. Heberle, Biophys. J. 79 (2000) 1629
- [3] P. Zavodszky et al., Proc. Natl. Acad. Sci. USA 95 (1998) 7406
- [4] I. Korndörfer et al., J. Mol. Biol. 246 (1995) 511
- [5] J. Fitter et al., Physica B (2001), in press

# How ATP induces structural changes of an archaeal chaperonin


- I. Gutsche, M. Rössle, H. Heumann, W. Baumeister (MPI für Biochemie, Martinsried)
- J. Holzinger (MPI für Biochemie, Martinsried & ILL)
- R.P. May (ILL)



**Chaperonins are double-ring protein folding machines fuelled by ATP binding and hydrolysis. Conformational changes upon ATPase cycling of bacterial chaperonins have been revealed mainly by means of cryo-electron microscopy and X-ray crystallography. For archaeal chaperonins, however, these methods have as yet failed to provide a correlation between the structural and the functional states. Small-angle neutron scattering experiments on D22 have given us an insight into the regulation of the *Thermoplasma acidophilum* thermosome by adenine nucleotides.**


One of the central problems in structural biology is to understand how proteins, synthetised as linear chains of amino acids, acquire their functional three-dimensional conformation. Over the past decade, it was realised that cellular protein folding critically depends on the assistance of a sophisticated machinery, for instance by so-called chaperonins. These essential multi-subunit protein assemblies exist in all three 'kingdoms' of life: bacteria, eucarya (higher organisms) and archaea (whose genome manifests both bacterial and eucaryotic features).

Chaperonins are double-ring structures with a central cavity that provides a compartment for ATP-driven folding of proteins. Binding and hydrolysis of ATP are thought to switch the chaperonins between an acceptor state, in which the cavity is open to receive an unfolded or a misfolded protein ('substrate'), and a folding-active state, encapsulating the substrate. The exact relationship between the nucleotide-bound state and the conformation of the folding machine has only been established for the bacterial protein GroEL [1]. However, it has still to be elucidated for the eukaryotic chaperonins and their simpler archaeal analogues known as thermosomes [2].

In the bacterium *Escherichia coli*, chaperonins consist of two major molecules, GroEL and GroES. GroEL can be described as a hollow cylinder formed by two heptameric rings ("double donut"). The co-factor GroES forms a cap that binds on top of the ATP-loaded GroEL to seal off the folding compartment. As for the thermosomes, they function without a GroES-like cofactor. How? The mechanism remained enigmatic until two structures of the archaeal *Thermoplasma acidophilum* were published, one obtained by cryo-electron microscopy [3] and the other by X-ray crystallography [4]. The difference between the two was amazing – the same protein appeared cylindrical in vitrified ice, but spherical in the crystal (Fig. 1). A transformation of one structure into the other requires a rotation of the outer regions of all subunits. Hence, it was realised that the thermosome possessed a built-in lid instead of a detachable cofactor. Therefore, by analogy with the GroEL/GroES system, the thermosome was proposed to be

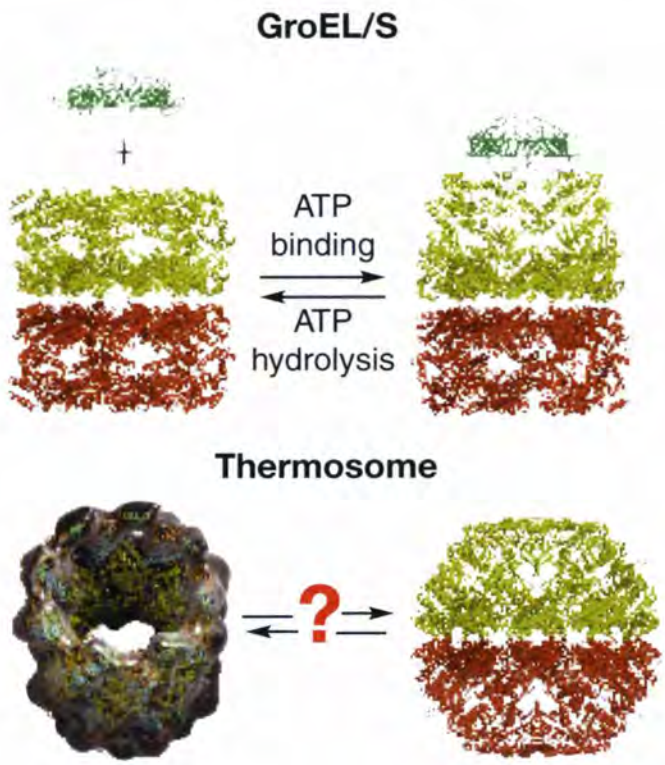


Figure 1: Conformational rearrangements of GroEL/ES and thermosome as proposed on the basis of cryo-electron microscopy and X-ray crystallography. One ring of the chaperonins is shown in red, the second in yellow. The cofactor GroES is shown in green. Note, that both the left (cryo-electron microscopic) and the right (X-ray crystal) structures of the thermosome were solved in the absence of nucleotides.

open in the absence of nucleotides, whereas the crystallisation conditions were presumed to have trapped it in a folding-active state. In solution, this state was postulated to occur only upon ATP binding [5]. Faced with conflicting data of cryo-electron microscopy and X-ray crystallography, we decided to verify these hypotheses with a third, independent technique, and chose small-angle neutron scattering. This method provides information about the overall structure and conformational changes of macromolecules in solution, where physiologically relevant conditions can be best approached. The experimental scattering curves were interpreted in terms of the pair-distance distribution function, p(r), which gives the weighted frequency of occurrence of distances between the elementary scatterers within the particle [6].

First of all, we recorded the scattering curve of the thermosome in the absence of any nucleotides, calculated the corresponding p(r), and compared it with the p(r) functions derived from the cryo-electron microscopic and the crystal data. In this way, we could show that in solution, in the absence of nucleotides, the conformation of the thermosome is well reflected by the open structure observed in vitrified ice.

Although the archaeon *Thermoplasma acidophilum* thrives only at 55 to 59 °C in hot sulphur springs, our biochemical [7] and small-angle neutron scattering analyses demonstrated that the thermosome from this organism could bind nucleotides (ADP, ATP or non-hydrolysable ATP analogues) already at 10 °C. The amplitude of the resulting conformational change was the same in the range of 10 to 55°C, and only the rate of ATP hydrolysis decreased with temperature.

Our results on the structural rearrangements of the thermosome during the reaction cycle are summarised in Fig. 2. Surprisingly, ATP binding does not induce a closure of the chaperonin as anticipated from the analogy to GroEL/GroES system. On the contrary, the thermosome seems even to expand a bit further. Then, it hydrolyses the nucleotide, proceeding through a transition state of nearly identical structure, and closes subsequently upon relaxation into an ADP-Pi species with a low affinity for inorganic phosphate. This closure represents the rate-limiting step of the cycle in the absence of denatured substrates. The release of phosphate triggers the re-opening of the chaperonin.

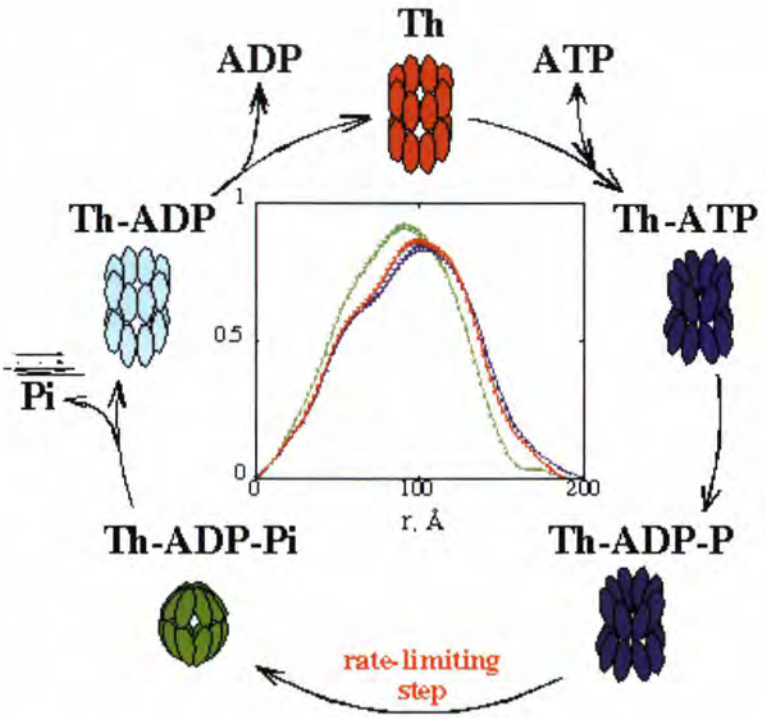


Figure 2: Model for the ATPase cycling of the thermosome based on small-angle neutron scattering data. Conformations of different nucleotide-bound species are schematised and colour-coded in accordance with the experimental p(r) functions, presented in the middle of the figure.

In order to mimic the transient hydrolytic intermediates ADP-P and ADP-Pi, we incubated the stable ADP-thermosome with $AlF_n$, known as a phosphate analogue with higher affinity and slower dissociation rate, and with inorganic phosphate, respectively. We verified that the closure of the thermosome, observed in ADP-Pi conditions, could not be triggered by phosphate ions alone, in the absence of ADP. Remarkably however, we found out that such a closure could be artificially induced in solution by the buffer used for thermosome crystallisation, which contained high concentrations of sulphate ions.

In conclusion, small-angle neutron scattering unravelled the reasons of the difference between the thermosome structures in the crystal and in vitrified ice, and gave us a first insight into conformational rearrangements of an archaeal chaperonin in solution upon ATP binding and hydrolysis [8]. The next step would now be to address the cycling of these folding machines in the presence of their cellular substrates.

Glossary:

- Adenine nucleotides, a class of molecules containing an adenine base, like ATP or ADP.
- ATP, Adenosine triphosphate, a molecule serving as energy source in biological reactions.
- ADP, Adenosine diphosphate, degradation product of ATP, can be reconverted into ATP.
- ADP-P, transition state of hydrolysis of Adenosine triphosphate.
- ADP-Pi, second transition state of hydrolysis of Adenosine triphosphate, where the inorganic phosphate is not yet released from its binding site.

**References**

[1] P.B. Sigler, Z. Xu, H.S. Rye, S.G. Burston, W.A. Fenton and A.L. Horwich, Ann. Rev. Biochem. 67 (1998) 581 • [2] I. Gutsche, L.-O. Essen and W. Baumeister, J. Mol. Biol. 293 (1999) 295 • [3] M. Nitsch, J. Walz, D. Typke, M. Klumpp, L.-O. Essen and W. Baumeister, Nature Struct. Biol. 5 (1998) 855 • [4] L. Ditzel, J. Lowe, D. Stock, K. O. Stetter, H. Huber, R. Huber and S. Steinbacher, Cell 93 (1998) 125 • [5] A. L. Horwich and H. R. Saibil, Nature Struct. Biol. 5 (1998) 333 • [6] O. Glatter, J. Appl. Crystallogr. 10 (1977) 415 • [7] I. Gutsche, O. Mihalache and W. Baumeister J. Mol. Biol. 300 (2000) 187 • [8] I. Gutsche, J. Holzinger, M. Rössle, H. Heumann, W. Baumeister and R. P. May Curr. Biol. 10 (2000) 405

# Formation of DNA-cationic vesicle complexes investigated by time-resolved small-angle neutron scattering

R. P. May (ILL)

P. C. A. Barreleiro, T.D. Le, B. Lindmän (Lund University)

**DNA and cationic vesicles form complexes that are promising candidates for gene therapy. The reaction between DNA and cationic vesicles was followed in the time range of seconds using the high flux small-angle neutron diffractometer D22. Different contrast conditions were used to examine the complexes as a function of charge ratio and membrane fluidity. Our experiments reveal that the formation of the complexes occurs in two steps, with characteristics times of about 10 and 50 s. These findings demonstrate the potential use of small-angle neutron scattering in the elucidation of structure and associated mechanism of fast reactions.**

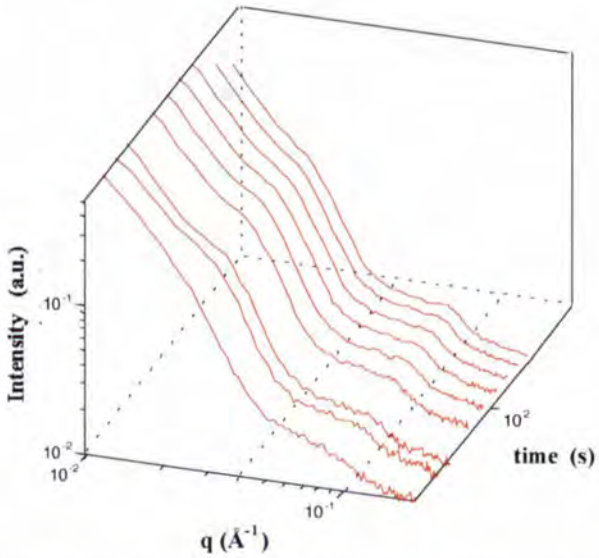


Figure 1: Time-resolved scattering intensity during the formation of DNA-cationic vesicle complexes in a DODAB:DOPE (1:1)/DNA mixture at a charge ratio of positive to negative charges of 2, 98% $^2H_2O$ and 25 °C. Interesting observations are that the neutron intensity decreases for low **q**, and the Bragg peak appearance at Q = 0.09 Å$^{-1}$ for times larger than 50 s. The initial counting time was 1 s (10 runs summed up), with an exponential increase of 1.053.

In the last few years gene therapy has attained considerable interest. Gene therapy involves the introduction and expression of recombinant genes in cells. Its purpose is to cure the cause of a disease while the traditional therapies often are limited to treat the symptoms of a disease. In gene and oligonucleotide therapy, the weak link is not the gene, but the vehicle used to deliver the gene, e. g., the ability of the vehicles to transport the gene inside the cells efficiently, safely and repeatedly. The most efficient gene transfer vectors currently in use are viruses that involve complex technologies and suffer from severe limitations. Artificial self-assembling vectors, formed by the complexation of cationic lipids and/or polymers with DNA, are currently being studied for transfection. These non-viral carriers appear promising because of their simplicity, apparent lack of immunogenicity and inflammatory response, larger carrier capacity and high fusogenic potential. A major drawback is their low transfection efficiency. The key role of the cationic lipid is to provide an electrostatic attraction between the vesicle and the DNA molecule. The introduction of neutral or zwitterionic lipids in the cationic vesicle has been shown to increase the transfection efficiency of the complexes in different cell lines *in vitro* as well as *in vivo*. However, their role is not well understood. Despite the increasing number of publications describing the structure and morphology little is known about the thermodynamics and kinetics of the formation of DNA-cationic lipid vesicle complexes. The knowledge of the mechanism of the complex formation is an important step for the improvement of gene therapy efficiency.

We have combined small-angle neutron scattering (SANS) with a "stopped-flow" apparatus, in which two solutions are injected rapidly into a measuring cell, to investigate the structural change occurring upon the interaction of DNA with cationic vesicles. A key advantage of the SANS technique is the ability to adjust the contrast in such a way that one component can be monitored at a time. Under different contrast conditions, we monitor the time-dependent structural change as a function of the charge ratio and membrane fluidity. The present time-resolved experiments, which are lacking in the literature, examine the time-dependent structural change that is useful for future developments and biological applications. Vesicles composed of a mixture of a cationic (dimethyldioctadecylammonium bromide) and a neutral lipid (1,2-dioleoyl-sn-glycero-3-phosphatidyethanolamine), are transformed into multilamellar structures upon DNA addition, as shown by small-angle X-ray [2] and neutron scattering experiments performed in our group.

The kinetic experiments were performed by rapidly mixing equal volumes of solutions containing cationic vesicles (200 nm diameter) and DNA (length 2000 base pairs) and measuring the time evolution of the scattering vector (Q)-dependent scattered intensity, *I(Q)*. The process was observed for a total of about 600 s using exponential exposure times, i.e., the initial 2D spectrum was recorded for 1 s, and subsequent spectra were recorded for a

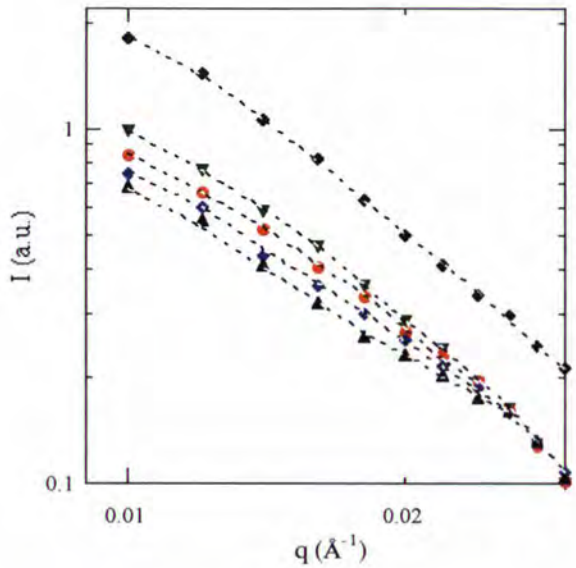


Figure 2: Scattering intensity from Fig. 1 for selected times at low Q. Times are, from top to bottom, (◆) 0 s; (▼) 2 s; (●) 3.1 s; (◆) 4.3 s; and (▲) 6.8 s at 25 °C.

duration of 1,053 times the preceding one. For improved statistics, each reaction was repeated 10 times, and the respective runs of each sample were summed up and analysed. An example of scattering curves obtained from a time-resolved small-angle neutron scattering experiment is shown in Fig. 1. The SANS intensity at low Q decreases with time till t ~ 10 s as is shown in Fig. 2 for times up to 6.8 s. This decrease comes from the mixing of the vesicles with DNA, since no change was observed when mixing vesicles with water. Cryo-TEM measurements on the DNA-cationic vesicle complex show the existence of clusters where the vesicles are deformed at the contact regions but are not ruptured. The flattening of the bilayers is caused by the addition of DNA. The "hump" at $Q = 0.025$ Å$^{-1}$ is interpreted as an intermediate occurring while forming the multilamellar complexes. The Bragg peak at $Q = 0.09$ Å$^{-1}$ corresponding to an interlamellar spacing of 68 Å, arises from lipid bilayer domains in the multilamellar complexes and only appears after ~50 s. The "hump" at $Q = 0.025$ Å$^{-1}$ becomes less pronounced as the time progresses. The two characteristic times (10 s and 50 s) suggest that the reaction occurs in at least two steps. The first time constant is attributed to the clustering of vesicles with DNA adsorbed on their surface; it has been independently confirmed by stopped-flow turbidity measurements performed in our laboratory [3]. The second time constant is made evident by the Bragg peak appearance. It is attributed to the reorganisation of the complex, resulting in the formation of multilamellar structures (Fig. 3). The fact that we do not observe the slower rate constant in the turbidity measurements indicates that the rearrangement of the complex may occur without a significant size increase. A very fast time constant in the millisecond time range, observed by stopped-flow, turbidity and fluorescence [3], was attributed to the binding of DNA to cationic vesicles.

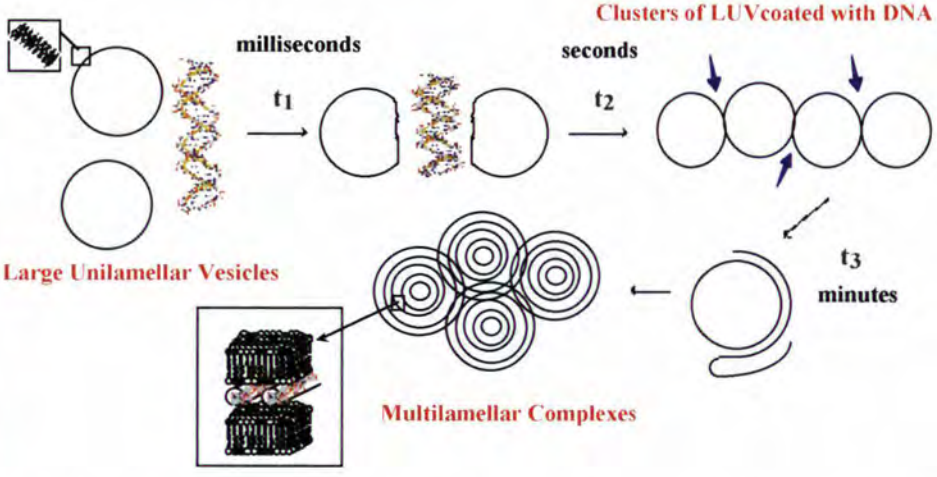


Figure 3: Schematic representation of the formation of DNA-cationic vesicle complexes suggested from cryo-TEM, stopped-flow turbidity and small-angle neutron scattering experiments.

The applicability of small-angle neutron scattering to probe the structural evolution during the DNA-cationic vesicles interaction in dilute solutions is demonstrated in this report. The combination of small-angle neutron scattering, turbidity and cryo-TEM measurements has given us the relevant time-scales for the different stages of the complex formation as well as the structures of the different intermediates.

Acknowledgements

We are very grateful to Manfred Rössle for the use and help with the stopped-flow apparatus. This work was supported by grants from The Swedish Research Council for Engineering Sciences (TFR), Sweden and PRAXIS XXI, FCT, Portugal (scholarship BD/13788/97).

## References

• [1] K. Roemer, T. Friedmann, Eur. J. Biochem. 208 (1992) 211 • [2] I. Koltover, T. Salditt, J.O. Rädler, C. R. Safinya, Science, 281 (1998) 78 • [3] P.C.A. Barreleiro, T. D. Le, B. Lindmän, Biochemistry, submitted

# Slow relaxation process in DNA
## at different levels of hydration


- A. P. Sokolov and A. Kisliuk (University of Akron, USA)
- H. Grimm (IFF, FZ Jülich)
- A. J. Dianoux (ILL)


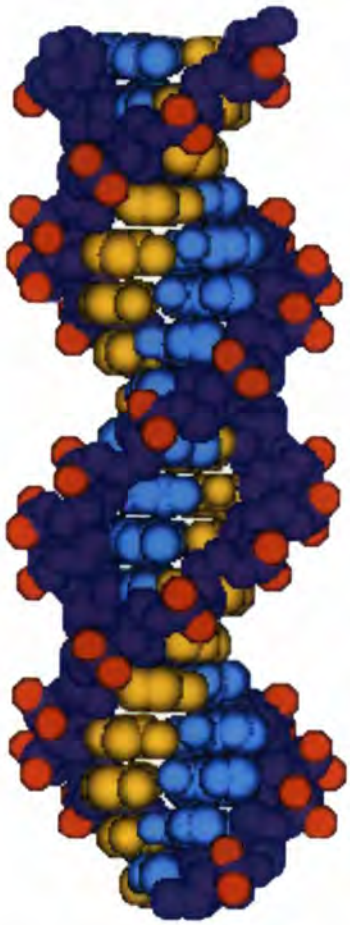

The structure of the most common form of the DNA molecule (B form). © CNRS.


**Sharp increase of atomic mean-squared displacements observed in hydrated bio-polymers at temperatures above T~200-230 K is usually ascribed to a dynamic transition. The nature of the dynamic transition is not yet clear but it is suggested that the dynamics transition is an important factor in enabling the protein's functions. Inelastic neutron scattering experiments have shown that the transition in DNA is related to the appearance of a slow relaxation process. Decreasing the hydration level suppresses the process and the dynamic transition. The decrease in water content is equivalent in terms of dynamics to a decrease in temperature. These results support the idea that the dynamic transition is mediated by the water of hydration, since bulk water has a dynamic transition around the same temperature.**


Oriented Li-DNA-fibers, hydrated with $D_2O$ to different levels (81%, 75% and 11%), have been studied on the time-of-flight spectrometer IN5 at the ILL. Incoming neutrons, of two different wavelengths (5 Å and 8 Å), were used in order to cover a sufficiently broad energy range. The quasielastic intensity demonstrates a strong increase at T above ~200 K for samples with high humidity level and a gradual increase for the "dry" sample. These results are similar to many previous observations obtained on bacteriorhodopsin[1], myoglobin[2] and other bio-polymers. They reflect a general trend in the dependence of the dynamics of bio-polymers on temperature and humidity.

In order to emphasize details in the quasielastic spectra, imaginary part of the susceptibility is shown in Fig. 1. Two processes can be readily identified: the "fast" one that dominates the spectra at $\nu$>100 GHz and the "slow" one that dominates the response at $\nu$<100 GHz. The latter exhibits a strong dependence on both T and relative humidity. Only the fast process is present at the lowest temperature and the quasielastic contribution to the spectrum in dry sample is stronger than in the samples with higher humidity (Fig. 1). This suggests that a decrease in water content increases flexibility of the DNA molecule at lower temperatures.

The situation changes at higher temperatures. Distinct differences develop at T~250 K, i.e. just above the dynamic transition: a decrease in the humidity level decreases the flexibility of DNA and is similar to a decrease in temperature.

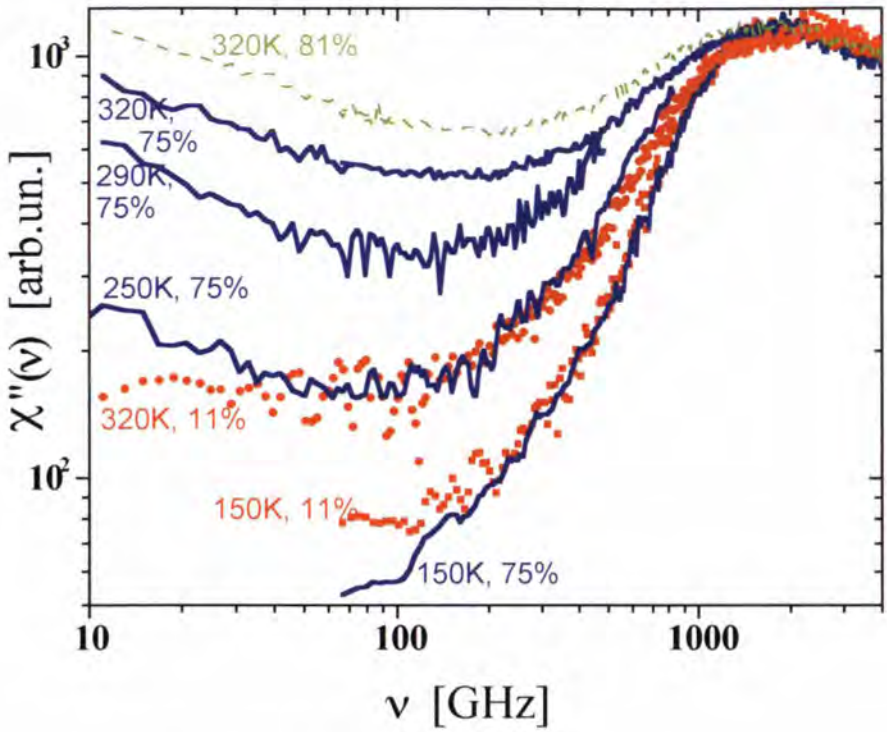


Figure 1: Susceptibility spectra of DNA samples at 11% r.h. (symbols), 75% r.h. (solid lines) and 81% r.h. (dashed line).

The most important observation in Fig. 1 is the absence of the slow process in the spectra of the "dry" sample. Even at the highest temperatures, T~320 K, only the tail of the fast process is evident at $\nu<100$ GHz. The fast process gives aharmonic contribution to $\langle x^2 \rangle$ observed as an increase of the quasielastic intensity even in the dry sample. However, this aharmonicity is weak. This result suggests that the sharp rise of $\langle x^2 \rangle$ at temperatures above ~210 K for the two "wet" samples is related to the slow process. Thus the decrease of the humidity level does not suppress in aharmonicity in general but suppresses the particular slow process. The nature of the slow process in bio-polymers is not known. Our data clearly indicate that the process is related to an intrinsic relaxational motion of DNA molecule (the contribution of $D_2O$ to our spectra is negligible in comparison with the contribution of DNA protons). We ascribe that process to cooperative motion of many DNA's monomers where all parts of the molecule, backbone and base-pairs, are involved.

The observed dependence of the dynamics on the level of hydration supports the idea of a strong influence of the solvent in bio-polymer dynamics. In particular, it supports our previous speculations[1] that the dynamic transition observed around 200-230 K can be related to the dynamic transition in bulk water observed at the same temperature range. The dynamic transition in water of hydration makes the DNA molecule more flexible and enable slow conformational variations. That can be important for opening of base-pairs. Thus our results suggest a possible explanation for suppression of biochemical activities by changes in the water content: the slow process appears to be strongly suppressed by a decrease in water content and the variations in dynamics appear to be similar to the variations caused by a decrease in temperature [4].


REFERENCES

• [1] M. FERRAND ET AL., PROC. NATL.AC.SCI. USA 90 (1993) 9668-9672 • [2] W. DOSTER, S. CUSACK, W. PETRY, NATURE 337 (1989) 754-756 • [3] A.P. SOKOLOV, H. GRIMM, R. KAHN, J.CHEM.PHYS. 110 (1999) 7053-7057 • [4] A.P. SOKOLOV ET AL., J.BIOL.PHYSICS 26 (2000) S1-S5

# Structure of clay-polymer-salt-water complexes: study by H/D isotope substitutions


- J. Swenson (Chalmers University of Technology, Göteborg)
- M.V. Smalley and H.L.M. Hatharasinghe (University College London)
- G. Fragneto (ILL)



**In this report we show how the intermediate-range structure of a complex four-component clay-polymer-salt-water system, consisting of *n*-butylammonium vermiculite, poly-(ethylene oxide) (PEO), *n*-butylammonium chloride and heavy water, can be determined by H/D isotope substitution of the butylammonium chains and PEO. By comparing the diffraction results of the four isotopically different samples we can show that a substantial part of the polymer chains is directly bound to the clay surfaces and that the remaining (at least 50%) polymer segments have a Gaussian-like distribution in the middle between the clay layers. A major part of the butylammonium ions are located in a 4-5 Å thick layer at a distance 12-16 Å from the centre of the clay platelets. The clay surfaces are therefore covered by, first, one layer of adsorbed ethylene oxide segments and water molecules, second, another molecular layer of water, and, third, the layer of butylammonium ions (1).**


Clay systems are not only a central problem of geology and soil science, they are also remarkably useful as model systems in colloid, polymer and biological science. Vermiculite clays consist of millions of negatively charged parallel silicate platelets that are held together by positively charged counterions located in the interlayer region.

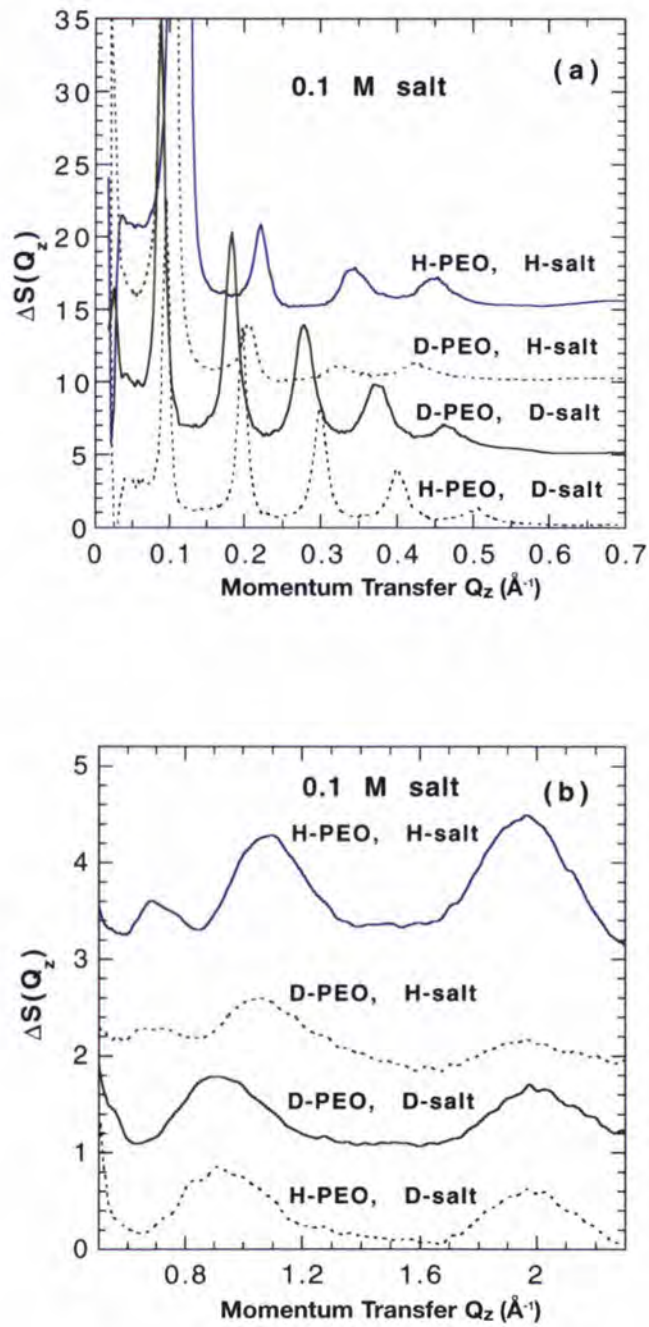


Figure 1: Difference structure factors $\Delta S(Q_z)$ (on different scales in (a) and (b)) obtained from neutron diffraction experiments on butylammonium vermiculite gels in 0.1 M salt concentration and a volume fraction of 4% PEO. The upper curves are shifted vertically for clarity.

The usefulness of the clays as colloidal model materials lies in their ability to swell (up to 50 times) in the direction perpendicular to the silicate platelets by taking up water, salts, polymers and other materials in the interlayer region. The clay gel formed is an ideal one-dimensional colloidal system suitable for studies of electrostatic interactions and interlayer structure in colloidal suspensions and polyelectrolyte solutions.

In the case of the present four-component system with added high molecular weight PEO the situation is rather complicated since one has to find the location of both the butylammonium chains and the polymer segments. However, due to the one-dimensional nature of the complex colloidal system and the use of four isotopically different samples (H-PEO and H-salt, D-PEO and H-salt, D-PEO and D-salt, H-PEO and D-salt) of each composition we have for the first time been able to determine the intermediate-range structure of this technologically important system (e.g. for stabilisation of drilling fluids and preparation of papers). Fig. 1 shows $\Delta S(Q_z)$ of these four isotope compositions of PEO and butylammonium ions in an 0.1 M butylammonium vermiculite gel, where $S(Q_z)$ of pure $D_2O$ has been subtracted from the measured $S(Q_z)$. The neutron diffraction experiments were performed on the D16 diffractometer. The volume fraction of PEO was 4% and the polymer molecular weight about 75000. In Fig. 1(a) we show the low Q-range of $\Delta S(Q_z)$, containing four orders of Bragg peaks arising from interplatelet correlations, whereas Fig. 1(b) shows the diffuse scattering caused mainly by clay platelet-solution correlations in the higher Q-range.The distribution of polymer segments were determined from analysis of the Fourier transfoms of the $\Delta S(Q_z)$ shown in Fig. 1, whereas the location of the butylammonium chains has been modelled by analysing the diffuse scattering and the intensity variation (as a function of ordering) of the Bragg peaks. The neutron structure factor, $S(Q_z)$, is related to the neutron scattering length density profile perpendicular to the clay platelets (along the z-axis), $\rho(z)$, via the crystallographic structure factor, $F(Q_z)$

$$S(Q_z)=M(Q_z)F(Q_z)F^*(Q_z)$$

$$F(Q_z) = \int_0^c \rho(z)[\cos(Qz) + i\sin(Qz)]dz$$

where c is the clay layer spacing and $M(Q_z)$ is a Lorentzian that takes into account the mosaic spread of the sample. This essentially

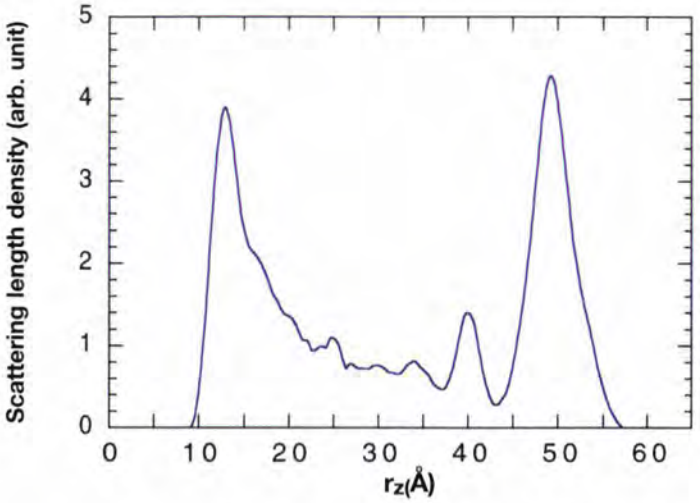


Figure 2: Scattering length density of butylammonium chains in the interlayer region as a function of $r_z$. The centre of the clay platelets are located at $r_z$=0 and $r_z$=63 Å. The result was obtained from a modelling (see the text) of the diffraction data shown in Fig. 1.

crystallographic description is a method to produce a single particle distribution function, $\rho(z)$, rather than a spatially averaged pair correlation function, $G(r_z)$.

Using this method, by means of an inverse Monte Carlo based program which simulates the scattering density along the z-axis simultaneously for several isotopically different samples, and the more traditional analysis of pair correlation functions, we have come to the following conclusions:

1. Polymer segments displace water molecules immediately adjacent to the clay surfaces, bonding directly to them by physical adsorption.
2. The remaining polymer segments show a Gaussian-like distribution with its centre in the middle of the interlayer region.
3. There are no indications that the presence of PEO affects the distribution of butylammonium ions. This is evident in Fig. 2, which shows that the majority of the butylammonium chains are, as in the case of the corresponding three-component system without added PEO, located in a 4-5 Å thick layer situated just outside the approximately 6 Å thick layer of adsorbed polymer segments and water molecules.


**References**

- [1] J. Swenson, M.V. Smalley, H.L.M. Hatharasinghe and G. Fragneto, Langmuir, in press

# Polymeric efficiency boosters in microemulsions: a SANS investigation of the polymer's role


- H. Endo, J. Allgaier, M. Monkenbusch, D. Richter (IFF, FZ Jülich)
- B. Jakobs, T. Sottmann, R. Strey (Univ. Köln)



**The boosting effect of amphiphilic block copolymers in the ternary microemulsion (water, oil and non-ionic surfactant) is investigated. Small amounts of PEP-PEO block copolymer lead to a dramatic expansion of 1 phase region where water and oil can be solubilised by the mediation of surfactant molecules. Small-angle neutron scattering experiments have made use of a sophisticated 2-dimensional contrast variation technique. The results demonstrate that the polymer is distributed uniformly on the surfactant membrane, owing to the variation of the membrane curvature elasticity.**


Microemulsions are thermodynamically stable and macroscopically homogeneous mixtures of oil and water, where the miscibility is mediated by surfactant molecules. Microscopically the surfactants form an extended interfacial film separating water and oil on a local scale. Recently we have discovered an enormous efficiency increase of the emulsification capacity of the non-ionic surfactant n-decyl-tetraoxyethylene ($C_{10}E_4$) by adding amphiphilic block copolymers of the polyethylenepropylene/ polyethylenoxide (PEP-PEO) [1]. Theoretically, a universal mechanism is proposed for the enhancement of the swelling behavior, which is due to the variation of the membrane curvature elasticity by polymer mushrooms anchored at the interface [2].

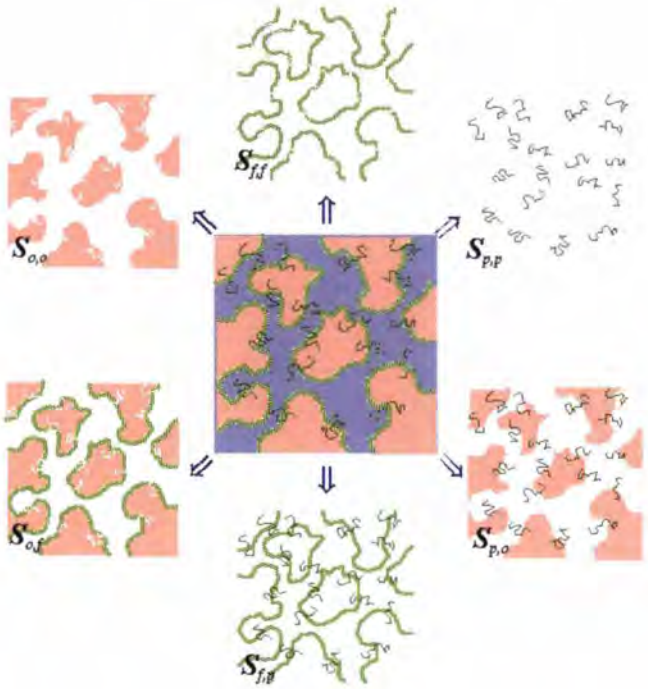


Figure 1: Scheme of the partial scattering functions $S_{i,j}$. The enough sets of SANS measurements with same components but different contrasts allow to decompose to each partial scattering function.

Here we report small angle neutron scattering (SANS) experiments with a high-precision contrast variation technique, which have been performed on samples in the bicontinuous microemulsions consisting of equal amounts of oil and water. With neutrons as probe, the contrast variation techniques based on H/D-replacement can be used to modify the visibility of the different components water, oil, surfactant film and polymer.

In bulk contrast, with deuterated water and protonated oil, the scattering is dominated by the three-dimensional structure of the water or oil network; contributions from any surfactant film or polymer are marginal. In principle, the location and structure of the polymer in the bicontinuous microemulsion can be examined in a system where all components except the polymer have exactly the same scattering densities $\rho_i$ [with i = *w, o, f, p* for water, oil, surfactant film and polymer, respectively]; i.e., deuterated and protonated contrasts have to be mixed such that $\rho_w = \rho_o = \rho_f \neq \rho_p$. However, since the scattering from such polymer is about 5 orders of magnitude lower than the bulk contrast and 2 orders of magnitude lower than the film contrast scattering (only surfactant protonated) the required perfect match of the scattering length densities of water, oil, and surfactant is practically unfeasible. On the other hand, a careful analysis of data obtained close to matching point yields (among others) the required polymer scattering functions. The scattering intensity $I(Q)$ is given by

$$I(Q) = \sum_{i,j=\{w,f,p\}} (\rho_i - \rho_w)(\rho_j - \rho_w) S_{ij}(Q)$$

where $S_{ij}$ is the partial scattering function of components *i* and *j* which originates from the interference between *i* and *j*. In Eq. (1), water is arbitrarily chosen as the component of the system that is considered as background, and

in this case the relevant partial scattering functions are $S_{o,o}$, $S_{f,f}$, $S_{p,p}$, $S_{o,f}$, $S_{f,p}$, and $S_{p,o}$. Figure 1 presents the partial scattering functions schematically.

The experiments have been performed at the high intensity SANS diffractometer D22. Contrast variation around the two-dimensional matching point was achieved by stepwise increment, adding tiny amounts of protonated decane and protonated surfactant to microemulsions containing fully deutrated water, oil and surfactant and protonated polymer. This measure allowed to vary $\rho_o$ and $\rho_f$ in small but defined steps and produced a set of 15 samples [Fig. 2]. Their scattering data were then used to extract the six partial scattering functions by inserting the measured intensities and the contrasts into Eq. (1) and solving the overdetermined set of equations by singular value decomposition separately for each $Q$ value.

Figure 3a shows the result for the polymer, $S_{p,p}$, and film, $S_{f,f}$, scattering functions. The comparison of the scattering curves indicates that the polymer scattering $Sp,p$ follows the form of $S_{f,f}$ for small $Q$ ($< 0.02$ Å$^{-1}$). This demonstrates clearly that the polymer "decorates" the surfactant film. Because of the dilution of scattering density, however, the corresponding intensity is about 2 orders of magnitude lower than the pure film-contrast scattering. For $Q > 0.03$ Å$^{-1}$, on the other hand, $S_{p,p}$ reflects the scattering from the polymer coils. The solid line in Fig. 2a shows a fit to the Zimm formula [3], which contains the Debye function and includes the effect of second virial coefficient to account the interactions in the interface. Any polymer-polymer aggregation (micellisation) would immediately lead to order of magnitude higher values for $S_{p,p}$ and can be safely excluded. The film- polymer scattering $S_{f,p}$, shown in Fig. 3b exhibits a minimum at $Q \approx 0.03$ Å$^{-1}$, which mainly corresponds to maxima of the polymer density on the film surface normal. The solid line is a fit of the Fourier transform of the monomer density including a $Q^{-2}$ factor to account for the random orientation of the membrane. The fitted average end-to-end radius amounts to 155 Å, which compares quite well with the end-to-end distance $R_{PEO} = 140$ Å as determined from homopolymer solutions; it is much smaller than the average bulk-domain size of 550 Å. The experimental results prove that the polymer is tethered to the interface, and that "mushrooms" formed by the PEP chain in the oil phase and by PEO chain in water are not noticeably influenced by the presence of neighboring membranes.

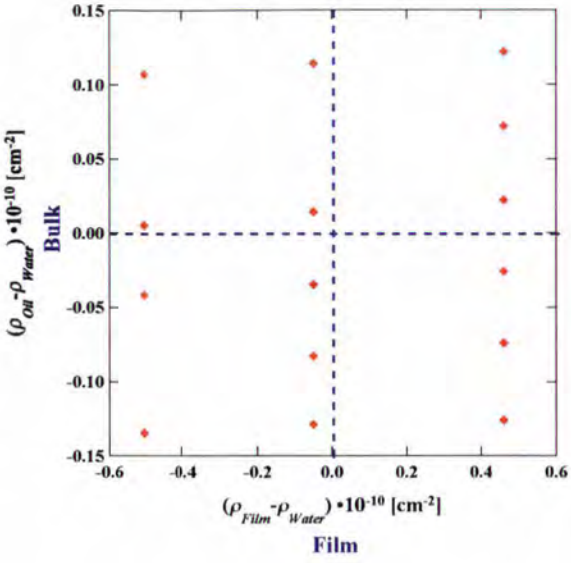


Figure 2: Location of the samples used for the contrast matching experiment in the scattering length density plane ($\rho_o$ - $\rho_w$), ($\rho_f$ - $\rho_w$).

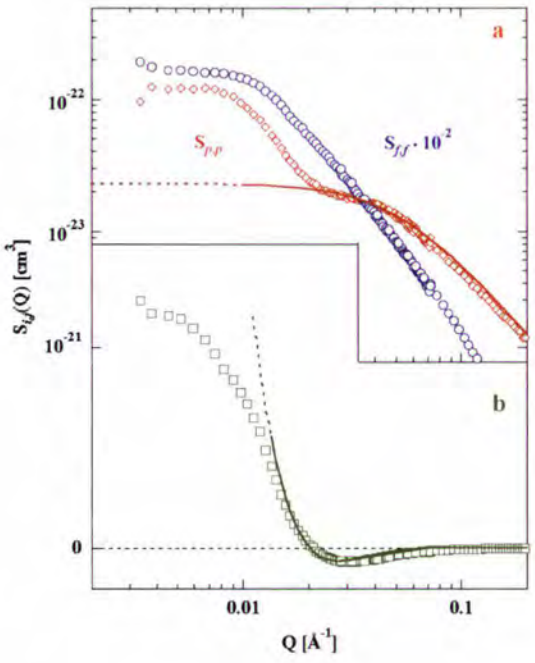


Figure 3: Experimental partial scattering functions. (a) $S_{p,p}$ (◇), in comparison with $S_{f,f}$ (○) and calculated polymer coil scattering (solid line); see text. (b) $S_{f,p}$ (□), which contains the interference between surfactant film and extended polymer layer, and fit to the calculated intensity (solid line) for ideal chains anchored to a planar membrane; see text. Note the linear scale of the ordinate of Fig. 3 (b).

Acknowledgements:
We thank Isabelle Grillo (ILL) for her assistance in performing the measurements at D22.

REFERENCES
● [1] B. Jakobs et al., Langmuir 15, (1999) 6707 ● [2] H. Endo et al., Phys. Rev. Lett. 85, (2000) 102 ● [3] J. S. Higgins and H. C. Benoit, Polymer and Neutron Scattering (Clarendon Press, Oxford, 1994)

# Is the dynamics of counter-ions a probe of the microscopic mechanisms of the electronic transport in conducting polyanilines ?


- D. Djurado, M. Bée (Université Joseph Fourier, Grenoble)
- J. Combet (ILL & Université Strasbourg)
- B. Dufour, P. Rannou, A. Pron, J.P. Travers (CEA-Grenoble)



**Polyaniline, protonated by an organic sulfonic acid, is a new generation of electronic conducting polymers. Stable, conducting, flexible films (conductivity = 150 to 500 S/cm at room temperature) can be cast from a solution. In general, these films exhibit a broad transition from a metal-like regime to an insulating one when the temperature is lowered. The origin of this transition is still debated [1]. Lattice disorder is generally thought to be responsible for this behaviour but the respective roles played by polymer chains and counter-ions in this transition remain unclear. Incoherent neutron scattering techniques have been used in order to study the lattice dynamics without being obscured by the presence of mobile electronic charges. The results suggest that the dynamical disorder of the counter-ions and the metal-like conduction regime are related.**


In the solid state, the system under study consists of polymeric chains separated by acid counter-ion layers (see Fig. 1a). In such systems the possible sources of dynamical molecular disorder are numerous and characteristic times of lattice dynamics may span a wide range of values. By using both the time of flight spectrometer IN6 and the high resolution backscattering spectrometer IN16 it was possible to cover the range of time scales from

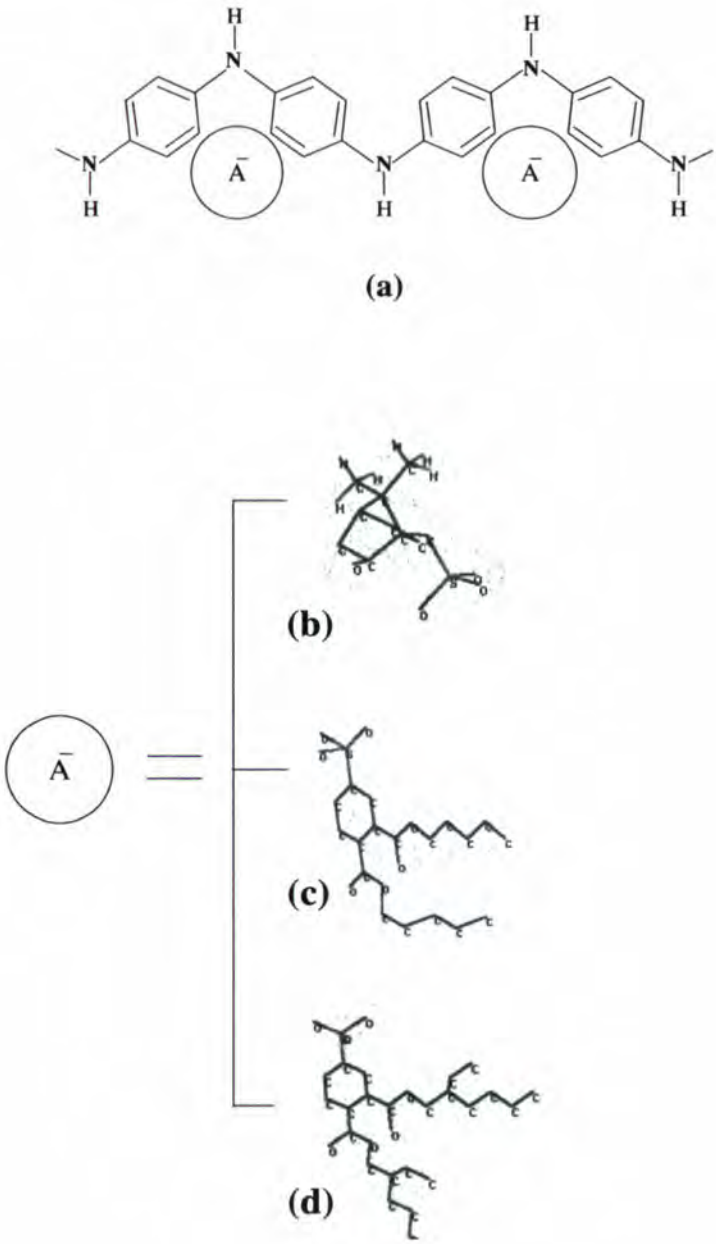


Figure 1: Chemical formula of components of studied compounds. (a) Emeraldine salt conducting form of polyaniline. (b) Camphor sulfonic acid. (c) Di n-pentyl ester of phthalosulfonic acid. (d) Di ethylhexyl ester of phthasulfonic acid.

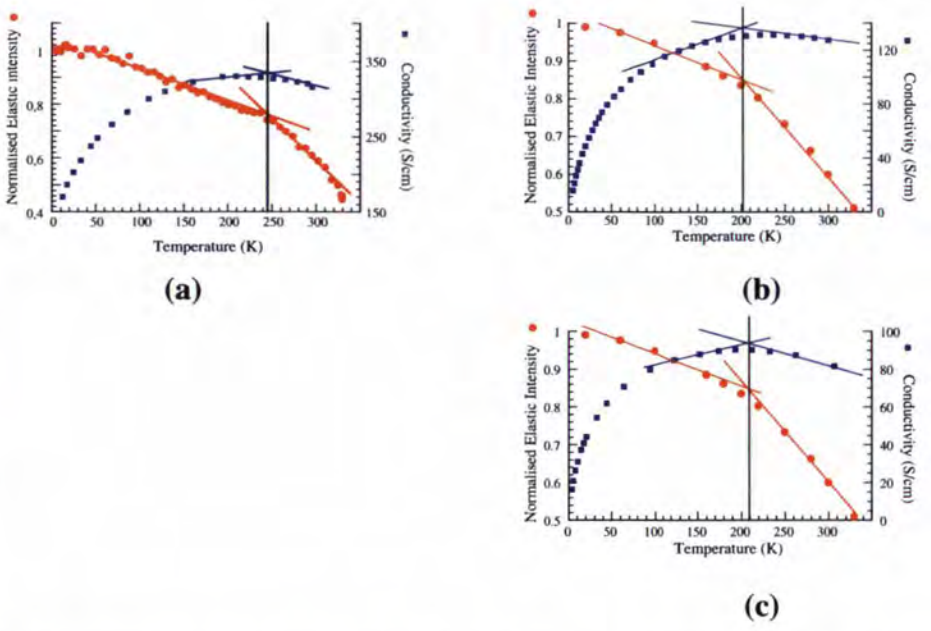


Figure 2: Comparison between thermal variations of electrical conductivity and elastic intensity of (a) polyaniline/camphorsulfonic acid, (b) polyaniline/di n-pentyl ester of phthalosulfonic acid, (c) polyaniline/di ethylhexyl ester of phthalosulfonic acid compounds.

$10^{-9}$ to $10^{-13}$s. In particular, systematic measurements of the elastic intensity have been carried out as a function of temperature. With this method any emergence of diffusive motion in the measuring window is easily detected since it results in a marked lowering of the intensity of the elastic peak. This was readily done on IN16 using the fixed window mode (Doppler drive stopped) while on IN6, scattered intensity in the two channels corresponding to the elastic peak maximum was traced as a function of temperature. Finally, the discrimination between contributions from polymeric chains and from counter-ions was made by comparing the results obtained from fully hydrogenated samples and samples in which the benzene rings of polyaniline chains were selectively deuterated. The different systems we have studied are shown in the Figs. 1 b, c, d.

An initial and somewhat surprising result is that in the whole time range probed in these experiments, the polyaniline chains behave as stiff, non-diffusive vibrating objects. This result has been confirmed by comparing the additional elastic intensity measured with fully hydrogenated samples to that obtained with partially deuterated ones. Accordingly, the whole quasielastic signal was attributed to the dynamics of the counter-ions.
Concerning the camphor sulfonic acid compound (Figs. 1 a & b) two distinct contributions have been found on IN6 and IN16. In the dynamic range of IN6, mainly the motion of methyl groups was observed. Above 300K the rotors could be described as one set of equivalent scatterers but, when the temperature is decreased, the values of correlation times become more and more widely distributed due to the progressive freezing of the molecular environment, which results in energetically inequivalent rotors. Results were successfully modelled with the so-called Rotation Rate Distribution Model developed for methyl groups in amorphous polymers [2]. In addition, the temperature dependence of the elastic intensity measured on IN16 exhibits two inflexion points (Fig. 2a). One is centred at 50 K and is also a signature of methyl group rotation. The second inflexion point is centred at 250 K and reveals the appearance of different dynamics, assigned to a rigid-body motion of the counter-ions. It is significant that the onset of counter-ion motion coincides with the temperature at which the sign of the slope of the conductivity curve is also inverted (Fig. 2a).

The correspondence between electrical and dynamical transitions was further confirmed by the results obtained with the two other compounds shown in figures 1a,c and 1a,d. With these counter-ions, while keeping similar electrical properties, the films exhibit an improved mechanical flexibility [3].

The temperature of the electrical transition is significantly lowered (Figs. 2b and 2c) and the dynamical transition is observed at a correspondingly lower temperature (Figs. 2b and 2c). However, in both of these cases, the dynamical transition is measured on IN6, the thermally activated motion probably being that of protons bound to the aliphatic tails of the counter-ions. The systematic correspondence of the temperature range of these two types of transition strongly suggests that the phenomena are related.

In conclusion, these results shed new light on the key role played by the dynamical disorder of counter-ions in influencing the transport properties in conducting polyaniline. Of course, many questions remain, for example:
i) Are the electronic excitations always confined on vibrating chains whose dynamics are modulated via the interaction with the counter-ions?
ii) In a given range of temperature, is any adiabatic transfer of electronic excitations to the counter-ions possible, as stated in an existing theory [4]?

These experiments have opened a new field of investigation of metal-insulator transitions in disordered, organic systems containing counter-ions. They should stimulate new theoretical studies, even if a detailed description of the microscopic interplay between the chains and the counter-ions is currently lacking.

**References**

• [1] see T.A. Skotheim, R.L. Elsenbaumer, J.R. Reynolds (eds), Handbook of conducting polymers, Marcel Dekker Inc. (1998) p. 27 and p. 85 • [2] R. Mukhopadhyay, A. Alegria, J. Colmenero, B. Frick, Macromolecules 31 (1998) 3985 • [3] T.E. Olinga, J. Fraysse, J.P. Travers, A. Dufresne, A. Pron, Macromolecules 33 (2000) 2107 • [4] L. Zuppiroli, M.N. Bussac, S. Paschen, O. Chauvet, L. Forro, Phys. Rev.B 50 (1994) 5196

# Quantum states of the neutron in the gravitational field


- V.V. Nesvizhevsky, A.K. Petukhov, H.G. Börner (ILL)
- H. Abele, S. Baessler, N. Haverkamp, F.J. Ruess, T. Stöferle, A. Westphal (University Heidelberg)
- A.M. Gagarsky (PNPI, Gatchina)
- A.V. Strelkov (JINR, Dubna)



**100 years ago, Max Planck introduced the concept of minimal energy quantum, which can be transmitted through physical interactions. Soon it became evident that quantum (discrete) properties of matter are dominant in a variety of phenomena: quantum states of electrons in an electromagnetic field are responsible for the structure of atoms, quantum states of nucleons in a strong nuclear field are responsible for the structure of atomic nuclei. An example for quantum effects in the weak interaction is the possible neutrino oscillations. We report here on the first observation of quantum states of neutrons in the gravitational field.**


The Pauli principle couples the Planck constant to the minimum values of the distance $\Delta z$ and the velocity $\Delta V$ at which the quantum phenomena become dominant for the particle with the mass $m$: $\Delta z \Delta V \sim \hbar / m$ ($\Delta V << c$). The smaller are $m$ and $\Delta V$, the larger is $\Delta z$. When the particle is placed in a potential well during a time period longer than $\Delta \tau \sim \hbar / \Delta E$, quantum states with an energy difference $\Delta E$ can be resolved. In order to allow for an experimental observation, all other interactions must be so small that their interference with the gravitational quantum phenomena can be neglected. The choice of a neutron, a neutral long-lived particle, satisfies the above mentioned conditions.

To our knowledge, the Planck constant and the neutron acceleration in the gravitational field have been considered simultaneously only in few papers (see for instance [1,2,3]). As pointed out in Ref. [4], it is possible to observe quantum states of neutrons in the Earth's gravitational field. Earlier, a complete analytical solution of the mathematical problem related to the quantum states of particles in a gravitational field was published in textbooks on quantum mechanics (see, for instance [5,6]). Ultracold neutrons provide a convenient method for such a study [7,8]. The experimental technique using ultracold neutrons was developed during the last 30 years. Recently a one-component neutron gravitational spectrometer of high resolution was built at the ILL [9]. The first measurement at the ultracold beam of the ILL [10] with this device showed the existence of the lowest neutron quantum state but hinted also to the potential for further investigations [11]. When neutrons with extremely low energy fall down in the Earth's gravitational field – above a reflecting mirror – then they do not move continuously along the vertical direction: they must fall in quantum bound states because they experienced a deep and wide potential well. Obviously, the Earth's gravitational field alone does not create such a potential well as it does not allow particles only to move upwards too high; the other wall of the well is obtained by introducing a horizontal reflecting mirror. A description of the interaction of neutrons with surface can be found in textbooks on neutron physics (for instance [12,13]). As in such a situation no forces act in the horizontal plane, quantum states can only be observed in the vertical direction.

Figure 1 illustrates how quantum states of neutrons in the Earth's gravitational field can be observed. The neutron wave is reflected from the bottom mirror and interferes with itself. Such self-interference provides a standing wave of neutron density. In a vertical slice, the neutron beam above the bottom mirror consists of plane neutron "jets" with a neutron density which varies with the vertical distance from the mirror.

One lets neutrons "flow" with a certain horizontal velocity distribution through a slit. An absorber/scatterer placed above the incident

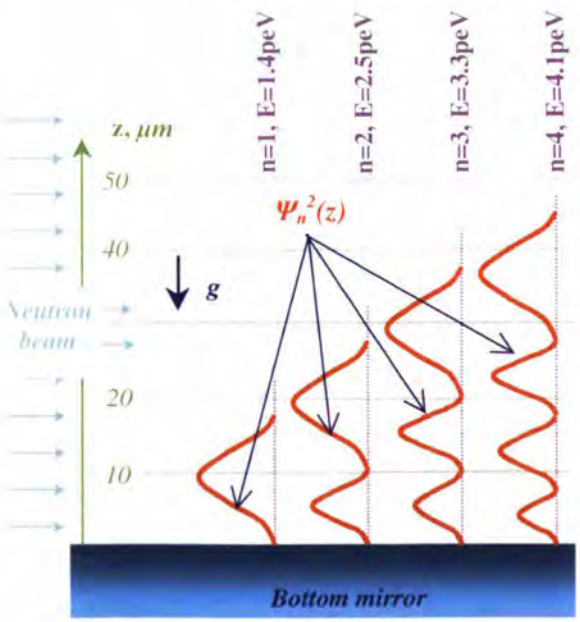


Figure 1: Quantum states of neutrons are formed in the potential well between the Earth's gravitational field on top and the horizontal mirror on bottom. The probability of finding neutrons at the height z, corresponding to the $n^{th}$ quantum state, is proportional to the square of the neutron wave function $\psi_n^2(z)$. The vertical axis z gives an idea about the spatial scale of this phenomenon.

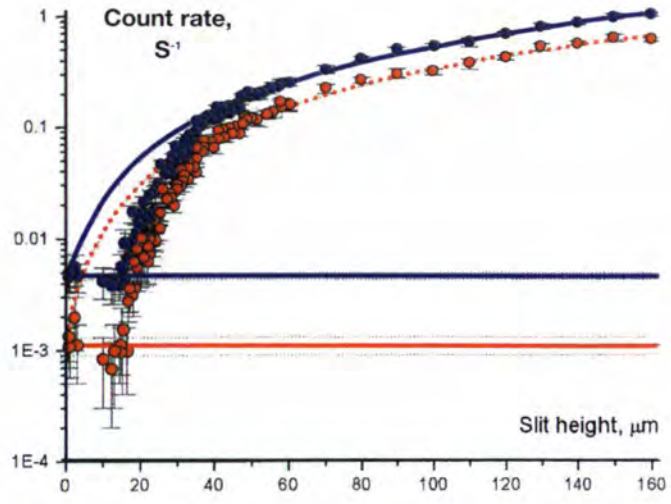


Figure 2: The count rate versus the slit height measured with a low-background gaseous $^3$He neutron detector. Blue circles show the data measured in the broad discrimination window of the detector signal. Solid blue curve is the classic $N \sim \Delta h^{1.5}$ fit for these data. Red circles correspond to the data measured in the narrow "peak" discrimination window. Dotted red curve is the corresponding classic fit. Horizontal straight lines show the detector background values and their uncertainties measured with the reactor "off".

neutrons and the reflecting mirror below act as a selector for the vertical velocity component. From Fig.1 we expect a stepwise dependence of the neutron flux as function of the height of the absorber: if its height is smaller than the spatial width of the lowest quantum state, then the neutron transmission should be zero. When the height is equal to the spatial width of the lowest quantum state then the transmission is expected to increase sharply. The height of such a step is equal to the first state population. Further increase in the absorber height should not increase the neutron transmission as long as the height is smaller than the spatial width of the second quantum state. Then again the transmission should increase stepwise. At sufficiently high absorber position one should approach the classical dependence and the stepwise increase should be washed out. Measurements at small absorber height showed the existence of the lowest quantum state; at sufficiently large absorber height the purely classical behavior is observed (Fig. 2) [11].

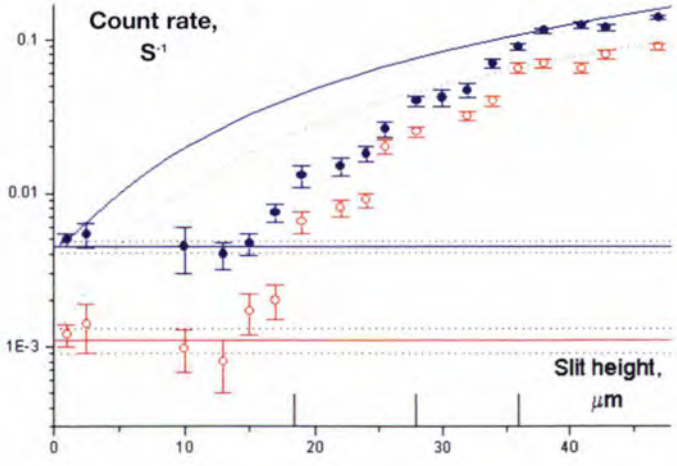


Figure 3: The dependence of the count rate versus the slit height. The data are summed up in intervals of 2μm. Solid and open circles and lines as well as the horizontal straight lines are analogous to those in Fig. 2. Vertical lines correspond to the height values, at which approximately a next step in the count rate is predicted by calculation.

The observed effects are consistent with the non-transparency of the slit formed by the bottom mirror and the absorber/scatterer for neutrons as long as the slit height is smaller than the spatial width of the lowest quantum state. Careful analysis of the experiment allowed to rule out any systematic errors. In particular, the shape of the transmission curve (Figs. 2,3) does not depend on the value of the horizontal velocity component but it depends only on the vertical velocity component, as expected. A 15 μm-wide slit is not yet transparent for neutrons but it is sufficiently large to observe its transparency for visible light. This is a good check of the setup as the light wavelength of ~0.4μm is much larger than the neutron wavelength of ~0.01μm . Evidently, the difference results from the fact that under normal laboratory conditions the Earth's gravitational field does not act noticeably on light beams but forms bound quantum states for neutrons.

Figure 3 shows in a larger scale and with additional statistics the initial part of the dependence analogous to Fig. 2. One can even notice here indications of the stepwise character of such a dependence not only for the lowest quantum level.

This first experimental observation of quantum state in the gravitational field showed once again the universality of the quantum properties of matter. As the parameters of quantum states are defined in such a system mainly by the interaction of the neutron with the gravitational field, the presented phenomenon can be considered as a tool for further investigations of fundamental properties of matter.


REFERENCES

● [1] R.A. COLELLA ET AL., PHYS. REV. LETT. 34 (1975) 1472 ● [2] V.G. BARYSHEVSKII ET AL., PHYS. LETT. A 153 (1991) 229 ● [3] A.I. FRANK, SOV. PHYS. USP. 34 (11) (1991) 980 ● [4] V.I. LUSCHIKOV AND A.I. FRANK, JETP LETT 28(9) (1978) 559-561 ● [5] L.D. LANDAU AND E.M. LIFSHITZ, IN QUANTUM MECHANICS, PAR. 28 (1963) ● [6] S. FLUGGE, IN PROBLEMS IN QUANTUM MECHANICS, PROBL. 40 (1971) ● [7] V.I. LUSCHIKOV ET AL., JETP LETT. 9 (1968) 40-45 ● [8] A. STEYERL, PHYS. LETT. 29B (1969) 33 ● [9] V.V. NESVIZHEVSKY ET AL., NIM 440(3) (2000) 754-759 ● [10] A. STEYERL ET AL., PHYS. LETT. A (1986) 347 ● [11] V.V. NESVIZHEVSKY ET AL., SUBMITTED TO PHYSICS LETTERS, ALSO IN ISINN-8, DUBNA (2000) ● [12] V.K. IGNATOVICH, "PHYSICS OF ULTRACOLD NEUTRONS", 1986 ● [13] R. GOLUB ET AL., "ULTRACOLD NEUTRONS", 1991

# Phase coexistence and phase transitions in finite nuclei


- R.F. CASTEN, V. ZAMFIR, M. CAPRIO (YALE UNIVERSITY)
- H.G. BÖRNER, M. JENTSCHEL, H. LEHMANN (ILL)


**Data from GRID measurements at the ILL, Grenoble, complemented by other measurements at Yale and Köln, are leading to a new understanding of structural evolution in nuclear systems. This work has raised the possibility that finite nuclei evolve in ways very close to those of systems showing real phase transitional behaviour, with coexisting phases, critical points, and order parameters.**

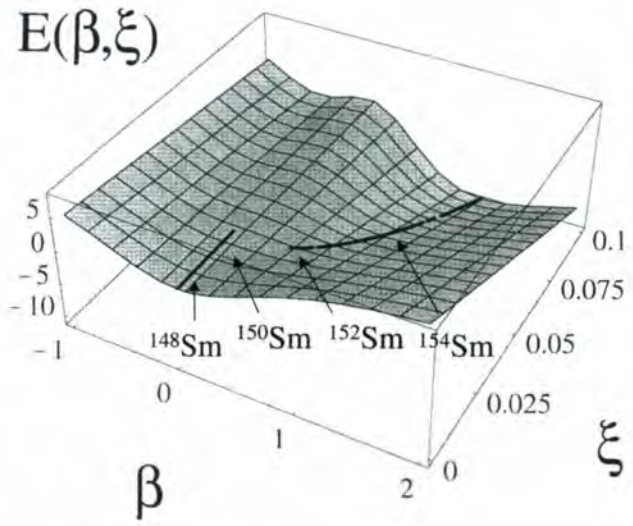


Figure 1: Energy surface in the Interacting Boson Model as a function of a phase transition parameter ξ, showing the discrete jump in β [5]. The positions of different Sm isotopes in the parameter space are also illustrated.

The nature of collectivity and coherence in nuclei and their evolution with proton and neutron number is one of the most fundamental issues in nuclear structure. Although nuclei can change properties rapidly with changes in the number of their constituents, phase coexistence and phase transitions, as a function of nucleon number, in the condensed matter sense of these concepts, have generally been discounted in finite nuclei. However, recent studies [1,2] mark a significant change in this situation: they have revealed that $^{152}$Sm is a rare example of phase coexistence with a deformed ground state and a more spherical set of vibrator-like excited states. This phenomenon differs from that of intruder states, as seen in Cd, Hg, and Pb nuclei in that both sets of shape coexisting states arise from a single set of basis states, that is, a single Hilbert space.

To further map out the phase transition, we have carried out GRID studies of lifetimes with GAMS 4 Spectrometer in $^{152}$Sm and in the spherical neighboring nuclei $^{148,150}$Sm. In the GRID technique [3] the lifetime of a nuclear state is obtained by an analysis of the Doppler broadening of a deexcitation γ-ray transition: highly excited nuclei are produced by thermal neutron capture. Those deexcite to lower energy states via emission of γ-quanta which induce a recoil to the nuclei. The excited atoms move in the bulk of the target material and are slowed down by collisions with the surrounding atoms. Meanwhile the still excited atomic nuclei deexcite by secondary γ emission. The probability of these emissions depends on the ratios ($t/\tau$) where t is counted from the emission of γ's inducing the recoil and τ is the lifetime of the intermediate state. If the nucleus is in motion when it deexcites ($t \approx \tau$) the γ-ray energy will be Doppler-shifted. If it is stopped, the normal transition energy will be measured. The Doppler effects are on the order of eV. Thus the γ-ray, typically with energy ~1 MeV, must be detected with a resolution of $\Delta E/E \approx 10^{-6}$, three orders of magnitude better than obtainable with the usual Ge semi-conductor detectors. Fortunately this is feasible for the GAMS4 and GAMS5 crystal spectrometers. The lifetimes τ of the excited states are directly related to absolute transition rates: The probability for the decay of an excited state is proportional to the square of the matrix element of the transition operator between the initial and final state wave functions.

An extensive set of about 50 new transition rates were measured for the first time and they provide a critical basis for evaluating the structure in this phase/shape transition region. In Fig. 2 is shown a typical example for a GRID profile. These results alter in a significant way our understanding of how collectivity and deformation develop in certain regions of nuclei. Instead of a gradual softening of the

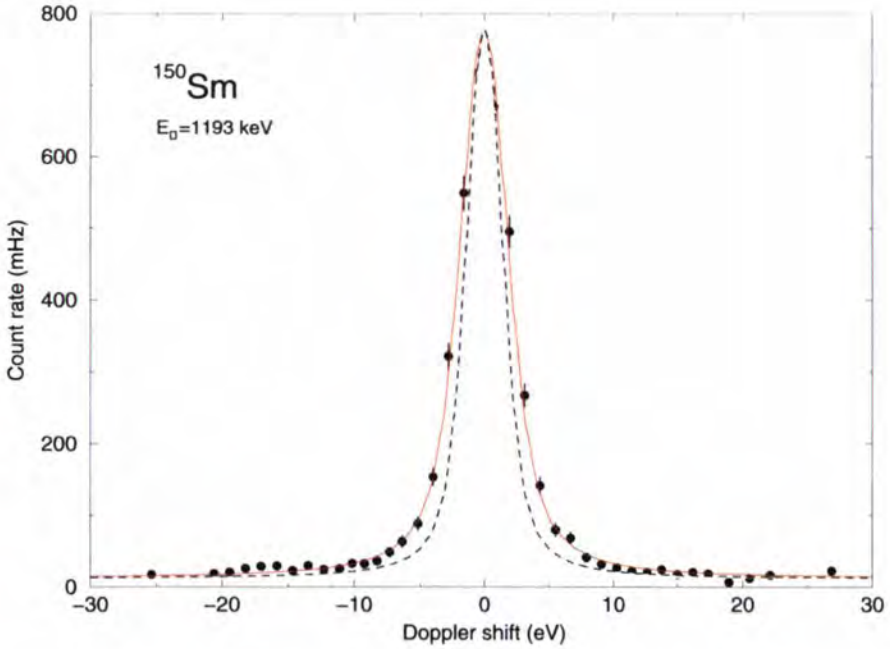


Figure 2: Example for a GRID profile: The 1193 keV $2^+_3 \rightarrow$ g.s. transition in $^{150}$Sm. The dashed line is the instrumental response, the full line is the fitted GRID line shape. The lifetime deduced from the fit is ~ 0.5 ps.

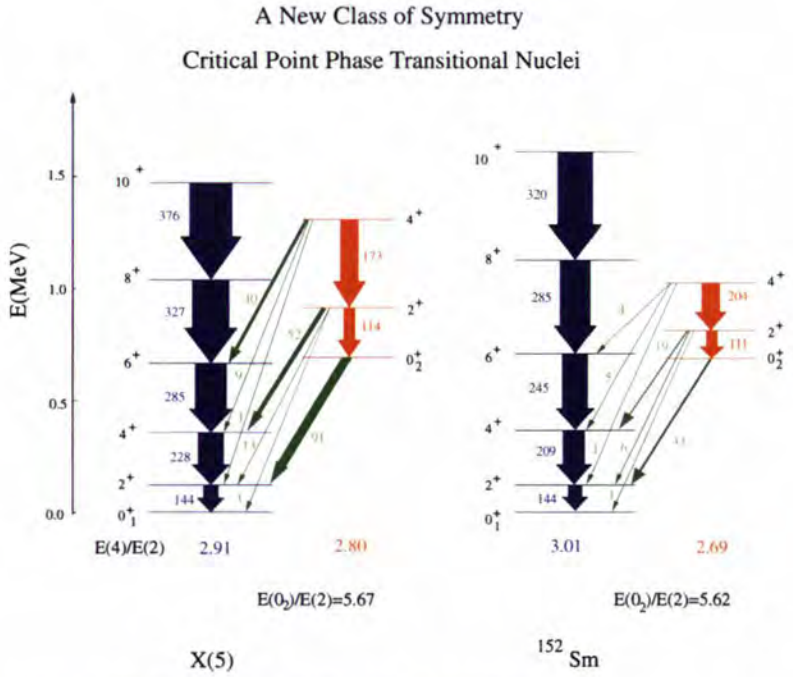


Figure 3: Comparison of X(5) and the data for $^{152}$Sm (based on ref. [9]).

nucleus to deformation as valence nucleons are added, the nucleus remains essentially spherical in going away from closed shells, albeit developing greater anharmonicities, until enough correlations build up that the nucleus 'snaps' to a deformed structure [4,5]. Geometrically, the deformation variable $\beta$, which describes the magnitude of ellipsoidal deformation, is 'bi-valued': either ~ 0 or fairly large, without a transitional region in between (Fig.1). The physical picture is that of a crossing of two potential energy surfaces, with spherical and deformed minima. The phase transition occurs at the crossing point of two intrinsic excitations. The mechanism seems to resemble a Jahn-Teller symmetry breaking in favor of the lower symmetry deformed state.

Interestingly, this feature appears in collective models such as the Interacting Boson Model or Geometric Collective Model, although it corresponds to a miniscule portion of their respective parameter spaces and was unrecognized before these structures motivated its discovery in the model framework. These results have directly inspired the theoretical development of a new class of dynamical symmetry for nuclei, the first dynamical symmetry applicable at a critical point itself, where structure is changing most rapidly [6].

There are two possibilities for this new class of symmetry, one describing a transition from a vibrator to a deformed $\gamma$ - unstable structure and the other a vibrator to axially symmetric transition region. These critical point symmetries are the first entirely new paradigms for the structure of atomic nuclei since the 1950's. Their empirical discovery has relied in a significant way on GRID data from the ILL. The first symmetry [6], called E(5), has been found [7] to exist empirically in $^{134}$Ba. The second symmetry [8], X(5) is manifested [9] in $^{152}$Sm as shown in Fig. 3. New GRID data will further test these ideas in this region. This new type of symmetry should have applications in other mesoscopic systems.


**References**

● [1] R.F. Casten et al., Phys. Rev. C57 (1998) R1553 ● [2] N.V. Zamfir et al., Phys. Rev. C60 (1999) 054312 ● [3] H.G. Börner and J. Jolie, J. Phys. G 19 (1993)217 ● [4] F. Iachello, N.V. Zamfir, and R.F. Casten, Phys. Rev. Lett. 81 (1998) 1191 ● [5] R.F. Casten, D. Kusnezov, and N.V. Zamfir, Phys. Rev. Lett. 82 (1999)5000 ● [6] F. Iachello, Phys. Rev. Lett. – 85 (2000) 3580 ● [7] R.F. Casten and N.V. Zamfir, Phys. Rev. Lett. – 85 (2000) 3584 ● [8] F. Iachello, to be published ● [9] R.F. Casten and N.V. Zamfir, to be published

## Preface

The following three articles reflect the growing use of numerical methods, based on modelling atom-atom interactions, in the analysis of experimental data. Once the model of interacting atoms has been shown to reproduce the existing experimental data, it can then be used to predict physical properties or effects, which are difficult to observe directly in measurements. Neutron scattering data lends itself particularly well to such numerical modelling since the neutrons are scattered principally by nuclei. It is sufficient, therefore, to determine the trajectories of nuclei, which can be done without recourse to the electronic structure, as in force-field based methods. However, in certain cases the electrons must be treated explicitly, using quantum chemistry techniques, in order to obtain more accurate results. A collection of twenty research articles in the field of neutron scattering and numerical modelling has recently been published in a special issue of Chemical Physics (vol. 261 nos. 1-2 (2000) Eds. M.R. Johnson, G.J. Kearley and J. Eckert). Nearly forty shorter articles can also be found in the proceedings of an ILL workshop (AIP conference proceedings 479 (1999) Eds. M.R. Johnson, G.J. Kearley and H.G. Büttner).

# Probing host-guest interactions in zeolites: a diffraction and molecular modelling study


- C. Baehtz, H. Fuess (TU-Darmstadt)
- M. Johnson, A.W. Hewat (ILL)



**Powder diffraction, Fourier analysis and Rietveld refinement were performed to localise guest molecules in mesoporous zeolites [1]. We are investigating 7,7,8,8-tetracyano-p-quinodimethane (TCNQ) and tetrathiafulvalene (TTF) separately and as a charge transfer complex in faujasite NaY (high sodium content) and HY (low sodium content). Diffraction patterns were recorded at 5 K at the neutron powder diffractometers D1A and D2B. Experimental results were compared with force-field-based adsorption simulations, modelling directly the host-guest interactions, for the NaY host.**


Interest in host-guest-systems has increased in the last few years, due to their potential applications in the field of sensors, gas separation and heterogeneous catalysis [2]. Also dyes are incorporated into mesoporous crystals. We have focussed on the nature of the binding of the guests in the host lattice, which is a basic question for the understanding of the host-guest interactions of these systems. TCNQ and TTF are model substances for the investigation of binding sites in zeolites.

The crystal structure of the host remains unchanged when guest molecules are incorporated, only the relative intensities of reflections at low scattering angle (< 60°) in the powder diffraction pattern change (Fig. 1). From these intensity changes, the non-zeolite framework scattering densities are extracted by difference Fourier analysis and reveal the positions of the adsorbed molecules. The position, orientation and occupancy (7 parame-

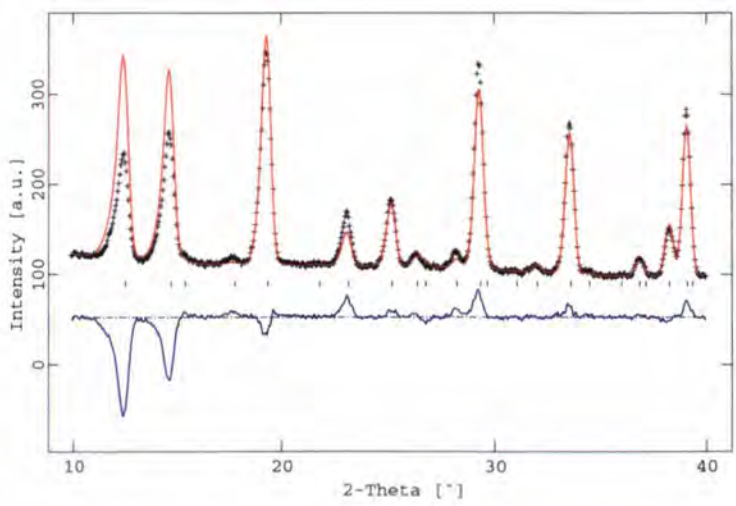


Figure 1: D1A diffraction data of TTF in the NaY zeolite (black crosses). The red curve is a fit to the bare zeolite pattern, the scattering densities for TTF are determined from the blue difference curve.

ters) of rigid guest molecules are then refined by the Rietveld method, introducing a minimum number of additional parameters (6). The NaY and HY zeolites show identical crystal structures but with different sodium content. The sodium content of HY at position II in the crystal structure, which is accessible for the guest, is 42% of the corresponding NaY.

Figure 2 displays the arrangement of TCNQ in the framework (yellow) of NaY and HY. The molecule is in the centre of a 12-ring window, which connects two supercages of the zeolite pore system. The cyano-groups point into these two cages and are coordinated to the sodium cations (pink) in front of the small 6-ring windows, the distance between sodium and nitrogen is 2.7 Å. The dimension and the high symmetry of TCNQ are such that the molecule fits precisely into this position. Such a 4-fold coordination of a guest to a zeolite framework has not been reported in literature before.

Adsorption simulations using the 'sorption' module in the Cerius$^2$ molecular modelling package and the Burchardt-Universal-Force-Field confirmed this binding site to be the most stable. For a rigid molecule adsorbate and a rigid zeolite framework, binding sites are probed randomly in the free volume of the cage using a Monte Carlo algorithm. Binding energies are determined in this way from Van der Waals and Coulomb interactions.

Although TTF and TCNQ have similar molecular dimensions, the binding of the two molecules in NaY is somewhat different. By simultaneous crystal structure refinement of the zeolite with one TTF molecule per super-cage, using neutron and synchrotron radiation diffraction patterns, a distribution of TTF sites, giving rise to good R-factors, is proposed. These sites have TTF in the super-cage with two sulphur atoms pointing to the cation in front of the 6-ring window (Fig. 3). The distance between the centre of mass of TTF and this cation varies between 3.5 and 4.4 Å, the rotation about the long molecular axis is also not well defined.

Again simulations give similar results, simulated adsorption giving a range of almost energetically degenerate sites. However, a coordination of all 4 sulphur atoms of TTF to the sodium with slightly lower sorption energy is

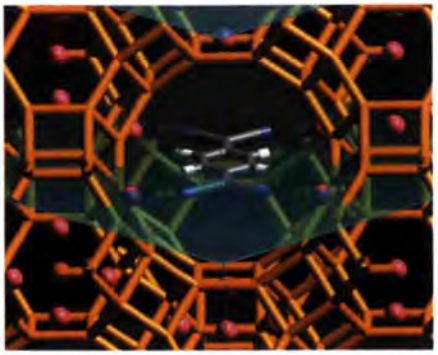

Figure 2: TCNQ in the 12-ring window of the NaY and HY framework: Na=pink, C=grey, H=white, N=blue; (200)-plane=blue.

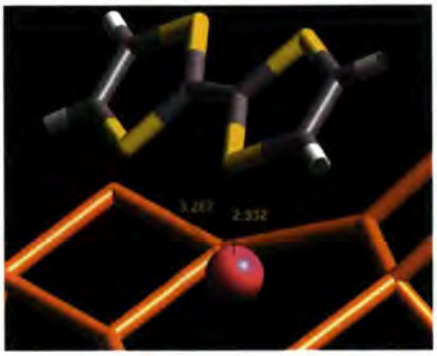

Figure 3: TTF in front of a sodium cation of the NaY and HY framework: Na=pink, C=grey, S=yellow, H=white.

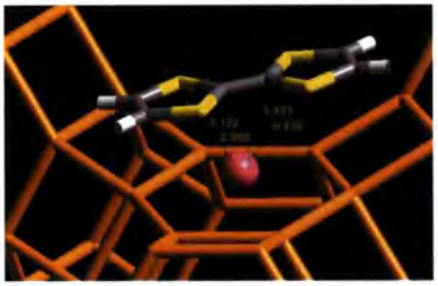

Figure 4: Second arrangement of TTF in the NaY framework: Na=pink, C=grey, S=yellow, H=white, found by simulation.

also observed (Fig. 4). This binding geometry was not obtained in the original refned set of binding sites, but retrospectively the diffraction data does not rule-out its existence. Simulations also confirm that the different nature of the binding of TTF and TCNQ arises from separation of the electronegative atoms which co-ordinate to the Na cations; 3.2 Å for TTF and 8.3 Å for TCNQ on the long molecular axis.

When the charge-transfer-complex of TCNQ and TTF is adsorbed in NaY, the two-molecule complex is distorted so that the guests are found in the positions as described above. So the intermolecular interactions between the guests are weaker than the host-guest-interactions. The complex could not be incorporated in the HY zeolite, because of its lower sodium concentration, only TTF penetrates into the pore system.

The overall agreement between experiment and adsorption simulation validates the force field used, in the rigid molecule approximation, and gives an energy-based confirmation of the diffraction results. The simulations also offer more information in the more difficultly determined binding sites of TTF. In principle, additional information concerning the deformation of the guest molecule and the host matrix could also be sought by unconstrained geometry optimisation in the simulation. However, UV spectroscopy reveals, through shifts in vibrational frequencies, significant modification of the molecule and host matrix electron densities on binding, which would not be well-modelled by force-field simulations. Changes in molecular geometry on binding are therefore not expected to be reproduced accurately using force-fields. Similarly, since the charge distribution of the guest molecules changes when forming the charge transfer complex and the lifetime and degree of electron transfer is unknown, no adsorption simulations of the complex were performed. Such electronic effects can only be investigated using quantum chemistry (QC) methods, which are typically employed following a force-field investigation. The size of the zeolite unit cell (15000 Å$^3$) presents a problem for solid state QC calculations and a more limited model of the binding sites would have to be constructed. Finally, the knowledge of the adsorption site of the guest molecules is the basis for the understanding of spectroscopic results [3]. Henceforth, this force field can be employed to model the dynamics of guest molecules in zeolite cages [4], which have an obvious importance, for example, in gas separation processes.


REFERENCES

• [1] H. KLEIN, C. KIRSCHHOCK, H. FUESS, J. PHYS. CHEM. 98 (1994) 12345-12360 • [2] D. WOEHRLE AND G. SCHULZ-EKLOFF, ADV. MATER. 6 (1994) 875-880 • [3] H. FÖRSTER ET AL. PHYS. CHEM. CHEM. PHYS. 1 (1999) 593-603 • [4] H. JOBIC AND M. BÉE, ILL ANNUAL REPORT 1997, P.16

# Dynamics of plastic crystals : a combined computer simulation and quasielastic neutron scattering analysis

J. COMBET, A. MARTIN
(ILL & UNIVERSITÉ STRASBOURG)

**Molecular dynamics simulation is a powerful technique for determining the structural and dynamical properties of molecular compounds. Molecular modelling and neutron scattering are complementary methods since they probe similar length and time scales (Å and ps-ns). Detailed analysis of the calculated trajectories enables to predict neutron scattering intensities. Thus, a comparison with experimental spectra provides a means for testing the accuracy of theoretical description. This report presents a molecular dynamics simulation performed on two plastic phases of a molecular compound: the norbornane.**

## The norbornane plastic crystal

Globular molecules often form plastic crystal below the melting point. These phases exhibit a high degree of disorder: while the centre of mass is rather well localised in space, the orientation varies from one site to another and changes with time. When the temperature is decreased, these substances exhibit one or several solid-solid transitions into a fully well ordered crystalline phase.

Norbornane (Fig. 1) is a simple bridged molecule and has been considered as a key compound for strained materials. This system is orientationally disordered at ambient temperature, transforming from cubic to hexagonal at 306 K and to a ordered monoclinic phase at 131 K.

The dynamics of norbornane in its two disordered phases has been extensively studied by NMR and incoherent quasielastic neutron scattering. Motions have been described as rapid isotropic reorientations. Long-range diffusion was also evidenced on a slower time scale. We have started molecular dynamics simulation in order to get a more accurate description of the dynamical properties of this compound, including greater insight into the phase transitions.

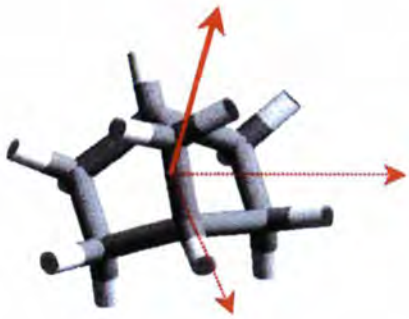

Figure 1: The molecular geometry of norbornane ($C_7H_{12}$), or bicyclo [2,2,1] heptane. The full arrow represents the axis of the dipole moment.

## Dynamical Simulations

We have used the COMPASS empirical force field implemented in the CERIUS2 package in order to simulate molecular dynamics. One week of calculation was needed to simulate around 200 ps on a biprocessor Silicon Graphics workstation (Origin 200).

Simulations were first realised in the NPT ensemble (constant number of molecules, pressure and temperature) to determine the evolution of the lattice parameters at different temperatures. The initial unit cell configuration was generated from the well-ordered, low temperature, monoclinic structure determined by X-ray powder diffraction [1]. The simulation box contained 27 unit cells and periodic boundary conditions were used in order to mimic an infinite crystalline environment.

The temperature was increased from 50 K to 320 K using 20 K steps. About 100 ps were simulated for each temperature in order to get a correct equilibration of the system. Lattice parameters extracted from these simulations exhibit high modifications around 155 K. The monoclinic ordered phase rapidly transforms toward a disordered hexagonal phase. This corresponds to the first order-disorder phase transition experimentally observed at 131 K. This very encouraging result indicates that the intermolecular interactions could be well represented by the COMPASS force field.

We also started NVT ensemble simulations (constant number of molecules, volume and temperature) in the two plastic phases in order to generate the molecular trajectories. The comparison with experimental quasielastic neutron scattering experiment was performed with the *n*MOLDYN package [2].

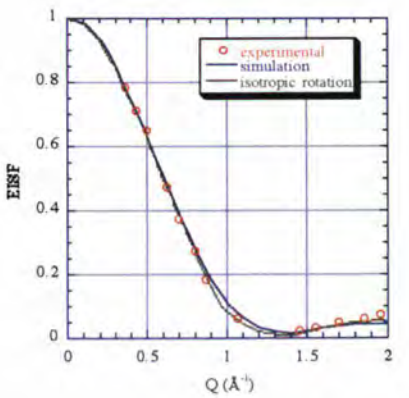


Figure 2: Experimental EISF extracted from IN6 experiment (similar in both plastic phases), simulated EISF extracted from the trajectories analysis (identical for both plastic phases), and theoretical evolution in case of isotropic rotation.

## Simulation analysis and neutron scattering

The simulation results were compared with the measurements performed at ILL on IN6 [3]. The trajectories analysis enable the EISF (Elastic Incoherent Structure Factor) to be extracted. This quantity is determined by the probability distribution of the hydrogen atoms, and thus provides a detailed description of the geometry of the motions. EISF are represented on Fig. 2.

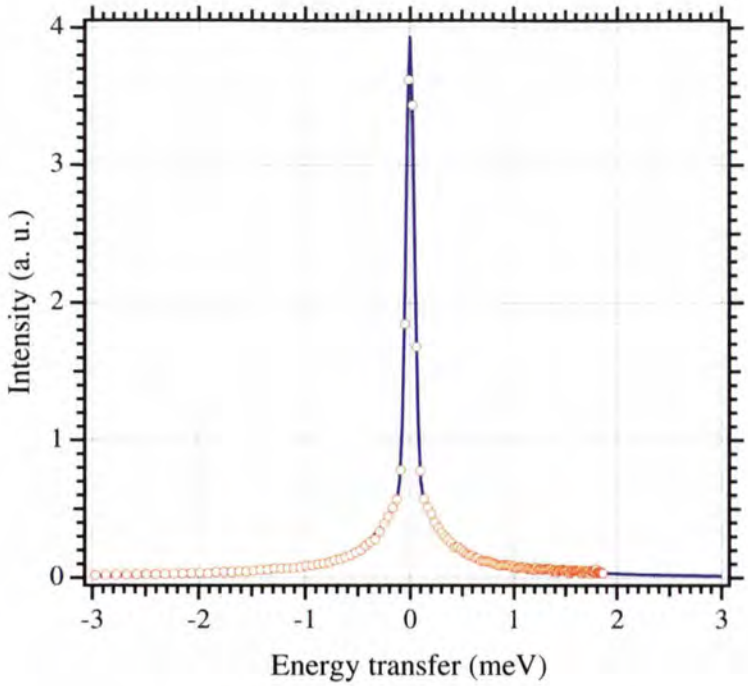


Figure 3: Comparison between experimental spectra and dynamical structure factor extracted from the molecular dynamics simulation in the cubic disordered phase ($Q = 0.7$ Å$^{-1}$)

The simulations are clearly able to explain the experimental evolution of the EISF. The small differencies observed between the isotropic rotation description and the simulated dynamics could be explained by the existence of preferential orientations and needs a careful investigation of the simulated trajectories.

phase. The excellent agreement definitively demonstrates the validity of the simulations and the accuracy of the empirical force field. The detailed analysis of the computed trajectories allowed the orientational distribution to be probed. Figure 4 represents the results for the dipole moment axis represented in Fig. 1

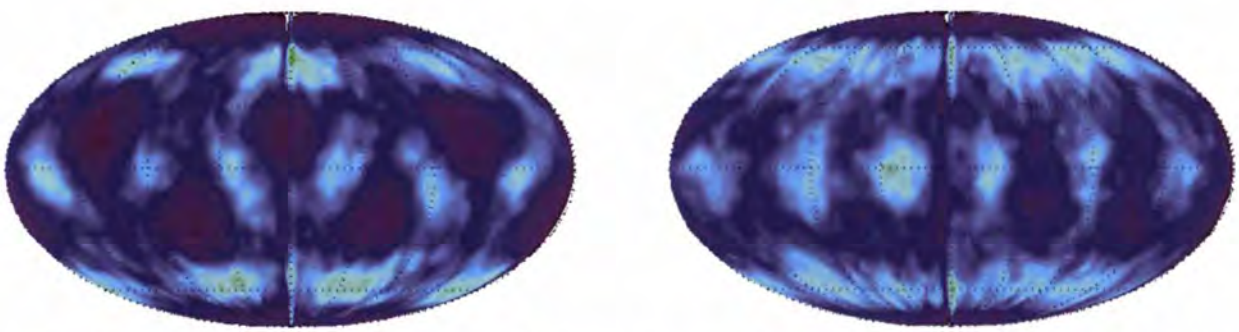

Figure 4: 2D representation of the orientational distribution of the molecular symmetry axis (representations realised with LAMP, the Large Array Manipulation Programme developed at the ILL). Left side: cubic phase, right side: hexagonal phase. Light blue spots indicate the occurrence of preferential orientations.

The EISF only gives geometrical information on the molecular motions. A more stringent test of the simulation involves comparing the experimental spectra with the dynamical structure factor extracted from the trajectories. Figure 3 represents the experimental and simulated spectra in the cubic disordered

for both plastic phases. Although the simulations are unable to reproduce directly the high temperature phase transition, stable simulations in the hexagonal and cubic phases show clearly broad maxima, indicating the existence of preferred orientations. The dynamics of norbornane molecules is therefore more complex than simple isotropic reorientation and the orientational distributions are different in each phase. Spectroscopic and diffraction measurements have been unable to detect these differences.

Molecular dynamics simulations is a powerful method for the description of structure and dynamics in molecular compounds. Combined studies with quasielastic neutron scattering experiments enable the same quantities to be probed, and thus offer a unique way to validate the simulations and, thereafter, exploit the wealth of microscopic information available from the simulation model.


**References**

• [1] A. N. Fitch and H. Jobic, J. Chem. Soc., Chem. Commun. 1993, 1516-1517 • [2] G. R. Kneller, V. Keiner, M. Kneller, M. Schiller, J. Comput. Phys. Commun. 23 (1977) 327 • [3] M. Bée, H. Jobic and C. Caucheteux, J. Chim. Phys. 83 (1986) 623

# Proton vibrational dynamics in nucleic acid building blocks

N. Leulliot, M.P. Gaigeot, M. Ghomi
(University P. & M. Curie, Paris)

H. Jobic
(Institut de Recherche sur la Catalyse, Villeurbanne)

**Inelastic neutron scattering (INS) spectra of two major RNA (RiboNucleic Acid) building blocks, i.e. adenosine (rA) and guanosine (rG), as well as those of two major DNA (DeoxyriboNucleic Acid) building blocks, i.e. 2'-deoxycytidine and 2'-deoxythymidine, have been recorded in solid phase at T = 15 K using the IN1-BeF spectrometer. These spectra gave us the opportunity to perform theoretical investigations at the density functional theory (DFT) level in order to access both geometrical and vibrational features of these molecular compounds. The joint use of INS spectra and ab initio calculations allowed us to particularly probe the hydrogen vibrational dynamics of the nucleic acid building blocks, and to analyse the effect of solid phase intermolecular H-bonding. This set of information is not accessible by traditional optical spectroscopy, i.e. Raman scattering and IR absorption.**

The knowledge of the structure of biological molecules is an important task in order to understand their functions. Nucleic acids (DNA and RNA) are linear polymers (Fig. 1a) which take part in various biological processes such as replication (DNA to DNA), transcription (DNA to RNA), translation (DNA to protein) and catalysis (RNA splicing or self-splicing). Nucleic acids have a great conformational flexibility and can adopt a variety of conformations (double-helices, hairpins, bulges, etc). The chemical repeat of an RNA is a *ribonucleotide*, whereas that of a DNA is a *2'-deoxyribonucleotide*. Each of these monomers is formed by a phosphate group, a sugar (ribose in RNA and 2'-deoxyribose in DNA) and a base (uracil): U (RNA), thymine: T (DNA), cytosine: C, guanine: G, adenine: A).

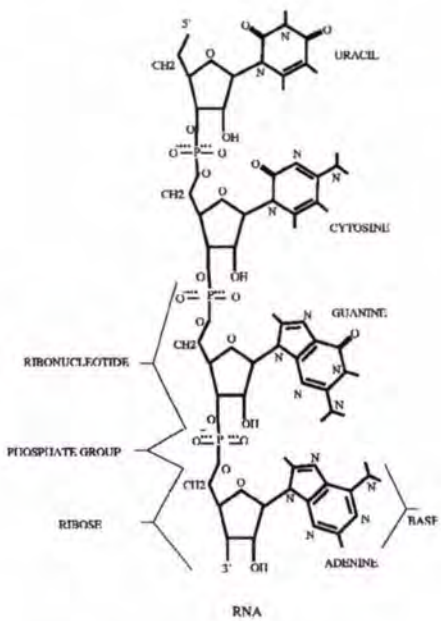


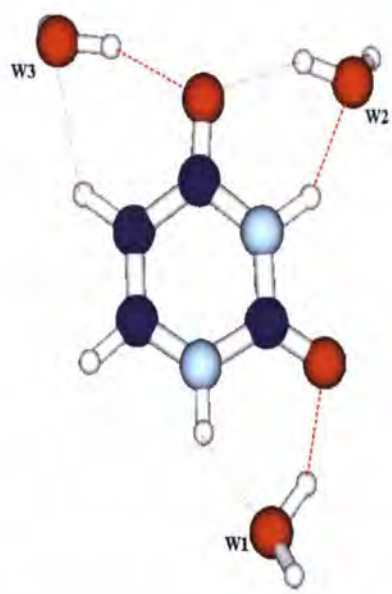


Figure 1: (a) Chemical structure of RNA. DNA chemical structure is similar, the O-H group in the 2'-position of sugar should be replaced by a hydrogen and uracil by a thymine (5-methyluracil). (b) Graphical representation of uracil bound to three water molecules through N-H, C=O and C5-H groups. Geometry optimisation has been made at the DFT/B3LYP/6-31++G* level [6].

A *ribonucleoside* or a *2'-deoxyribonucleoside*, which is formed by a base and a sugar, can also be considered as an important RNA or DNA building block. Hence, there are four major ribonucleosides, i.e. uridine (rU), cytidine (rC), guanosine (rG) and adenosine (rA), and four major 2'-deoxyribonucleosides, i.e. 2'-deoxythymidine (dT), 2'-deoxycytidine (dC), 2'-deoxyguanosine (dG) and 2'-deoxyadenosine (dA). To study the conformational flexibility of nucleic acids by different theoretical methods, the knowledge of the intra and inter-molecular forces is necessary. To achieve this task for RNA and DNA building blocks, vibrational data can be used in junction with quantum mechanical calculations. Raman scattering and IR absorption cannot give sufficient data in this framework, because their intensities are basically monitored by the displacements of heavy atoms (e.g. C, N, O and P). Hydrogen vibrational dynamics can only be accessed by inelastic neutron scattering (INS) spectra in which the vibrational modes arising from hydrogen atoms are particularly exalted.

To give an example of our investigations on ribonucleosides and 2'-deoxyribonucleosides, we present in Fig. 2 the INS spectra of rG and rA recorded at T=15 K on IN1-BeF, in the spectral region below 2000 $cm^{-1}$ (250 meV). To analyse these spectra, we resorted to DFT calculations with B3LYP exchange-correlation

functional and 6-31G* (or 6-31++G*) basis sets [1-5]. First-order INS spectra calculated with the harmonic force field of isolated rA and rG, are reported in Fig. 2 for comparison [4].

We can emphasize here the new information obtained from the INS analysis of these molecular compounds. First of all, in all ribonucleosides and 2'-deoxyribonucleosides, one can observe intense INS bands in the 1500-1200 $cm^{-1}$ (185 – 150 meV) spectral region which mainly arise from the CCH, OCH, COH and NCH angular bendings of sugar [3]. We have verified the above-mentioned assignments with the use of the INS spectra obtained from the labile hydrogen deuterated species also recorded on the IN1-BeF. Moreover, the C-H and N-H waggings of the bases as well as the torsion modes of the bases and sugars, which induce large hydrogen displacements, can also be observed in the 900-700 $cm^{-1}$ (110 – 85 meV) spectral region. All this vibrational information is not accessible in Raman and IR spectra.

On the basis of the careful analysis of the whole set of results, we can conclude that the calculated INS spectra of isolated nucleic acid building blocks reproduce satisfactorily the observed ones in the 2000-900 $cm^{-1}$ (250 – 110 meV) region. However, some discrepancies appear in the spectral region below 900 $cm^{-1}$ (Fig. 2). We have shown [4] that the poor agreement below 900 $cm^{-1}$ (110 meV) between the calculated and observed INS spectra, is mainly due to intermolecular H-bonding that affect (*i*) the base vibrational N-H wagging motions in the 900-500 $cm^{-1}$ (110 – 60 meV) region, and (*ii*) the ring (base or sugar) torsional motions in the region below 500 $cm^{-1}$ (60 meV). We have attempted to account for the intermolecular H-bonding through simple theoretical models in which the main acceptor and donor sites of RNA building blocks interact with water molecules. The example which is completely treated up to now, is that of uracil bound to three water molecules (Fig. 1b) mimicking the solid phase H-bond network. The calculated results based on these models have shown, that the main H-bonding effects appear in the N-H wagging modes which are upshifted by ~250 $cm^{-1}$ (~30 meV) in going from the isolated to H-bonded uracil, thus in good agreement with the observed INS spectrum in solid phase [5-6].

In conclusion, such modelling (Fig. 1b) represents acceptable compromise to account for complicated intermolecular H-bonding in solid phase, at a reasonable computational cost. Similar calculations are now in progress on other bases, as well as on ribonucleosides and 2'-deoxyribonucleosides.

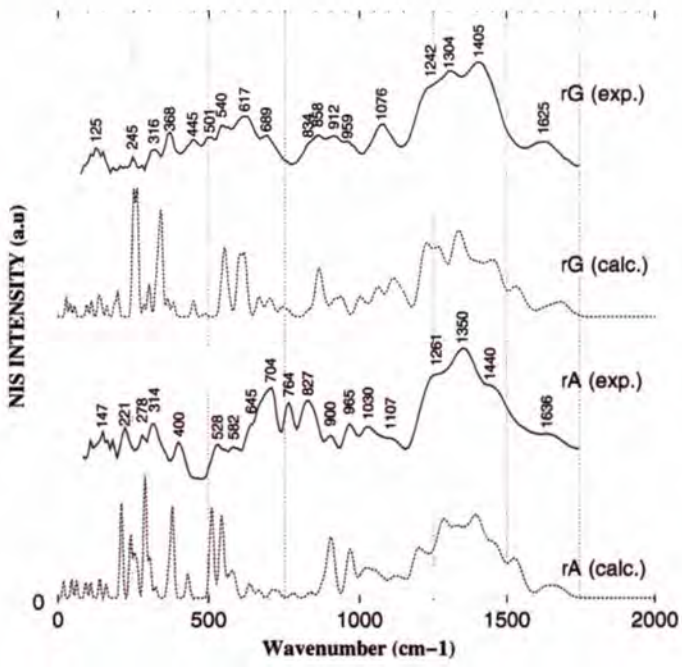


Figure 2: Comparison between the observed (powder samples at T=15 K) and calculated (first-order) INS spectra of rG and rA in the spectral region below 2000 $cm^{-1}$(250 meV), as obtained from the quantum mechanical calculations at the DFT/B3LYP/6-31G* level.


REFERENCES

• [1] N. Leulliot, H. Jobic, M. Ghomi, In Neutrons and Numerical Methodes-N2M, Ed. M.R. Johnson, G.J. Kearley and H.G. Büttner, AIP, New York (1999) 179 • [2] N. Leulliot, M. Ghomi, G. Scalmani, G. Berthier, J. Phys.Chem. A 103 (1999) 9716 • [3] N. Leulliot, M. Ghomi, H. Jobic, O. Bouloussa, V. Baumruk, C. Coulombeau J. Phys.Chem. B 103 (1999) 10934 • [4] M.P. Gaigeot, N. Leulliot, M. Ghomi, H. Jobic, O. Bouloussa, C. Coulombeau, Chem. Phys. 261 (2000) 217 • [5] M. Ghomi, A. Aamouche, B. Cadioli, G. Berthier, L. Grajcar, M. H. Baron, J. Mol. Struct. 411 (1997) 323 • [6] M.P. Gaigeot, N. Leulliot, H. Jobic, M. Ghomi, Chem. Phys. 261 (2000) 217

# Network of hydrogen bonds
## as a medium for DNA interaction in solvents


- V.L. Golo (University of Moscow)
- E.I. Kats (ILL & on leave from Landau Institute, Moscow)
- Yu.M. Yevdokimov (Institute of Molecular Biology, Moscow)



**We suggest that the DNA molecules could form a cholesteric phase owing to an interaction mediated by the network of the hydrogen bonds (H-network) in the solvent. Using the experimental data for the cholesteric phase of the DNA dispersion, we obtain a rough estimate for the energy given by our model, and show that it should be taken into account as well as the energy due to the steric repulsion, Van der Waals, and electrostatic forces, generally used for studying the DNA molecules. The elastic constant of the H-network generating the interaction between the DNA molecules is determined by the energy due to the proton's vibration in the hydrogen bonds.**


It is generally accepted that the formation of the cholesteric phases of the DNA dispersions is intimately related to the interplay among the basic properties of the DNA and the solvent, but the nature of the interactions between the molecules of DNA in the dispersions has remained obscure. It is worth noting that the hydrogen bonds, although weak (5 kcal/mol), are still larger than the Van der Waals ones, and are strong enough to hold the water molecules in a rigid structure in solid water (ice) [1]. The structures of the water and the ice are similar, and either of them is determined by the network of the hydrogen bonds [2], even though in liquid water some of the hydrogen bonds are broken, their number depending on temperature. The whole system may be visualised as a fisherman's net: the knots represent the oxygen atoms and the threads correspond to the hydrogen bonds. The conformation of the net and the distribution of the protons are determined by Bernal-Fowler's rules [2], i.e. there are two protons in the neighbourhood of an atom of the oxygen, and one proton is assigned to each hydrogen bond. Defects also should be allowed for: some of the threads (H-bonds) can be considered as broken due to the thermal fluctuations. The conformation of the network of the hydrogen bonds in the DNA dispersions has certain properties which make it quite different from the network of the hydrogen bonds in the bulk solvent, so that the interaction between the DNA molecules which are separated by less than 50 Å, may induce new phenomena. Experimental data and numerical simulations [3] - [10] suggest that the inter-molecular medium of the DNA dispersions plays an important role in the phase stability. Indeed, the transitions from the cholesteric to the nematic phases, which are observed in the DNA dispersions, have a number of features which cannot be understood within the conventional framework of electrostatic and Van der Waals forces [8]. In the presence of DNA molecules, the network of the hydrogen bonds has a conformation which is different close to the DNA molecules and in the bulk, a few layers of the water molecules away from the DNA. One can imagine that close to the DNA molecules, the net is rolled round a pole; it is spreading more leisurely away from the DNA molecules. Interaction between DNA molecules and solvent leads to substantial modification of the structure of H-bonds in the nearest aqueous environment. If we believe that very close to DNA molecules the network of the H-bonds is more or less stable (on characteristic time-scale relevant for intermolecular interactions), there is a certain elasticity of the net (it means that for any deformation

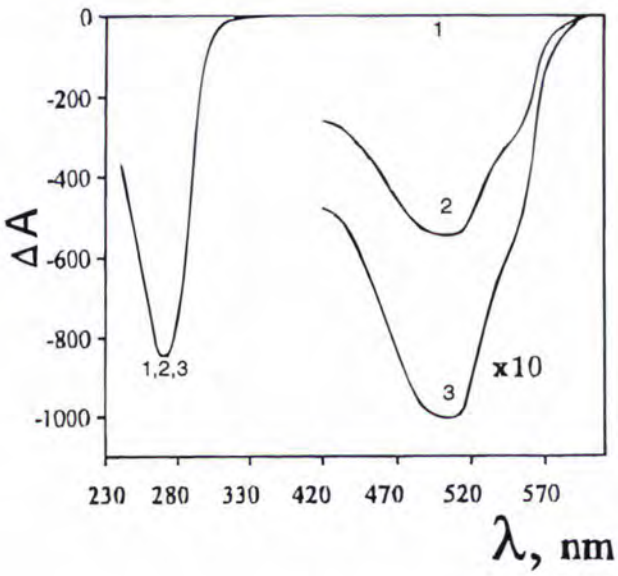


Figure 1: The CD (circular dichroism) spectra of the liquid-crystalline dispersion treated by daunomycin (DAU) (curve1 - $C_{DAU}$ = 0, curve 2 - $C_{DAU}$ = 6.8 ·10$^{-6}$ M, curve 3 - $C_{DAU}$ = 27.2 ·10$^{-6}$ M, where $C_{DAU}$ is the concentration of daunomycin.

of its structure one has to pay a certain energy) and therefore effective elastic interaction between DNA molecules mediated by the H-net. Therefore, we shall assume that the network of the H-bonds in solvent has a certain amount of elasticity (see also [11]), and in fact enough to account for the interaction of DNA molecules. The total energy, which contains the elastic and the entropy term under the constraints imposed by the boundary effects, should result in an effective interaction between the DNA molecules, through the medium of the network of the hydrogen bonds. The picture given above implies that in the neighbourhood of the DNA molecule in the solvent, the conformation of water molecules is strongly influenced by the geometry of the DNA helix. In this neighbourhood, which spreads out at a distance of approximately 10 Å, the conformation of the H-bonds follows the grooves of the DNA and has the shape resembling that of the helix. In this respect, it differs considerably from that in the bulk (compare [4], [5]).

It is important that stringent topological conditions are imposed on the network owing to the requirements due to the structure of ice [1], i.e. among 16 possible combinations of the protons round an atom of the oxygen only 6 are allowed, so that the residual entropy of ice turns out to be equal to $S_0 = Nk_B \ln(3/2)$. The topological constraints are also essential for the proton dynamics of the H-bonds. In fact, the deformation of the net by DNA molecules can be described in certain cases as the deformation field created by the dislocation in the net, i.e. by topological constraints, and besides the interaction changes the probability of proton tunnelling (near DNA the potential for tunnelling is not the same as is is in bulk water). In this respect it is worth noting the phenomenon reported in [4] that the protons could perform cooperative or concerted motions (flip-flop) by jumping from one state to another. Saenger et al. [4] claim that one could find chains of the water hydroxyl groups O – H ··· O – H ··· O – H in which the protons would oscillate clockwise and anti-clockwise in a flip- flop manner. Obviously, the choice of the circles allowing for the flip- flop motion is determined by the topology of the network of the H-bonds.

Our hypothesis on the nature of the interaction between DNA molecules that leads to the formation of the cholesteric phase, is in agreement with experimental data [10] (see Fig.1 and Fig.2), which show the change in the sense of the cholesteric twist due to the intercalation of DNA molecules by the daunomycin. At this intercalation, from the viewpoint of molecular properties, modification of the DNA molecules is quite negligible and therefore one can only expect a small modification of the direct interparticle interaction (electrostatic or Van der Waals) rather than the fundamental rearrangement of the entire structure observed experimentally [10].

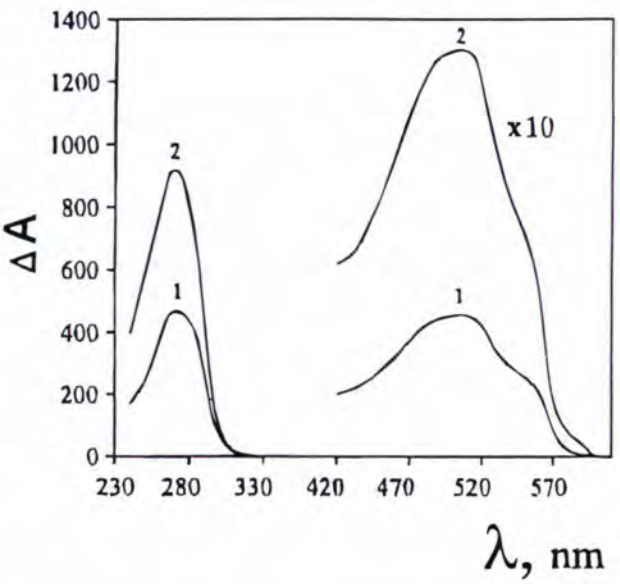


Figure 2: The CD spectra of the liquid-crystalline dispersions formed by DNA - DAU complexes (curve 1 - $C_{DAU} = 13.6 \cdot 10^{-4}$ M ; curve 2 – $C_{DAU} = 37.6 \cdot 10^{-4}$ M).


**References**

- [1] L. Pauling, The Nature of Chemical Bond, Cornell University Press (1960)
- [2] J.D. Bernal and R. Fowler, J. Chem.Phys. 1 (1933) 515
- [3] S. Neidle, H.M. Berman, and H.S.Shieh, Nature 288 (1980) 129
- [4] W. Saenger, Ch. Betzel, B. Hingerty, and G.M. Brown, Nature 296 (1982) 581
- [5] P. Gallo, Single Particle Slow Dynamics of Confined Water, cond-mat/0003027 (2000)
- [6] D.C. Rau and V.A. Parsegian, Biophys.J. 61 (1992) 260
- [7] R. Podgornik, D.C. Rau, and V.A. Parsegian, Biophys. J. 66 (1994) 962
- [8] A.A. Kornyshev and S. Leikin, Phys.Rev.Lett. 84 (2000) 2537
- [9] Yu.M. Yevdokimov, V.I. Salyanov, A.T. Dembo, and F. Spener, Sensory Systems13, (1999), 158
- [10] Yu.M.Yevdokimov, S.G. Skuridin, S.V. Semenov, V.I. Salyanov, and G.B. Lortkipanidze, Biophysics 43 (1998) 240
- [11] D. Farago and Y. Kantor, The elastic behaviour of entropic "Fisherman's Net", cond-mat/0004276 (2000)

# Off-diagonal geometric phases

F. Pistolesi (ILL)

N. Manini (Istituto Nazionale per la Fisica della Materia, INFM & International School for Advanced Studies, Trieste)

**We have investigated the adiabatic evolution of a set of parameterised wavefunctions. Their relative phase change can be related to geometric measurable quantities that extend the familiar concept of Berry phase to the evolution of more than one state. These concepts can be applied to several physical systems. We discuss an experiment on microwave cavities for which off-diagonal phases have been determined from published data.**

When a quantum system undergoes a cyclic evolution, the initial and final wave functions differ by at most a phase factor. This phase factor has an intrinsically geometric component, as it was first recognised by Berry [1]. In this context, "geometric" means that the phase depends only on the sequence of quantum states visited by the system. A simple classical analogous is the rotation by a finite angle of a parallel-transported reference frame along a closed loop on a curved surface, as drawn in Fig. 1.

Berry's phase is almost ubiquitous in present-day physics, and it has been a fruitful tool for interpreting disparate physical phenomena. A well-known example is the molecular Aharanov-Bohm effect. Here the electronic wavefunctions acquire a geometric phase while following the nuclear coordinates around a loop. Such a phase does not affect the classical motion of the nuclei. However, as soon as the nuclear coordinates are quantised, the geometric phase determines the symmetries of the vibronic levels [2]. Among others, a field where Berry's phase has provided a particularly useful interpretation scheme is the theory of the electric polarisation in crystals [3].

In Berry's formulation, the geometric phase concerns any quantum state $|\psi_k(\boldsymbol{s})\rangle$ driven along a cycle. The more general case of open paths $\Gamma$ (joining $\boldsymbol{s}_1$ to $\boldsymbol{s}_2$) was considered in a pioneering work of Pancharatnam's [4]. For a noncyclic evolution, the final wavefunction $|\psi_k(\boldsymbol{s}_2)\rangle$ need not be simply proportional to $|\psi_k(\boldsymbol{s}_1)\rangle$. Pancharatnam considered the phase associated to the *projection* $\langle\psi_k(\boldsymbol{s}_1)|\psi_k(\boldsymbol{s}_2)\rangle$ of a parallel-transported state to the same state at the beginning of the path. It can be shown that this phase factor is also a geometric measurable quantity, except of course in the case where the final state is orthogonal to the initial one ($\langle\psi_k(\boldsymbol{s}_1)|\psi_k(\boldsymbol{s}_2)\rangle=0$).

In general, in a noncyclic evolution, the final wavefunction $|\psi_k(\boldsymbol{s}_2)\rangle$ will have nonzero components along the other orthogonal initial states $|\psi_k(\boldsymbol{s}_1)\rangle$. Recently we have thus investigated the phase factor $\sigma_{jk}^{\Gamma}$ of $\langle\psi_j(\boldsymbol{s}_1)|\psi_k(\boldsymbol{s}_2)\rangle$ for two *different* eigenstates [5]. Indeed, $\sigma_{jk}^{\Gamma}$ can be rigorously defined (in terms of parallel-transported vectors) and made independent of an arbitrary continuous phase change at each point along the path. However, $\sigma_{jk}^{\Gamma}$ still depends on the relative phase of the two vectors $|\psi_j\rangle$ and $|\psi_k\rangle$ at the initial point $\boldsymbol{s}_1$, thus $\sigma_{jk}^{\Gamma}$ is not a geometric quantity. The above phase relation is indeed arbitrary, as it relates orthogonal states. We found [5] that such arbitrariness can be eliminated only by introducing the product:

$$\gamma_{jk}^{\Gamma}=\sigma_{jk}^{\Gamma}\,\sigma_{kj}^{\Gamma} \qquad (1)$$

The factors $\gamma_{jk}$ are truly geometric and constitute a generalisation of the Berry phase to the evolution of several states. For a cyclic path, assuming nondegenerate states, all off-diagonal overlaps $\langle\psi_j(\boldsymbol{s}_1)|\psi_k(\boldsymbol{s}_2=\boldsymbol{s}_1)\rangle$ vanish, and the

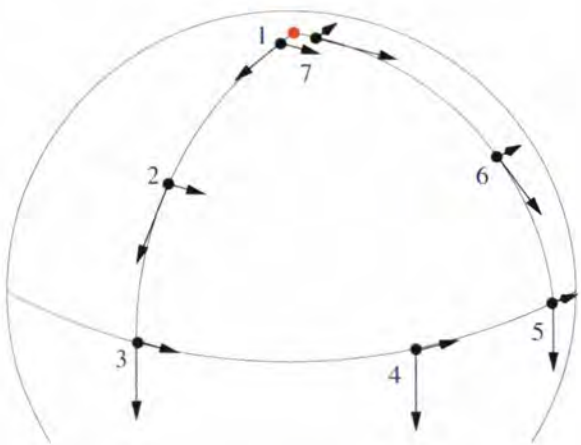


Figure 1: Two vectors tangential to a curved surface are driven along a path. Despite being parallel-transported along the path (remaining as parallel as possible to the direction they were pointing at before each infinitesimal displacement), when they return to the original point, the two vectors find themselves rotated with respect to the initial directions. These rotation angles measure the curvature of the surface enclosed in the loop, and are analogous to the Berry phase acquired by the quantum wavefunctions.

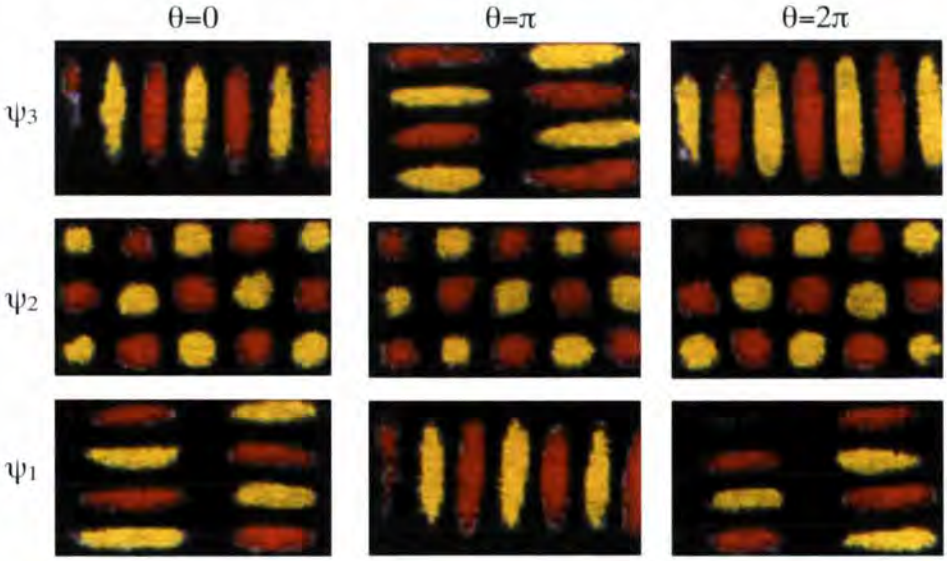


Figure 2: The observed initial (θ=0, left), intermediate (θ=π, central) and final (θ=2π, right) eigenstates of the microwave cavity deformed following adiabatically the path of Ref. [6] around a 3-fold degenerate point. Red/yellow indicate opposite signs of the wavefunctions.

only geometric phase information is represented by the diagonal Berry phases $\sigma_{jj}^{\Gamma}=\gamma_j^{\Gamma}$. For a generic non-cyclic path, both diagonal $\gamma_j^{\Gamma}$ and off-diagonal $\gamma_{jk}^{\Gamma}$ phase factors carry the same kind of information, and can be considered on the same footing. When the $n$ final states are a nontrivial *permutation* of the initial ones, the diagonal scalar products $\langle\psi_j(\mathbf{s}_1)|\psi_k(\mathbf{s}_2)\rangle$ vanish and the usual Pancharatnam-Berry phase $\gamma_j^{\Gamma}$ is not defined. In this particularly important situation, all but $n$ $\sigma_{jj}^{\Gamma}$'s are undefined, since $|\psi_k(\mathbf{s}_2)\rangle=e^{i\alpha}|\psi_j(\mathbf{s}_1)\rangle$ (with $j \neq k$). Here, the only phase information about the permuted eigenstates is contained in the off-diagonal products $\langle\psi_j(\mathbf{s}_1)|\psi_k(\mathbf{s}_2)\rangle$, and it is synthesized in the corresponding cyclic products $\gamma_{jk}^{\Gamma}$.

We consider now a few examples of the newly introduced off-diagonal geometric phases. Although the definition (1) is completely general, as discussed above, the most transparent examples of the off-diagonal phases occur when the final states approximate a permutation of the initial ones. We thus concentrate on this specific case in the following.

Consider first a parametrised Hamiltonian $H(\mathbf{s})$, that reverses its sign at the ends of a path in parameters' space: $H(\mathbf{s}_2)=-H(\mathbf{s}_1)$. Thus the uppermost eigenstate (ordered in energy) becomes the lowest one and vice versa. Such a situation is met rather frequently in physics. To be more concrete, consider the deformed microwave resonator experiment by Lauber et al. [6]. Here off-diagonal phase factors can be easily measured for open paths [7]. In this case, $\mathbf{s} = (s\cos\theta, s\sin\theta)$ parameterises the displacement of the upper right corner of the resonator away from the rectangular-shape position. At this position, three energy levels are degenerate. In this experiment, the three nearly degenerate wavefunctions are followed adiabatically as the distortion is driven in small steps through a loop θ=0 to 2π around the degenerate point. In Fig. 2 we report the initial (θ=0), half-way (θ=π) and final (θ=2π) eigenfunctions from the original pictures of Ref. [6]. The $\sigma_{jk}=\pm 1$ factors defined above are easily identified in Fig. 2 from the recurrence of the wave patterns and the sign changes. In particular, the swap of wavefunctions $|\psi_1\rangle$ and $|\psi_3\rangle$ shows that this system satisfies the symmetry relation $H(\pi)=-H(0)$ at mid loop. Thus, for the path θ=0 to π the only well-defined diagonal phase is that of the central state $\sigma_{22}=\gamma_2=-1$. The upper and lower states exchange, giving $\sigma_{13}=1$ and $\sigma_{31}=1$, thus an observable gauge-independent product $\gamma_{13}=1$. This kind of result gives information on the "curvature" of the space of wavefunctions. It is well known that the presence of degeneracies in the parameters space determines the value of the usual Berry phase. The off-diagonal geometric phase is indeed a similar probe for the presence of degeneracies. In this simple example it can be shown that the observed value of $\gamma_{13}=1$ signals the presence of additional 2-fold degeneracies near the 3-fold one [7].

Nontrivial perturbational cases are more common than one might suspect. Indeed, the quantum states of any physical system affected by some external disturbance will evolve in such a way that the energy levels would cross. Whenever no special symmetry selection rule prevents level repulsion, we will get a sequence of avoided crossings with the characteristic approximated swapping of the pair of involved states. Basically, after each avoided crossing, we have a permutation of the original states. In the region between two avoided crossings, the only well-defined geometric phases are the off-diagonal ones associated to that specific permutation.

The off-diagonal geometric phases can be a useful tool to characterise the evolution of any multi-dimensional quantum system.

Specifically, they could be observed for example with neutron interferometry experiments similar to those used successfully to measure diagonal phases [8]. Very recently, the neutron-spin off-diagonal phase has been succesfully measured at the ILL [9].


**References**

• [1] M. V. Berry, Proc. R. Soc. Lond. A 392 (1984) 45 • [2] F.S. Ham, Phys. Rev. Lett. 58 (1987) 725; N. Manini and P. De Los Rios, Phys. Rev. B 62 (2000) 29 • [3] R. Resta, J. Phys.: Condens. Matter 12 (2000) R107. • [4] S. Pancharatnam, Proc. Ind. Acad. Sci. A 44 (1956) 247 • [5] N. Manini and F. Pistolesi, Phys. Rev. Lett. 85 (2000) 3067. • [6] H.-M. Lauber, P. Weidenhammer, and D. Dubbers, Phys. Rev. Lett. 72 (1994) 1004. • [7] F. Pistolesi and N. Manini, Phys. Rev. Lett. 85 (2000) 1585 • [8] H. Rauch and S. A. Werner, Neutron interferometry. Lessons in experimental quantum mechanics, edited by S.W. Lovesey and E.W.J. Mitchell (Oxford University Press, Clarendon Press, Oxford, 2000) • [9] Y. Hasegawa, R. Lodl, M. Baron, G. Badurek and H. Rauch, to be published in PRL

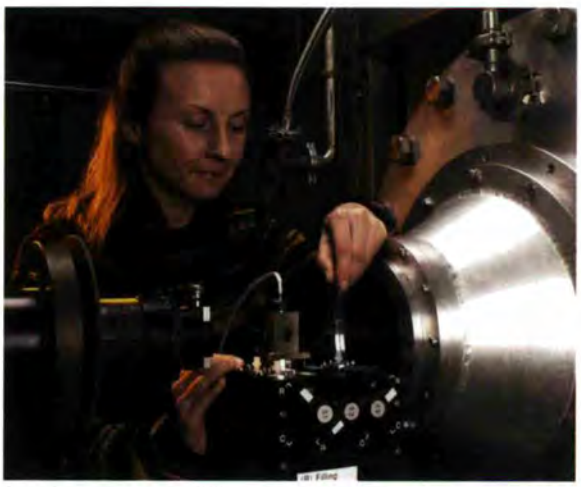

Isabelle Grillo fills the D22 stop-flow apparatus.

The PERKEO installation at the new beam of polarised/unpolarised cold neutrons for Particle Physics PF1B. View of the collimation system and the spectrometer in the iron shielding and the people involved in the project (from left): M. Kreuz (University of Heidelberg), V. Nesvizhevsky (ILL), C.Vogel and U. Mayer (University of Heidelberg).

Rebuilding the D20 multidetector.

Giovanna Fragneto making model membranes on the ILL Langmuir trough.

# Millennium programme
## and new developments

A sustained effort has been devoted this year into establishing a solid foundation for the regeneration of the Institute's instruments and infrastructure through the launching of the ILL's Millennium Programme. Perhaps it is more than symbolic that ILL is an integral part of the word millennium. Such an ambitious programme requires a concurrence of three essential ingredients – motivated and well-qualified manpower, adequate sources of finance and inspired ideas. It also requires good luck and a willingness to take risks. As the first year of the Millennium Programme draws to a close, there are hopeful signs that all these elements are in place. Building upon the newly rebuilt reactor, the momentum generated by instrument projects already in place, the increasingly youthful staff and the guidance of our users, our funding bodies have responded to our appeal for the investment necessary to fulfil the vision which is illustrated in the ILL's long-term strategy document – the Road Map.

# The ILL
## millennium programme

C.J. CARLILE

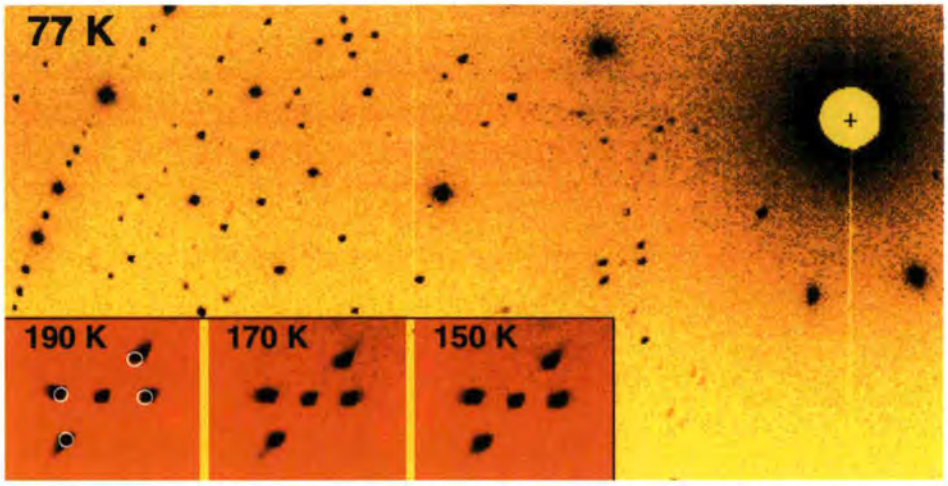


Part of the Laue diffraction pattern of 4% Ga-doped $FeGe_2$ at 77 K, observed in a trial with the LADI image-plate detector on a thermal beam. Shown in inset is the evolution of one set of magnetic satellites towards the commensurate 1/10 phase below ~170 K.

The third Millennium rolls on – only 999 years left until we celebrate the next one. But in the meantime there is much activity in the Millennium Programme at the ILL with five projects currently on the menu. VIVALDI, the Very Intense, Vertical Axis, Laue Diffractometer (previously known as Thermal LADI) with its image plate detector is well into its manufacturing phase. We expect delivery of the complete instrument - a collaboration with the EMBL - during spring 2001 and installation on its guide position before summer. Tests with the prototype version gave remarkably good quality data with none of the background problems which had been feared. Weak superlattice reflections in magnetic materials were clearly seen. E.F. Schumacher's catch phrase "Small is Beautiful" appears to apply here and we shall be exploring other possible applications of image plates. Certainly speed of manufacture, relative cheapness and small sample size, are all qualities in favour of such instruments.

The rebuild of the single crystal diffractometer D3 as a spherical polarimeter is also moving ahead quickly, but it is conceptually and technologically much more complex and will come on line gradually over a three to four year period of development and commissioning. Decpol, a spin sensitive detector for the new instrument, comprising polarised $^3$He plus a $^3$He detector within its magnetic shield, has already been received and commissioned on the instrument.

Elsewhere, as part of our continuing detector development programme, we have commissioned and received five prototype linear position sensitive detectors 7 mm active diameter and 1 m active length. The aim to achieve a position resolution of 7 mm along the length of the detector by an appropriate mix of absorber/quench gases and anode voltage has been exceeded in recent tests. An array of 140 such detectors would then deliver the appropriate spatial resolution (7 mm x 7 mm) for the D22 and later the D11 small-angle scattering machines at an overall count rate of 2 MHz. Commissioning tests indicate that a rate of 5 MHz can be achieved with dead time losses of 10%. Currently these instruments are limited to around 50 kHz and must use beam attenuators in order to avoid data corruption, even with the detectors at large distances from the sample. A hundred-fold increase in data rate will now allow experiments only dreamed of to be tackled.

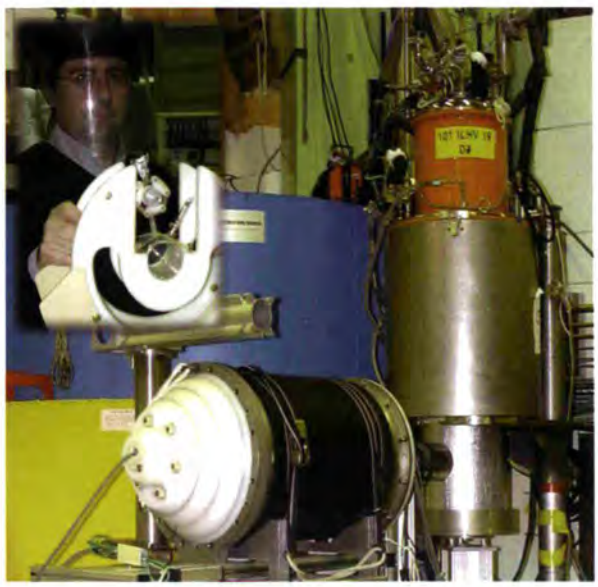

The first experiment carried out on D3 with Decpol, a compact single detector with spin analysis, aimed at measuring the antiferromagnetic form factor of Co in $LiCoPO_4$ using polarimetric scattering. Upper left: Hubert Humblot delivering a $^3$He spin filter.

The Strain Imager is a joint project financed partly by the ILL and partly via a grant to Prof. Philip Withers of the University of Manchester. Beam line design is now complete, integrating D1A, D1B, the Strain Imager and VIVALDI along the same

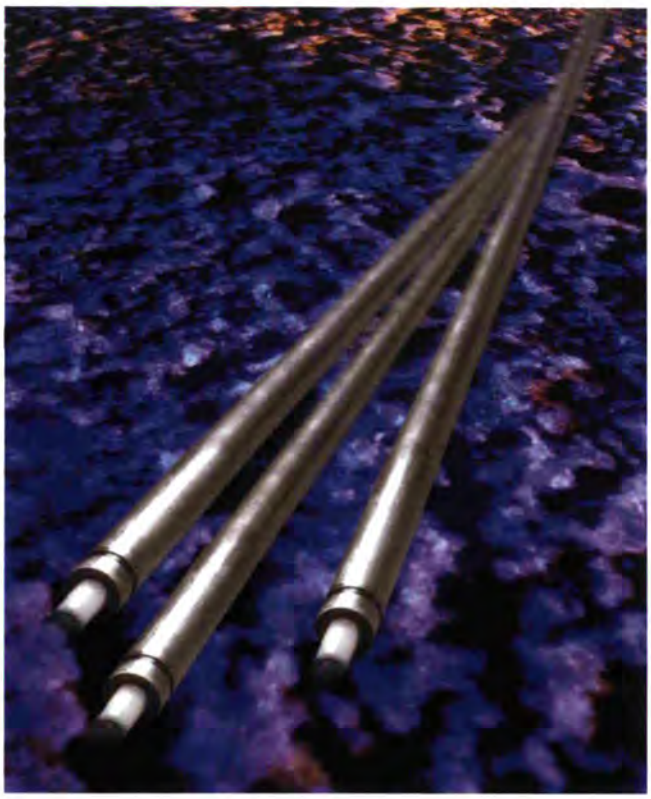

**Prototypes of the D22 tubular position sensitive detectors (length of the tube: 1m)**

renewed neutron guide. The site for the instrument has already been excavated down to a 2 metre depth ready for the foundations which will support the 1 tonne capacity, 10 μm precision hexapod orientation device which will sit on the granite sample table.

A considerably increased polarised neutron flux of $6x10^7$ n per $cm^{-2}s^{-1}$ on the sample will be obtained by remodelling the IN20 primary spectrometer. A larger beam tube using a source diameter of 170 mm has been installed in January 2001 which will be implemented together with a new large (230 mm x 140 mm) double focussing Heusler monochromator in spring 2001.

BRISP, the Brillouin scattering spectrometer being built as a CRG by an Italian INFM team comprising Professors Fabrizio Barocchi, Caterina Petrillo and Francesco Sacchetti, together with Professor Jens-Boie Suck from Chemnitz, is now out of the starting blocks following an intense year of engineering optimisation. In particular the seismic stability of the large instrument, to be installed on an inclined beam hole in the reactor hall, has had to be meticulously simulated. This has been an iterative process with initial in-house seismic calculations acting as input to the engineering design prior to the final quality-assured simulations by accredited consultants. The first pillars have already appeared during the present winter shutdown and the 2-dimensional detector has already been ordered.

During 2001 we will start the upgrade of the D7 polarisation analysis spectrometer with its huge programme of supermirror spin analysers, to begin the rebuild of the D2b high resolution powder diffractometer from the monochromator to the detector, and we intend also to implement the Miniball detector options for Lohengrin aimed at investigating the properties of short-lived isotopes near the neutron drip line to furnish data for cosmological models. At the same time we will start the neutron guide renewal programme with the rebuild of the D11 guide and collimation system as well as the guide feeding D1A, D1B, the Strain Imager and VIVALDI.

**Schematic drawing of the new IN20 monochromator assembly, the biggest one ever built (230x150 $mm^2$, composed of 75 crystals).**

We also recognise that ILL cannot, from within even the increased budget voted by the Associates at the November 2000 Steering Committee, finance all the projects necessary to fully rejuvenate the instrument suite, the neutron guides and the ancillary infractructure which are necessary to deliver the best science for our users. We therefore have entered into a number of collaborative ventures with teams of users to bid for additional funds to accelerate instrument renewal. These include the Strain Imager, PF1 bis, D2b, D19 and IN13 as well as bids for a Facility for Materials Engineering FaME (in collaboration with the ESRF) and for a Bacteriological Deuteration Facility (in collaboration with the EMBL).

We still have a large number of projects queued up to follow on from the nine identified above, but we are very keen to ensure that bright new ideas continue to be added to the list of contenders. We therefore strongly encourage anyone with such ideas to contact one of the Directors so that we can see whether it is possible. Equally well, we encourage consortia of users interested to bid for funds from external sources for their favourite instrument or project also to contact us.

# Review of developments in instrumentation

C.J. CARLILE

Simon Wood on D16.

**The instrument rebuild programme is now firmly established as a central and continuous theme in ILL life and earlier investments are bearing fruit whilst the new projects in the Millennium Programme have been launched. In addition, the need for infrastructure renewal has been recognised and we shall begin replacing two neutron guides in 2001.**

## Progress with Ongoing Upgrades

Whilst the Millennium Programme is now in full swing, the earlier investment programme, colloquially known as UFI – the Upgrade of Five Instruments – is taking centre stage. In some senses the two programmes now form a single continuous programme of instrument build which we intend to maintain as a constant thread in ILL's activities.

The D16 long wavelength diffractometer has been operating in its new configuration with scheduled experiments for over a year now. Special sample environment equipment – shear cells and controlled humidity cells – has been commissioned. The project for an improved detector is underway and a prototype two-dimensional wire device, designed and assembled in-house, has been tested with great success.

After major commissioning work, the D17 reflectometer is open to users in both monochromator and time-of-flight modes. Spurious signals and sources of background have been hunted down and reflectivity patterns over eight decades of intensity are now feasible. By the implementation of an intelligent pulse recognition algorithm the maximum count-rate of the delay line detector has been lifted from its original specification of 175 kHz to 400 kHz. Undoubtedly this is a really welcome addition to the ILL's instrument park.

The rebuild of the D4 liquids and amorphous diffractometer was completed in June 2000 and the nine sets of microstrip detectors in their new shielding and collimator housing were installed on the beam-line. The instrument immediately operated successfully and within days first users were quickly brought in to assay the quality of the new instrument. The original aim to improve the precision of the instrument by an order of magnitude through improved counting statistics and reduced systematic errors appears to have been realised. A five times increase in data rate is combined with a five times improvement in detector stability – much improved on even what was previously the most stable liquids instrument in the world.

The IN4 time-of-flight spectrometer, an ILL/INFM Italy collaboration, is nearing the end of a painful rebirth. The two new horizontal axis choppers are both installed on the instrument and operational. Final authorisation has been given to remove the aluminium beam blocker, signalling the start of first measurements which we eagerly await. Improvements to the instrument have been made in parallel – detector electronics have been replaced, the radial collimator has been refurbished and the low-angle detector has been put in place for neutron tests.

The D20 microstrip detector in its mark-II version is now delivering high quality data to the user programme. The meticulous manu-

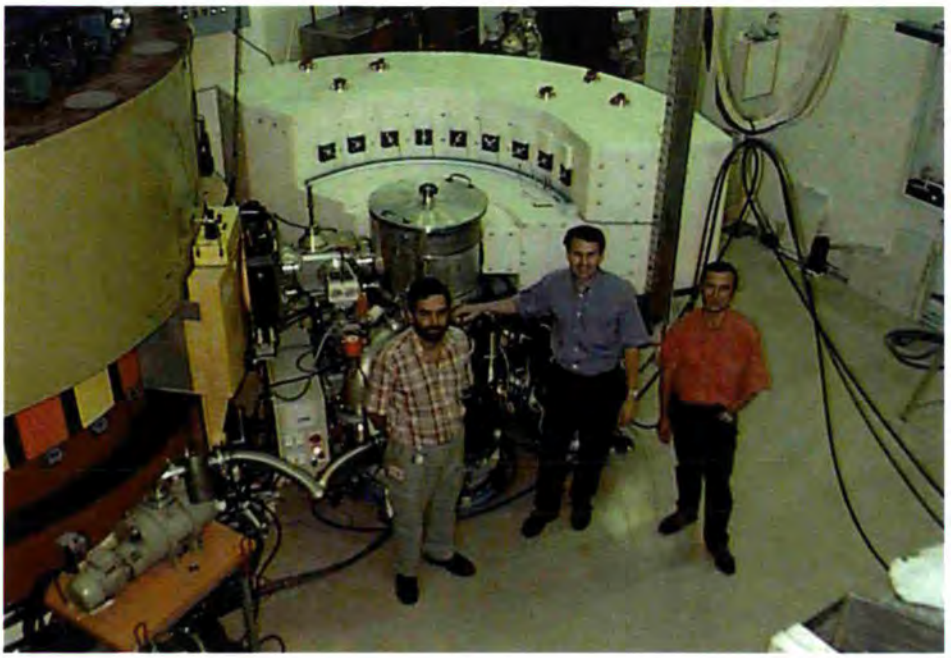

Gabriel Cuello, Henry Fischer and Pierre Palleau during the first tests of D4.

facturing and assembly process, combined with online diagnostic software to monitor the detector conditions, appears to have paid off. First diffraction patterns from standard samples including vanadium were taken in September and the delicate task of balancing all detector channels is complete and since October the user programme has taken off to great acclaim. At the same time as the mark-II detector was installed, the ability to take off at 122° from the monochromator was implemented by a long overdue modification to the shielding of the neighbouring instrument. We shall now set in place a programmed sequence of detector maintenance.

The new wheel choppers of IN4 (maximum speed: 5500 rpm).

The new triple-axis spectrometer IN8, an ILL/CSIC Spain collaboration, is showing visible progress on-site. The monochromator drum was received in late September and all monochromator crystals have been spark-eroded at ILL for the 3-faced monochromator itself. First neutrons are expected during summer 2001.

The rebuild of the IN5 primary spectrometer is underway. Work commenced immediately following the end of reactor operations in mid-December 2000 with the removal of the present guide and chopper systems and the new focussing guide and chopper pedestals are currently being installed. The manufacture of the precision discs for the choppers has passed a significant milestone with the successful machining of four of the aluminium chopper blades. A number of initial manufacturing techniques had failed to achieve the necessary precision at the circumference of the disc until a cold-rolled (and hence preferentially oriented) aluminium ingot was used. Rather counter-intuitively this has resulted in a disc well within specification and rotational tests are to begin shortly. The IN5 upgrade, when completed at the end of 2001, promises an order of magnitude increase in data rate. We are presently looking at design options for the secondary spectrometer.

A new high-intensity cold neutron guide – H113, built in collaboration with the University of Heidelberg – is now delivering neutrons to the rebuilt PF1 machine in the ILL's first guide hall. The guide, with a supermirror coating and a cigar-shaped profile along its length, is a so-called ballistic guide and delivers an astonishing intensity 80 metres from the cold source of almost $10^{12}$ n/sec.

# A strain imager at the ILL

THILO PIRLING AND STEVEN ROWE (ILL)

**As part of the ILL Millennium Programme, ILL is constructing a neutron strain imager, dedicated to the determination of (residual) stresses, in collaboration with the University of Manchester and partly funded by EPSRC. Its construction and commissioning is foreseen to last for 4 years, after which time the instrument will become a fully scheduled ILL instrument.**

A strain imager is an instrument for the non-destructive determination of residual stresses inside matter. Thanks to the high penetration power of neutrons, both small and large components can be investigated. The technique covers a large range of applications in basic, applied and industrial research and materials testing. Examples include welds, interfaces, coatings, hardening, composite materials and fatigue processes. Both high penetration and high resolution are required at the same time to allow high position accuracy for the smallest and the largest sample.

The construction of a reliable instrument dealing with such a broad range of applications and specimens is the challenge of the strain imager project. Not only are the technical specifications our concern, but also a user-friendly operation.

The project was started at ILL in January 2000 and the design and feasibility studies of the overall instrument have already been completed. During the summer we have carried out simulations of the monochromator and the neutron guide design. The specifications of the monochromator and the guide have now been defined. During the current reactor shut-down, the excavation work for the experimental area – down to a depth of 2 metres - has begun.

## General design and technical aspects of the strain imager

A well-defined monochromatic neutron beam with a cross section of typically 1 mm² penetrates the sample. Part of the beam is reflected by crystalline planes of the specimen and is imaged on the detector by secondary optics. The primary and secondary optics determine the size of the gauge volume which defines the lateral resolution. The stress distribution in the specimen is mapped by scanning across the sample. The precise position of the scattered peak contains information about the variation of the lattice spacing (strain $\varepsilon$) in the crystalline material, which is related to stress by Hooke's law. In principle our strain imager is a 2-axis high resolution powder diffractometer, applied with special optics for the definition of the gauge volume [1].

The strain imager will be located in the first guide-hall, on the H22 guide, between D1A / D1B and the new VIVALDI instrument. Space is an essential requirement for the

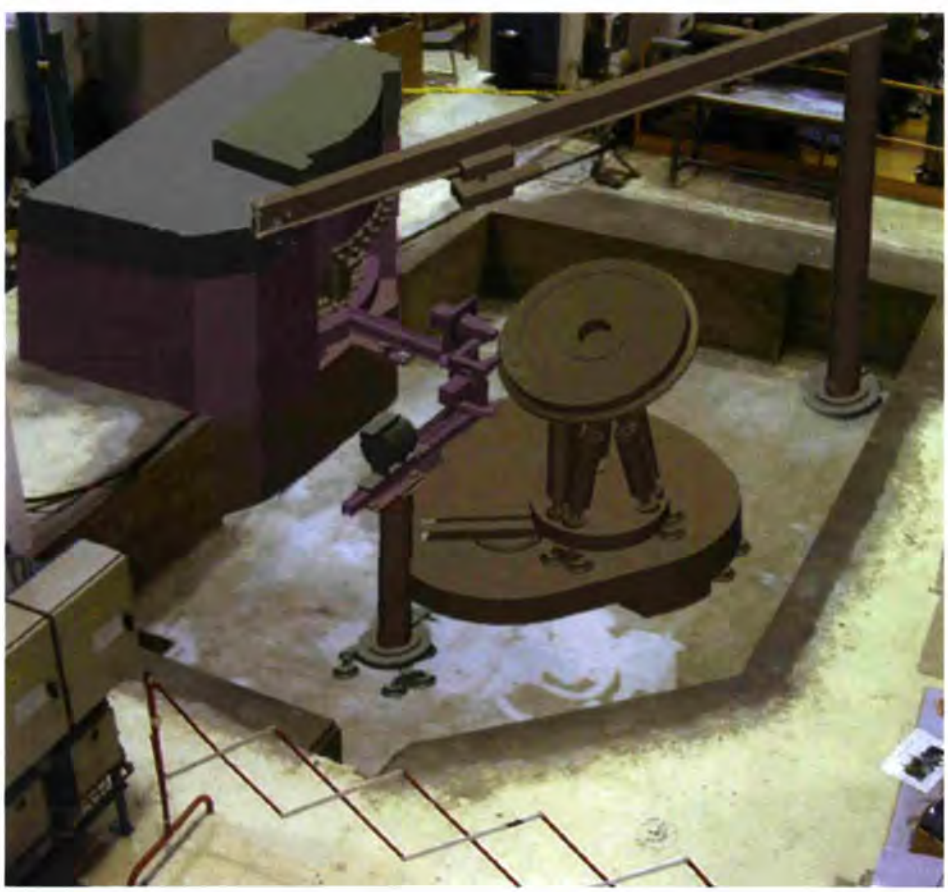

Design study of the new strain imager.

study of large samples. Therefore, the experimental area will be quite extensive sitting about 1.6 m below the beam axis. Fig.1 shows the overall view of the future instrument. A 50° range in the take-off angles for the monochromator will enable a continuous choice of wavelengths between 1.3 and 4.5 Å. The instrument will slide on air-pads over a marble floor.

Compared to most of the instruments at ILL, a strain imager deals with "real" engineering components. They can have any shape, but they must be very precisely aligned, often in orientation not easy to handle.

Our sample table (a Steward platform, or hexapod known from flight simulators for pilots) is ideal for this task. In fact, it is capable of positioning a sample over a large range of tilting angles and translations. Rotations around any freely defined pivot point and scans along a freely defined trajectory are possible. It will be possible to load samples up to 1000 kg and position them to an accuracy of 10 μm on short range.

Lasers and a closed circuit TV camera system will help us to align any sample in a quick and reliable way.

In order to be able to mount a specimen with its centre of gravity above the centre of the sample table, the hexapod can be displaced on the omega table, using an air cushion system. A displacement of 60 cm is easily possible, but we are envisaging up to 1 m. This would give us the possibility to mount samples of 2 m length. A feasibility study is in progress.

Monte Carlo calculations, performed by Jan Šaroun (Nuclear Physics Institute of Řež, Prague), have shown that the optimum design of the monochromator is a double focusing assembly, consisting of bent Ge-crystals. The curvature must be variable in both directions: horizontal and vertical. It has to be optimised for each diffracting angle $2\Theta$ and it shows best resolution over a relatively small $2\Theta$ range. But this matches well to the needs of strain measurements, since there is only one reflection under investigation at a time.

Radial collimators are best suited to a double focusing monochromator for the definition of the gauge volume. They take advantage of the divergent neutron beam and focus it on to the sample, shaping a precisely defined gauge volume. This concept was developed and tested on D1A [1]. To be efficient, the monochromator itself requires a minimum divergence from the neutron guide. The calculations have shown that a super-mirror guide with a relative angle of total reflection of m=2 provides the optimum divergence. Fortunately H22 will be replaced by such a guide starting in 2001. Compared to the present situation on D1A, this will provide a gain in neutron flux of between 3 and 5, depending on wavelength.

The neutron strain imager is unique in several respects: not only will it be the first ILL instrument to use a hexapod sample positioning system, but it will also incorporate a variable double focusing monochromator - the first of its kind at the ILL.

The year 2000 has seen a lot of progress towards the realisation of the instrument. We are looking forward to the collaboration with Prof. Withers and his co-workers (University of Manchester), starting in 2001 which will inspire and push forward the project tremendously.

REFERENCES

• [1] SEE ARTICLE "NEW BEAM OPTICS FOR THE D1A STRAIN-IMAGER" IN THIS REPORT (P. 86 )

# Optics for strain imaging: radial collimators or slits?

T. PIRLING (ILL)

**A number of neutron strain imaging applications require high resolution [1]. These are mainly measurements at interfaces or surfaces, and along steep stress gradients. Unfortunately, the available flux of a neutron source sets practical limits to the smallest useable gauge size, and thus to the lateral resolution. Furthermore, the choice of the beam optics is crucial due to the so-called surface error, which occurs during interface, or surface scans, when the sample does not entirely fill the gauge volume.**

Most strain imagers (or scanners) use slit apertures for the definition of the gauge volume. But just where the highest lateral resolution is demanded - at interfaces - they introduce the largest errors. To overcome the experimental inaccuracies, the strain imager option on D1A has been equipped successfully with a secondary radial collimator in 1997 [2]. Many inaccuracies and inconveniences could be improved [3]. But the surface error still remained. It lies in the range of several 100% to several 1000%! Its correction is very difficult and uncertain since the measuring conditions are not very well defined by the primary slit and, of course, big numbers have to be corrected to obtain relatively small values.

The work on D1A has shown [4] that the surface-error is mainly caused by the wavelength distribution in the primary beam, which is caused by the monochromator / slit combination. A collimator in place of a primary slit can equalise the wavelength-distribution and therefore reduce the surface error. Only a small geometrical error remains which can be analytically corrected, thanks to the perfect definition of the experimental conditions by the collimators. During the year 2000 we have installed a primary radial collimator and tested it successfully. It has led to better performance, higher resolution and to more reliable results at surfaces and interfaces. This will extend the range of applications of the neutron strain imaging technique. First experiments have already been performed at ILL, using the new optics.

## The principle of strain imaging

The idea of strain imaging is to determine the strain in the crystalline lattice of the material, from which the stress is then calculated. The strain $\varepsilon$ is defined by the variation of the lattice spacing $d$ relative to a stress-free reference value $d_0$. A diffraction method is very well suited for its determination. By differentiating the Bragg equation we get a relation that allows us to determine strain just by measuring the variation $\Delta\theta$ of the diffracted peak position referred to its position $\theta_0$ in a stress free sample:

$$\varepsilon = \frac{d - d_0}{d_0} = -\Delta\theta \cot\theta_0$$

Strain is mostly reported in με ($10^{-6}$ ε) which is 1 ppm lattice distortion. Hooke's law connects strain ε and stress σ. Here the general formula for a cubic material:

$$\sigma_{ij} = \frac{E}{(1+\nu)}\varepsilon_{ij} + \frac{\nu E}{(1+\nu)(1-2\nu)}\delta_{ij}\varepsilon_{kk}$$

Whereas ν is the Poissons-ratio and $E$ Youngs modulus. To determine the stress tensor, measurements in 6 different orientations have to be performed. In most cases, the direction of the principal axes can be assumed to coincide with the principal axes of the sample. In this case three measurements in these directions are sufficient to determine the complete tensor.

To understand the difficulties of a measurement and the different error sources, the principle of the experiment will be explained.

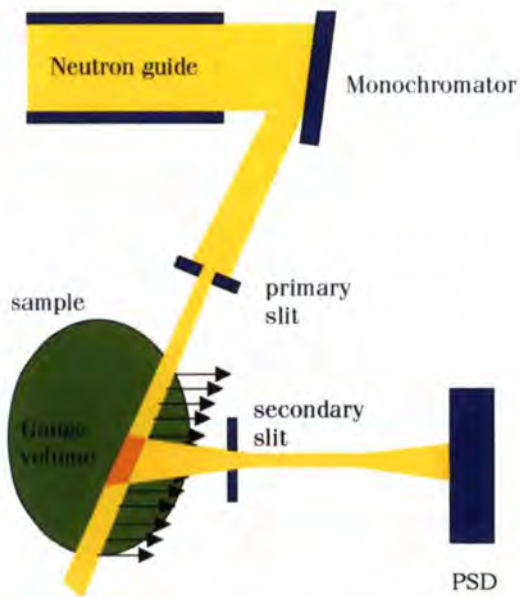


Figure 1: Set-up of a strain imager, using slits for the definition of the gauge volume. Due to the divergence of the neutron beams the slits should be positioned as close as possible towards the sample. The gauge volume is diffuse and diverging, even in a 90° scattering geometry.

Fig. 1 and 2 show a sketch of different experimental configurations. The primary optics defines a neutron beam with a specific cross-section, which penetrates the sample and is scattered by the material. The secondary optics selects a fraction of the scattered beam and images it onto the detector. The intersection of the two beams is the gauge volume. The precision of the definition of the gauge volume determines the lateral resolution. In the simplest case the optical components are just slit apertures as in Fig. 1. At ILL we are using radial collimators, as shown in

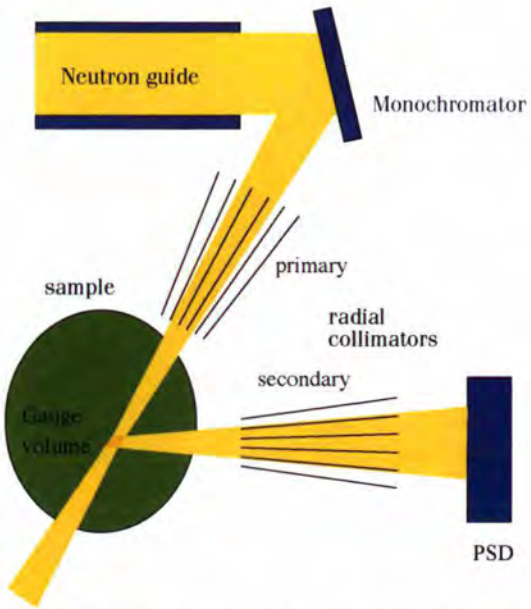


Figure 2: A strain imager equipped with radial collimators for the gauge definition. The collimators focus the whole diverging neutrons onto the sample, but define a perfectly shaped gauge volume with parallel borders, which is rhombic for any scattering geometry. Due to the fixed distance of the collimators, no realignment needs to be done after sample changes. The focal length of the collimators – at D1A 150 mm – leaves a lot of space for sample movement and sample environment.

Fig. 2. To be efficient, the detector is a PSD (Position Sensitive Detector) since it detects the whole of a reflected peak at one time. To perform a complete mapping, the sample is scanned.

From this we can deduce the requirements on the experimental set-up: a well-defined and sharp-edged gauge volume for high lateral resolution; perfect imaging of the peak shape; and high angular resolution for precise determination of strain and thus stress. High neutron flux enables either small gauge volumes for better lateral resolution to be probed or enables measurements to be made deeper inside large samples.

## Slit optics

Using slits for the definition of the gauge volume is relatively simple and allows a flexible design because it is easy to adapt the gauge size to the sample. But it has many weak points.

To achieve good lateral resolution, the slits should be positioned as close as possible to the gauge volume. The reason is that on the primary side the beam divergence and secondary the peak width increases the gauge size. For good results the distance should not exceed 20 mm. This complicates the alignment and increases the risk of collisions during the scan. Apart from surface scans the slits are further away and measurements can only be performed with less resolution than expected from the slit dimensions. This is a big disadvantage for the investigation of internal interfaces. Furthermore, the slit optics provides wrong values when scanning along steep stress gradients, getting worse with increasing distance of the slits.

Especially in the vertical direction, this error is extremely high, particularly when a focusing monochromator is installed. But for the efficient use of neutrons this is indispensable. On D1A a 200 mm high beam is focussed down to about 15 mm on the sample table over a distance of 1500 mm. The resulting beam divergence is about 7.5°. Under these conditions the gauge volume defined by a slit aperture is several times bigger than the aperture and quite diffuse, even at relatively small distances to the gauge. A high-resolution vertical scan is not feasible. This is unsatisfactory, because the appeal of vertical scans is that they are not affected by one of the biggest problems of neutron strain-scanning: the surface error!

## Surface error

The surface error is an instrumental effect, which occurs during scans in the scattering plane when the diffracting material passes out of the gauge volume. This is the case at surfaces or at interfaces between two different materials. The peak fit provides shifts, which easily can be between 4 and 10 times higher than the real variation in the sample. Three different effects cause these shifts: geometrical position of the centre of gravity, peak clipping and the wavelength distribution across the primary beam.

The geometrical shift occurs because the centre of gravity of the effective scattering gauge volume is moving while the sample is passing out of the gauge volume.

This leads to a movement of the peak position on the PSD, which can be misinterpreted as an angular peak shift. Furthermore the reflected beam profile is cut by the slits. This leads to an asymmetric peak with a reduced peak width. Since the original peak profile can not be reconstructed, an erroneous determination of the peak position and width is the result, which creates errors in the stress values.

The third source of error, the wavelength distribution in the primary beam, contributes the biggest fraction [4]. It is caused by the primary slit: for any point in the gauge volume the slit aperture cuts out a different fraction of the divergent neutrons from the monochromator. Since the wavelength is related to divergence, the wavelength-distribution across the beam is not homogeneous. In surface scans when the sample passes out of the gauge volume, the varying wavelength-distribution leads to huge peak shifts.

Whilst the errors, caused by the first effects described are in the range of several 100 με, the latter adds several 1000 με! A correction is not reliable and neither is it practical, due to changing measuring geometries.

## Focusing collimators

Replacing the slits by collimators has however many practical advantages. Since their focus is fixed, they stay at the same position and no changes have to be made when changing the scan direction or the sample. No realignment is necessary and neither does the experimenter need to worry about the best location of the optical elements - unlike slits. Furthermore, the lateral resolution is only determined by the collimators. Scans at interfaces deep inside the material can be performed with the same precision as at surfaces. Since the focal length is quite large, in the case of the collimators on D1A it is 150 mm, there is the necessary space for sample movements and for large samples. So this technique is very well matched to one of the biggest advantages of neutrons, which is their penetration power. Furthermore, sample environment - like i.e. a furnace, stress-rig, or cryostat – does not allow slits to be placed close to the sample. Collimators leave enough room for the equipment.

The gauge size is defined only by the collimators and does not depend on the beam divergence or peak width [3]. The collimator takes advantage of the beam divergence without reducing the resolution. So the primary collimator can also be used to define the vertical gauge height by turning it 90°. Vertical scans can then be performed with the same high resolution as horizontal scans. This is a big advantage, since these scans, as we have said earlier, are not affected by the surface error!

But that is not all: the negative effects, described in the last section, for scans in the scattering plane, are avoided or reduced. Peak clipping is totally inhibited by the secondary collimator. Peak shape analysis, used for the evaluation of second order stresses, can therefore be performed close to the surface or interface. Since the primary collimator focalises the whole divergence of the neutron beam coming from the monochromator onto the sample, the wavelength-distribution inside the gauge volume is equalised. This means, that the mean wavelength is constant across the gauge, which, as described in the previous section, eliminates the biggest part of the surface-error.

Only the geometrical error remains, since the combination PSD / secondary collimator is not a totally angle sensitive system. But due to the perfect defined gauge volume, and the well-defined measuring geometry, this error can be corrected analytically.

Fig. 3 shows a comparative measurement of a primary slit and a collimator set-up. The sample was an iron powder to make sure that there is no strain gradient. Such an experiment shows directly the surface error. In case of a 2 mm wide secondary gauge width and taking into account the detector distance of 800 mm, the pure geometrical error should be maximally 604 με and 360 με for a gauge size of 1.2 mm. This is perfectly verified by the measurements. The maximum measured error of the slit set-up is 1600 με using a 1 mm primary slit. And this is the optimum slit configuration of D1A. Often the error reaches more than 2000 με.

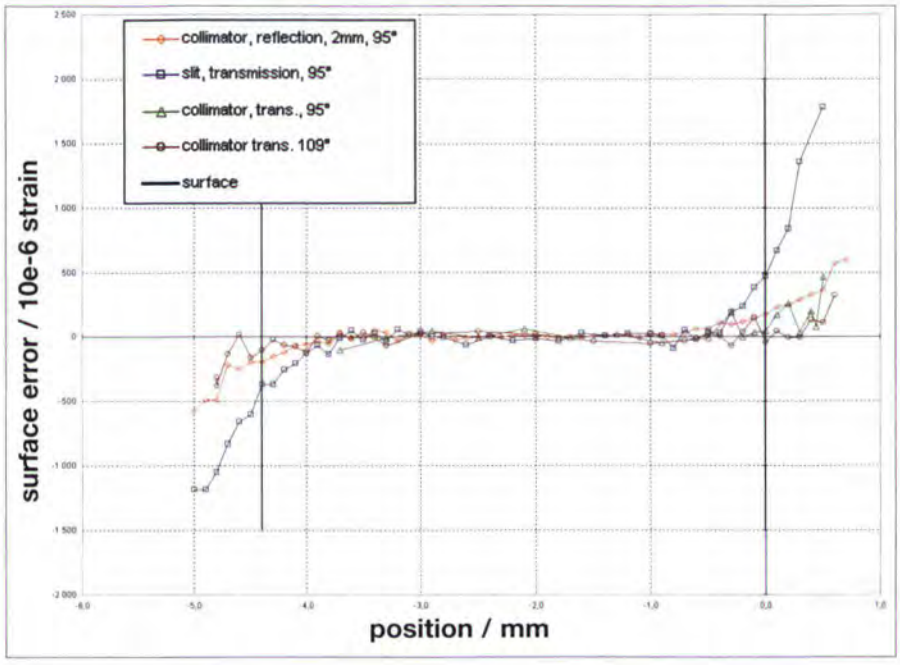


Figure 3: Through-surface scans of an iron powder sample in different scattering geometries. The Sary slit. All other curves were measured using the two collimators. The diffracting angle was 95 (Fe(110)) and 109 2Θ (Fe(211)). In one case the secondary collimator was approximated to the sample so that the gauge size was 2 mm (red curve). The error of the collimator configuration does not exceed the geometrical error.

## Conclusion

The introduction of a primary radial collimator on the strain imaging option at D1A has solved the outstanding problem of the surface error. This makes high resolution experiments possible. Furthermore, radial collimators provide a precise defined gauge volume, and ensure a constant high lateral resolution at any point inside the sample. They leave room for large samples, sample environment and sample movement. And last but not least, they simplify the alignment.

Radial collimators fit very well to a – horizontal and vertical - focusing monochromator since they focalise the whole divergent neutrons onto the sample while at the same time achieving high resolution. We are now optimising the mechanical support for the two-collimator configuration. Unfortunately the space on the D1A diffractometer is limited. So only small samples up to approximately 100*100*30 mm³ can be measured in the new arrangement. They will be mounted on an eulerian cradle, equipped with a small xy-table. For larger samples the primary slit system in combination with the secondary collimator will be used, as before.

The gained experience will be applied to the design of the new strain-imager currently under construction.


### References

[1] see as well "The ILL strain-imager" in this annual report, p. 84 [2] T. Pirling, R.C. Wimpory, Stress measurements on D1 A: a new high precision strain scanner, ILL annual report 1997, 87-89 [3] T. Pirling, A new high precision strain scanner at the ILL, Materials Science Forum Vols 312-324 (2000) 206-211 [4] T. Pirling, Neutron strain scanning at interfaces: optimised beam optics to reduce the surface effect; Materials Science Forum Vols 347-349 (2000), 207-112

# New 1.8 K cryogen free cryostat available to the users

M. De Palma, F. Thomas and S. Pujol (ILL)

**The ILL Sample Environment Service has developed a Joule-Thomson low temperature low cooling power stage to expand the temperature range of commercial cryocoolers down to 1.8 K. Two prototypes have been made. The first one is incorporated into an ILL top-loading cryocooler and therefore, routinely available to the ILL users. The second one is mounted on the four-circle bottom-loading cryocooler of the XMAS line, the UK CRG at ESRF.**

A descriptive of the Joule-Thomson stage is shown in Fig. 1. Special attention has been paid to achieving a compact design and a base temperature below 2 K. This stage can be added to any commercial cryocooler which can reach base temperature below 10 K. The overall dimensions of the stage are typically 34 mm diameter x 85 mm high.

Fig. 2 shows the ILL top-loading cryocooler (left) and the XMAS bottom-loading cryocooler (right). In the foreground, one can see the sample holder of the top-loading machine. This sample holder is very similar to those used in an Orange Cryostat, with the same outer diameter, and an adjustable length with a sample at low temperature. In the photograph, the actual length is 910 mm.
Fig. 3 describes schematically the bottom-loading cryocooler set-up. To operate it, one needs only a standard pressurised helium-gas bottle, a liquid-nitrogen trap and a 5 $m^3/h$ primary pump. The working pressure on the condensing line is around 10 bar and the helium-gas consumption is 4 $m^3$ / week STP.

Figure 1: Picture of the Joule-Thomson stage of the XMAS cryocooler.

Figure 2: Picture of the ILL top-loading cryocooler (left) and of the XMAS bottom-loading cryocooler (right). In foreground, the sample-holder of the top-loading machine (length 910 mm).

For the top-loading cryocooler, the set-up is similar except that the liquid-nitrogen trap is not needed.
The base temperature is 1.8 K, and the maximum tilt angle to keep the base temperature below 2 K is 50°. The typical cooling power is 2 mW at 2 K in a vertical position. Further improvements of the devices await users' comments following field tests currently underway. Should these tests prove positive, we plan to put more such cryostats into operation since they use less material resources than an Orange Cryostat, do not need frequent cryogenics fluids filling, and promise greater reliability.

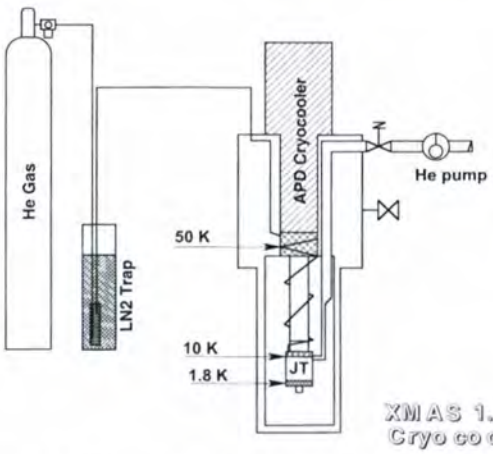


Figure 3: Schematic drawing of the XMAS cryocooler set-up. The Joule-Thomson (JT) stage is added to an APD cryocooler to expand the temperature range down to 1.8 K.

# H113 neutron guide

W. KAISER (ILL)

**The project for a new guide on the vertical could source was first proposed by P. Ageron, J.M. Astruc and A. Robert in 1991. It has been finally realised with supplementary external funding of the Universities of Darmstadt, Munich and Heidelberg and delivers by far the highest intensity cold beam from a guide, exceeding $10^{12}$n/sec. The new H113 guide is designed on a so called ballistic guide. The present guide has a divergent section at its entrance and a converging section at its exit which provides a very rough approximation to this profile.**

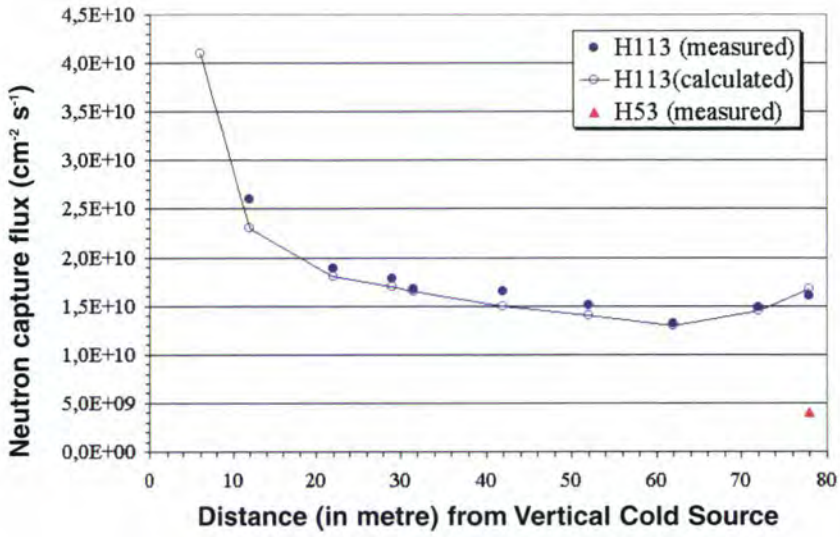


Figure 1: Neutron capture flux measured (filled circles) and calculated (empty circles) along the ballistic supermirror cold-neutron guide H113. For comparison, the capture flux at the present beam station PF1 (H53) is also given.

## Design, Manufacture, Mounting and Flux Measurements

### In-pile part

The H113 guide starts 2.2 m away from the vertical cold source of the reactor. Over a length of 3.7 m the guide is straight and slightly convergent with a cross section of 200 x 68 mm², exit section 200 x 62 mm² and is coated with Ni58. The in-pile part of the H113 guide, mounted during the reactor shutdown in 1994, is made of borated (19% $B_2O_3$) glass with low soda content (0.4% $Na_2O$) from Corning, designed and manufactured by Cilas in Orléans.

### Out-of-pile part

In the out-of-pile part the guide is designed as a "ballistic guide", straight and divergent over 10 m, expanding to an exit section of 200 x 90 mm² and curved with R = 4 km over 52 m, then straight and convergent over 10 m to 200 x 60 mm². It is coated with supermirror m = 2. This section was designed and manufactured in collaboration with the University of Heidelberg and the company Sputter-Dünnschichttechnik, also in Heidelberg.

The 6 m out-of-pile part length in the swimming pool, installed during the July/August 1999 reactor shutdown, is made in 6 mm thick float glass, again with m = 2 supermirror coating, assembled with Aluminium profiles. The $B_2O_3$ content of the glass to avoid radiation damage in this case is less than 1% and the $Na_2O$ content is about 12 to 15%. The guide elements are activated by (n,γ) reactions in Na and Al. A 0.5 mm thick cadmium foil around the guide elements protects the housings which were made in a stainless steel with low cobalt content (~ 0.1%). This guide section penetrates half a metre into the swimming pool door in the H1-H2 casemate in the reactor hall up to the safety valve.

The succeeding part, 20 m in length, passes through the reactor hall and the reactor shell. The guide elements were installed during the May 1999 reactor shutdown. These guide elements were made in 6.5 mm thick borated float glass from Schott in Mainz, using the same supermirror coating and assembly technology. The $B_2O_3$ content is about 12%, and the $Na_2O$ content around 8%. The housings downstream from the safety valve were made from normal steel and the guide elements were able to be mounted without cadmium foils.

The final part in the neutron guide hall, and 46 m in length, has been installed during the winter shutdown 1999/2000 with the design identical to the 20 m upstream section. The guide comes to the end in the primary casemate of the new PF1B beam facility. Flux measurement with gold foils confirm the computer simulation [1].

The installation of this intense neutron guide has been a story of determination, which in the end has paid off handsomely. The beam flux can be further increased by the addition of a multi-bladed mirror assembly. Amongst other aims, this beam position will be used to push down further the upper limit of the electric dipole moment of the neutron.

### REFERENCES

[1] H. HANSEN ET AL., NUCL. INSTR. METH. A, 2001, SUBMITTED

# The D17 reflectometer

R. Cubitt (ILL)

**The main requirements for a reflectometer are high flux, flexible resolution, accurate collimation and precise spatial detection. D17 has all of these properties. This article shows some of the first results taken with D17 using the time-of-flight (TOF) option, including data from the first official experiment.**

The principal reason for having a TOF option on this instrument was to enable experiments on the kinetics of planar materials to be performed. This is possible because a range of q is measured simultaneously using a white beam as opposed to the monochromatic mode where the sample angle has to be rotated for each point in q. The TOF is less efficient than the monochromatic mode in terms of the flux available at each q point as the flux at the extremes of usable wavelengths are much lower than the peak flux used in the monochromatic mode. Having a chopper system where the resolution can be continuously varied, however, compensates for this as flux can be gained when high resolution is not required. A second advantage is that when setting up experiments it is easy to check the alignment of the sample after only a few seconds of data acquisition. For example, Fig. 1 shows raw data from counting for only 10 seconds. The vertical resolution of the detector has been summed resulting in a picture with horizontal pixels corresponding to 2θ, and vertical pixels representing wavelength. It can be seen that above the critical wavelength where total reflection occurs there is no intensity in the direction of the incoming beam. This means that no neutrons fly past the sample surface and this surface is under illuminated and correctly aligned with respect to the incoming beam. The picture demonstrates the fact that neutrons obey simple optical laws. It can be seen that below the critical wavelength the transmitted beam is refracted towards the horizon showing that neutrons, unlike light, have a refractive index less than one (for a material with positive scattering length density). The curvature of the diffracted beam with wavelength is due to the fact that the formula for neutron refractive index has a wavelength squared term.

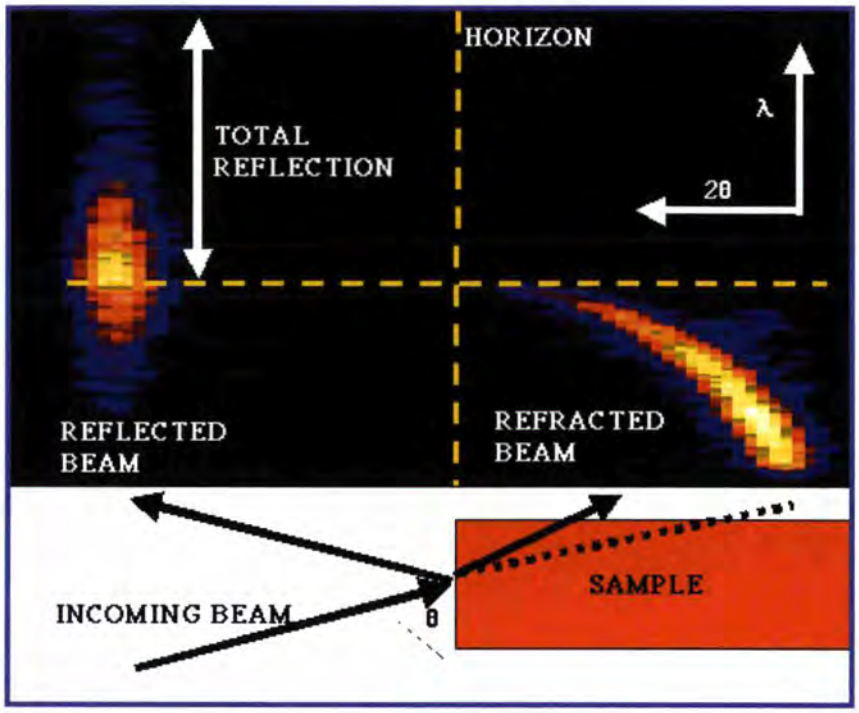


Figure 1: TOF alignment data taken in 10 seconds. The sample was a Si/$D_2O$ interface. The right-hand side shows the transmitted refracted beam and on the left is the specular reflection.

For the first officially scheduled experiment (July 2000) neutron reflectivity curves were measured from adsorbed lipid bi-layers at a silicon/water interface [1,2]. The lipid layers undergo a phase transition from a gel to a fluid phase and it is known that around the transition a substantial increase of the thickness at the interface is due to an increase in the quantity of water between the two bi-layers. The q-range explored on D17 (see Fig. 2) was larger than that measured in the past on this kind of sample as the lowest reflectivity is usually limited by background from bulk water and sample cell. With the high flux and wide-angle multi-detector [3], reflectivities of ~$10^{-7}$ could be measured in the reasonable time of one hour. Analysis is still in progress but the increased q-range should give additional information for modelling cell membranes. As the water thickness is largely defined by the first minimum in the reflectivity, a limited q-range (0.005-0.05 Å$^{-1}$ measurable in 7 minutes) is sufficient to follow the water thickness through the transition. In the

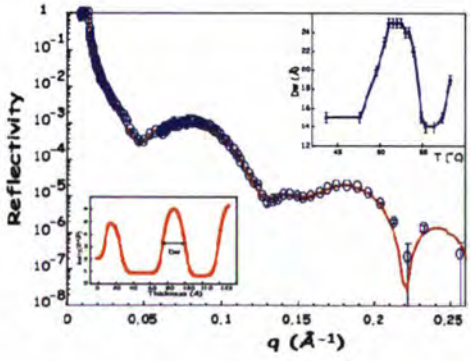


Figure 2: TOF reflectivity from a lipid bi-layer at 57°C in the fluid phase in $D_2O$ on a Si base. The bottom left insert shows the scattering length density profile fitted to the data with the water layer thickness Dw. The top right insert is the fitted water thickness as a function of temperature showing the sharp transitions. Measurement time was 90 minutes.

top-right insert of Fig. 2 the fitted thickness of the water layer between the two bi-layers is given at the different temperatures shown.

In addition to the ability to subtract incoherent backgrounds more efficiently there is another advantage in having a large area multi-detector. About the specular reflection there can be off-specular scattering arising from surface roughness or, as in the case described below, low-angle diffraction. The sample was a diffraction grating consisting of a glass substrate with thousands of strips of nickel, 900 Å deep separated by 10 μm (Ott and Menelle, Saclay). If this grating were placed perpendicular to the incoming beam then 10 Å neutrons would be diffracted only a few thousandths of a degree ($qx = 6x10^{-3}$ Å$^{-1}$), beyond the range of any existing small angle instrument. However, if the incoming beam strikes the grating surface at a glancing angle, then many diffraction orders can be seen in both the reflected and transmitted beams at measurable angles of deflection (Fig. 3). In addition to information on the stripe separation, the depth profile (consistent with 900 Å) is revealed in the ripples of intensity found running along the specular line and the various reflected diffraction orders.
The diagonal line of intensity coming from where the specular line just totally reflects is a Yoneda wing and is a consequence of the roughness along the surface of the nickel strips.

D17 is ideally suited to investigate not just structures as a function of depth but also within the plane such as magnetic grain boundaries or polymer droplets. Recently, both the monochromatic and the polarised neutron modes of the instrument have been successfully tested. The polarisation analyser will be installed in the winter shutdown 2000.

| | |
|---|---|
| Useful wavelength range | 2-20 Å |
| Qz range (normal to a surface) | $2x10^{-3}$ - 3 Å$^{-1}$ |
| Qx range (within a surface): | $1x10^{-6}$ - $2x10^{-2}$ Å$^{-1}$ |
| white beam flux | $10^{10}$ n/s/cm$^2$ |
| Detector size | 250 x 500 mm |
| Detector resolution | 1.5 x 3 mm |

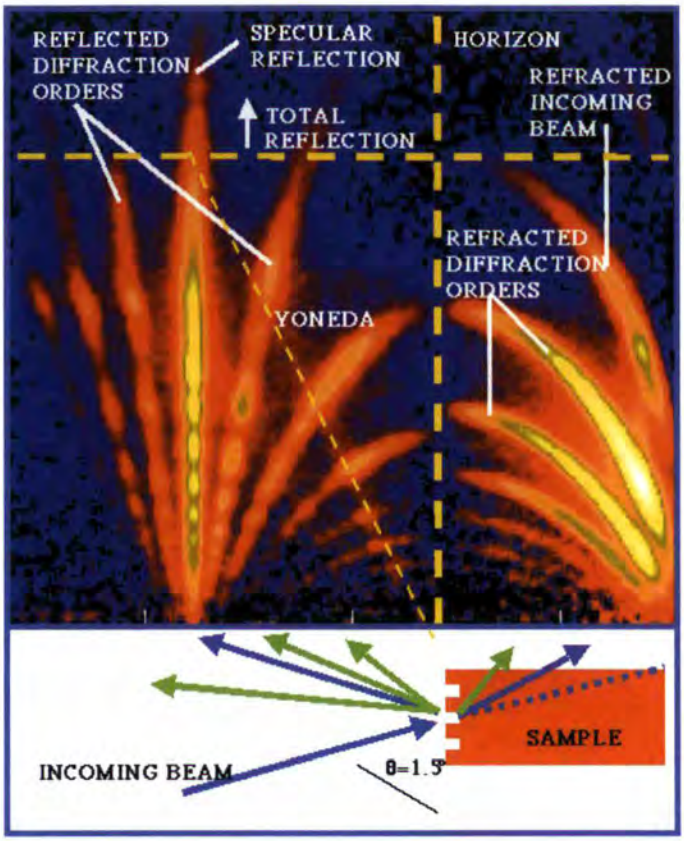


Figure 3 : TOF diffraction and subsequent refraction, reflection and interference from a Ni grating on a glass substrate. Measurement time was 30 minutes.


REFERENCES

- [1] T. Charitat et al., Eur. Phys. J. B (1999) 583
- [2] G. Fragneto et al., Eur. Phys. J.B., in press
- [3] Gabriel et al. J. Macromol. sci. phys. B37 (4) (1998) 463

# The D4C diffractometer
## for liquids and glasses


H.E. FISCHER (LURE, ORSAY)

G.J. CUELLO, P. PALLEAU, D. FELTIN (ILL)



**Immediately following its successful commissioning tests in May/June 2000, the D4C instrument became operational and welcomed its first users. Although the absence of the hot source allowed only 0.7 Å neutrons to be used, the first D4C experiments confirmed the anticipated performance of the new instrument. The scientific motivation of the D4C project was to increase the overall precision of the former D4B instrument by nearly an order of magnitude, implying not only a large increase in counting rate to reduce random error, but also a corresponding reduction in systematic error through improvements in detector stability and background counts. Higher instrumental precision was necessary to extend the capacity of D4 to a greater range of samples and in particular to new elements for which isotopic substitution experiments can be performed, such as silicon and carbon, the latter being useful for determining partial structure factors of biological solutions, for example.**


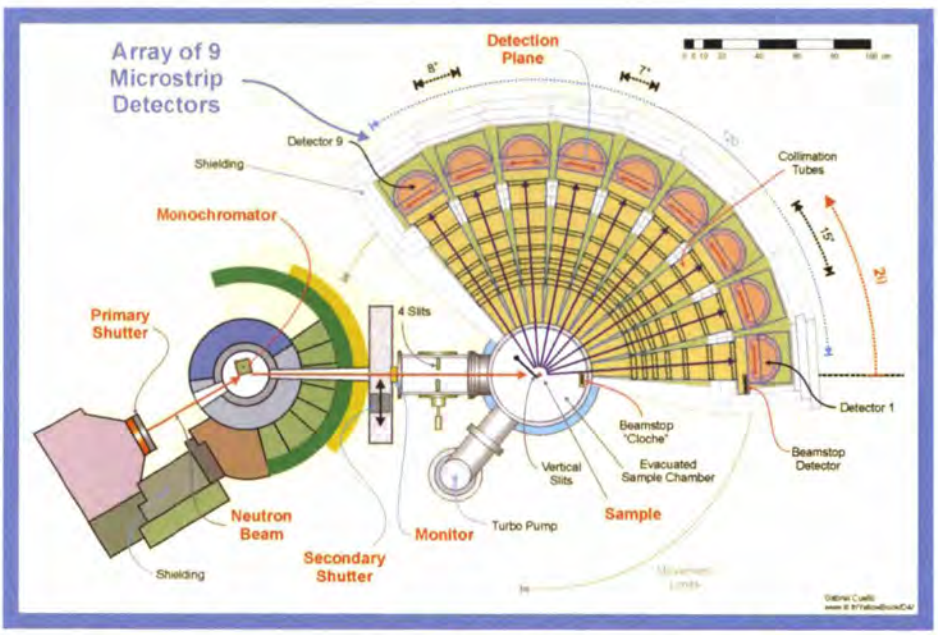


Figure 1: Top-view schematic of D4C showing the arrangement of the 9 microstrip detectors and their collimation tubes.

To increase detection solid angle and stability, the D4C project replaced the 2 multiwire detectors of the D4B liquids/glasses diffractometer with 9 microstrip detectors in a fan-like array (Fig. 1), and also made upgrades in neutron shielding, detector collimation and electronics. Both detector types use $^3$He as detection gas and have 64 cells allowing position-sensitive detection along one dimension (the scattering angle 2θ), but the cells of D4C are 100 mm high as compared to 70 mm for D4B. The usual configuration for D4B placed its two detectors at radii of about 1.5 m and 0.75 m (giving 2θ widths of 0.1° and 0.2° per cell, respectively). The 9 D4C detectors at a radius of 1.146 m (0.125° per cell) provide a factor of 4 increase in total solid angle of detection as compared to D4B's usual configuration, amounting to a factor of 5 increase in total counting rate for typical scans due to reduced detector movement time for D4C. For scattering angles of less than about 50°, the increase in counting rate over D4B is in fact a factor of about 10. Average statistical precision of 0.1 % (per 0.125°) can be obtained in a couple hours on D4C for 10 % scatterers of typical sample dimensions.

The mechanical stability and other advantages of the microstrip technology [1] permit a greatly enhanced counting stability for D4C's detectors (Fig. 2) as compared to the multiwire technology of D4B. Previous tests first verified the proper functioning of the D4C prototype detector and its associated electronics [2] and then finalised the designs for detector collimation, beamstops and neutron shielding [3]. A detector counting rate stability of $2 \cdot 10^{-4}$ over nearly 3 days was first measured for the D4C prototype detector as compared to only $10^{-3}$ for a D4B detector (Fig. 3), and then confirmed for the 9 D4C detectors during the May/June 2000 commissioning tests . The factor of 5 increase in total counting rate for D4C is thus matched by a factor of 5 increase in detector stability, as compared to D4B.

Each of the 9 microstrip detectors has an angular range of 8° in 2θ, which is slightly larger than half of the 15° fixed angular separation between detectors, allowing the execution of a complete 135.5° scan with sufficient overlap via a 7.5° displacement of the 9-detector ensemble on an air-suspension (Tanzboden) surface. This reasonably quick two-step scan technique allows some real-time diffraction studies to be performed at D4C. The minimum and maximum scattering angles for typical scans are about 1.5° and 137°.

The D4C detector collimation design assures that any point on the detection surface sees the solid angle subtended by the sample volume

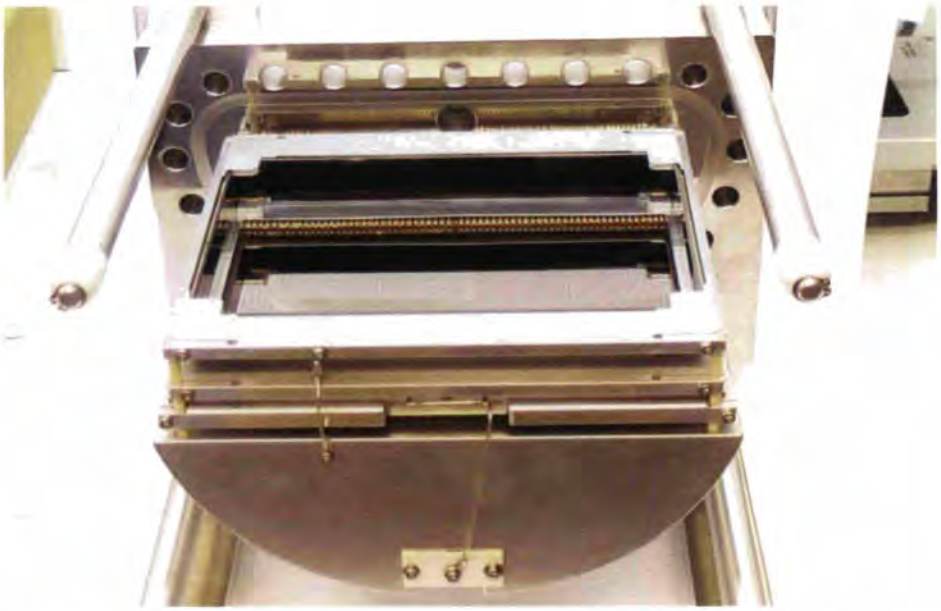

Figure 2: The interior of a D4C microstrip detector, showing the front face of the microstrip plate: a glass (Schott S8900) substrate supporting the chromium metallisation of the 64 microstrip detection cells, each 2.5 mm wide and consisting of 2 anodes and 2 cathodes. A depth of 30 mm for the $^3$He detection gas at 15 bar provides a detection efficiency of about 90 % at 0.7 Å and 69 % at 0.35 Å neutron wavelength. Electrically polarised guard plates at the four sides of the microstrip plate assure a uniform drift field and thus an undistorted diffractogramme.

to be surrounded by neutron-absorbing $B_4C$ plates placed ring-like within the evacuated collimation tubes of each detector [4]. A series of collimation rings is the most effective way to minimize the (partially neutron-diffusing) collimation surface area that is visible to both the detectors and to the sample or direct beam, thus reducing background counts to a minimum. To further reduce the background from direct-beam scattering at the lowest angles, the first detector's collimation uses isotopically enriched $^{10}B_4C$ (neutron absorption constant of 160 cm$^{-1}$ for a wavelength of 0.7 Å) and includes a mobile beamstop of $^{10}B_4C$ just before the detector. A second mobile $^{10}B_4C$ beamstop is placed further upstream in the sample bell jar, cutting off about half of the direct beam. This collimation+beamstops geometry prevents direct beam and parasitic peaks (e.g. from the aluminium bell jar window) from striking all 9 detectors for both scan positions and for all three standard wavelengths used at D4 (0.7, 0.5 and 0.35 Å). The neutron shielding is effected by 100 mm of thermalising polyethylene, followed by 10 mm of borated polymer, surrounding the 9-detector ensemble. The addition of Cd sheet would be superfluous since tests [3] showed the remaining very small background count rate to result principally from non-thermalised neutrons.

The independent instrument control systems for D4C and D4B facilitated a rapid instrument changeover prior to the D4C commissioning tests (0.7 Å wavelength neutrons only). Further tests at 0.5 and 0.35 Å will be made once the new hot source is installed. On-line software at D4C now provides for data normalisation and regrouping into diffractogrammes, the calibration of detector cell efficiences, the monitor deadtime correction, and for most other aspects of data reduction and analysis.

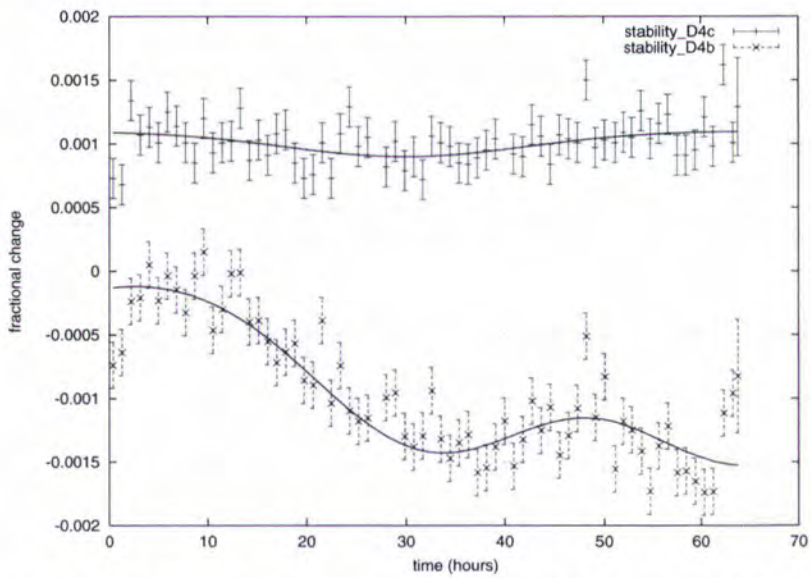


Figure 3: Stability of the D4C prototype microstrip detector (upper curve) as compared to that of a D4B multiwire detector (lower curve) when counting simultaneously on a vanadium sample (counts integrated over all 64 cells in both cases). Taking into account the counting statistics error bars, we estimate the stability of the D4C prototype detector to be $2 \cdot 10^{-4}$ over nearly 3 days, as compared to $10^{-3}$ at best for the D4B detector. The solid curves serve as guides to the eye.

Thanks and acknowledgement to participants in the D4C project, including:
Gilbert Viande, Steve Rowe, Jacques Loppé, Loïc Pajou, Roland Gandelli, Jo Pellegrino, Othman Jeddi, Pierre Thomas, Jean-Louis Champon and Anthony Pascaud, Jacques Munnier, Jean-Jacques Vernier, Raymond Rouquès, Bruno Guerard, Michel Gamon, Franck Cecillon, John Allibon, Marie-Claude Filhol.

## References


- [1] A. Oed, Nucl. Instr. and Meth. A 367 (1995) 34; A. Oed, Nucl. Instr. and Meth. A 263 (1988) 351.
- [2] H. Fischer, ILL Annual Report 1997, p. 85.
- [3] H.E. Fischer, P. Palleau and D. Feltin, ILL Report No. ILL98FI15T, 17 November 1998, 99pp.
- [4] H.E. Fischer, P. Palleau and D. Feltin, Physica B 276&278 (2000) 93.

# USANS:
# Ultra Small-Angle Neutron Scattering on S18

M. Baron, M. Hainbuchner, R. Loidl, H. Rauch (Atominstitut, Wien)

**Bonse-Hart small-angle scattering camera with channel-cut perfect crystals has been installed at S18 to extend the accessible Q-range by at least two orders of magnitude. This permits investigations of rather large structures as they exist in composed and micro-structured materials, in sedimentary rocks and macromolecular systems. A substantial improvement of the peak/background ratio makes the new instrument applicable to many new topics.**

Configured as a double Silicon crystal diffractometer the CRG(C) instrument S18 (neutron interferometer) can be operated as an ultra small-angle scattering instrument. In this mode of operation a momentum transfer range between $2.10^{-5}$ – $5.10^{-3}$ $Å^{-1}$ can be covered. In 2000, users from five different countries have used this new method for the structural investigation of minerals, composite, plastic, and micro-structured materials and cement pastes under different sample conditions.

Channel-cut perfect silicon crystals in a Bonse-Hart arrangement [1] are used as monochromator and analyser crystals. A so-called Agamalian-cut (an additional groove is cut into the long crystal plate where a cadmium absorber is inserted [2]) reduces parasitic reflections from the back-surfaces of the crystals and provides a peak to background ratio better than $10^{5}$ [3]. The use of a perfect crystal as monochromator provides a very small wavelength spread leading to a low intensity of the reflected neutron beam. Therefore the peak intensity is about 6000n/s, which corresponds directly to the luminosity of the source because nearly perfect reflecting components exist between the source and the detector. The schematic layout of the instrument is shown in Fig. 1. Test measurements showed a smooth transition of the scattering pattern measured with SANS and USANS. Thus USANS extends

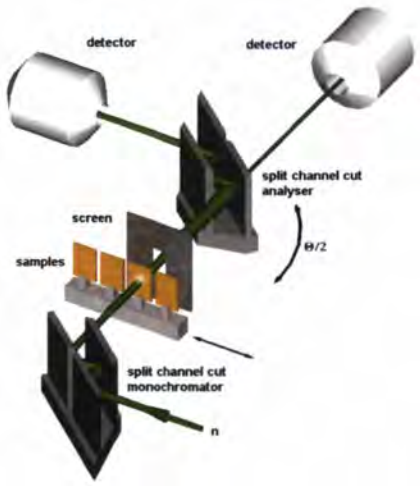


Figure 1: Sketch of the ultra small-angle neutron scattering system installed at the S18 neutron interferometer set-up.

the measurable Q-range by more than two orders of magnitude and permits together with the SANS technique the measurement of the scattering pattern over ten decades in scattering intensities. Inhomogeneities from 5 nm to 30 μm can now be investigated. Fig. 2 shows a typical combined SANS (D22) and USANS (S18) scattering pattern of a sedimentary rock sample. The two scattering curves show a clear overlap in the region around $10^{-3}Å^{-1}$ and the fractal scattering behaviour can be recognised obviously over 3 orders of length scales [4].

The inset of p.96 shows the types of samples that have been studied so far.

The measurements with the SiC/SiC$_f$ ceramic composite material will be described in some more detail. This material is considered to become an alternative first wall material for fusion systems [5]. The composite material has better ductile properties than pure SiC, but its gas permeability is still questioned, because unavoidable pores cause gas penetration and gas emissions. The behaviour of these pores under different conditions – thermal, radiation and gas atmospheres - can be studied by USANS. Fig. 3 shows the different USANS scattering patterns for two different SiC/SiC$_f$ samples thermally treated at 1750 and 1900 °C. The signal is related to the size of the pores. New SiC/SiC material is under development, which should be even more resistant against temperature, stress and radiation effects.

The USANS technique probes the microscopic structure of various materials and contributes to the future material developments. The intensities can be converted to an absolute differential cross section. Thus, USANS is an adequate extension to SANS measurements and should therefore become a standard method for material science.

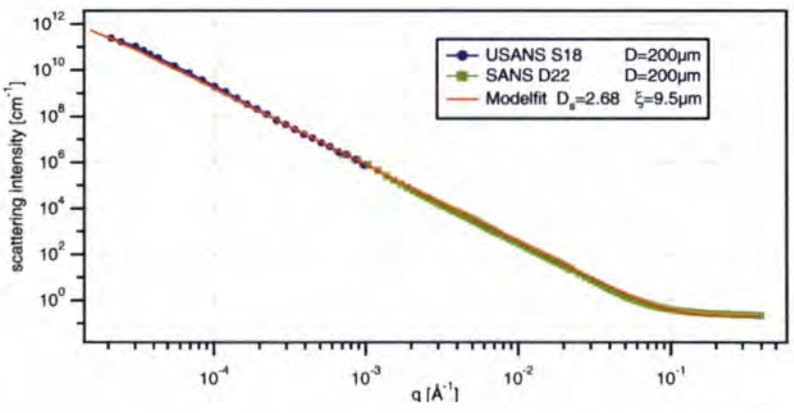


Figure 2: Combined scattering pattern of a Vosgian sandstone (200 mm) measured at D22 (SANS) and S18 (USANS). The fractal scattering behaviour manifests itself over more than three orders of magnitude in length scale with an upper fractal size limit of 9.5 μm.

- SiC/SiC$_f$ [1] composite materials: co-operation with L. Gobert, SEP, Bordeaux, France and with Euratom
- MHPC[2] samples: co-operation with H. Vogel, University of Freiburg, Germany
- Petroliferous sedimentary rocks: co-operation with A.P. Radlinski, Geological Survey, Australia
- MCM[3] biological samples: co-operation with H. Amenitsch, Elettra Trieste, Italy
- NbTi Superconductors and Portland cement pastes: co-operation with S. Mazumder, BARC-Bombay, India
- Plastic samples with silica fillers: co-operation with R. Triolo, University of Palermo, Italy
- Artificially structured materials: co-operation with Siemens, Munich, Germany

[1] silicon carbide fibre material
[2] methyl-hydroxy-propyl cellulose
[3] mobil oil composite material

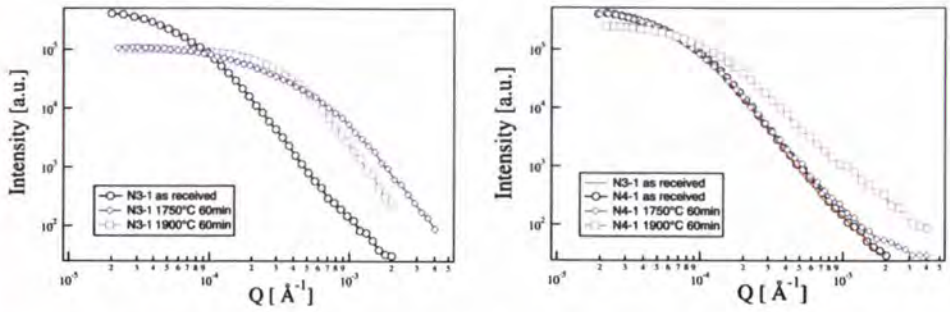


Figure 3: USANS scattering pattern of thermally treated N3-1(a) and N4-(b) SiC/SiCf compounds compared to the untreated specimen. Structural changes caused by the heat treatment can clearly be obtained. This material is considered as a new first wall material for fusion machines.


**REFERENCES**

● [1] U. BONSE, M. HART, APPL. PHYS. LETT. 7 (1965) 238 ● [2] M. AGAMALIAN, G. D. WIGNALL, R. TRIOLO, J. APPL. CRYST. 30 (1997) 345 ● [3] M. HAINBUCHNER, M. VILLA, G. KROUPA, G. BRUCKNER, M. BARON, H. AMENITSCH, E. SEIDL, H. RAUCH; J.APPL. CRYST. 33 (2000) 851 ● [4] A.P. RADLINSKI, E.Z. RADLINSKA, M. AGAMALIAN, G.D. WIGNALL, P. LINDNER, O.G. RANDL, PHYS. REV. LETT. 82 (1999) 3078 ● [5] A.S. PEREZ RAMIREZ, A. CASO, L. GIANCARLI, N. LE BARF, G. CHAUMAT, J.F. SALAVY, J. SZCZEPANSKI, J. NUCL. MAT. 233-237 (1996) 1257-1261


# Inelastic spin-echo on IN20: first experiments


● E. FARHI, J. KULDA, C.M.E. ZEYEN (ILL)

● B. FÅK (ISIS FACILITY, UK)



**We have employed the spin-echo option of the IN20 three-axis spectrometer to measure the line-width of the roton excitation in superfluid helium and to study the anharmonic behaviour of a zone-boundary 'transverse acoustic' phonon in germanium.**
**As the present results demonstrate, information on line-width and frequency variation in the range of 0.001 - 0.1 meV can be obtained for excitations with energies up to 10 meV.**


The access to experimental information on weak anharmonic effects in lattice dynamics, such as thermal variation of phonon frequencies and their natural line-widths in crystals far from phase transitions, is a long-standing problem. While light scattering can provide such information on optically active phonons near the Brillouin zone center, the extraction of similar information from neutron spectrometry data for phonons at arbitrary positions in the Brillouin zone is almost impossible. Analogous problems are encountered also in other fields like magnetism or physics of quantum liquids. Much improvement to this situation is expected from the combination of thermal beam three-axis spectrometers (TAS) with the neutron spin-echo (NSE) technique to access the momentum and energy transfer ranges of several Å$^{-1}$ and several tenths of meV and to achieve an energy resolution of the order of $10^0$ - $10^1$ μeV at the same time.

The TASSE option of the IN20 polarised thermal beam three-axis spectrometer is one of the prototypes of such a set-up [1]. It comprises two 1.6 m long superconducting precession coils (Fig. 1) inserted between the monochromator, sample and analyser tables, respectively. Their optimised field shape (OFS) guarantees a negligible cross-talk between the incident and scattered beam precession fields up to their maximum values of 1.4 T. Two pairs of spiral Fresnel coils are used to maintain a homogeneous field inte-

Figure 1: The three-axis spin-echo (TASSE) precession coils mounted on IN20.

gral value of up to 1 Tm across the whole beam cross-section. The maximum Fourier time of 3.2 ns for neutrons with $k = 2.661$ Å$^{-1}$ provides for a quasi-elastic resolution about 10 neV as verified in the quasielastic scattering experiments on a $KDCO_3$ crystal [1].

For the first inelastic scattering tests, we have chosen the roton line-width in superfluid helium, which has been studied extensively by neutron spin-echo [2] and back-scattering [3] experiments. The IN20 TAS instrument with $k_f = 2.662$ Å$^{-1}$ has been set up for the momentum ($Q = 1.925$ Å$^{-1}$) and energy ($\Delta E = 0.743$ meV) transfers corresponding to the roton minimum in the elementary excitation dispersion curve. The amplitude and phase of the NSE signal have then been measured as a function of the Fourier time for several temperatures [4]. Fig. 2 displays the results concerning the line-width being in excellent agreement with the previous work [3]. That finite width observed for the roton at T = 0.5 K is of instrumental origin and goes back to the condition to obtain an inelastic echo signal, which is not given by equal spin precession phases in the two coils, but rather by a phase difference stationary with respect to the energy transfer [5]. In the linear approximation the latter condition leads to

$$\frac{\Phi_M}{\Phi_A} = \left(\frac{v_i}{v_f}\right)^3 = \left(\frac{k_i}{k_f}\right)^3$$

where $\Phi_i$ are the field integrals in the first (M) and second (A) precession coil and $v_i$ and $v_f$ are the incident and scattered neutron velocities, respectively. In the case of helium rotons this condition is still fulfilled in a large range of Fourier times, but for energy transfers comparable to the neutron energy the non-linearity of the condition leads to a fast damping of the echo signal.

The importance if this effect is demonstrated on the case of a 9.8 meV phonon in germanium (cf. Fig. 1 inset) investigated with 14 meV neutrons [6]. These phonons, lying on the flat part of the 'transverse acoustic' branch along the [ξ00] direction (ξ = 0.8), are interesting because of their negative Gruneisen constant, responsible for the negative thermal expansion coefficient in Si, Ge and most of the III-V type superconductors. Although their dispersion relation is almost flat, providing optimum resolution conditions for the NSE, the observed line-widths at 13 K and at 298 K are

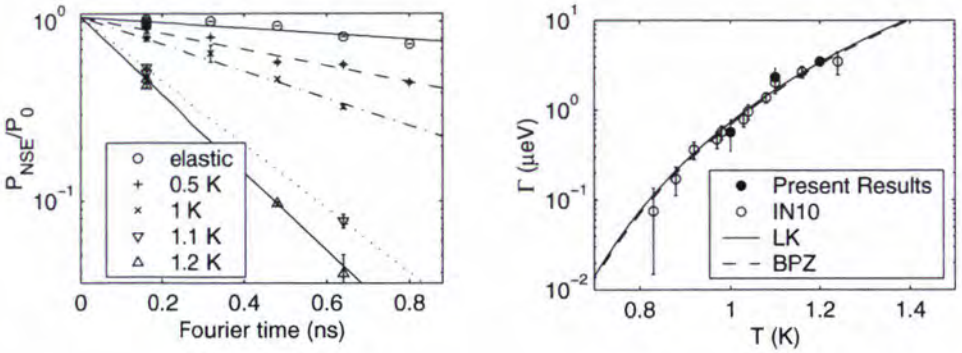


Figure 2: Decrease of the NSE contrast as a function of Fourier time for elastic scattering and for inelastic roton signal in superfluid $^4$He (a) and the resulting roton linewidth (b) compared to the previous IN10 results [3] and to the theoretical predictions.

157 (15) μeV and 266 (5) μeV, respectively. In absence of a more involved analysis we may assume that the low-temperature intrinsic line-width is negligible and that the observed value is entirely due to the non-linear terms beyond the condition (1). The room-temperature intrinsic phonon line-width would then amount to the difference 110 (20) μeV of the two observed values.

Fig. 3 displays the temperature dependence of the echo phase shift, obtained in the same experiment at a fixed Fourier time of 0.015 nsec and providing information on the temperature variation of the phonon frequency. The observed data can be described by an anharmonic model of Barron, used already in Ref. [7]. According to this approach the phonon frequency renormalises with the total vibrational energy of the crystal rather than with the crystal volume expansion as predicted by the popular quasiharmonic model. The fit of our low-temperature data in Fig. 3 results in the same parameter values as the fit of the high-temperature (300 -1000 K) data in Ref. [7] and proves that, even at low temperatures, the quasiharmonic model is not applicable.

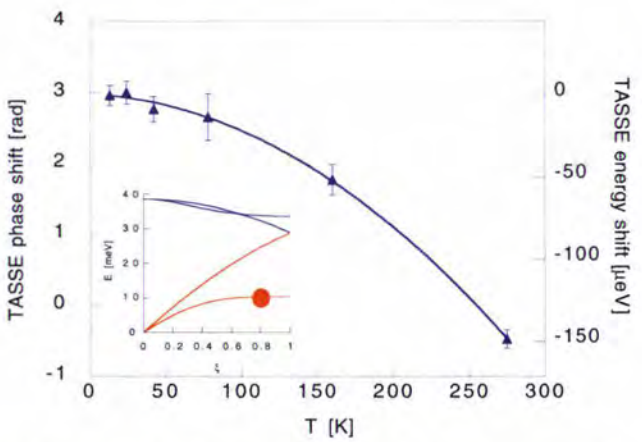


Figure 3: Temperature variation of the germanium [0.8 0 0] TA phonon frequency (cf. red point on the [100] phonon dispersion in the inset), the curve is a fit to Barron's model.


**References**

● [1] C.M.E. Zeyen, J. Phys. Chem. Solids 60 (1999) 1573 ● [2] F. Mezei, Phys. Rev. Lett. 44 (1980) 1601 ● [3] K.H. Andersen, J. Bossy, J.C. Cook, O.G. Randl, J.L. Ragazzoni, Phys. Rev. Lett. 77 (1996) 4043 ● [4] E. Farhi, B. Fåk, C.M.E. Zeyen, J. Kulda, Physica B in press, ● [5] F. Mezei in: Neutron Spin Echo, ed. F. Mezei, Lecture Notes in Physics Vol. 128, (Springer Verlag, Berlin, Heidelberg, New York 1980), p 9 ● [6] J. Kulda, E. Farhi, C.M.E. Zeyen, Physica B, in press ● [7] G. Nelin, G. Nilsson, Phys. Rev. B10 (1974) 612

# Spin-dependent neutron scattering length of $^3$He: a precise determination on IN15


- O. ZIMMER, W. KETTER (UNIVERSITY OF MAINZ)
- G. EHLERS, B. FARAGO, H. HUMBLOT (ILL)
- R. SCHERM (PTB BRAUNSCHWEIG)



**We have applied a new method to measure the poorly known spin-dependent neutron scattering length of $^3$He. The obtained result is of importance for the interpretation of the quantum liquid $^3$He, and for the few body theory in nuclear physics. The method relies only on relative measurements of neutron intensities without any absolute calibration. It employs polarised gaseous $^3$He and the unconventional use of neutron spin echo spectrometry.**


Compilations of neutron scattering lengths for the different isotopes are very useful for anyone who employs neutron scattering to study structure and dynamics of condensed matter. So far, scientists who study excitations in liquid $^3$He had to live with the disappointing fact that the spin-dependent scattering length of $^3$He was only known with poor precision. Its real part, $\mathrm{Re}(b_N)$, in the past could not be determined to better than 25% ($b_N$ denotes the difference of the triplet and the singlet scattering length). An improved knowledge of this value would be of great help for the interpretation of existing inelastic neutron scattering data, in order to reveal to which extent observed excitations in the quantum liquid originate from spin or density fluctuations. A second motivation to measure this quantity is to test nuclear theory. In fact, the nuclear four-body problem can be described with a relatively simple model, whose predictions can be tested through experimental results.

$^3$He is a strongly spin-dependent neutron absorber with a huge capture cross section for slow neutrons. At first glance a precise measurement of $\mathrm{Re}(b_N)$ thus seems ambitious. However, through the new method described below, the well known cross section for neutron capture of $^3$He turns out to be the only required information needed to determine $\mathrm{Re}(b_N)$.

Our method employs two types of neutron transmission experiments. The first one is a measurement of the "pseudomagnetic field" which can be attributed to any spin polarised sample as a consequence of the spin-dependent strong neutron-nucleus forward scattering. Its observable effect is a precession of the neutron spin around the axis of nuclear polarisation on propagation through the sample [1].

The pseudomagnetic precession angle $\varphi_{pm}$ is related to $\mathrm{Re}(b_N)$ via

$$\varphi_{pm} = \frac{1}{2}\lambda PNd \cdot \mathrm{Re}(b_N)$$

where $\lambda$ is the neutron wavelength, $P$ the nuclear polarisation, N the number density of the polarised $^3$He nuclei, and $d$ is the thickness of the sample.

A second type of experiment serves to determine the proportionality factor between $\varphi_{pm}$ and $\mathrm{Re}(b_N)$. Here the trick is to obtain the whole product $\lambda PNd$ from relative measurements, rather than from absolute measurements of its four individual factors.

Using non-polarised neutrons, we can measure the transmission of the polarised sample, $T(P)$, and of the non-polarised sample, $T(0)$. Their ratio is given by

$$R = \frac{T(P)}{T(0)} = \cosh\left[K_c \cdot \lambda PNd\right]$$

$K_c\lambda = \sigma_c$ is the cross section for neutron capture by $^3$He. $K_c = 2.963(5)$ fm is constant

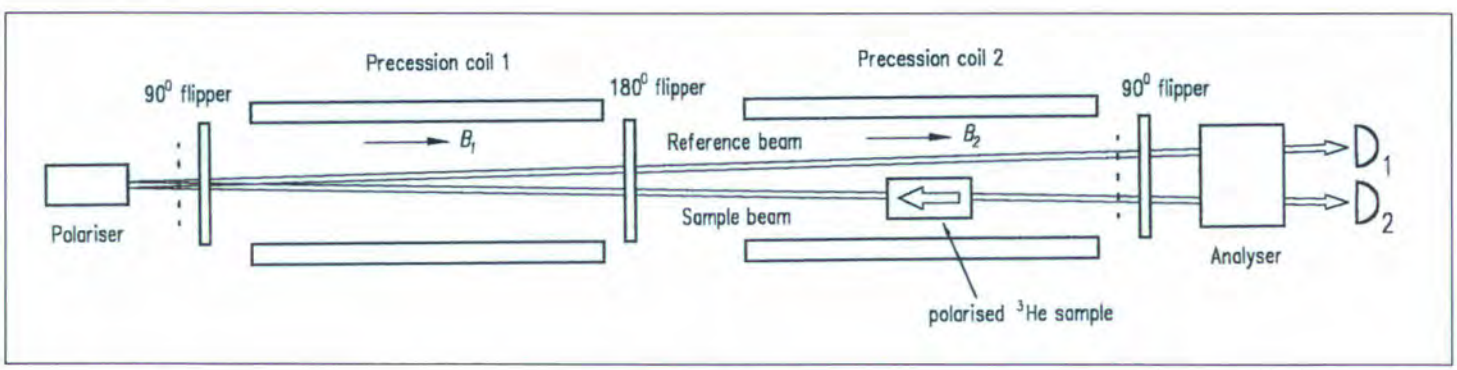


Figure 1: Beam configuration and sample position within the spin echo spectrometer IN15. The dotted lines indicate the two iron shims used to depolarise the beam for the measurement of $R$. In all measurements we related the neutron intensity through the sample to a "reference beam" passing by the sample. Common drifts in both beams thus are strongly suppressed (this two-beam technique was also employed in a prior measurement of the scattering length densities of SiBe, quartz and graphite).

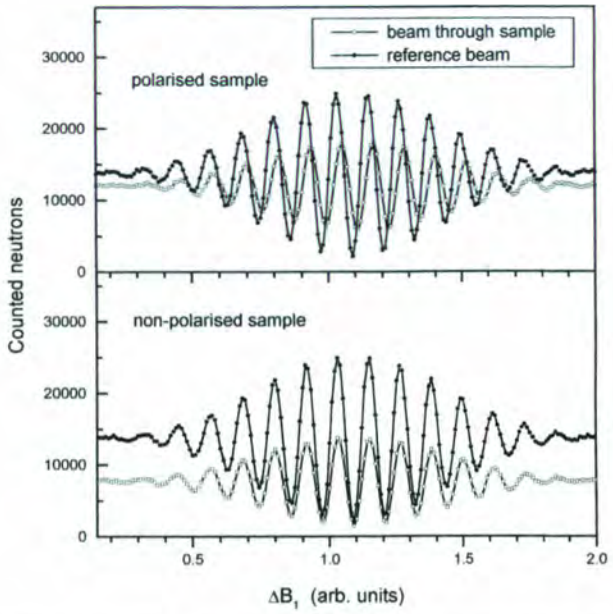


Figure 2 : Spin echo signals with the sample polarised, respectively, non-polarised. $\Delta B_1$ indicates the sweep of the magnetic field in the first precession coil (see Fig.1) which results in the intensity oscillations. The pseudomagnetic phase shift, caused by the nuclear polarisation of the $^3$He, is visible in comparing the upper and the lower figure.

because for slow neutrons $\sigma_C$ is proportional to $\lambda$. Obviously, it is the only absolute value one has to know. Its relative uncertainty of only 0.17 % limits the precision with which one can determine Re($b_N$) using the two equations. Of course, we felt challenged to approach this limit in real measurements.

Fig. 1 shows the experimental set-up. The measurements of $R$ were performed with thin iron shims inserted before and behind the sample, which completely depolarised the neutrons. Fig. 2 shows the first signals measured with polarised neutrons (shims taken out). According to the spin echo principle [2], the lowest intensity minimum intensity minimum corresponds to equal numbers of neutron spin precessions in the first and the second coil. The polarisation of the sample adds the pseudomagnetic field to $B_2$. We can extract $\varphi_{pm}$ as a phase shift, comparing the signals obtained with and without nuclear polarisation respectively. In the example shown, $\varphi_{pm}$ is about 50 degree. The measuring time for each pair of signals was 20 min. This should be compared to the drift of the phase difference between the two beams (less than 0.05 degree during 12 hours), and to the spin relaxation time of the $^3$He samples (120 hours). Note that the spin-dependent neutron absorption only reduces the amplitude of the spin echo signals but does not affect $\varphi_{pm}$.

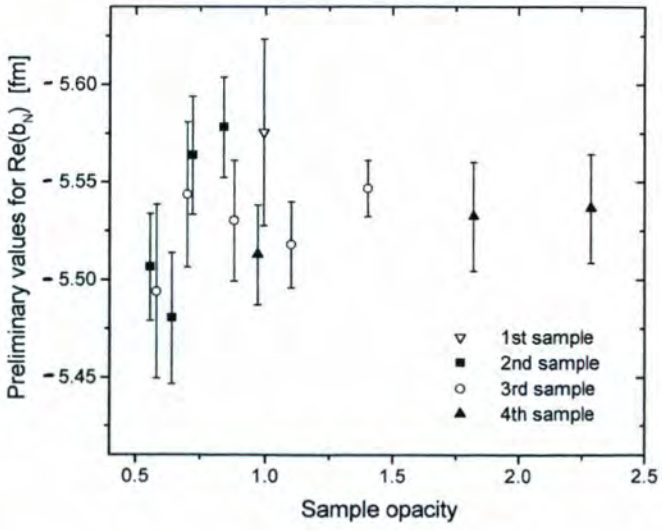


Figure 3: Preliminary values for Re($bN$). The abscissa is the so-called sample opacity, defined as $\sigma cPNd$. The nuclear polarisation can easily be reduced in steps, applying a depolarising magnetic field gradient for a short moment. Thus we could obtain several values with a single sample. The independence of the values of Re($bN$), measured under various conditions, demonstrates the reliability of our method.

Fig. 3 shows preliminary results for Re($b_N$), measured with four $^3$He samples of different gas pressure and at two different neutron wavelengths. For the final result, which will be published by the time of appearance of this report, we expect a precision of better than 0.3 %.

We note that pseudomagnetic precession in the past has been employed to determine Re($b_N$) of many isotopes [3]. In our present study we have used for the first time a spin echo spectrometer for this purpose. The combination with non-polarised neutron transmission results in a value of Re($b_N$) on an excellent level of precision. The quality of the data obtained is due to the stability of IN 15, the quality of the polarised $^3$He cells of the ILL, and a method which avoids any absolute calibrations.

Acknowledgement:
We are very grateful to the Directors of the ILL for giving beamtime on their discretion to this experiment. One of us (W.K.) was supported by a DFG grant (contract number OT 33-17-1).

REFERENCES

● [1] A. Abragam and M. Goldman, Nuclear magnetism: order and disorder, Clarendon Press, Oxford 1982, chapter 7 ● [2] F. Mezei, Neutron spin echo, Lecture notes in physics 128, Springer, Berlin 1980 ● [3] H. Glättli and M. Goldman, Methods of experimental physics, Vol. 23, part C, Academic Press, New York 1987

# Spin precession optics
## on the IN15 spin-echo spectrometer


- A. Frank, A.V. Kozlov, I.V. Bondarenko (FLNP, Dubna)
- G. Ehlers, P. Høghøj (ILL)



**The Larmor precession of neutron spins has been used as a clock to measure the delay in neutron time-of-flight caused by different neutron transit velocities in vacuum and in matter, respectively. The bound coherent scattering length density has been measured for a number of materials with an accuracy of a few percents. The absolute accuracy of the measurement of the neutron's delay time in matter achieved (3 - 5) x $10^{-10}$ s, which will make it possible in the future to perform many new experiments on the interaction time of the neutron with different quantum objects. It was found that the diamagnetic properties of the samples, especially pyrolytic graphite, affect the results remarkably.**


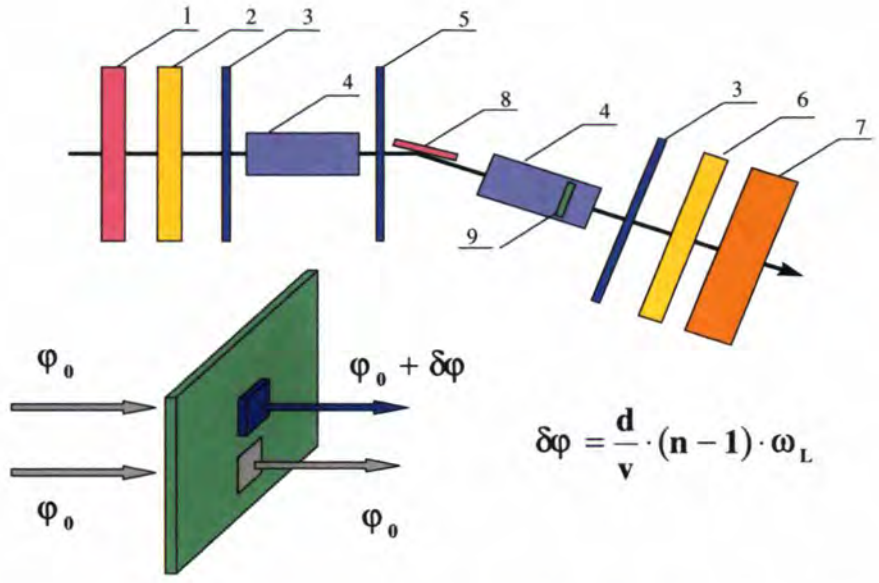


Figure 1: Scheme of the experiment. 1- velocity selector, 2- polariser, 3- π/2 flipper, 4- precession coils, 5- π flipper, 6- analyser, 7- position sensitive detector, 8- multi-layer monochromator, 9- position of the diaphragm with the sample holder (shown in the lower part).

Neutron spin-echo spectrometry is based on the comparison of neutron velocities before and after scattering by the sample under investigation. On its way to the sample, the neutron passes through a precession coil that provides a permanent magnetic field which is orthogonal to the spin direction. Another identical coil is located behind the sample. The change of the neutron velocity due to inelastic scattering in the sample results in a different time-of-flight through the second precession coil and hence causes a difference of the total precession phases. In fact, the Larmor precession of the neutron spin is used as a clock to measure the neutron velocity. If the neutron-sample interaction is purely coherent and elastic, as in all kinds of neutron optical phenomena, only the direction of the neutron's $\boldsymbol{k}$-vector changes but not its absolute value. It might appear therefore that in this case there is nothing to measure by spin-echo. But this is not exactly correct. The point is that the neutron spends some time during the interaction itself, i. e. the total time-of-flight also changes due to this interaction. This delay time can be measured by the Larmor clock in slightly modified experimental conditions, by placing the sample inside the precession path. Then the neutron will precess during the interaction at the Larmor frequency $\omega_L = \frac{2\mu B}{\hbar}$ and a delay time $\Delta t$ will introduce an additional precession phase $\Delta\varphi = \Delta t \cdot \omega_L$ which can be measured in the experiment. Here $\mu$ is the neutron magnetic moment and $\boldsymbol{B}$ is the magnetic induction.

In terms of stationary quantum mechanics the state of a precessing neutron is interpreted as the interference of two coherent waves with different spin projection onto the magnetic field vector. Since in a magnetic field the two spinor components have different wave vector $k_{\pm} = k_0\left(1 \mp \frac{\mu B}{E}\right)^{1/2}$, with $k_0$ the neutron wave vector in the absence of a field and $E$ its kinetic energy, a neutron-sample interaction will result in different phase variations for both waves. This gives an extra precession angle $\Delta\varphi$ which can be measured in the experiment.

For $\Delta t$ we can write $\Delta t = \frac{\Delta\varphi}{\omega_L} = \hbar\frac{\Delta\varphi}{2\mu B} = \hbar\frac{\Delta\varphi}{\Delta E}$, where $\Delta E = 2\mu B$ is the Zeeman energy splitting. This may be compared to the Bohm-Wigner formula $\Delta t = \hbar\frac{\partial\varphi}{\partial E}$, obtained from wave packet arguments [1,2]. This is the approach used for theoretical investigations of neutron optical phenomena in the presence of a magnetic field. The effect of multiple frequency neutron spin precession in Bragg diffraction [3] and an additional spin precession angle in neutron wave refraction were theoretically predicted long ago [4,5].

Experimental activity in neutron spin precession optics started some years ago [6]. In 1999 we demonstrated that the unique characteristics of the IN15 spin-echo spectrometer can contribute to this kind of experiment [7]. Here we report on some recent results obtained during a second experiment [8].

For a neutron passing through a sample with refractive index $n$ the additional precession phase may be expressed as $\Phi = \omega_L\frac{(1-n)d}{v}$, where $d$ is is the sample thickness and $v$ is the neutron velocity. This leads to $\Phi \propto \lambda^3$, because

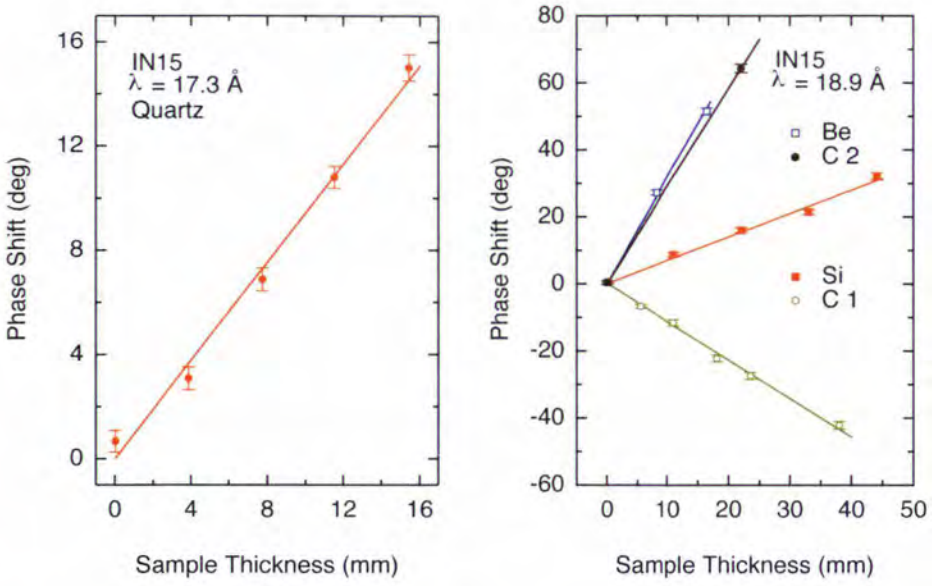


Figure 2: Phase differences between the two beams caused by refraction. C1 and C2 refer to carbon (graphite) with the beam parallel and perpendicular to the c axis, respectively.

$n - 1 = 2\pi\rho_b / \boldsymbol{k}^2$ where $\rho_b$ is the coherent scattering length density. The basic experimental idea was to directly compare the precession phases of two parallel beams, one passing through the sample (see Fig. 1), while the other does not interact with the sample. The sample was installed in the second precession coil. A multi-layer monochromator was used giving $\Delta\lambda/\lambda = 5\%$. The sample holder was designed such that the sample could be moved periodically and remotely between the two beams. The experimental procedure thus eliminated slow global phase drifts in the spectrometer. The measured phase differences between the two beams are presented in Fig. 2 for a number of materials in a field of B=1300G.

A surprising result was obtained for pyrolytic graphite. For this material the value and the sign of the phase shift depend on the orientation of the crystal (see Fig. 2). Furthermore, as we show below, if the neutron beam is parallel to the c axis, the phase shift does not follow the predicted $\Phi \propto \lambda^3$ law. We explain this effect by the large and anisotropic diamagnetic susceptibility of pyrolytic graphite, which has been documented in the literature [9]. The magnetic induction $\boldsymbol{B}$ and, consequently, the Larmor frequency inside the graphite is significantly smaller than outside. This gives a negative contribution $\Phi_{dia}$ to the phase difference which is proportional to the time the neutron spends in the sample and therefore proportional to wavelength: $\Phi_{dia} \propto \lambda$. We tested this hypothesis by measuring the phase shift at different wavelengths, and the result for graphite is given in Fig. 3. The solid line represents the best fit to a modified law $\Phi = A\lambda + B\lambda^3$. The fit parameters are $A=(-201\pm1)\times10^{-3}$ deg.mm$^{-1}$.Å$^{-1}$ and $B=(396\pm5)\times10^{-6}$deg.mm$^{-1}$.Å$^{-3}$. The diamagnetic susceptibility $\chi$,= defined as, $\chi = B_{int}/B_{ext}$ that corresponds to this value of $A$, is $\chi = (-0.574\pm0.003) \times 10^{-3}$. To check that this giant value is correct, the susceptibility $\chi$

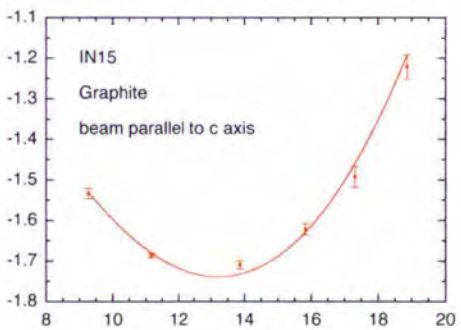


Figure 3: Dependence of the specific phase shift from the wavelength for pyrolytic graphite. The fit is discussed in the text.

was measured in a magnetometer at Laboratoire Louis Néel, Grenoble, using a small sample that was cut from the one used in the neutron experiment. This resulted in $\chi = (-0.574\pm0.003) \times 10^{-3}$ for the susceptibility measured with the external field parallel to the c axis, and a huge anisotropy: $\chi_\perp = \chi_\parallel$ [23] (field perpendicular to $c$), thus giving a reasonable agreement with the IN15 experiment. The bound coherent scattering length of graphite can be extracted from the parameter: $B$: $\rho b = 7.2\times10^{-6}$ Å$^{-2}$, which has to be compared to the table value $\rho b = 7.5\times10^{-6}$ Å$^{-2}$. Actually, even for silicon and beryllium (much smaller susceptibility) a term linear in wavelength can be observed.

The future perspectives of Larmor clock applications should be discussed from (at least) two points of view. As noted above, the additional phase in refraction is proportional to $(1-n)d$, which is actually the difference between the geometrical and optical paths. This could be used for the development of a phase contrast imaging technique in neutron optics [10]. Due to the $\lambda^3$ dependence of the phase shift it is preferable to use very slow neutrons. Note that we were able to measure the very small phase shift introduced by a 4 mm thick quartz sample using 17 Å neutrons: $\varphi = 3{,}07\pm0{,}44$deg . A general conclusion from our experiment is that such an imaging technique can be quite sensitive to magnetic properties of the samples, depending on the wavelength used.

Another aspect is the unique possibility to measure the interaction time with a quantum object. The absolute accuracy of the measurement of the interaction time in the present experiment was about $3\text{-}5\times10^{-10}$s, and was not limited by counting statistics. In our opinion a precision of $1\,10^{-10}$s may be reached soon because of the high phase stability of IN15. We plan in the future to perform a number of experiments to measure tunneling through two- and multi-barrier structures, and the time the neutron spends in the process of total reflection.

Acknowledgement:
Special thanks are due to Eric Eyraud, Laboratoire Louis Néel, Grenoble, for his assistance in the susceptibility measurement.

## References

● [1] Bohm, Quantum Theory (Prentice-Hall, New York, 1951) ● [2] E.P. Wigner, Phys.Rev. 98 (1955) 145 ● [3] V.G. Baryshevsky, JETP Lett, 33 (1981) 74 ● [4] A.I. Frank, Nucl. Inst. Meth. A284 (1989)161 ● [5] V.G. Baryshevsky, S.V. Cherepitsa, A.I. Frank, Phys.Lett. A153 (1991) 229 ● [6] N. Achiva et al., J.Phys. Soc. Jpn. 65 Suppl. A (1996) 183 ● [7] A.I. Frank, et al. Proceeding of the ISINN7 conference, Dunba, 1999, pp. 126-128. ● [8] A.I. Frank, et al. Proceeding of the PNCM-2000 conference, Gatchina, June 2000. To be published in Physica B ● [9] Landolt-Börnstein Numerical Data and Functional Relationships in Science and Technology, Group II, Vol. 16, edited by K.-H. Hellwege and A. M. Hellwege, Springer, Berlin, New York, chapter 9.1, and references therein ● [10] A.I. Frank, Usp. Fiz. Nauk, (Sov. Phys. Uspechy) 161 (1991) 95, A.I. Frank. SPIE , 1738, 323

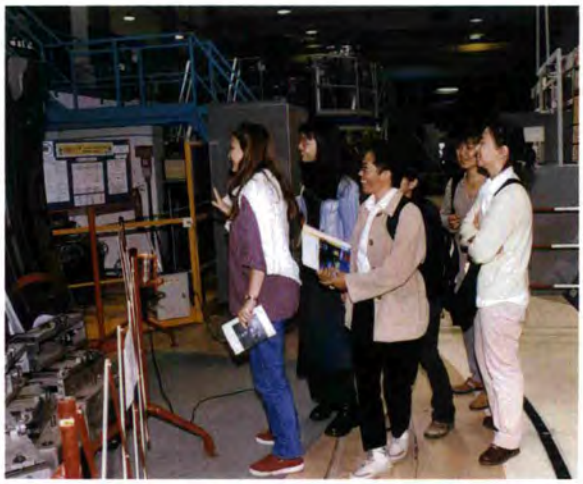

Magic mirrors demonstration on IN10, during the Open Days in May 2000.

Remembering the good old days: Diana Dijoux with John White, the British ILL director from 1975 to 1980.

Ross Stewart (left) and Andrew Wildes (right) singing goodbye to Herma Büttner on the day of her leaving pot in January 2000.

From the left: Pierre Convert, Michel Mollier and Olivier Isnard enjoying the break during the Journée D4, in September 2000.

# Workshops

## Workshops in which ILL was a major player in the year 2000:

| | | | |
|---|---|---|---|
| **Dynamics in Confinement** | organised by Bernhard Frick (ILL), Reiner Zorn (Jülich) and Herma Büttner (ILL) | ILL | 26-29 January |
| **Monte Carlo Simulation of Neutron Spectrometers (SINS)** | organised by Ian Anderson, Ron Ghosh and Emmanuel Farhi (ILL) | ILL | 31 January |
| **European Neutron Polarisation Initiative (ENPI)** | organised by Francis Tasset and Trevor Forsyth (ILL) | ILL | 24-25 February |
| **Neutron characterisation of Industrial Materials** | organised by Peter Lindner and Albert Wright (ILL) | ILL | 29 June |
| **Journée D4** | organised by Pierre Palleau and Gabriel Cuello (ILL) | ILL | 15 September |
| **Workshop on Correlated Fermions** | organised by Christian Vettier (ILL) and Yves Petroff (ESRF) | ILL | 30-31 October |
| **Ultracold Neutron Anomalies** | organised by Peter Geltenbort, James Butterworth and Thomas Brenner (ILL) | ILL | 25 November |

## International Workshop on 'Dynamics in Confinement'

More than one hundred participants, at least half of them not being neutron scatterers, attended the 4-day international workshop on Dynamics in Confinement on 26 January 2000.

Reiner Zorn, Herma Büttner and Martine Espitallier at the poster session of the workshop 'Dynamics in Confinement'.

The meeting - held in the Chadwick amphitheatre of the ILL - focussed on the changes of dynamics due to confinement in relation to bulk properties, especially in supercooled liquids and glass transitions. The scope of the workshop has been broadened by adding classical topics such as small molecule dynamics in confinement, adsorbates and fringe topics where the importance of confinement is less obvious. The workshop was structured into 7 sessions: "Theory and simulation", "Liquids and Glasses in Confinement" , "Adsorbates, Atoms & Molecules in Confinement", "Quantum Liquids in Confinement", "Water in Confinement", "Biological, Colloidal and Polymeric Confined Systems" and "Confinement in Thin Films". Besides the 13 invited speakers a further 26 speakers from different countries presented results from experiments, simulations and theory. There were also two poster sessions, where an additional 42 contributions were presented.
The sessions were well attended and lively discussions took place. The meeting brought together many scientists working in this field using very different methods and different types of samples. Furthermore, it provided a complete review of the experimental and theoretical situation. The organisers of the workshop have encouraged some participants to consider inelastic neutron scattering methods as an appropriate investigation tool.

## Monte Carlo SImulation of Neutron Spectrometers (SINS)

The SINS workshop reviewing Monte Carlo (MC) methods under development in Europe was held at the ILL on 31 January 2000. The aim was to bring together groups developing different simulation packages, potential users and component developers. About thirty-five scientists from the ILL-ESRF joint site attended the meeting. Recent advances have shown that the accurate simulation of neutron instruments enables the optimisation of the instrument configuration: accurate determination of good resolution functions is vital for data analysis. Furthermore, it is vital in studies for instrument improvements or new designs.
The meeting was opened by a general introduction and an overview of the important points to be considered in a MC neutron ray-tracing programmes. The rest of the meeting was then devoted to talks describing the different packages available:
- the VITESS programme (HMI, Berlin), initially designed to simulate spallation source instruments is now available for various operating systems. The presentation included the demonstration of an attractive Graphical User

Jan Šaroun and Thomas Hansen debating the merits of ResTrax at the SINS practical demonstration session.

Interface for both simulation design and usage:
- the McStas package (Risø) has a source code, including instrument design and visualisation tools, now available for most platforms. As an example of application, a single crystal diffraction pattern simulation was highlighted;
- the ResTrax (NPI and ILL) programme, optimised for simulating triple-axis spectrometers, has recently also proved very useful for simpler two-axis problems. However, at present ResTrax only runs on a limited number of systems;
- lastly, the possibility to adapt the Shadow X-ray tracing simulation program (ESRF) to neutrons was presented. This evolution seems quite promising, but still requires substantial effort.

The meeting concluded with most of the participants having an opportunity to debate the various merits of each programme with the authors during a practical demonstration session. Despite the limited time available the workshop proved really useful. Further information on the workshop as well as some bibliographic references can be found at the following address:
http://www.ill.fr/tas/mcstas/workshop0100.html.

## European Neutron Polarisation Initiative (ENPI)

The first ENPI meeting was held at the ILL on 24 and 25 February 2000. ENPI is a network of eight laboratories co-ordinated by the ILL. It is funded over three years to the tune of 0.9 M € by the European Commission FP5 programme. The primary objectives of ENPI are:

- to improve and make widely available tools for neutron polarisation;
- to equip instruments at European facilities with such tools;
- to train young scientists and technicians in using them.

The ENPI network has stemmed from the highly successful XENNI programme for neutron instrumentation and is one of several EU neutron scattering initiatives in FP5. These include the PECNO, TECHNI, SCANS, Vesuvio and Cool Neutrons programmes and the Neutron Round Table.

Thomas Brückel (Jülich) and Roger Eccleston (ISIS) in a friendly discussion during ENPI meeting.

The meeting started with the scientific session, opened by an introduction to the network and which was then devoted to talks from each of the partner laboratories on their current roles and future projects within the network. The day was rounded off with a very pleasant working dinner at the Château de Sassenage. The second day was devoted to the more managerial aspects of the network. The organisation of the project was discussed and the programme until the next meeting in June at PNCMI'2000 was decided. The co-ordinators were then given guided tours of the Neutron Optics Laboratories before the meeting ended. For further information refer to the ENPI web-site http://enpi.vitamib.com.

## Neutron characterisation of Industrial Materials

A one-day workshop on the Characterisation of Industrial Materials using Neutrons was held at the ILL on 29 June. One goal of this workshop was to bring together research scientists from publicly-funded applied research laboratories and those from private industrial laboratories. Participants were shown how neutron techniques are currently being used in pre-competitive applied research and confidential proprietory research. The other purpose of this meeting was to provide a forum for all those concerned to meet and to discuss how joint projects using these advanced resources could be launched. The industrial and public sectors were equally represented both in terms of speakers and participants.

The first morning session was devoted to a brief introduction of the ILL facilities and to the presentation of experimental techniques relevant to industrial research, such as small-angle neutron scattering, neutron diffraction and neutron reflectometry. The second morning and the afternoon sessions turned to contributions from ILL users on specific research applied to real industrial materials. Speakers outlined the usefulness of the small-angle neutron scattering technique in such fields as surfactant science for the development of detergents, the study of polymer blends, fuel additives and latex dispersions, the study of filtration processes and food science. Further contributions underlined the use of neutron diffraction in the characterisation of natural and industrial fibres, in the observation of hydrogen bonding in water-sensitive fibres such as cellulose, and in the application of neutron diffraction for studying active porous materials such as zeolites and catalysts. Finally, the neutron strain scanning technique was presented as an ideal method for the control of linear friction welding techniques now being developed

Roberto Coppola (Frascati) and Albert Wright discussing the use of neutrons in materials for the future: plastic!

for the production of the next generation of turbine blades for air engines. The examples from applied research presented during the meeting are indicative of the broad range of applications for which neutrons are now used to characterise industrial materials. The workshop provided a forum for all those concerned to meet and discuss how to set up joint projects using the unique facilities available at ILL.

## Journée D4

We are happy to announce to the whole neutron community, but especially to those working with liquids and amorphous systems, that the upgrade of the D4 diffractometer was achieved with success and within the planned time scale, and that the instrument is now available and awaiting beamtime proposals. The results of the commissioning tests and of the first scheduled experiments showed that all the objectives of the project have been reached and, notably, the increase of the overall counting rate by a factor of 5 and the increase of the detection stability by a factor of 5, to become $2x10^{-4}$ over several days. The project was completed within budget, in time and to specification.

A half-day workshop, the "Journée D4", was held on 15 September to celebrate this success. This inauguration brought together the previous D4 instrument responsibles, as well as a number of "regular" D4 users. The workshop was divided into two sessions, the first being opened by Pierre Chieux, who presented the history of the D4 diffractometer, followed by Pierre Palleau and Dominique Feltin, who described the technical and instrumental aspects of the diffractometer up-grading (neutron shielding, detector collimation, microstrip detector design and operation). The second session was devoted to the presentation of the results from the D4 tests (Henry Fischer, LURE) and the results of the first scheduled experiments (Françoise Leclercq, Lille, and Adrian Barnes, Bristol). A big hurrah to the D4-team!


Anton Oed explaining to Patrick Van Esch the avalanche mechanism in a microstrip detector.

## Workshop on Correlated Fermions

Philippe Nozières has been leading the Theory Group at the ILL for 28 years. He has stepped down from his position while remaining a visiting scientist at the ILL. Philippe's pivotal role in the field of condensed matter physics and his personality have attracted many theoreticians and have contributed considerably to the development of theoretical physics. The ILL and the ESRF organised a lively and friendly meeting on 30 and 31 October, which focused on one of Philippe's favourite subjects of interest: Correlated Fermions. The meeting consisted of invited presentations related to the central theme. A wide range of topics was covered and a significant amount of time was left open for discussions and exchanges. Further information concerning the programme and the participants can be found at: http://www.ill.fr/Events/nozieres.html.

Philippe Nozières during the Workshop on Correlated Fermions, organised by the ILL and ESRF to mark his retirement.

Philippe Nozières is still present at the ILL, sharing his free time between CNRS LEPES Laboratory (Laboratoire d'études des propriétés électroniques des solides) and the ILL Theory Group. The ILL is very grateful to Philippe Nozières for the activity he has developed to make the Theory Group so attractive and visible.

## Ultracold Neutron Anomalies Where Do We Stand?

A "mini-workshop" was organised to review the latest results on ultra-cold neutron storage and spectroscopy. This work was initiated at ILL several years ago to shed more light on recurrent reports indicating that the lifetimes measured for ultra-cold neutron (UCN) stored in traps with material walls are always shorter than expected, presumably due to enhanced wall reflection losses. Long storage lifetimes are especially needed for precise measurements of the neutron lifetime for beta-decay.
About 25 participants vividly discussed the contributions which dealt with:

- depolarisation and UCN spectroscopy; neutron-gamma data, storage lifetimes and spectroscopy;
- analysis of quasi-elastic processes;
- theory of wall losses; scrutiny of the neutron optical model;
- reflectivity of VCN - very cold neutrons and spectroscopy ;
- UCN efflux from the trap

It became clear that no commonly accepted explanation of the "anomalies" has been reached so far. Among other proposals, a new type of "low-temperature Fomblin" material (perfluorinated poly-formaldehydes with low melting temperatures) should be studied as a possible low-loss wall coating, and the role of quasi-elastic processes and of surface cleanliness should be further investigated - although ultra-high-purity surface conditions are difficult to achieve in the large and complex UCN traps needed in UCN storage experiments. A detailed report of the meeting can be obtained from Peter Geltenbort (geltenbort@ill.fr).

Roger J. Stewart (right), Reading University, and Jessica Cheung prepare their experiment on D22.

Jonathan Goff (right), Liverpool, back on D10 again with his student Simon Lee (left).


Winfried Petry (T.U. München), happy user on the up-graded IN13. From the left, Claude Pfister, Frédéric Marchal, Alessandro Paciaroni, Winfried Petry and Jérôme Locatelli.

The up-graded D4 welcomes its first users: from the left, Fabrice Cavillon, Pierre Damay and Françoise Leclercq, Lille.

# Experimental programme

**Reactor operation**

**Instrument list**

**Beam-time allocation**

**Instrument performance**

**Industrial use of neutrons**

**User forum**

**User satisfaction**

# List of instruments (Dec. 2000)

## ILL INSTRUMENTS

| | | |
|---|---|---|
| D1A (50%) | powder diffractometer | operational |
| D2B | powder diffractometer | operational |
| D3* | single-crystal diffractometer | operational |
| D4 (50% with IN1)* | liquids diffractometer | operational |
| D7 | diffuse-scattering spectrometer | operational |
| D9* | single-crystal diffractometer | operational |
| D10 | single-crystal diffractometer | operational |
| D11 | small-angle scattering diffractometer | operational |
| D16 | small momentum-transfer diffractometer | operational |
| D17 | reflectometer | operational |
| D19 | single-crystal diffractometer | operational |
| D20 | powder diffractometer | operational |
| D22 | small-angle scattering diffractometer | operational |
| IN1 (50% with D4)* | three-axis spectrometer | operational |
| IN3 | three-axis spectrometer | operational |
| IN4 | time-of-flight spectrometer | commissioning |
| IN5 | time-of-flight spectrometer | under reconstruction |
| IN6 | time-of-flight spectrometer | operational |
| IN8 | three-axis spectrometer | operational |
| IN10 | backscattering spectrometer | operational |
| IN11 | spin-echo spectrometer | operational |
| IN14 | three-axis spectrometer | operational |
| IN16 | backscattering spectrometer | operational |
| IN20 | three-axis spectrometer | operational |
| PF1 | neutron beam for fundamental physics | operational |
| PF2 | ultracold neutron source for fundamental physics | operational |
| PN1 | fission product mass-spectrometer | operational |
| PN3 | gamma-ray spectrometer | operational |
| *Strain Imager* | | *under construction* |
| *VIVALDI* | *thermal neutron Laue diffractometer* | *under construction* |

* hot neutron instruments

## JOINTLY FUNDED INSTRUMENTS

| | | |
|---|---|---|
| DB21 (50%) | single-crystal diffractometer | operational, with EMBL |
| LADI (50%) | LAUE diffractometer | operational, with EMBL |
| IN15 | spin-echo spectrometer | operational, with FZ Jülich and HMI Berlin |

## CRG INSTRUMENTS

| | | |
|---|---|---|
| ADAM | reflectometer | CRG-B operational |
| BRISP | Brillouin spectrometer | CRG-B under development |
| D1A | powder diffractometer | potential CRG |
| D1B | powder diffractometer | CRG-A operational |
| D15 | single-crystal diffractometer | CRG-B operational |
| D23 | single-crystal diffractometer | CRG-B commissioning |
| EVA | reflectometer | CRG-B operational |
| IN12 | three-axis spectrometer | CRG-B operational |
| IN13 | backscattering spectrometer | CRG-A operational |
| IN22 | three-axis spectrometer | CRG-B commissioning |
| S18 | interferometer | CRG-C operational |

## TEST BEAMS

| | |
|---|---|
| CT1, CT2 | detector test facilities |
| S42 | Laue-crystal alignment facility |
| T3 | neutron optics test facility |
| T13A,C | monochromator test facility |
| T17 | cold neutron test facility |

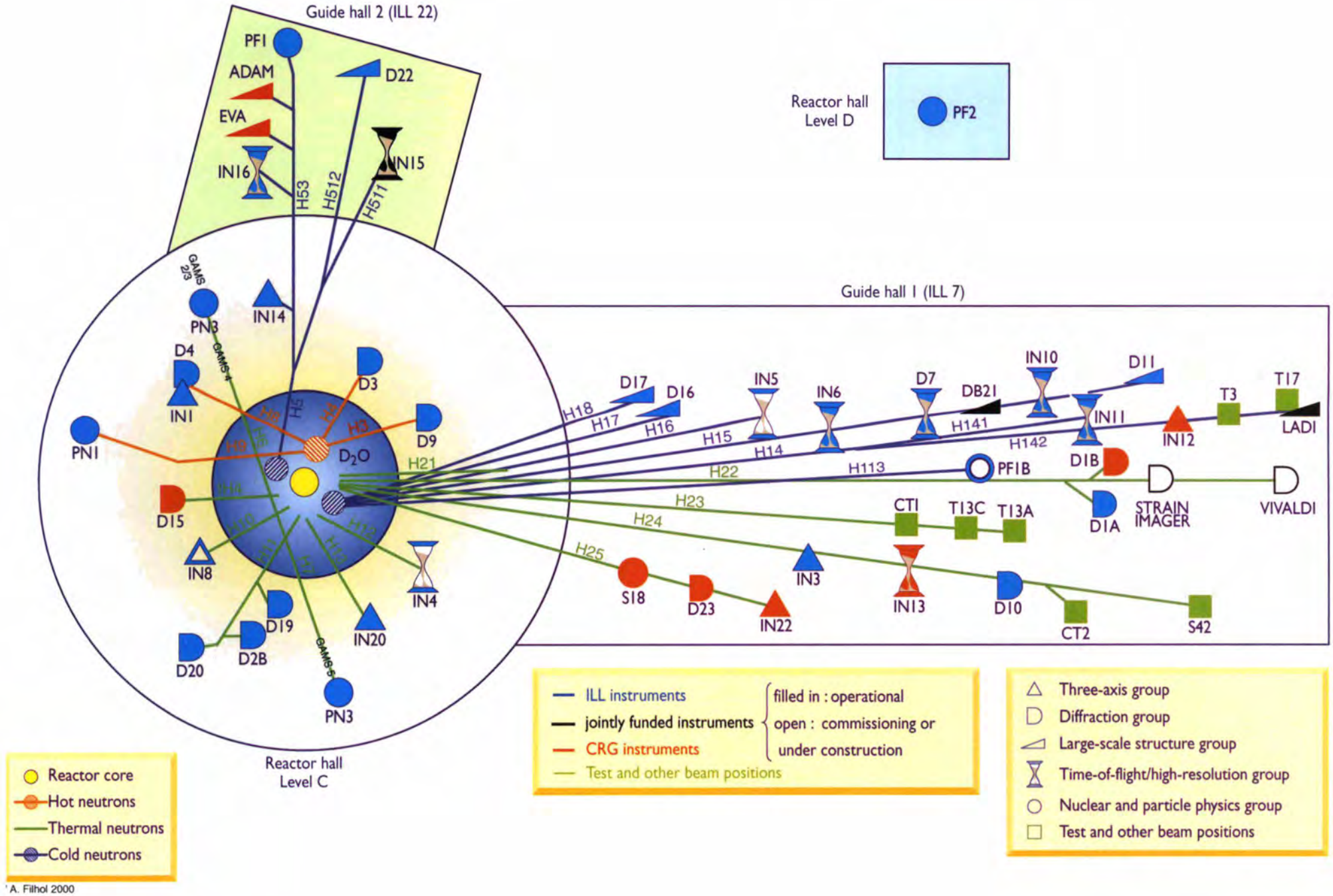


A. Filhol 2000

# Reactor operation

| Cycle | starting date | finishing date | days scheduled | days of operation | unscheduled shutdowns |
|---|---|---|---|---|---|
| 121-2 | 15/02/00 | 02/03/00 | 16 | 16 | 0 |
| 122 | 14/03/00 | 04/05/00 | 50 | 51 | 0 |
| 123 | 23/05/00 | 12/07/00 | 50 | 50 | 0 |
| 124 | 17/08/00 | 06/10/00 | 50 | 50 | 1 |
| 125 | 18/10/00 | 08/12/00 | 50 | 49 | 1 |
| **Total** | | | **216** | **216** | **2** |

Table 1: Reactor operation in 2000.

Replacing the H10 guide: Jacques Italia checks the dose rate before starting operations.

work will increase the instrument PN1's performance and will allow users to alternate between periods of irradiation and monitoring the count-rate on a particular sample. Two detritiation operations were performed in the second half of the year. In the first operation a little over 60 m³ of water from the reactor were treated, with tritium activity in the reactor water being reduced by a factor of two.

The second operation concerned the treatment of 2 m³ of water, to reduce its activity to about 10 mCi/l. This water with a very low tritium level will be used for rinsing the unloading flasks, in order to reduce the levels of liquid waste produced during these operations. Following these detritiation operations, the equivalent of approximately 15 gm of tritium were sent to the CEA. Prior to the operations the tritium letdown equipment had been modified and requalified, to adapt it to the new transport flasks.

The hot source was removed from the reactor to the storage pool in December 1999, and the reactor has operated without hot source during the year 2000. The design of the new source has been completed and the construction will be subcontracted to an external manufacturing company. The new hot source is expected to arrive before the end of 2001. In the meantime, the instruments D3, D4, D9 and IN1 will continue operating with thermal neutrons.

More information about the instrument performance can be found on the ILL web under http://www.ill.fr/hotsource.html.

The 216-day programme of operations planned for scientific work in the year 2000 was completed successfully. Any time lost due to the unscheduled shutdowns noted above was compensated by an extension of cycles 122 and 125. The first unscheduled shutdown involved a suspension of the cycle 124 for about one hour as a result of technical problems with a compressor used on the refrigeration circuit for the cold sources. A longer shutdown during the cycle 125 was decided by the Management following industrial action.
The maintenance programme, since the replacing of the reactor block six years ago, is proceeding smoothly and this year work was carried out as scheduled to replace the safety rod absorbers on the H9 and H10 guides. Amongst the new projects, the "source changer" tube for H9 has been transformed, as well as its associated control system. This

Preparing the H10 guide for replacement (N. Laurens, M. Samuel and N. Della-Gatta).

# Instruments

The instrumental facilities at the ILL are shown in the schematic diagram on p.111. Besides the 30 ILL instruments there are 9 CRG-instruments, which are operated by external Collaborating Research Groups. There are currently three different categories of CRG instruments.

- CRG-A in which the external group leases an instrument owned by ILL. They have 50% of the beam time at their disposal and for the other 50% they support ILL's scientific user programme.
- The CRG-B category owns their instrument and have 70% of the beam time, supporting the ILL programme for the other 30%.
- Finally, CRG-C instruments are used full time for specific research programmes by the external group who has exclusive use of the beam.

DB21, LADI and IN15 have a special status, since they are a joint venture of ILL with other laboratories: in the case of DB21/LADI with EMBL and for IN15 with FZ Jülich and HMI Berlin.

The list of instruments as of December 2000 is summarised below (CRG instruments are marked with an asterisk *):

- powder diffractometers: D1A, D1B*, D2B, D20
- liquids diffractometer: D4
- single-crystal diffractometers: D3, D9, D10, D15*, D19, DB21, D23*, LADI
- small-angle scattering: D11, D22
- low momentum-transfer diffractometer: D16
- reflectometers: ADAM*, D17, EVA*
- diffuse-scattering and polarisation analysis spectrometer: D7
- three-axis spectrometers: IN1, IN3, (IN8 under reconstruction), IN12*, IN14, IN20, IN22*
- time-of-flight spectrometers: IN4, IN5, IN6,
- backscattering and spin-echo spectrometers: IN10, IN11, IN13*, IN15, IN16
- nuclear physics instruments: PN1, PN3
- fundamental physics instruments: PF1, PF2

Details of the instruments can be found on the web under http://www.ill.fr.

S18*, an interferometer, is a CRG-C instrument and is normally not available as a 'user' instrument. Some beam time was made available for prototype tests of USANS.

# Beam-time allocation for 2000

Overall the Subcommittees of the Scientific Council (meetings in October 1999 and April 2000) scrutinised 924 proposals, out of which 677 proposals received beam time, allocating 4450 days of beam time on the different instruments. About 750 experiments were carried out. Table 2 shows the request and allocation of beam time per instrument.

Note that D4 and IN1 share a beam and that the CRG instruments offer a reduced number of days for ILL users. For PF2 several experiments share the beam taking neutrons alternatively, so the table contains the beam-days allocated but gives the total number of experiments running simultaneously.

| Instrument | days requested | days allocated† | number of experiments | days used†† | days lost |
|---|---|---|---|---|---|
| *ADAM* | *79* | *55* | *11* | *186* | *6* |
| D10 | 268 | 177 | 19 | 187 | 4 |
| D11 | 242 | 163 | 64 | 165 | 10 |
| *D15* | *33* | *36* | *5* | *111* | *80* |
| D16 | 231 | 160 | 17 | 162 | 4 |
| D17 * | 74 | 7 | 1 | | |
| D19 | 302 | 190 | 17 | 196 | 12 |
| D1A | 156 | 122 | 32 | 123 | 9 |
| *D1B* | *168* | *87* | *42* | *197* | *8* |
| D20 | 105 | 91 | 35 | 41 | 0 |
| D22 | 333 | 163 | 69 | 150 | 25 |
| *D23* | *9* | *34* | *3* | *185* | *15* |
| D2B | 361 | 168 | 75 | 190 | 9 |
| D3 | 280 | 160 | 17 | 162 | 33 |
| D4 | 142 | 57 | 14 | 64 | 8 |
| D7 | 341 | 180 | 17 | 185 | 5 |
| D9 | 310 | 179 | 31 | 185 | 6 |
| DB | 2131 | 25 | 2 | 59 | 0 |
| *EVA* | *74* | *41* | *4* | *208* | *2* |
| IN1 | 133 | 56 | 9 | 68 | 4 |
| IN10 | 103 | 139 | 16 | 156 | 4 |
| IN11 | 230 | 173 | 19 | 170 | 8 |
| *IN12* | *93* | *52* | *6* | *205* | *3* |
| *IN13* | *232* | *82* | *11* | *199* | *0* |
| IN14 | 362 | 167 | 21 | 177 | 14 |
| IN15 | 162 | 59 | 8 | 123 | 30 |
| IN16 | 321 | 160 | 22 | 184 | 12 |
| IN20 | 244 | 164 | 18 | 170 | 8 |
| *IN22* | *100* | *61* | *7* | *198* | *8* |
| IN3 | 32 | 57 | 7 | 109 | 0 |
| IN4* | 19 | 30 | 7 | | |
| IN5 | 208 | 148 | 30 | 193 | 7 |
| IN6 | 376 | 168 | 40 | 182 | 17 |
| LADI | 220 | 205 | 11 | 145 | 3 |
| PF1 | 565 | 200 | 6 | 216 | 0 |
| PF2 | 371 | 225** | 16 | 215 | 1 |
| PN1 | 239 | 180 | 11 | 131 | 58 |
| PN3 | 377 | 141 | 7 | 189 | 4 |
| **Total** | **7555** | **4450** | **747** | **5790** | **415** |

Table 2: Beam-time request / allocation by instrument and instrument performance. ILL use of the CRG instruments (italic and blue) corresponds to 30 or 50% of the total beam time used.
† 'days allocated' refers to only those days reviewed by the subcommittees (i.e., excluding CRG days)
†† 'days used' refers to the total number of days delivered (i.e., inxcluding CRG days)
(* D17 and IN4 were not officially scheduled in 2000; **PF2 consists of several long-term experiments so the number of days scheduled is given as an estimation).

In 2000, the member countries of the ILL were as follows: France, Germany, UK, Spain, Switzerland, Austria, Italy, the Czech Republic and Russia.

In calculating the statistics of beam-time per country, shown in Table 3, the attribution is based on the location of the laboratory of the proposers, not their individual nationality. For a proposal involving laboratories from more than one member country, the total number of days is divided equally amongst the collaborating countries. When a proposal involves a collaboration with a non-member country, the allocated time is attributed entirely to the collaborating member country (or countries). When ILL scientists are proposers or co-proposers, the allocated ILL time' is attributed amongst the member countries according to their financial contributions to ILL. Local contacts are not counted as proposers.

The ILL welcomed 1207 users in 2000. Approximately 80% came from the member countries including 290 from France, 225 from Germany and 236 from the UK (Fig.1). Many of our visitors were received more than once. There were thus almost 1900 visits in which about 750 experiments were carried out.

The distribution of beam time for these experiments amongst the different 'Colleges' is shown in Fig.2: 7% of the days were allocated to nuclear and fundamental physics (college 3), 10% to structural and magnetic excitations (college 4), 40% to crystal and magnetic structures (college 5a + 5b), 7% to structure and dynamics of liquids and glasses (college 6), 11% to materials science, surfaces and spectroscopy (college 7), 10% to biology (college 8) and 15% to structure and dynamics of soft-condensed matter (college 9).

| Country | Requested days | Requested % | Allocated days | Allocated % |
|---|---|---|---|---|
| AUT + CZ | 118.9 | 1.5% | 60.2 | 1.4% |
| CH | 254.4 | 3.3% | 180.5 | 4.0% |
| D | 2154.5 | 27.8% | 1313.2 | 29.5% |
| E | 363.7 | 4.7% | 190.7 | 4.3% |
| F | 2108.3 | 27.2% | 1257.2 | 28.2% |
| GB | 1971.2 | 25.4% | 1078.8 | 24.2% |
| I | 307.0 | 3.9% | 148.3 | 3.3% |
| RUS | 476.1 | 6.1% | 229.8 | 5.2% |
| **Total** | **7754.1** | **100%** | **4450.6** | **100%** |

Table 3: Distribution of beam-time request and allocation amongst the member and scientific-member countries.

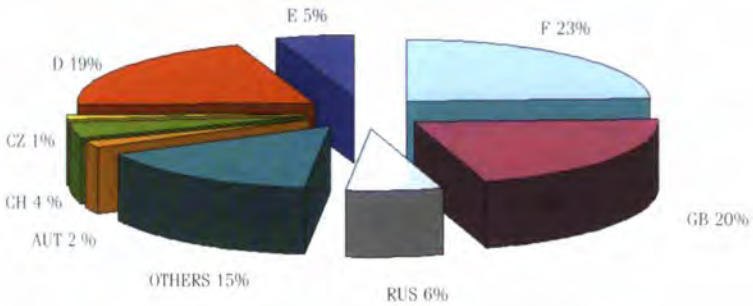


Figure 1: Nationality of the users who came to the ILL in the year 2000.

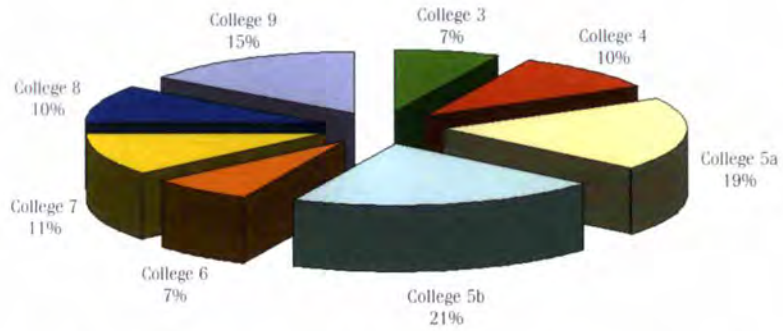


Figure 2: Beam-time allocation in 2000: distribution amongst the different colleges.

# Instrument performance

Table 2 on page 113 gives a summary of instrument performance for 2000. For each cycle a record is kept of any time lost from the total available beam-time, and the reasons for the lost time are analysed for all the instruments. The table gives a global summary for the year. In 2000, 415 days were lost due to various malfunctions, which represents about 7% of the total available beam-time (lost time in 1999 was 11.2%). However, the majority of this time is returned to users because usually time for minor breakdowns, tests, calibrations, scheduling difficulties and director's discretion time is allowed for in the scheduling process.
Detailed comments on the larger beam-time losses (20 days or more) are as follows:

- D3 had various problems with bad connectors involving polarisation instabilities and with a cryo-pad malfunction due to a leak between the bath and the vacuum. In addition, beam time could not be used efficiently due to problems on the user side (bad sample); it proved impossible to find replacement experiments at short notice.
- D22 suffered time loss due to a magnetic field interference with the neighbourhood instrument IN15. Solutions to avoid this kind of problem in future are under investigation.
- IN15 struggled with the mechanics and electronics of its chopper for the time-of-flight option.
- A longer shut down period on PN1 was due to a failure of the target changing mechanism, which eventually was totally reconstructed by the reactor department.

Reasons for beam time loss in 2000

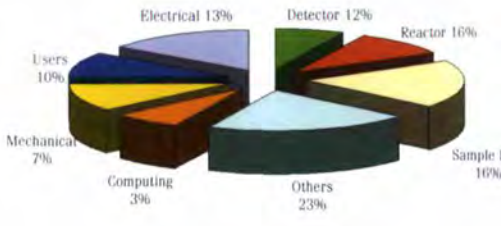

# Industrial use of neutrons

The year 2000 has been a remarkably good year for relations with industry, both in terms of completed neutron experiments and in terms of new contracts with high profile industrial companies. Most of the experiments were performed in the field of small-angle neutron scattering (instruments D11 & D22), while other measurements required the use of neutron strain imaging (instrument D1A). Furthermore, D20 was used for industrial tests.
The sales figures for 2000 were as follows:

| | in 2000 | in 1999 |
|---|---|---|
| Number of customers | 9 | 4 |
| Number of new customers | 5 | 1 |
| Number of instrument days | 17 | 8.5 |

Bearing in mind that it takes from 6 to 12 months to convert a serious contact into an industrial experiment, these figures speak for themselves as a reflection of the combined effort made by all members of the Industrial Liaison Group (Pierre Convert, Peter Lindner, Thilo Pirling and Albert Wright). Building up a continuous and effective industrial activity is a long-term effort.

The role of the Industrial Liaison Group (ILG) is to stimulate a continuous programme of communications and exchanges. In 2000, the ILG organised a wide programme of meetings and presentations of neutron-related industrial work. In April 2000, ILL experts presented neutron techniques to Engineering Schools and the University Claude Bernard in Lyon which resulted in a new user for strain measurements with close links to industry [1].
A one-day workshop was held on 29 June 2000, dedicated to the "Characterisation of industrial materials using neutrons", to enable industry and applied research laboratories to learn more about what neutrons can be used for [2].
In September 2000, the ILL presented two posters at the "Materials Week"* in Munich. This also provided the opportunity to make useful contacts with many German-based companies at the associated trade fair.

Johannes Zipfel mounting the high-temperature sample changer on D11.

For 2001, it is planned to establish a forum for industrial engineers and applied scientists, interested in the use of neutron methods. Our aim is to create a network to promote the industrial applications of neutrons in different fields of interest. ILL will animate seminars and meetings for this forum during the year to come in order to build exchange and to develop a strategy for neutron applications for the benefit of all parties.

* Organised by Werkstoffwoche-Partnerschaft GBRmbH, Frankfurt.


REFERENCES

● [1] ILL NEWS FOR REACTOR USERS, N° 33 (JUNE 2000) P. 3 ● [2] THIS ANNUAL REPORT (EDITION 2000), WORKSHOP SECTION, P.106


# User forum

The ILL values feed-back from the users as an indicator of how well our facility is fulfilling their needs and to initiate actions when we are not. Therefore this year for the first time we have instigated the idea of a User Forum. Those users already on site for scheduled experiments were invited to an informal meeting with the ILL directors, the physicists' representatives, and the Group Leaders (DS and DPT) and were given the opportunity to comment on several points of interest such as instruments and service at the ILL. We have organised two User Forums in 2000. The first one - held in March - was already considered to be a success, but the second one in October was even more constructive. Clearly we are on a positive learning curve here! Many positive suggestions were made ranging from instrument up-grading and new sample environments to network connections in the Guest House rooms. We very much appreciated the enthusiasm and co-operation of our users in giving their views, and every effort will be made to implement suggestions. To date, our electronic proposal submission has already been further improved following your initial comments, and the possibility of strengthening the technical support outside working hours is being looked into.

# User satisfaction

User satisfaction has been tested since July 2000 via a questionnaire - the User Satisfaction Form - received by all users upon arrival at the ILL. The results of the survey – as can be seen in Fig.4 - showed in most cases a very high satisfaction ( higher than 90% ) with the staff support, ILL equipment and human comfort. From the comments on the sheets we are pleased to see that ILL is considered as an excellent facility to carry out research and a great place to come for experiments. We will do our best to keep up the good work!

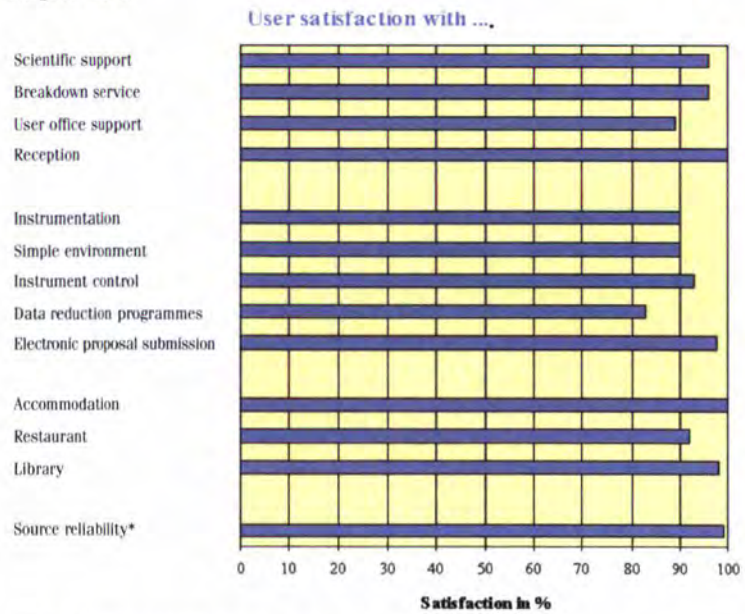


Figure 4: User satisfaction survey results (July 2000 – December 2000).
* The source reliability has been calculated from Tab.1.

Florian Nettesheim (University of Kiel) loading a sample into the Bohlin rheometer.

Anton Oed checks a microstrip plate before mounting.

Thilo Pirling fits out the area for the future Strain Scanner.

David Weddle (left) and Roger Chung mount the new low-angle multidetector on IN4.

Jane Brown and Jens-Boie Suck (Chemnitz University) during the first ILL User Forum, held in March 2000.

Alan Hewat and Maria Teresa Fernandez Diaz enjoy the Subcommittee lunch.

# Facts and figures

## Facts and Figures for 2000

**Name** Institut Max von Laue - Paul Langevin (ILL)

**Founded** 1967

**Associates**
France: Commissariat à l'énergie atomique (CEA)
Centre national de la recherche scientifique (CNRS)
Federal Republic of Germany: Forschungszentrum Jülich
United Kingdom: Engineering and Physical Sciences Research Council (EPSRC)

**Countries with Scientific membership**

**Spain** Ministerio de Ciencia y Tecnologìa (MCYT)

**Switzerland** Schweizer Bundesamt für Bildung und Wissenschaft (SBBW)

**Italy** Istituto Nazionale per la Fisica della Materia (INFM)

**Russia** MINATOM

**MENI (Middle European Neutron Initiative) Consortium, composed of**
Austria: Österreichische Akademie der Wissenschaften
Czech Republic: Charles University of Prague

**Staff** 409 people including 52 experimentalists in the scientific sector
259 French, 52 German, 56 British, 42 others.

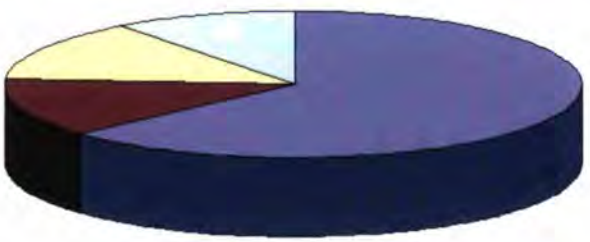

| | | |
|---|---|---|
| French | 259,5 | 63,37% |
| British | 56 | 13,68% |
| German | 52 | 12,70% |
| Others | 42 | 10,26% |

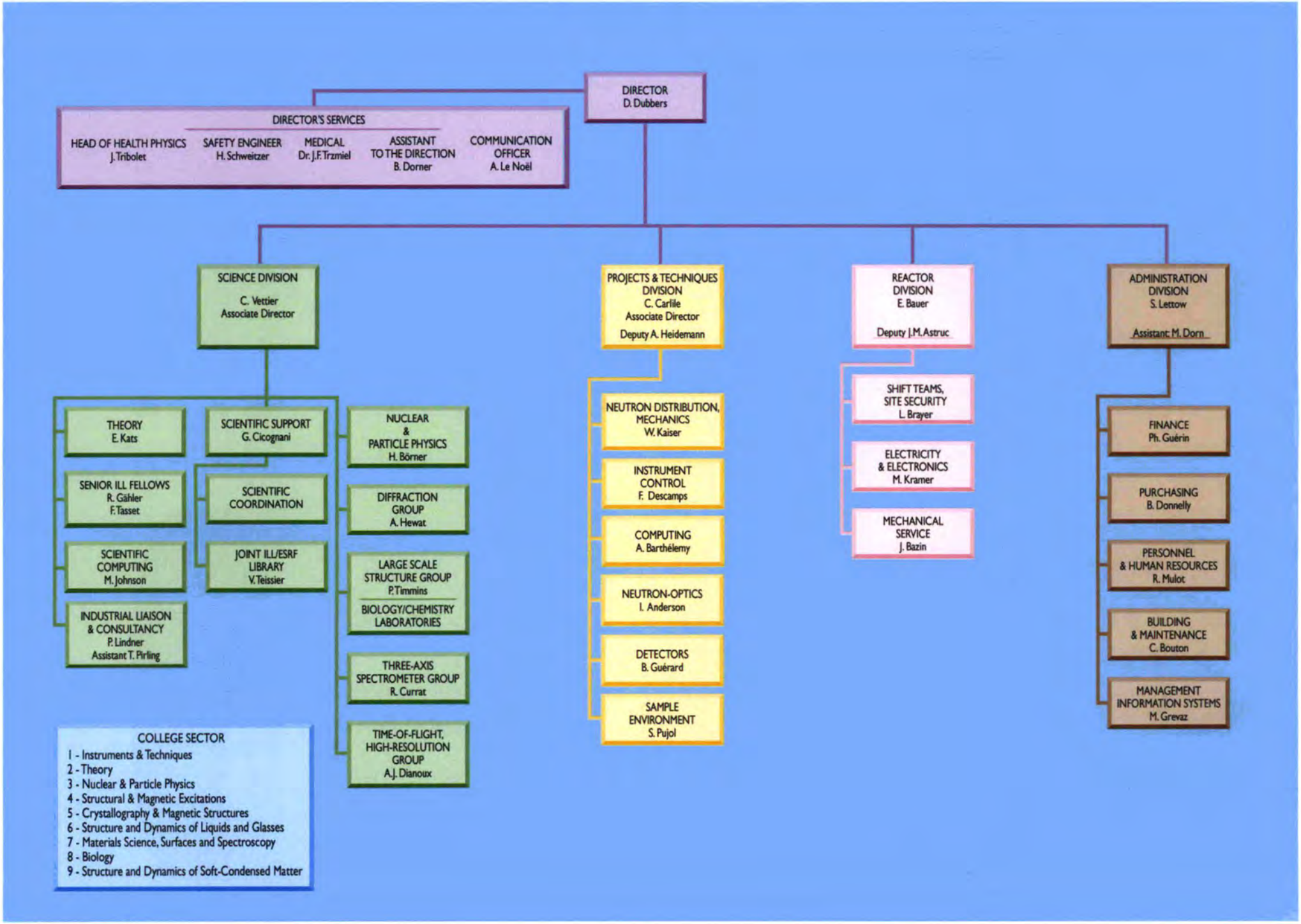
DIRECTOR
D. Dubbers
DIRECTOR'S SERVICES
HEAD OF HEALTH PHYSICS
J. Tribolet
SAFETY ENGINEER
H. Schweitzer
MEDICAL
Dr. J.F. Trzmiel
ASSISTANT TO THE DIRECTION
B. Dorner
COMMUNICATION OFFICER
A. Le Noël
SCIENCE DIVISION
C. Vettier
Associate Director
PROJECTS & TECHNIQUES DIVISION
C. Carlile
Associate Director
Deputy A. Heidemann
REACTOR DIVISION
E. Bauer
Deputy J.M. Astruc
ADMINISTRATION DIVISION
S. Lettow
Assistant: M. Dorn
THEORY
E. Kats
SENIOR ILL FELLOWS
R. Gähler
F. Tasset
SCIENTIFIC COMPUTING
M. Johnson
INDUSTRIAL LIAISON & CONSULTANCY
P. Lindner
Assistant T. Pirling
SCIENTIFIC SUPPORT
G. Cicognani
SCIENTIFIC COORDINATION
JOINT ILL/ESRF LIBRARY
V. Teissier
NUCLEAR & PARTICLE PHYSICS
H. Börner
DIFFRACTION GROUP
A. Hewat
LARGE SCALE STRUCTURE GROUP
P. Timmins
BIOLOGY/CHEMISTRY LABORATORIES
THREE-AXIS SPECTROMETER GROUP
R. Currat
TIME-OF-FLIGHT, HIGH-RESOLUTION GROUP
A.J. Dianoux
NEUTRON DISTRIBUTION, MECHANICS
W. Kaiser
INSTRUMENT CONTROL
F. Descamps
COMPUTING
A. Barthélemy
NEUTRON-OPTICS
I. Anderson
DETECTORS
B. Guérard
SAMPLE ENVIRONMENT
S. Pujol
SHIFT TEAMS, SITE SECURITY
L. Brayer
ELECTRICITY & ELECTRONICS
M. Kramer
MECHANICAL SERVICE
J. Bazin
FINANCE
Ph. Guérin
PURCHASING
B. Donnelly
PERSONNEL & HUMAN RESOURCES
R. Mulot
BUILDING & MAINTENANCE
C. Bouton
MANAGEMENT INFORMATION SYSTEMS
M. Grevaz
COLLEGE SECTOR
1 - Instruments & Techniques
2 - Theory
3 - Nuclear & Particle Physics
4 - Structural & Magnetic Excitations
5 - Crystallography & Magnetic Structures
6 - Structure and Dynamics of Liquids and Glasses
7 - Materials Science, Surfaces and Spectroscopy
8 - Biology
9 - Structure and Dynamics of Soft-Condensed Matter

**Income (MF)**

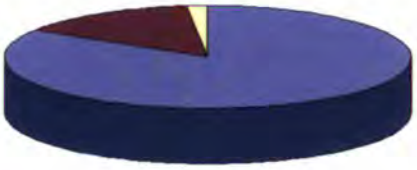

| | | |
|---|---|---|
| Income from Associates *(Divided: F 37.87%; D 37.113%; UK 25%)* | 315.8 | 84.00% |
| Income from scientific members | 53.4 | 14.20% |
| Own Income | 6.8 | 1.80% |
| **Total** | **376** | **100%** |

**Expenditure (MF)**

| | | |
|---|---|---|
| Staff costs | 187.4 | 49.84% |
| Operating costs | 70.8 | 18.83% |
| Investment costs | 43.4 | 11.54% |
| Fuel cycle | 74.4 | 19.79% |
| **Total** | **376** | **100%** |

**Distribution of ILL purchases (MF, excluding taxes)**

| | | |
|---|---|---|
| France | 52.1 | 66.88% |
| Germany | 7.5 | 9.64% |
| United Kingdom | 4.5 | 5.79% |
| Others | 13.8 | 17.72% |
| **Total** | **77.9** | **100%** |

**Budget**

376 MF (excluding taxes)

**Bodies**

Steering Committee, meeting twice a year
Scientific Council with 8 Subcommittees, meeting twice a year
Management Board, meeting weekly

**Reactor**

58 MW, running 4.5 cycles in 2000 (with cycles of 50 days)

**Experimental Programme**

747 experiments (allocated by subcommittees) on 25 ILL-funded and 8 CRG instruments
1207 visitors coming from 33 countries
924 proposals submitted and 677 accepted

**Experiment Selection by the Scientific Council via its 8 subcommittees**

Nuclear and fundamental physics (college 3)
Structural and magnetic excitations (college 4)
Crystallographic structures (college 5a)
Magnetic structures (college 5b)
Structure and dynamics of liquids and glasses (college 6)
Materials science, surfaces and spectroscopy (college 7)
Structure and dynamics of biological systems (college 8)
Structure and dynamics of soft-condensed matter (college 9)

**Scientific Life**

based on 10 colleges
8 of which map on to the subcommittees plus two others:
instruments and techniques (college 1); theory (college 2)

Ralph Siebrecht can't believe how lucky he is, surrounded by this smiling bunch of ILL young scientists: from the left, Isabelle Grillo, Laurence Perino, Giovanna Fragneto and Claudia Mondelli.

Stéphanie Pouget (right) explaining the principle of the spin-echo technique.

Jean Paul Gonzales checks the inside of the 6mK dilution refrigerator.


Sending out the Annual Report!

# Publications

In 2000, the ILL received notice of 475 publications by ILL staff and users of which 285 were published as journal articles, 187 as conference proceedings in journals, books or reports and 3 as book chapters. The distribution by subject is as follows: 41 in instruments and methods, 11 in theory, 64 in fundamental and nuclear physics, 42 in structural and magnetic excitations, 77 in crystallographic structures, 79 in magnetic structures, 45 in structure and dynamics of liquids and glasses, 54 in materials science, surfaces and spectroscopy, 31 in biology, 31 in structure and dynamics of soft-condensed matter.

This list gives publications received during 2000 resulting from research carried out at the ILL. It was generated from the library database LORIS-DORIS and can be consulted on the Web at http://www.ill.fr

# Papers published in scientific periodicals, books and conference proceedings


ABELE H., BOUCHER A., GELTENBORT P., KLEIN M., SCHMIDT U., STELLMACH C. Radio frequency-induced polarization of ultra-cold neutrons or how to pump a two-level system.
Nuclear Instruments and Methods in Physics Research A **440**, 760-763 (2000)

ACET M., ROESSEL T., WASSERMANN E.F., ANDERSEN K.H., KULDA J., MURANI A.P., WILDES A. Moment fluctuations and volume enhancements in anti-Invar.
Journal of the Physical Society of Japan Supplement A **69**, 108-111 (2000)

ACET M., WASSERMANN E.F., ANDERSEN K.H., KULDA J., MURANI A.P., WILDES A. Large spin fluctuations and moment-volume coupling in Fe in an FCC environment.
Physica B **276-278**, 728-729 (2000)

ACET M., WASSERMANN E.F., PEPPERHOFF W. Relevance of magnetic instabilities to the phase stabilities of Fe alloys.
Philosophical Magazine B **80**, 127-139 (2000)

ADAMS S. CDW superstructures in hydrogen molybdenum bronzes $H_xMoO_3$.
Journal of Solid State Chemistry **149**, 75-87 (2000)

ADELMANN P., RENKER B., SCHOBER H., BRADEN M., FERNANDEZ-DIAZ F. Lattice dynamics of Li-ZrNCl: An electron doped layered superconductor.
Journal of Low-Temperature Physics **117**, 449-453 (1999)

AGTERBERG D.F., HEEB R., KEALEY P.G., RISEMAN T.M., FORGAN E.M., MACKENZIE A.P., GALVIN L.M., PERRY R.S., LEE S.L., PAUL D.MCK., CUBITT R., MAO Z.Q., AKIMA S., MAENO Y. Vortex lattice structures and pairing symmetry in $Sr_2RuO_4$.
Physica C **341-348**, 1643-1646 (2000)

AKSENOV V.L., KOZHEVNIKOV S.V., NIKITENKO Y.V., LAUTER H.J. Reflection and refraction of spin-flip neutrons in a Fe-Gd structure.
Physica B **276-278**, 179-180 (2000)

ALONSO J.A., MARTINEZ-LOPE M.J., CASAIS M.T., FERNANDEZ-DIAZ M.T. Evolution of the Jahn-Teller distortion of $MnO_6$ octahedra in $RMnO_3$ perovskites (R = Pr, Nd, Dy, Tb, Ho, Er, Y): A neutron diffraction study.
Inorganic Chemistry **39**, 917-923 (2000)

ALONSO J.A., MARTINEZ-LOPE M.J., CASAIS M.T., GARCIA-MUNOZ J.L., FERNANDEZ-DIAZ M.T. Room-temperature monoclinic distortion due to charge disproportionation in $RNiO_3$ perovskites with small rare-earth cations ($R$ = Ho, Y, Er, Tm, Yb, and Lu): A neutron diffraction study.
Physical Review B **61**, 1756-1763 (2000)

ALONSO J.A., MARTINEZ-LOPE M.J., CASAIS M.T., MARTINEZ J.L., DEMAZEAU G., LARGETEAU A., GARCIA-MUNOZ J.L., MUNOZ A., FERNANDEZ-DIAZ M.T. High-pressure preparation, crystal structure, magnetic properties, and phase transitions in $GdNiO_3$ and $DyNiO_3$ perovskites.
Chemistry of Materials **11**, 2463-2469 (1999)

ALONSO J.A., MARTINEZ-LOPE M.J., CASAIS M.T., MARTINEZ J.L., FERNANDEZ-DIAZ M.T. Large increase in magnetoresistance and cluster-glass behavior in defect $Tl_{2-x}Mn_2O_{7-y}$ pyrochlores.
Chemistry of Materials **12**, 1127-1133 (2000)

ALONSO J.A., MARTINEZ-LOPE M.J., CASAIS M.T., VELASCO P., MARTINEZ J.L., FERNANDEZ-DIAZ M.T., DE PAOLI J.M. Enhancement of ferromagnetic coupling in Sb-substituted $Tl_2Mn_2O_7$ pyrochlores (Rapid communications).
Physical Review B **60**, R15024-R15027 (1999)

ALONSO J.A., SANZ J., SANTAMARIA J., LEON C., VAREZ A., FERNANDEZ-DIAZ M.T. On the location of $Li^+$ cations in the fast Li-cation conductor $La_{0.5}Li_{0.5}Ti_{03}$ perovskite.
Angewandte Chemie International Edition English **39**, 619-621 (2000)

ALONSO J.A., VELASCO P., MARTINEZ-LOPE M.J., CASAIS M.T., MARTINEZ J.L., FERNANDEZ-DIAZ M.T., DE PAOLI J.M. Unprecedented magnetoresistance in Cd-substituted $Tl_2Mn_2O_7$ pyrochlores.
Applied Physics Letters **76**, 3274-3276 (2000)

ALVAREZ L., RIGHI A., ROLS S., ANGLARET E., SAUVAJOL J.L. Excitation energy dependence of the Raman spectrum of single-walled carbon nanotubes.
Chemical Physics Letters **320**, 441-447 (2000)

AMORETTI G., CACIUFFO R., COMBET J., MURANI A.P., CANESCHI A. Inelastic neutron scattering below 85 μeV and zero-field splitting parameters in the $Fe_8$ magnetic cluster.
Physical Review B **62**, 3022-3024 (2000)

ANDERSEN K.H., BOURGEAT-LAMI E., DREYER J., HEIL W., HOFMANN D., HUMBLOT H., IVANOV S., KULDA J., LELIEVRE-BERNA E., PETOUKHOV A., PUJOL S., REGNAULT L.P., ROBERTS T.W., STEWART J.R., TASSET F., THOMAS M., WILDES A.R. Recent news on ILL polarised $^3$He developments.
Physica B **276-278**, 65-66 (2000)

ANDERSON C.R., STIRLING W.G., ANDERSEN K.H., SOKOL P.E., DIMEO R.M. Two-dimensional excitations of superfluid $^4$He confined in 72% porosity xerogel.
Physica B **276-278**, 820-821 (2000)

ANDERSON I.S., HAMELIN B., HØGHØJ P., COURTOIS P., HUMBLOT H. Novel trends in neutron optics.
In: 'Frontiers of Neutron Scattering. Proceedings of the Seventh Summer School on Neutron Scattering', FURRER A. (Ed.) (World Scientific, 2000) pp. 44-71

ANDREICA D., GYGAX F.N., PINKPANK M., SCHENCK A., CHATTERJI T., SURYANARAYANAN R., DHALENNE G., REVCOLEVSCHI A. Charge/orbital and antiferromagnetic ordering in $LaSr_2Mn_2O_7$.
Physica B **289-290**, 65-68 (2000)

ANTONOV V.E., CORNELL K., DORNER B., FEDOTOV V.K., GROSSE G., KOLESNIKOV A.I., WAGNER F.E., WIPF H. Neutron spectroscopy of γ manganese hydride.
Solid State Communications **113**, 569-572 (2000)

ANTONOV V.E., FEDOTOV V.K., GNESIN B.A., GROSSE G., IVANOV A.S., KOLESNIKOV A.I., WAGNER F.E. Anisotropy in the inelastic neutron scattering from fcc NiH.
Europhysics Letters **51**, 140-146 (2000)

APRAHAMIAN A., DE HAAN R.C., BÖRNER H.G., LEHMANN H., JENTSCHEL M. The nature of $K^\pi = 0^-$ excitations in deformed nuclei.
AIP Conference Proceedings **529**, 51-57 (2000)

ARZEL L., HEHLEN B., CURRAT R., HENNION B., COURTENS E. Dynamics of coupled modes in $SrTiO_3$.
Physica B **276-278**, 230-231 (2000)

ARZEL L., HEHLEN B., CURRAT R., HENNION B., SAINT-PAUL M., COURTENS E. The effect of domains on spectral anomalies of $SrTiO_3$ below the structural transition.
Ferroelectrics **236**, 81-92 (2000)

ARZUMANOV S., BONDARENKO L., CHERNYAVSKY S., DREXEL W., FOMIN A., GELTENBORT P., MOROZOV V., PANIN Y., PENDLEBURY J., SCHRECKENBACH K. Neutron lifetime measured by monitored storing of ultra-cold neutrons.
Nuclear Instruments and Methods in Physics Research A **440**, 511-516 (2000)

ARZUMANOV S., BONDARENKO L., CHERNYAVSKY S., DREXEL W., FOMIN A., GELTENBORT P., MOROZOV V., PANIN Y., PENDLEBURY J., SCHRECKENBACH K. Neutron life time value measured by storing ultracold neutrons with detection of inelastically scattered neutrons.
Physics Letters B **483**, 15-22 (2000)

ARZUMANOV S., BONDARENKO L., GELTENBORT P., KOROBKINA E., MOROZOV V., PANIN Y., FOMIN A., CHERNJAVSKY S. Investigation of the radiative capture of UCN at the matter surface.
Nuclear Instruments and Methods in Physics Research A **440**, 690-694 (2000)

ASO N., ROESSLI B., BERNHOEFT N., CALEMCZUK R., SATO N.K., ENDOH Y., KOMATSUBARA T., HIESS A., LANDER G.H., KADOWAKI H. Neutron-scattering study of the magnetic response in the heavy-fermion superconductor $UNi_2Al_3$ (Rapid communications).
Physical Review B **61**, R11867-R11870 (2000)

BAFILE U., BAROCCHI F., CILLOCO F., HOCHGESAND K., WINTER R., FISCHER H.E. The microscopic structure of liquid mercury from neutron and X-ray diffraction.
Physica B **276-278**, 452-453 (2000)

BALAGUROV A.M., SHEPTYAKOV D.V., AKSENOV V.L., ANTIPOV E.V., PUTILIN S.N., RADAELLI P.G., MAREZIO M. Structure of $HgBa_2CaCu_{1-\delta}$ ($0.06<\delta<0.19$) at ambient and high pressure.
Physical Review B **59**, 7209-7215 (1999)

BALDINOZZI G., CALVARIN G., SCIAU P., GREBILLE D., SUARD E. Neutron Rietveld refinement of the incommensurate phase of the ordered perovskite $Pb_2CoWO_6$.
Acta Crystallographica B **56**, 570-576 (2000)

BÄR N.K., ERNST H., JOBIC H., KÄRGER J. Combined quasi-elastic neutron scattering and NMR study of hydrogen diffusion in zeolites.
Magnetic Resonance in Chemistry **37**, S79-S83 (1999)

BÄR N.K., JOBIC H., KÄRGER J. Diffusion of hydrogen in various zeolites studied by pulsed-field gradient NMR and quasi-elastic neutron scattering techniques.
In: '12. International Zeolite Conference' (MRS, 1999) pp. 77-84

BARNES A.C., HAMILTON M.A., BECK U., FISCHER H.E. A determination of the structure of liquid $Ag_2Te$ using neutron diffraction and isotopic substitution and its comparison to $Ag_2Se$.
Journal of Physics Condensed Matter **12**, 7311-7322 (2000)

BASTIE P., HAMELIN B., COURTOIS P. Méthode de Laue refocalisée à haute énergie : intérêts et apports de la spectrométrie des faisceaux diffractés.
Journal de Physique IV **10**, Pr10-21-Pr10-26 (2000)

BECVAR F., KRTICKA M., JENTSCHEL M. Simulations of gamma cascades and modelling atomic collision chains.
Journal of Research of the National Institute of Standards and Technology **105**, 113-123 (2000)

BENITES G.M., FERNANDEZ GUILLERMET A., CUELLO G.J., CAMPO J. Structural properties of metastable phases in Zr-Nb alloys. I. Neutron diffraction study and analysis of lattice parameters.
Journal of Alloys and Compounds **299**, 183-188 (2000)

BERMEJO F.J., FÅK B., BENNINGTON S.M., FERNANDEZ-PEREA R., CABRILLO C., DAWIDOWSKI J., FERNANDEZ-DIAZ M.T., VERKERK P. Microscopic collective dynamics in liquid *para*-$H_2$.
Physical Review B **60**, 15154-15162 (1999)

BERMEJO F.J., JIMENEZ-RUIZ M., CRIADO A., CUELLO G.J., CABRILLO C., TROUW F.R., FERNANDEZ-PEREA R., LÖWEN H., FISCHER H.E. Rotational freezing in plastic crystals: A model system for investigating the dynamics of the glass transition.
Journal of Physics Condensed Matter **12**, A391-A397 (2000)

BERMEJO F.J., KINUGAWA K., CABRILLO C., BENNINGTON S.M., FÅK B., FERNANDEZ-DIAZ M.T., VERKERK P., DAWIDOWSKI J., FERNANDEZ-PEREA R. Quantum effects on liquid dynamics as evidenced by the presence of well-defined collective excitations in liquid para-hydrogen.
Physical Review Letters **84**, 5359-5362 (2000)

BERMEJO F.J., SABOUNGI M.L., PRICE D.L., ALVAREZ M., ROESSLI B., CABRILLO C., IVANOV A.S. Persistence of well-defined collective excitations in a molten transition metal.
Physical Review Letters **85**, 106-109 (2000)

BERNE B.J., CICCOTTI G., COKER D.F. Book Review: Classical and quantum dynamics in condensed phase simulations.
Journal of Statistical Physics **97**, 419-420 (1999)

BERNHOEFT N., ROESSLI B., SATO N., ASO N., HIESS A., LANDER G.H., ENDOH Y., KOMATSUBARA T. Order parameter symmetry in $UPd_2Al_3$.
Physica B **281-282**, 993-995 (2000)

BICOUT D.J. Incoherent neutron scattering functions for diffusion inside two concentric spheres.
Physical Review E **62**, 261-271 (2000)

BIENFAIT M., ASMUSSEN B., JOHNSON M., ZEPPENFELD P. Methane mobility in carbon nanotubes.
Surface Science **460**, 243-248 (2000)

BIOTTEAU G., MOUSSA F., HENNION M., RODRIGUEZ-CARVAJAL J., WILDES A., PINSARD L., REVCOLEVSCHI A. Strong change in spin dynamics close to percolation in $La_{1-x}Ca_xMnO_3$.
Physica B **276-278**, 562-563 (2000)

BLASIE J.K., TIMMINS P.A. Neutron scattering in structural biology and biomolecular materials.
Materials Research Bulletin **24**, 40-47 (1999)

BOMBARDI A., BOURDAROT F., BURLET P., SANCHEZ J.P., VULLIET P., COLINEAU E., REBIZANT J., WASTIN F., LANDER G.H., VOGT O., MATTENBERGER K. Evolution of magnetic structures in $NpAs_{1-x}Se_x$ solid solutions.
Physical Review B **62**, 14920-14927 (2000)

BOMBARDI A., GRENIER B., BURLET P., LANDER G.H., REGNAULT L.P., MATTENBERGER K., VOGT O. Observation of ferromagnetic correlation in diluted UTe.
Physica B **276-278**, 606-607 (2000)

BONDARENKO I.V., BALASHOV S.N., CIMMINO A., GELTENBORT P., FRANK A.I., HØGHØJ P., KLEIN A.G., MASALOVICH S.V., NOSOV V.G. UCN gravity spectrometry using neutron interference filters for fundamental investigations in neutron optics.
Nuclear Instruments and Methods in Physics Research A **440**, 591-596 (2000)

BONETTI E., PASQUINI L., SAMPAOLESI E., DERIU A., CICOGNANI G. Vibrational density of states of nanocrystalline iron and nickel.
Journal of Applied Physics **88**, 4571-4575 (2000)

BORDET P., BOUGEROL CHAILLOUT C., GREY I.E., HODEAU J.L., ISNARD O. Structural characterization of the Engineered Scavenger Compound, H-$Li_2Ti_3O_7$.
Journal of Solid State Chemistry **152**, 546-553 (2000)

BORISOV Y., HEIL W., LEDUC M., LOBASHEV V., OTTEN E.W., SOBOLEV Y. Feasibility study of a $^3$He-magnetometer for neutron electric dipole moment experiments.
Nuclear Instruments and Methods in Physics Research A **440**, 483-488 (2000)

BÖRNER H.G., JENTSCHEL M., LEHMANN H., KESSLER E.G. Gamma ray spectroscopy with ppm resolving power.
AIP Conference Proceedings **529**, 35-42 (2000)

BÖRNER H.G., JENTSCHEL M., LEHMANN H., KESSLER E.G. Ultra-high precision gamma-ray spectroscopy.
BgNS Transactions **5**, 13-17 (2000)

BOTTI S., CICOGNANI G., COPPOLA R., LAPP A., MAGNANI M. Particle size and optical performances of photoluminescent laser synthesized Si nanopowders.
Physica B **276-278**, 860-861 (2000)

BOUCHERLE J.X., GIVORD F., SCHWEIZER J., GUKASOV A., MIGNOT J.M., LELIEVRE-BERNA E., AOKI H., OCHIAI A. Polarized neutron investigation in the mixed-valence compound $Sm_3Te_4$ at different temperatures.
Physica B **281-282**, 139-140 (2000)

BOURGES P., SIDIS Y., FONG H.F., REGNAULT L.P., BOSSY J., IVANOV A.S., KEIMER B. The spin excitation spectrum in superconducting $YBa_2Cu_3O_{6.85}$.
Science **288**, 1234-1237 (2000)

BOUZERAR G., LEGEZA Ö., ZIMAN T. Minimal model to describe the magnetism of $CuGeO_3$.
Physical Review B **60**, 15278-15284 (1999)

BOVE L.E., SACCHETTI F., PETRILLO C., DORNER B. Neutron investigation of collective excitations in liquid K-Cs alloys: The role of the electron density.
Physical Review Letters **85**, 5352-5355 (2000)

BRAND R.A., DIANOUX A.J., CALVAYRAC Y. Vibrational density of states in the archetypical icosahedral quasicrystal $i$-$Al_{62}Cu_{25.5}Fe_{12.5}$: Neutron time-of-flight results.
Physical Review B **62**, 8849-8861 (2000)

BRAZOVSKII S., KIROVA N., REQUARDT H., NAD F.Y., MONCEAU P., CURRAT R., LORENZO J.E., GRÜBEL G., VETTIER C. Plastic sliding of charge density waves: X-ray space resolved-studies versus theory of current conversion.
Physical Review B **61**, 10640-10650 (2000)

BRENNER T., BUTTERWORTH J., GELTENBORT P., HINO M., MALIK S.S., OKUMURA K., SARKISOV D., STEYERL A., UTSURO M. Looking for surface states of ultra-cold neutrons.
Nuclear Instruments and Methods in Physics Research A **440**, 722-728 (2000)

BROWN P.J., NEUMANN K.U., WEBSTER P.J., ZIEBECK K.R.A. The magnetization distributions in some Heusler alloys proposed as half-metallic ferromagnets.
Journal of Physics Condensed Matter **12**, 1827-1835 (2000)

BUDAYOVA-SPANO M., LAFONT S., ASTIER J.P., EBEL C., VEESLER S. Comparison of solubility and interactions of aprotinin (BPTI) solutions in $H_2O$ and $D_2O$.
Journal of Crystal Growth **217**, 311-319 (2000)

BURDIN S., GEORGES A., GREMPEL D.R. Coherence scale of the Kondo lattice.
Physical Review Letters **85**, 1048-1051 (2000)

CACIUFFO R., RINALDI D., BARUCCA G., MIRA J., RIVAS J., SENARIS-RODRIGUEZ M.A., RADAELLI P.G., FIORANI D., GOODENOUGH J.B. Structural details and magnetic order of $La_{1-x}Sr_xCoO_3$ ($x \leq 0.3$).
Physical Review B **59**, 1068-1078 (1999)

CAMPBELL A.J., PAUL D.MCK., MCINTYRE G.J. Neutron diffraction study of metamagnetic phases in $ErNi_2B_2C$.
Solid State Communications **115**, 213-216 (2000)

CAMPBELL A.J., PAUL D.MCK., MCINTYRE G.J. Neutron-diffraction study of the metamagnetic phases in $HoNi_2B_2C$.
Physical Review B **61**, 5872-5875 (2000)

CAPOGNA L., RADAELLI P.G., CHEONG S.W., MAREZIO M. Charge, orbital and magnetic ordering in $La_{0.333}Ca_{0.667}MnO_3$.
Materials Science Forum **321-324**, 818-822 (2000)

CARSUGHI F., MAY R.P., PLENTEDA R., SAROUN J. Sample geometry effects on incoherent small-angle scattering of light water.
Journal of Applied Crystallography **33**, 112-117 (2000)

CASALTA H. Les spectromètres à temps de vol .
Journal de Physique IV **10**, Pr1-15-Pr1-26 (2000)

CASALTA H., SCHLEGER P., BELLOUARD C., HENNION M., MIREBEAU I., EHLERS G., FARAGO B. Low $Q$ measurement of super-paramagnetic fluctuations in monodomain Fe particles.
Physica B **276-278**, 664-665 (2000)

CAVADINI N., HEIGOLD G., HENGGELER W., FURRER A., GÜDEL H.U., KRÄMER K., MUTKA H. Quantum magnetic interactions in $S = 1/2$ $KCuCl_3$.
Journal of Physics Condensed Matter **12**, 5463-5472 (2000)

CAVADINI N., HENGGELER W., FURRER A., GÜDEL H.U., KRÄMER K., MUTKA H. Magnetic excitations and spin gap in $KCuCl_3$.
Physica B **276-278**, 540-542 (2000)

CHACON C., ISNARD O. Determination of the substitution scheme of gallium and magnetic features of $Nd_2Fe_{14-x}Ga_xB$.
Journal of Applied Physics **88**, 3570-3577 (2000)

CHACON C., ISNARD O. Structure of $Nd_2Fe_{14-x}Si_xBH_y$ measured by neutron diffraction.
Journal of Applied Physics **88**, 2342-2348 (2000)

CHACON C., ISNARD O. Study of the $Y(Co,Fe)_4B$ phases.
Physica B **276-278**, 652-653 (2000)

CHAPPEL E., NUNEZ-REGUEIRO M.D., CHOUTEAU G., ISNARD O., DARIE C. Study of the ferrodistorsive orbital ordering in $NaNiO_2$ by neutron diffraction and submillimeter wave ESR.
European Physical Journal B **17**, 615-622 (2000)

CHATTERJI T., FRICK B. Nuclear spin excitations in $Nd_2CuO_4$.
Physica B **276-278**, 252-253 (2000)

CHATTERJI T., MCINTYRE G.J., CALIEBE W., SURYANARAYANAN R., DHALENNE G., REVCOLEVSCHI A. Reentrant behavior of the charge and orbital ordering and antiferromagnetism in $LaSr_2Mn_2O_7$.
Physical Review B **61**, 570-574 (2000)

CHEN D.Y., WU M.K., PARKINSON N.G., DU C.H., HATTON P.D., CHIEN F.Z., RITTER C. Magnetic ordering in the superconducting mixed ruthenium-copper oxide $Sr_2Y(Ru_{1-x}Cu_x)O_6$.
Physica C **341-348**, 2157-2158 (2000)

CICOGNANI G., MUTKA H., SACCHETTI F. The thermal neutron time-of-flight spectrometer IN4C.
Physica B **276-278**, 83-84 (2000)

CICOGNANI G., MUTKA H., WEDDLE D., HAMELIN B., MALBERT P., SACCHETTI F., PETRILLO C., BABUCCI E. The double focussing monochromator of IN4C.
Physica B **276-278**, 85-86 (2000)

COAD S., HIESS A., MCMORROW D.F., LANDER G.H., AEPPLI G., FISK Z., STEWART G.R., HAYDEN S.M., MOOK H.A. Magnetic response in $UBe_{13}$.
Physica B **276-278**, 764-765 (2000)

COAD S., HIESS A., PAOLASINI L., BERNHOEFT N., DERVENAGAS P., KACZOROWSKI D., CZOPNIK A., TROC R., LANDER G.H. Magnetic excitations in $UGa_3$.
Physica B **281-282**, 200-201 (2000)

COLE J.M., WILSON C.C., HOWARD J.A.K., CRUICKSHANK F.R. Quantitative analysis of hydrogen bonding and atomic thermal motion in the organic non-linear optical material DCNP using X-ray and neutron diffraction.
Acta Crystallographica B **56**, 1085-1093 (2000)

COLMENERO J., MORENO A.J., ALEGRIA A., ALVAREZ F., MUKHOPADHYAY R., FRICK B. Methyl group dynamics in glassy polymers by neutron scattering: From classical to quantum motions.
Physica B **276-278**, 322-325 (2000)

COMBET J., FRICK B., LOSSERAND O., GAMON M., GUERARD B. Simultaneous diffraction and inelastic scattering on the backscattering instrument IN16.
Physica B **283**, 380-385 (2000)

COMBET J., JOHNSON M., GABRIEL A., VOGL G., PETRY W. New position-sensitive detector for the IN10 backscattering spectrometer.
Physica B **276-278**, 154-155 (2000)

CONVERT P., HANSEN T., TORREGROSSA J. The high intensity two axis neutron diffractometer D20 first results.
Materials Science Forum **321-324**, 314-319 (2000)

COPLEY J.R.D., HAYES C., LARTIGUE C. Performance comparisons for the ILL neutron spin echo spectrometer IN15 in its standard and focusing mirror configurations.
Proceedings SPIE **3767**, 296-310 (1999)

COPPOLA R., MAGNANI M., MAY R.P., MOESLANG A. He bubble growth in a martensitic steel for fusion reactors.
Journal of Applied Crystallography **33**, 469-472 (2000)

CORBEL G., SUARD E., EMERY J., LEBLANC M. OH–F disorder in non-centrosymmetric $Zn_3(BO_3)(OH)_{0.7}F_{0.3}$: Ab initio structure determination and NMR study; comparison with tridymite and fluoride borates.
Journal of Alloys and Compounds **305**, 49-57 (2000)

CORDONE L., FERRAND M., VITRANO E., ZACCAI G. Harmonic behavior of trehalose-coated carbonmonoxy-myoglobin at high temperature.
Biophysical Journal **76**, 1043-1047 (1999)

COSTI T.A. Kondo effect in a magnetic field and the magnetoresistivity of Kondo alloys.
Physical Review Letters **85**, 1504-1507 (2000)

CRIADO A., JIMENEZ-RUIZ M., CABRILLO C., BERMEJO F.J., FERNANDEZ-PEREA R., FISCHER H.E., TROUW F.R. Rotational dynamics in the plastic-crystal phase of ethanol: Relevance for understanding the dynamics during the structural glass transition.
Physical Review B **61**, 12082-12093 (2000)

CRIADO A., JIMENEZ-RUIZ M., CABRILLO C., BERMEJO F.J., GRIMSDITCH M., FISCHER H.E., BENNINGTON S.M., ECCLESTON R.S. Role of low-frequency vibrations on sound propagation in glasses at intermediate temperature.
Physical Review B **61**, 8778-8783 (2000)

CRISTOFOLINI L., DIANOUX A.J., DAMAY P. A particle jumping in an octahedron studied by QENS.
Physica B **276-278**, 316-317 (2000)

CRISTOFOLINI L., FACCI P., FONTANA M.P., CICOGNANI G., DIANOUX A.J. Lithium diffusion and $C_{60}$ dynamics by quasielastic and inelastic neutron scattering in $Li_{12}C_{60}$ fulleride.
Physical Review B **61**, 3404-3409 (2000)

CRITCHLOW G.W., SWALLOWE G.M., WIMPORY R.C., PIRLING T. Longitudinal stresses in lap joints measured using neutron strain scanning.
In: 'Proceeding of the 22. Annual Meeting of the Adhesion Society' SPETH D.R. (Ed) (The Adhesion Society, 1999) pp. 348-350

CURRAT R. Inelastic scattering using the three-axis spectrometer technique
KFKI-1999-04/E.
In: '2nd European Conference on Neutron Scattering' KADAR G., ROSTA L. (Eds.) (1999)

CURRAT R. Neutron scattering studies of incommensurate systems.
Ferroelectrics **236**, 11-22 (2000)

CUSSEN L.D. On the resolution of neutron scattering instruments.
Journal of Applied Crystallography **33**, 1399-1404 (2000)

CUSSEN L.D. Resolution calculations for novel neutron beam elements.
Journal of Applied Crystallography **33**, 1393-1398 (2000)

CZIHAK C., MÜLLER M., SCHOBER H., VOGL G. Ice formation in amorphous cellulose.
Physica B **276-278**, 286-287 (2000)

CZIHAK C., MÜLLER M., SCHOBER H., VOGL G. Relaxational motion and ice formation of water adsorbed to cellulose.
Journal de Physique IV **10**, Pr7-199-Pr7-202 (2000)

DAWBER P.G., BYRNE J., VAN DER GRINTEN M.G.D., HABECK C., SHAIKH F., SPAIN J.A., BAKER C.A., GREEN K., SCOTT R.D., ZIMMER O. Determination of the electron-antineutrino correlation coefficient *a* in neutron β decay by measurement of the integrated proton spectrum.
Nuclear Instruments and Methods in Physics Research A **440**, 543-547 (2000)

DE HAAN R.C., APRAHAMIAN A., BÖRNER H.G., DOLL C., JENTSCHEL M., BRUCE A.M., LESHER S.R. Lifetime measurements in $^{180}$Hf.
Journal of Research of the National Institute of Standards and Technology **105**, 125-131 (2000)

DEME B., HESS D., TRISTL M., LEE L.T., SACKMANN E. Binding of actin filaments to charged lipid monolayers: Film balance experiments combined with neutron reflectivity.
European Physical Journal E **2**, 125-136 (2000)

DEME B., ZEMB T. Measurement of sugar depletion from uncharged lamellar phases by SANS contrast variation.
Journal of Applied Crystallography **33**, 569-573 (2000)

DERIU A., PACIARONI A., ZACCAI J., PFISTER C. First experimental results from the IN13-Collaborative Research Group (CRG) at the I.L.L..
Physica B **276-278**, 512-513 (2000)

DERTINGER A., KREYSSIG A., RITTER C., LOEWENHAUPT M., BRAUN H.F. Superconductivity, magnetic ordering, and its interplay in $HoNi_2{}^{11}B_2C$.
Physica B **284-288**, 485-486 (2000)

DERVENAGAS P., BURLET P., BONNET M., BOURDAROT F., HIESS A., BUD'KO S.L., CANFIELD P.C., LANDER G.H., KIM J.S., STEWART G.R. Magnetic structure of $HoBe_{13}$ in an applied magnetic field.
Physical Review B **61**, 405-412 (2000)

DETLEFS C., BOURDAROT F., BURLET P., DERVENAGAS P., BUD'KO S.L., CANFIELD P.C. Ordering wave vectors of metamagnetic states in $HoNi_2B_2C$: One dimension is not enough (Rapid communications).
Physical Review B **61**, R14916-R14919 (2000)

DOLL C., BÖRNER H.G., VON EGIDY T., FUJIMOTO H., JENTSCHEL M., LEHMANN H. GAMS5.
Journal of Research of the National Institute of Standards and Technology **105**, 167-171 (2000)

DOLL C., LEHMANN H., BÖRNER H.G., VON EGIDY T. Lifetime measurement in $^{172}$Re.
Nuclear Physics A **672**, 3-20 (2000)

DÖNNI A., FISCHER P., KELLER L., HERRMANNSDÖRFER T., FAUTH F., KOMATSUBARA T. Neutron diffraction study of a $Nd_3Pd_{20}Ge_6$ sample with three successive magnetic phase transitions.
Physica B **281-282**, 155-157 (2000)

DORE J.C., BLAKEY D.M., CHIEUX P., PALLEAU P. Neutron diffraction studies of an argon/amorphous ice co-deposit using isotopic substitution.
Physical Chemistry - Chemical Physics **2**, 1603-1606 (2000)

DORNER B. Brillouin scattering with neutrons and X-rays.
In: 'Frontiers of Neutron Scattering. Proceedings of the Seventh Summer School on Neutron Scattering', FURRER A. (Ed.) (World Scientific, 2000) pp. 27-43
DOXASTAKIS M., KITSIOU M., FYTAS G., THEO-

DOROU D.N., HADJICHRISTIDIS N., MEIER G., FRICK B. Component segmental mobilities in an athermal polymer blend: Quasielastic incoherent neutron scattering versus simulation.
Journal of Chemical Physics **112**, 8687-8694 (2000)

DREßLER S., TAYLOR J.W., OULADDIAF B., NEUMANN K.U., ZIEBECK K.R.A. Suppression of the martensitic phase transition and the effect on superconductivity in $HfV_2$.
Solid State Communications **113**, 649-651 (2000)

DREYER J., REGNAULT L.P., BOURGEAT-LAMI E., LELIEVRE-BERNA E., PUJOL S., THOMAS F., THOMAS M., TASSET F. Cryopol: A superconducting magnetostatic cavity for a $^3$He neutron spin filter.
Nuclear Instruments and Methods in Physics Research A **449**, 638-648 (2000)

DUBBERS D. Physics with low-energy neutrons and neutrinos.
Hyperfine Interactions **127**, 355-363 (2000)

DUBOIS M., BELLONI L., ZEMB T., DEME B., GULIK-KRZYWICKI T. Formation of rigid nanodiscs: Edge formation and molecular separation.
Progress in Colloid and Polymer Science **115**, 238-242 (2000)

DUFFY J.A., HAYDEN S.M., MAENO Y., MAO Z., KULDA J., MCINTYRE G.J. Polarized-neutron scattering study of the cooper-pair moment in $Sr_2RuO_4$.
Physical Review Letters **85**, 5412-5415 (2000)

DUNN R.V., REAT V., FINNEY J.L., FERRAND M., SMITH J.C., DANIEL R.M. Enzyme activity and dynamics: Xylanase activity in the absence of fast anharmonic dynamics.
Biochemical Journal **346**, 355-358 (2000)

EHLERS G., RITTER C., KNORR K., SCHNEIDER R., HOHLWEIN D., MEIßNER M., MALETTA H. Pressure-induced change of magnetic order in $Tb_{1-x}Y_xNiAl$ and $TbNi_{1-x}CuxAl$.
Physica B **276-278**, 650-651 (2000)

ENDERLE M., KIEFER K., KLÖPPERPIEPER A., ALBERS J., MCINTYRE G. J., LEFMANN K., SCHMIDT W., VAN DE KAMP R. Quantum features in the spin dynamics of $S=\frac{1}{2}$ and 1 Heisenberg antiferromagnets in spite of long-range ordered phases.
Physica B **276-278**, 782-783 (2000)

ESSAYEM N., TONG Y.Y., JOBIC H., VEDRINE J.C. Characterization of protonic sites in $H_3PW_{12}O_{40}$ and $Cs_{1.9}H_{1.1}PW_{12}O_{40}$: A solid-state $^1$H, $^2$H, $^{31}$P MAS-NMR and inelastic neutron scattering study on samples prepared under standard reaction conditions.
Applied Catalysis A: General **194-195**, 109-122 (2000)

FÅK B., PLANTEVIN O., GLYDE H.R. Liquid helium in confinement.
Journal de Physique IV **10**, Pr7-163-Pr7-167 (2000)

FÅK B., PLANTEVIN O., GLYDE H.R., MULDERS N. Phonons, rotons, and layer modes of liquid $^4$He in aerogel.
Physical Review Letters **85**, 3886-3989 (2000)

FAN L., SVERGUN D.I., VOLKOV V.V., AKSENOV V.L., ALGALAROV C.C., SELIVANOVA O.M., SHCHERBAKOVA I.V., KOCH M., GILLES R., WIEDENMANN A., MAY R.P., SERDYUK I.N. Structural studies of the 30S subunit of ribosomes Thermus thermophilus by small-angle neutron and X-ray scattering.
Journal of Applied Crystallography **33**, 515-518 (2000)

FARHI E., TAGANTSEV A.K., CURRAT R., HEHLEN B., COURTENS E., BOATNER L.A. Low energy phonon spectrum and its parameterization in pure $KTaO_3$ below 80 K.
European Physical Journal B **15**, 615-623 (2000)

FARHI E., TAGANTSEV A.K., HEHLEN B., CURRAT R., BOATNER L.A., COURTENS E. The broad Brillouin doublets and central peak of $KTaO_3$.
Physica B **276-278**, 274-275 (2000)

FARHI E., TAGANTSEV A.K., HEHLEN B., CURRAT R., BOATNER L.A., COURTENS E. The extra Brillouin doublets and central peak of $KTaO_3$: Second sound vs. two-phonon difference scattering.
Ferroelectrics **239**, 895-902 (2000)

FERNANDEZ-DIAZ M.T., ALONSO J.A., MARTINEZ-LOPE M.J., CASAIS M.T., GARCIA-MUNOZ J.L., ARANDA M.A.G. Charge disproportionation in $RNiO_3$ perovskites.
Physica B **276-278**, 218-221 (2000)

FISCHER H.E., PALLEAU P., FELTIN D. The D4c neutron diffractometer for liquids and glasses.
Physica B **276-278**, 93-94 (2000)

FISCHER P., HERRMANNSDÖRFER T., BONELLI T., FAUTH F., KELLER L., BAUER E., GIOVANNINI M. Antiferromagnetic rare-earth ordering in the intermetallic compounds $R_2Pd_2In$ (R = Pr, Nd).
Journal of Physics Condensed Matter **12**, 7089-7098 (2000)

FITTER J. Confined molecular motions of globular proteins studied in powder samples and in solution.
Journal de Physique IV **10**, Pr7-265-Pr7-270 (2000)

FITTER J., HEBERLE J. Structural equilibrium fluctuations in mesophilic and thermophilic α-amylase.
Biophysical Journal **79**, 1629-1636 (2000)

FONG H.F., BOURGES P., SIDIS Y., REGNAULT L.P., BOSSY J., IVANOV A.S., MILIUS D.L., AKSAY I.A., KEIMER B. Spin susceptibility in underdoped $YBa_2Cu_3O_{6+x}$.
Physical Review B **61**, 14773-14786 (2000)

FORGAN E.M., KEALEY P.G., JOHNSON S.T., PAUTRAT A., SIMON C., LEE S.L., AEGERTER C.M., CUBITT R., FARAGO B., SCHLEGER P. Measurement of vortex motion in a type-II superconductor: A novel use of the neutron spin-echo technique.
Physical Review Letters **85**, 3488-3491 (2000)

FÖRSTER H., FUESS H., GEIDEL E., HUNGER B., JOBIC H., KIRSCHHOCK C., KLEPEL O., KRAUSE K. Adsorption of pyrrole derivatives in alkali metal cation-exchanged faujasites: Comparative studies by surface vibrational techniques, X-ray diffraction and temperature-programmed desorption augmented with theoretical studies. Part I - Pyrrole as probe molecule.
Physical Chemistry - Chemical Physics **1**, 593-603 (1999)

FRAGNETO G., BELLET-AMALRIC E., CHARITAT T., DUBOS P., GRANER F., PERINO-GALLICE L. Neutron and X-ray reflectivity studies at solid-liquid interfaces: The interaction of a peptide with model membrane.
Physica B **276-278**, 501-502 (2000)

FRAGNETO G., GRANER F., CHARITAT T., DUBOS P., BELLET-AMALRIC E. Interaction of the third helix of Antennapedia homeodomain with a deposited phospholipid bilayer: A neutron reflectivity structural study.
Langmuir **16**, 4581-4588 (2000)

FRAGNETO G., SU T.J., LU J.R., THOMAS R.K., RENNIE A.R. Adsorption of proteins from aqueous solutions on hydrophobic surfaces studied by neutron reflection.
Physical Chemistry - Chemical Physics **2**, 5214-5221 (2000)

FRAGNETO-CUSANI G. Biology at ECNS'99.
Neutron News **11**, 12-13 (2000)

FREY F., WEIDNER E., HRADIL K., BOISSIEU M. DE, CURRAT R., SHIBATA K., TSAI A.P., SATO T.J. On the one-dimensional 8 Å periodic superstructure in decagonal phases.
Philosophical Magazine A **80**, 2375-2391 (2000)

FRICK B., FRANCO L., SUBIRANA J., XENOPOULOS A. Temperature dependence of the dynamics of methylene chains in aliphatic nylons of different chain length.
Physica B **276-278**, 421-422 (2000)

FRICK B., ZORN R., BÜTTNER H.G. ILL hosts "Dynamics in confinement".
Neutron News **11**, 8 (2000)

FRONTERA C., GARCIA-MUNOZ J.L., LLOBET A., RITTER C. Reply to "Comment on 'Tetragonal to monoclinic transition in the metallic antiferromagnet $Pr_{0.5}Sr_{0.5}MnO_3$'".
Physical Review B **62**, 6822-6824 (2000)

FRONTERA C., GARCIA-MUNOZ J.L., LLOBET A., RITTER C., ALONSO J.A., RODRIGUEZ-CARVAJAL J. Dependence of the physical properties of $Nd_{0.5}Ca_{0.5}MnO_{3-\delta}$ on the oxidation state of Mn.
Physical Review B **62**, 3002-3005 (2000)

FRONTERA C., LLOBET A., GARCIA-ARANDA M.A., RITTER C., GARCIA-MUNOZ J.L. Phase coexistence and magnetic structures of $Bi_{1-x}Sr_xMnO_3$ ($x = \frac{1}{7}, \frac{1}{2}$).
Physica B **276-278**, 793-794 (2000)

GALEZ P., LOMELLO-TAFIN M., HOPFINGER T., OPAGISTE C., BERTRAND C. Crystal structure of $Ca_{4.78}Cu_6O_{11.60}$.
Journal of Solid State Chemistry **151**, 170-180 (2000)

GARCIA-MUNOZ J.L., RESPAUD M., FRONTERA C., LLOBET A., BROTO J.M., RAKOTO H., GOIRAN C. *H-T* diagrams of $Ln_{1-x}Ca_xMnO_3$ (x = 1/2, 1/3) in pulsed fields up to 50 T.
Journal of Applied Physics **85**, 5570-5572 (1999)

GARNIER A., GIGNOUX D., OULADDIAF B., SCHMITT D., SHIGEOKA T. Double-Q magnetic structures and strong planar anisotropy in tetragonal $ErRu_2Ge_2$ and $ErRu_2Si_2$.
European Physical Journal B **16**, 423-427 (2000)

GASPARD P.P., BEATTY A.M., CHEN T., HAILE T., LEI D., WINCHESTER W.R., BRADDOCK-WILKING J., RATH N.P., KLOOSTER W.T., KOETZLE T.F., MASON S.A., ALBINATI A. Tris(triisopropylsilyl)silane and the generation of bis(triisopropylsilyl)silylene.
Organometallics **18**, 3921-3932 (1999)

GEIDEL E., JOBIC H., PARKER S.F. Vibrational spectroscopic investigations of pyrrole adsorption in faujasites: Studies by infrared, Raman and neutron spectroscopy.
In: '12. International Zeolite Conference' (MRS, 1999) pp. 2609-2614

GENEVEY J., PINSTON J.A., FAUST H., FOIN C., OBERSTEDT S., REJMUND M. New high-spin microsecond isomers in $^{130}$Sb.
European Physical Journal A **9**, 191-195 (2000)

GENEVEY J., PINSTON J.A., FAUST H., FOIN C., OBERSTEDT S., WEISS B. On the nature of the 17 μs isomer of the $^{131}$Sb valence nucleus.
European Physical Journal A **7**, 463-465 (2000)

GENILLOUD L., BÖRNER H.G., CORMINBOEUF F., DOLL C., DRISSI S., JENTSCHEL M., JOLIE J., KERN J., LEHMANN H., WARR N. Erratum to "Study of the vibrational nucleus $^{98}$Ru by the $^{98}$Mo(α, 2γ) and $^{98}$Ru(n,γ) reactions" [Nucl. Phys. A 662 (2000) 3-43].
Nuclear Physics A **669**, 407-449 (2000)

GENILLOUD L., BÖRNER H.G., CORMINBOEUF F., DOLL C., DRISSI S., JENTSCHEL M., JOLIE J., KERN J., LEHMANN H., WARR N. Study of the vibrational nucleus $^{98}$Ru by the $^{98}$Mo(α, 2γ) and $^{98}$Ru(n,γ) reactions.
Nuclear Physics A **662**, 3-43 (2000)

GENILLOUD L., JOLIE J., BÖRNER H.G., LEHMANN H., BECVAR F., KRTICKA M., ZAMFIR N.V., CASTEN R.F. Lifetimes of negative parity states in $^{166}$Er.
Physical Review C **62**, 034313-1-034313-8 (2000)

GENILLOUD L., JOLIE J., BÖRNER H.G., LEHMANN H., BECVAR F., ZAMFIR N.V., CASTEN R.F. Study of octupole vibrations in $^{166}$Er.
AIP Conference Proceedings **529**, 654-656 (2000)

GERGIDIS L.N., THEODOROU D.N., JOBIC H. Dynamics of alkane mixtures in silicalite pores.

Journal de Physique IV **10**, Pr7-143-Pr7-146 (2000)

GERGIDIS L.N., THEODOROU D.N., JOBIC H. Dynamics of *n*-butane–methane mixtures in silicalite, using quasielastic neutron scattering and molecular dynamics simulations.
Journal of Physical Chemistry B **104**, 5541-5552 (2000)

GHOSH R.E., RENNIE A.R. Assessment of detector calibration materials for SANS experiments.
Journal of Applied Crystallography **32**, 1157-1163 (1999)

GIBBS M.R., STIRLING W.G., ANDERSEN K.H., SCHOBER H. Pressure dependence of the multiphonon excitations of superfluid $^4$He.
Journal of Low-Temperature Physics **120**, 55-64 (2000)

GILBERT R.J.C., HEENAN R.K., TIMMINS P.A., GINGLES N.A., MITCHELL T.J., ROWE A.J., ROSS-JOHN J., PARKER M.W., ANDREW P.W., BYRON O. Studies on the structure and mechanism of a bacterial protein toxin by analytical ultracentrifugation and small-angle neutron scattering.
Journal of Molecular Biology **293**, 1145-1160 (1999)

GIOVANNINI M., MICHOR H., BAUER E., HILSCHER G., ROGL P., BONELLI T., FAUTH F., FISCHER P., HERRMANNSDÖRFER T., KELLER L., SIKORA W., SACCONE A., FERRO R. Effect of nonstoichiometry on the transition from ferromagnetism to antiferromagnetism in the ternary iodides $Ce_{1+\varepsilon}Pd_{2+2\delta}In_{1-3\varepsilon}$ and $Ce_{1+\varepsilon}Pd_{1+\delta}In_{1-\varepsilon}$.
Physical Review B **61**, 4044-4053 (2000)

GLYDE H.R., PLANTEVIN O., FÅK B., CODDENS G., DANIELSON P.S., SCHOBER H. Dynamics of liquid $^4$He in Vycor.
Physical Review Letters **84**, 2646-2649 (2000)

GONZALEZ M.A., ENCISO E., BERMEJO F.J., BEE M. Glassy dynamics in supercooled liquid and glassy ethanol: A molecular dynamics study.
Physical Review B **61**, 6654-6666 (2000)

GONZALEZ M.A., ENCISO E., BERMEJO F.J., JIMENEZ-RUIZ M., BEE M. Molecular approach to the interpretation of the dielectric relaxation spectrum of a molecular glass former.
Physical Review E **61**, 3884-3895 (2000)

GOOSSENS D.J., WILDES A.R., RITTER C., HICKS T.J. Ordering and the nature of the spin flop phase transition in $MnPS_3$.
Journal of Physics Condensed Matter **12**, 1845-1854 (2000)

GOREMYCHKIN E.A., OSBORN R., RAINFORD B.D., MURANI A.P. Evidence for anisotropic Kondo behavior in $Ce_{0.9}La_{0.1}Al_2$.
Physical Review Letters **84**, 2211-2214 (2000)

GORRIA P., FERNANDEZ BARQUIN L., GARITAONANDIA J.S., BARANDIARAN J.M., GARCIA-ARRIBAS A., CONVERT P. Joule heating nanocrystallization of Fe/Zr/Cu/B glass studied by neutron diffraction.
Physica B **276-278**, 461-462 (2000)

GOUPIL C., PAUTRAT A., SIMON C., KEALEY P.G., FORGAN E.M., LEE S.L., JOHNSON S.T., LAZARD G., PLACAIS B., SIMON Y., MATHIEU P., CUBITT R., DEWHURST C. Small angle neutron scattering and vortex lattice dynamical phase diagram.
Physica C **341-348**, 999-1002 (2000)

GOYAL R., FITCH A.N., JOBIC H. Powder neutron and X-ray diffraction studies of benzene adsorbed in zeolite ZSM-5.
Journal of Physical Chemistry B **104**, 2878-2884 (2000)

GRATZ E., BERNHOEFT N., PAUL-BONCOUR V., CASALTA H., MURANI A.P. Use of magnetization density fluctuation spectra to estimate the electrical resistivity in $YCo_2$.
Journal of Physics Condensed Matter **12**, 5507-5518 (2000)

GRENIER B., REGNAULT L.P., LORENZO J.E., BOUCHER J.P., HIESS A., DHALENNE G., REVCOLEVSCHI A. Magnetic field effects on spin excitations in the spin-Peierls compound $CuGeO_3$.
Physical Review B **62**, 12206-12215 (2000)

GRENIER B., REGNAULT L.P., LORENZO J.E., RENARD J.P., DHALENNE G., REVCOLEVSCHI A. Phase diagram of Si-doped spin-Peierls compound $CuGeO_3$.
Physica B **280**, 313-314 (2000)

GROENEWEGEN W., EGELHAAF S.U., LAPP A., VAN DER MAAREL J.R.C. Neutron scattering estimates of the effect of charge on the micelle structure in aqueous polyelectrolyte diblock copolymer solutions.
Macromolecules **33**, 3283-3293 (2000)

GUTIERREZ J., PENA A., BARANDIARAN J.M., PIZARRO J.L., HERNANDEZ T., LEZAMA L., INSAUSTI M., ROJO T. Structural and magnetic properties of $La_{0.7}Pb_{0.3}(Mn_{1-x}Fex)O_3$ ($0 \le x \le 0.3$) giant magnetoresistance perovskites.
Physical Review B **61**, 9028-9035 (2000)

GUTSCHE I., HOLZINGER J., RÖBLE M., HEUMANN H., BAUMEISTER W., MAY R.P. Conformational rearrangements of an archaeal chaperonin upon ATPase cycling.
Current Biology **10**, 405-408 (2000)

GYGAX F.N., SOLT G., AMATO A., ANDERSON I.S., PINKPANK M., SCHENCK A., UDOVIC T.J. Light hydrogen isotope $\mu^+$ in Sc and ($\alpha$-$ScH_x$) solid solutions.
Physical Review B **61**, 168-183 (2000)

HAARMANN F., JACOBS H., ASMUSSEN B., NÖLDEKE C., KEARLEY G.J., COMBET J. Reorientational motion of the HS ions in hydrogensulfides of alkali metals (NaHS, KHS, RbHS): A quasielastic neutron scattering study.
Journal of Chemical Physics **113**, 8161-8167 (2000)

HAMBSCH F.J., VIVES F., SIEGLER P., OBERSTEDT S. Study of the $^{237}$Np(n,f)-reaction at MeV neutron energies.
Nuclear Physics A **679**, 3-24 (2000)

HAMMERMANN M., BRUN N., KLENIN K.V., MAY R.P., TOTH K., LANGOWSKI J. The diameter of the DNA superhelix decreases with salt concentration: SANS measurements and Monte Carlo simulations.
Journal of Applied Crystallography **33**, 526-529 (2000)

HAMMERMANN M., TOTH K., RODEMER C., WALDECK W., MAY R.P., LANGOWSKI J. Salt-dependent compaction of di- and trinucleosomes studied by small-angle neutron scattering.
Biophysical Journal **79**, 584-594 (2000)

HARRIS P.G., BAKER C.A., GREEN K., IAYDJIEV P., IVANOV S., MAY D.J.R., PENDLEBURY J.M., SHIERS D., SMITH K.F., VAN DER GRINTEN M.G.D., GELTENBORT P. New experimental limit on the electric dipole moment of the neutron.
Physical Review Letters **82**, 904-907 (1999)

HARRIS P.G., MAY D.J.R., PENDLEBURY J.M., SHIERS D., SMITH K.F., VAN DER GRINTEN M.G.D., BAKER C.A., GREEN K., IAYDJIEV P., IVANOV S., GELTENBORT P. The neutron EDM experiment at the ILL.
Nuclear Instruments and Methods in Physics Research A **440**, 479-482 (2000)

HAYWARD M.A., GREEN M.A., ROSSEINSKY M.J., SLOAN J. Sodium hydride as a powerful reducing agent for topotactic oxide deintercalation: Synthesis and characterization of the nickel(I) oxide $LaNiO_2$.
Journal of the American Chemical Society **121**, 8843-8854 (1999)

HEFFNER R.H., SONIER J.E., MACLAUGHLIN D.E., NIEUWENHUYS G.J., EHLERS G., MEZEI F., CHEONG S.W., GARDNER J.S., RÖDER H. Observation of two time scales in the ferromagnetic manganite $La_{1-x}Ca_xMnO_3$, $x \approx 0.3$.
Physical Review Letters **85**, 3285-3288 (2000)

HERNANDO A., CRESPO P., CASTANO F.J., ARCAS J., MULTIGNER M., BARANDIARAN J.M., FERNANDEZ-BARQUIN L. Thermoremanence anomaly in Fe-Zr(B,Cu) Invar metallic glasses: Volume expansion induced ferromagnetism.
Physical Review B **61**, 3219-3222 (2000)

HETZER M., KARAKATSANIS P., CASALTA H., HIRSCH A., CAMPS X., VOSTROWSKY O., BAYERL T.M. Diffusion and molecular dynamics of lipo-fullerenes in phospholipid membranes studied by NMR and quasi-elastic neutron scattering.
Journal of Physical Chemistry A **104**, 5437-5443 (2000)

HIESS A., BOUCHERLE J.X., GIVORD F., SCHWEIZER J., LELIEVRE-BERNA E., TASSET F., GILLON B., CANFIELD P.C. Magnetism in intermediate-valence $YbAl_2$: A polarized neutron diffraction study.
Journal of Physics Condensed Matter **12**, 829-840 (2000)

HIESS A., CURRAT R., SAROUN J., BERMEJO F.J. ILL renewed thermal three-axis spectrometer IN3.
Physica B **276-278**, 91-92 (2000)

HILL R.E., ANAYA J.M., BOWLES T.J., GREENE G.L., HOGAN G., LAMOREAUX S., MAREK L.,

MORTENSON R., MORRIS C.L., SAUNDERS A., SEESTROM S.J., TEASDALE W., HOEDL S., LIU C.Y., SMITH D.A., YOUNG A., FILIPPONE B.W., HUA J., ITO T., PASYUK E., GELTENBORT P., GARCIA A., FUJIKAWA B., BAESSLER S., SEREBROV A. Performance of the prototype LANL solid deuterium ultra-cold neutron source.
Nuclear Instruments and Methods in Physics Research A **440**, 674-681 (2000)

HILLIER A.D., CYWINSKI R., RITTER C. Evolution of magnetic order and loss of superconductivity in $Er_{1-x}Th_xNi_2B_2C$.
Physica B **276-278**, 658-659 (2000)

HOFFMANN S., WILLNER L., RICHTER D., ARBE A., COLMENERO J., FARAGO B. Origin of dynamic heterogeneities in miscible polymer blends: A quasielastic neutron scattering study.
Physical Review Letters **85**, 772-775 (2000)

HØGHØJ P., ABELE H., ASTRUC HOFFMANN M., BÄßLER S., REICH J., NESVIZHEVSKY V.V., ZIMMER O. Neutron long wavelength cut-off filter.
Nuclear Instruments and Methods in Physics Research B **160**, 431-434 (2000)

HOLZINGER J., HEUMANN H., MANAKOVA E., RÖßLE M., VANATALU K., WIEDENMANN A., MAY R.P. GroEL single-ring solution structure obtained by small-angle neutron scattering.
Physica B **276-278**, 528-529 (2000)

HUFFMAN P.R., BROME C.R., BUTTERWORTH J.S., COAKLEY K.J., DEWEY M.S., DZHOSYUK S.N., GOLUB R., GREENE G.L., HABICHT K., LAMOREAUX S.K., MATTONI C.E.H., MCKINSEY D.N., WIETFELDT F.E., DOYLE J.M. Magnetic trapping of neutrons.
Nature **403**, 62-64 (2000)

HUPFELD D., SCHWEIKA W., STREMPFER J., MATTENBERGER K., MCINTYRE G.J., BRÜCKEL T. Element-specific magnetic order and competing interactions in $Gd_{0.8}Eu_{0.2}S$.
Europhysics Letters **49**, 92-98 (2000)

HUXLEY A., RODIERE P., PAUL D.MCK., VAN DIJK N.H., CUBITT R., FLOUQUET J. Realignment of the flux-line lattice by a change in the symmetry of superconductivity in $UPt_3$.
Nature **406**, 160-164 (2000)

IRODOVA A.V., SUARD E. Order–disorder phase transition in the deuterated hexagonal (C14-type) Laves phase $ZrCr_2D_{3.0}$.
Journal of Alloys and Compounds **299**, 32-38 (2000)

ISOBE M., ONODA M., OHTA T., IZUMI F., KIMOTO K., TAKAYAMA-MUROMACHI E., HEWAT A.W., OHOYAMA K. Low-temperature crystal and magnetic structures of the chain-ladder composite material $Sr_{0.4}Ca_{13.6}Cu_{24+y}O_{41+z}$: Hole redistribution and antiferromagnetic order.
Physical Review B **62**, 11667-11676 (2000)

IVANOV A.S., RUMIANTSEV A.Y. Phonon dispersion in vanadium metal.
Physica B **276-278**, 197-199 (2000)

JAMES S.S., DEWHURST C.D., DOYLE R.A., PAUL D.MCK., PALTIEL Y., ZELDOV E., CAMPBELL A.M. Flux pinning, surface and geometrical barriers in $YNi_2B_2C$.
Physica C **332**, 173-177 (2000)

JAVORSKY P., NISHIGORI S., OULADDIAF B. Magnetic structures in DyPdIn.
Physica B **276-278**, 730-731 (2000)

JENTSCHEL M., BÖRNER H.G., LEHMANN H., DOLL C. The GRID technique: Current status and new trends.
Journal of Research of the National Institute of Standards and Technology **105**, 25-32 (2000)

JERICHA E., SCHWAB D.E., JÄKEL M.R., CARLILE C.J., RAUCH H. Neutron beam tailoring by accumulation between perfect crystal mirrors.
Physica B **283**, 414-417 (2000)

JESINGER P., KÖTZLE A., GAGARSKI A.M., GÖNNENWEIN F., DANILYAN G., PAVLOV V.S., CHVATCHKIN V.B., MUTTERER M., NEUMAIER S.R., PETROV G.A., PETROVA V.I., NESVIZHEVSKY V.V., ZIMMER O., GELTENBORT P., SCHMIDT K., KOROBKINA K. Observation of a triple correlation in ternary fission: Is time reversal invariance violated?
Nuclear Instruments and Methods in Physics Research A **440**, 618-625 (2000)

JOBIC H. Diffusion of linear and branched alkanes in ZSM-5. A quasi-elastic neutron scattering study .
Journal of Molecular Catalysis A: Chemical **158**, 135-142 (2000)

JOBIC H. Dynamics of molecules in confinement and technical relevance.
Journal de Physique IV **10**, Pr7-125-Pr7-130 (2000)

JOBIC H. Molecular dynamics of n-pentane in NaX zeolite studied by quasi-elastic neutron scattering.
Physical Chemistry - Chemical Physics **1**, 525-530 (1999)

JOBIC H., BEE M., FRICK B., METHIVIER A. Diffusivities of xylenes in x-type zeolites, a quasi-elastic neutron scattering study.
In: 'Proceedings of the 12. International Zeolite Conference', TREACY M.M.J. et al. (Eds.) (1999) pp. 59-66

JOBIC H., BEE M., POUGET S. Diffusion of benzene in ZSM-5 measured by the neutron spin–echo technique.
Journal of Physical Chemistry B **104**, 7130-7133 (2000)

JOBIC H., FITCH A.N., COMBET J. Diffusion of benzene in NaX and NaY zeolites studied by quasi-elastic neutron scattering.
Journal of Physical Chemistry B **104**, 8491-8497 (2000)

JOHNSON M., COMBET J., FRICK B. Les spectromètres à haute résolution.
Journal de Physique IV **10**, Pr1-27-Pr1-44 (2000)

JOLIE J., STRITT N., JENTSCHEL M., BÖRNER H.G., LEHMANN H. Study of intermetallic potentials using high precision gamma-ray spectroscopy.
AIP Conference Proceedings **529**, 136-143 (2000)

JORIO A., CURRAT R., MYLES D.A.A., MCINTYRE G.J., ALEKSANDROVA I.P., KIAT J.M., SAINT-GREGOIRE P. Ferroelastic phase transition in $Cs_3Bi_2I_9$: A neutron diffraction study.
Physical Review B **61**, 3857-3862 (2000)

JOUMARD I., KLEIN T., MARCUS J., CUBITT R. Neutron diffraction from the flux line lattice near the entanglement transition in $(K, Ba)BiO_3$.
Physica C **341-348**, 2131-2132 (2000)

KAISERMAYR M., COMBET J., IPSER H., SCHICKETANZ H., SEPIOL B., VOGL G. Nickel diffusion in *B2*-NiGa studied with quasielastic neutron scattering.
Physical Review B **61**, 12038-12044 (2000)

KAISERMAYR M., COMBET J., SEPIOL B., THIESS H., VOGL G. Self-diffusion in the B2-ordered alloy NiGa.
Physica B **276-278**, 270-271 (2000)

KARMANN A., WESCH W., WEBER B., BÖRNER H.G., JENTSCHEL M. Application of GRID to foreign atom localization in single crystals.
Journal of Research of the National Institute of Standards and Technology **105**, 177-182 (2000)

KEALEY P.G., RISEMAN T.M., FORGAN E.M., GALVIN L.M., MACKENZIE A.P., LEE S.L., PAUL D.MCK., CUBITT R., AGTERBERG D.F., HEEB R., MAO Z.Q., MAENO Y. Reconstruction from small-angle neutron scattering measurements of the real space magnetic field distribution in the mixed state of $Sr_2RuO_4$.
Physical Review Letters **84**, 6094-6097 (2000)

KEARLEY G.J., BÜTTNER H.G., SCHIEBEL P. Lattice-parameter dependence of translation/rotation coupling potentials.
Physica B **276-278**, 258-259 (2000)

KEARLEY G.J., NICOLAÏ B. Méthodes numériques et simulations.
Journal de Physique IV **10**, Pr1-237-Pr1-249 (2000)

KEIMER B., BOURGES P., FONG H.F., GU G.D., HE H., IVANOV A.S., KOSHIZUKA N., LIANG B., LIN C.T., REGNAULT L.P., SIDIS Y., SCHOENHERR E. Spin excitations in cuprates: From underdoped to overdoped state.
Physica C **341-348**, 2113-2116 (2000)

KEIZER R.J., DE VISSER A., MENOVSKY A.A., FRANSE J.J.M., FÅK B., MIGNOT J.M. Neutron-diffraction study of the evolution of antiferromagnetic order in $UPt_3$ doped with Pd.
Physical Review B **60**, 6668-6677 (1999)

KERNAVANOIS N., BOUCHERLE J.X., DALMAS DE REOTIER P., GIVORD F., LELIEVRE-BERNA E., RESSOUCHE E., SANCHEZ J.P., SATO N. Magnetization density in the heavy-fermion superconductor $UNi_2Al_3$.
Physica B **276-278**, 797-798 (2000)

KERNAVANOIS N., BOUCHERLE J.X., DALMAS DE REOTIER P., GIVORD F., LELIEVRE-BERNA E., RESSOUCHE E., ROGALEV A., SANCHEZ J.P., SATO N., YAOUANC A. Polarized neutron scattering and X-ray magnetic circular dichroism studies of the heavy-fermion superconductor $UNi_2Al_3$.
Journal of Physics Condensed Matter **12**, 7857-7867 (2000)

KESSLER E.G., DEWEY M.S., DESLATTES R.D., HENINS A., BÖRNER H.G., JENTSCHEL M., LEHMANN H. Accurate determination of high energy gamma-ray standards.
AIP Conference Proceedings **529**, 400-407 (2000)

KHARCHENKO A., ENGLISCH U., GEUE T., GRENZER J., PIETSCH U., SIEBRECHT R. Investigation of partially deuterated organic multilayers by means of X-ray and polarized neutron reflectometry.
Neutron News **11**, 29-32 (2000)

KIAT J.M., BALDINOZZI G., DUNLOP M., MALIBERT C., DKHIL B., MENORET C., MASSON O., FERNANDEZ-DIAZ M.T. Anharmonicity and disorder in simple and complex perovskites: A high energy synchrotron and hot neutron diffraction study.
Journal of Physics Condensed Matter **12**, 8411-8425 (2000)

KLEIN T., JOUMARD I., MARCUS J., CUBITT R. Neutron scattering from the flux line lattice in the cubic (*K, Ba*)$BiO_3$ superconductor.
Journal of Low-Temperature Physics **117**, 1353-1357 (1999)

KNEE C.S., WELLER M.T. Structure of $TlSr_2NiO_{5+\delta}$ by high-resolution neutron powder diffraction.
Journal of Solid State Chemistry **144**, 62-67 (1999)

KNEE C.S., WELLER M.T. Synthesis and structure of a new family of nickelates: $Tl(Ln_2Sr_2)Ni_2O_9$, *Ln* = La, Pr, Nd, Sm, Eu, and Gd.
Journal of Solid State Chemistry **150**, 1-13 (2000)

KOCH T., HEINIG K.H., JENTSCHEL M., BÖRNER H.G. Study of interatomic potentials in ZnS–crystal-GRID experiments versus ab initio calculations.
Journal of Research of the National Institute of Standards and Technology **105**, 81-87 (2000)

KÖTZLE A., JESINGER P., GÖNNENWEIN F., PETROV G.A., PETROVA V.I., GAGARSKI A.M., DANILYAN G., ZIMMER O., NESVIZHEVSKY V.V. Parity nonconservation in nuclear fission: Does it depend on fragment mass/energy?
Nuclear Instruments and Methods in Physics Research A **440**, 750-753 (2000)

KRÄMER K.W., GÜDEL H.U., ROESSLI B., FISCHER P., DÖNNI A., WADA N., FAUTH F., FERNANDEZ-DIAZ M.T., HAUSS T. Magnetic ordering in the erbium honeycomb lattices of $ErX_3$ (X = Cl, Br, I).
Physica B **276-278**, 674-675 (2000)

KREISEL J., VINCENT H., TASSET F., PATE M., WOLFERS P. A single-crystal neutron diffraction study of the magnetic anisotropy change in Babexaferrites.
Physica B **276-278**, 688-689 (2000)

KREISEL J., VINCENT H., TASSET F., WOLFERS P. The magnetic anisotropy change of $BaFe_{12-2x}Ir_xCo_xO_{19}$: A single-crystal neutron diffraction study of the accompanying atomic and magnetic structures.
Journal of Magnetism and Magnetic Materials **213**, 262-270 (2000)

KREYSSIG A., FREUDENBERGER J., RITTER C., HOSER A., HOFMANN M., FUCHS G., MÜLLER K.H., LOEWENHAUPT M. Magnetic structures and their propagation vectors in diluted holmium nickel borocarbides.
Physica B **276-278**, 554-555 (2000)

KRIMMEL A., LOIDL A., KLEMM M., HORN S., SCHOBER H. Competition between heavy fermion behavior and magnetism in the *d*-metal system $Li_{1-x}Zn_xV_2O_4$ (Oral presentation).
Physica B **281-282**, 26-27 (2000)

KRIMMEL A., LOIDL A., KLEMM M., HORN S., SCHOBER H. Interplay between spin glass and heavy fermion behavior in the *d*-metal oxides $Li_{1-x}Zn_xV_2O_4$.
Physical Review B **61**, 12578-12581 (2000)

KRIMMEL A., LOIDL A., KLEMM M., HORN S., SCHOBER H. Magnetic properties of the d-metal heavy-fermion system $Li_{1-x}Zn_xV_2O_4$.
Physica B **276-278**, 766-767 (2000)

KROUPA G., BRUCKNER G., BOLIK O., ZAWISKY M., HAINBUCHNER M., BADUREK G., BUCHELT R.J., SCHRICKER A., RAUCH H. Basic features of the upgraded S18 neutron interferometer set-up at ILL.
Nuclear Instruments and Methods in Physics Research A **440**, 604-608 (2000)

KULDA J., MIKULA P., SAROUN J. Elastically bent perfect Ge crystal analyser.
Physica B **276-278**, 73-74 (2000)

KUZNETSOV I.A., RUDNEV Y.P., SEREBROV A.P., SOLOVEI V.A., STEPANENKO I.V., VASILIEV A.V., MOSTOVOY Y.A., ZIMMER O., YEROZOLIMSKY B.G., DEWEY M.S., WIETFELDT F. An experiment to measure $\lambda = G_V/G_1$ from a combination of angular correlation coefficients in the beta decay of polarized neutrons.
Nuclear Instruments and Methods in Physics Research A **440**, 539-542 (2000)

LANDER G.H. X-rays and neutrons as complementary probes to muons in magnetism: A view from reciprocal space.
Physica B **289-290**, 1-9 (2000)

LAPORTE P., ABROSIMOV N., BASTIE P., CORDIER B., DI COCCO G., EVRARD J., GIZZI L., HAMELIN B., JEAN P., LAURENT P., PALTANI P., SKINNER G.K., SMITHER R.K., VON BALLMOOS P. CLAIRE – Towards the first light for a gamma-ray lens.
Nuclear Instruments and Methods in Physics Research A **442**, 438-442 (2000)

LAUTER-PASYUK V., LAUTER H.J., LORENZ M., PETRENKO A., NIKONOV O., AKSENOV V.L., LEIDERER P. Magnetic field distribution around flux-lines in $YBa_2Cu_3O_7$ superconducting thin films in a parallel field.
Physica B **276-278**, 776-777 (2000)

LAUTER-PASYUK V., LAUTER H.J., TOPERVERG B., NIKONOV O., KRAVTSOV E., MILYAEV M.A., ROMASHEV L., USTINOV V. Magnetic off-specular neutron scattering from Fe/Cr multilayers.
Physica B **283**, 194-198 (2000)

LEE S.L., KEALEY P.G., FORGAN E.M., LLOYD S.H., RISEMAN T.M., PAUL D.MCK., JOHNSON S.T., SIMON C., GOUPIL C., PAUTRAT A., CUBITT R., SCHLEGER P., DEWHURST C., AEGERTER C.M., AGER C. Small-angle scattering from the vortex lattice in high-$T_c$ and other superconductors.
Physica B **276-278**, 752-755 (2000)

LEHNERT H., BOYSEN H., SCHNEIDER J., FREY F., HOHLWEIN D., RADAELLI P., EHRENBERG H. A powder diffraction study of the phase transition in $LaAlO_3$.
Zeitschrift für Kristallographie **215**, 536-541 (2000)

LENNE P.F., BONOSI F., RENAULT A., BELLET-AMALRIC E., LEGRAND J.F., PETIT J.M., RIEUTORD F., BERGE B. Growth of two-dimensional solids in alcohol monolayers in the presence of soluble amphiphilic molecules.
Langmuir **16**, 2306-2310 (2000)

LEULLIOT N., GHOMI M., JOBIC H., BOULOUSSA O., BAUMRUK V., COULOMBEAU C. Ground state properties of the nucleic acid constituents studied by density functional calculations. 2. Comparison between calculated and experimental vibrational spectra of uridine and cytidine.
Journal of Physical Chemistry B **103**, 10934-10944 (1999)

LEVASSEUR S., MENETRIER M., SUARD E., DELMAS C. Evidence for structural defects in non-stoichiometric HT-$LiCoO_2$: Electrochemical, electronic properties and $^7$Li NMR studies.
Solid State Ionics **128**, 11-24 (2000)

LEVELUT C., FAIVRE A., PELOUS J., JOHNSON M., DURAND D. $\alpha$–$\beta$ crossover in glass formers as a function of molecular architecture.
Physica B **276-278**, 431-432 (2000)

LEVELUT C., SCHEYER Y., PELOUS J., DURAND D. Inelastic neutron scattering experiments on polyurethane: Microscopic origin of the $\beta$ relaxational process.
Philosophical Magazine B **79**, 1881-1887 (1999)

LI S., HALL M.B., ECKERT J., JENSEN C.M., ALBINATI A. Transition metal polyhydride complexes. 10. Intramolecular hydrogen exchange in the octahedral iridium(III) dihydrogen dihydride complexes $IrH_2(\eta^2\text{-}H_2)(PR_3)_2$ (X = Cl, Br, I).
Journal of the American Chemical Society **122**, 2903-2910 (2000)

LIDSTRÖM E., MANNIX D., HIESS A., REBIZANT J., WASTIN F., LANDER G.H., MARRI I., CARRA P., VETTIER C., LONGFIELD M.J. Resonant X-ray magnetic scattering from $U_{1-x}Np_xRu_2Si_2$ alloys.
Physical Review B **61**, 1375-1385 (2000)

LINDNER P. ILL : au coeur de la matière.
Industrie & Territoire, 27 (2000)

LINDNER P. Water calibration at D11 verified with polymer samples.
Journal of Applied Crystallography **33**, 807-811 (2000)

LINDNER P., LECLERCQ F., DAMAY P. Analysis of water scattering used for calibration of small-angle neutron scattering (SANS) measurements.
Physica B **291**, 152-158 (2000)

LINE C.M.B., KEARLEY G.J. An inelastic incoherent neutron scattering study of water in small-pored zeolites and other water-bearing minerals.
Journal of Chemical Physics **112**, 9058-9067 (2000)

LIVINGSTON R.A., NEUMANN D.A., ALLEN A.J., FITZGERALD S.A., BERLINER R. Application of neutron scattering to Portland cement.
Neutron News **11**, 18-24 (2000)

LLOBET A., GARCIA-MUNOZ J.L., FRONTERA C., RESPAUD M., RAKOTO H., LORD J.S. Magnetic dynamics and discommensuration in charge-ordered $Pr_{1-x}Ca_xMnO_3$ ($x = \frac{1}{3}$ and $\frac{1}{2}$).
Physica B **289-290**, 73-76 (2000)

LLOBET A., GARCIA-MUNOZ J.L., FRONTERA C., RITTER C. Charge reallocation in the tetragonal to monoclinic transition in $Pr_{1/2}Sr_{1/2}MnO_3$.
Physica B **276-278**, 790-792 (2000)

LORIMIER J., BERNARD F., ISNARD O., BERAR J.F., NIEPCE J.C. Diffraction anomale et composition cationique d'une titanomagnétite nanométrique.
Journal de Physique IV **10**, Pr10-27-Pr10-31 (2000)

LYCHAGIN E.V., MUZYCHKA A.Y., NESVIZHEVSKY V.V., NEKHAEV G.V., STRELKOV A.V. Experimental estimation of the possible subbarrier penetration of ultracold neutrons through vacuum-tight foils.
JETP Letters **71**, 447-450 (2000)

MA G., BARLOW D.J., LAWRENCE M.J., HEENAN R.K., TIMMINS P.A. Small-angle neutron-scattering studies of nonionic surfactant vesicles.
Journal of Physical Chemistry B **104**, 9081-9085 (2000)

MANINI N., PISTOLESI F. Off-diagonal geometric phases.
Physical Review Letters **85**, 3067-3071 (2000)

MANNIX D., COAD S., LANDER G.H., REBIZANT J., BROWN P.J., PAIXAO J.A., LANGRIDGE S., KAWAMATA S., YAMAGUCHI Y. Neutron and synchrotron diffraction study of UPtGe.
Physical Review B **62**, 3801-3810 (2000)

MANUEL P., HILLIER A.D., KILCOYNE S.H. Observation of the flux line lattice in an amorphous superconductor.
Physica B **276-278**, 818-819 (2000)

MARGADONNA S., PRASSIDES K., BROWN C.M., SHIMODA H., IWASA Y., CASALTA H. Rotational tunneling of ammonia in $(NH_3)K_3C_{60}$.
Journal of Chemical Physics **111**, 10969-10973 (1999)

MARMEGGI J.C., CURRAT R., BOUVET A., LANDER G.H. Incommensurate phase associated with the 43 K soft phonon-mode displacive transition in α-U.
Physica B **276-278**, 272-273 (2000)

MARTUCCI A., CRUCIANI G., ALBERTI A., RITTER C., CIAMBELLI P., RAPACCIUOLO M.T. Location of Brønsted sites in D-mordenites by neutron powder diffraction.
Microporous and Mesoporous Materials **35-36**, 405-412 (2000)

MENEGHINELLO E., ALBERTI A., CRUCIANI G., SACERDOTI M., MCINTYRE G.J., CIAMBELLI P., RAPACCIUOLO M.T. Single crystal neutron diffraction study of the natural zeolite barrerite in its $ND_4^+$-exchange form.
European Journal of Mineralogy **12**, 1123-1129 (2000)

MESHCHEROV B.R., GELTENBORT P. Neutron transport in ultradisperse copper layers under strong scattering conditions.
Physics of the Solid State **42**, 1908-1910 (2000)

MESOT J., METOKI N., BÖHM M., HIESS A., KADOWAKI K. The magnetic resonance in underdoped Bi2212 and its relation to the electronic spectra: An inelastic neutron scattering study.
Physica C **341-348**, 2105-2106 (2000)

MEZEI F., EHLERS G., PAPPAS C., RUSSINA M., HICKS T.J., LING M.F. What neutrons do tell us about the nature of (spin) glasses?
Physica B **276-278**, 543-546 (2000)

MIDDENDORF H.D., TRAORE A., FOUCAT L., RENOU J.P., FERRAND M. Dynamics of collagen hydration by quasielastic neutron scattering.
Physica B **276-278**, 518-519 (2000)

MIKULA P., KULDA J., LUKAS P., ONO M., SAROUN J., VRANA M., WAGNER V. Bragg diffraction optics in neutron diffractometry.
Physica B **283**, 289-294 (2000)

MIKULA P., KULDA J., LUKAS P., ONO M., VRANA M., WAGNER V. Instrumentation components of focusing diffraction used in NPI, ILL, KURRI and PTB.
Physica B **276-278**, 174-176 (2000)

MILLANGE F., BRION S. DE, CHOUTEAU G. Charge, orbital, and magnetic order in $Nd_{0.5}Ca_{0.5}MnO_3$.
Physical Review B **62**, 5619-5626 (2000)

MILLOT B., METHIVIER A., JOBIC H., MOUEDDEB H., BEE M. Diffusion of isobutane in ZSM-5 zeolite: A comparison of quasi-elastic neutron scattering and supported membrane results.
Journal of Physical Chemistry B **103**, 1096-1101 (1999)

MONDELLI C., MUTKA H., PAYEN C., FRICK B., ANDERSEN K.H. Temperature dependence of the spin dynamics in the strongly frustrated antiferromagnet $SrCr_{8p}Ga_{12-8p}O_{19}$ (SCGO).
Physica B **284-288**, 1371-1372 (2000)

MONDELLI C., TAGLIERI G., OULADDIAF B., MUTKA H., PAYEN C. Neutron and X-ray diffraction study of the $SrCr_8Ga_4O_{19}$ kagomé compound synthesized by citrate route.
Materials Science Forum **321-324**, 828-833 (2000)

MORELON N.D., BEE M., COMBET J. Molecular dynamics simulation of a channel type inclusion compound: Comparison with neutron scattering experiments.
Chemical Physics **261**, 75-88 (2000)

MORENO A.J., ALEGRIA A., COLMENERO J., FRICK B. Methyl group rotational tunnelling in glasses: A direct comparison with the crystal.
Physica B **276-278**, 361-362 (2000)

MULLER F., DELSANTI M., AUVRAY L., YANG J., CHEN Y.J., MAYS J.W., DEME B., TIRRELL M., GUENOUN P. Ordering of urchin-like charged copolymer micelles: Electrostatic, packing and polyelectrolyte correlations.
European Physical Journal E **3**, 45-53 (2000)

MÜLLER M., CZIHAK C., BURGHAMMER M., RIEKEL C. Combined X-ray microbeam small-angle scattering and fibre diffraction experiments on single native cellulose fibres.
Journal of Applied Crystallography **33**, 817-819 (2000)

MÜLLER M., CZIHAK C., SCHOBER H., NISHIYAMA Y., VOGL G. All disordered regions of native cellulose show common low-frequency dynamics.
Macromolecules **33**, 1834-1840 (2000)

MÜLLER T.M., DUBBERS D., HAUTLE P., BUNYATOVA E.I., KOROBKINA E.I., ZIMMER O. Measurement of the γ–anisotropy in $\vec{n}+\vec{p}\rightarrow d+\gamma$.
Nuclear Instruments and Methods in Physics Research A **440**, 736-743 (2000)

MÜLLER-BUSCHBAUM P., GUTMANN J.S., CUBITT R., STAMM M. Probing the in-plane composition of thin polymer films with grazing-incidence small-angle neutron scattering and atomic force microscopy.
Colloid and Polymer Science **277**, 1193-1199 (1999)

MÜLLER-BUSCHBAUM P., GUTMANN J.S., STAMM M. Dewetting of confined polymer films: An X-ray and neutron scattering study.
Physical Chemistry - Chemical Physics **1**, 3857-3863 (1999)

MÜLLER-BUSCHBAUM P., GUTMANN J.S., STAMM M., CUBITT R., CUNIS S., VON KROSIGK G., GEHRKE R., PETRY W. Dewetting of thin polymer-blend films examined with GISAS.
Physica B **283**, 53-59 (2000)

MUNOZ A., ALONSO J.A., MARTINEZ-LOPE M.J., CASAIS M.T., MARTINEZ J.L., FERNANDEZ-DIAZ M.T. Magnetic structure of hexagonal $RMnO_3$ ($R$ = Y, Sc): Thermal evolution from neutron powder diffraction data.
Physical Review B **62**, 9498-9510 (2000)

MUNOZ A., ALONSO J.A., MARTINEZ-LOPE M.J., FERNANDEZ-DIAZ M.T. Magnetic structure evolution of $Pr_{1-x}MnO_3$ perovskite from neutron powder

diffraction data.
Solid State Communications **113**, 227-231 (2000)

MUNOZ A., ALONSO J.A., MARTINEZ-LOPE M.J., GARCIA-MUNOZ J.L., FERNANDEZ-DIAZ M.T. Magnetic structure evolution of $NdMnO_3$ derived from neutron diffraction data.
Journal of Physics Condensed Matter **12**, 1361-1376 (2000)

MURANI A.P. Comment on "Dramatic change of the magnetic response in $LiV_2O_4$: Possible heavy fermion to itinerant *d*-metal transition".
Physical Review Letters **85**, 3981 (2000)

NESVIZHEVSKY V.V., BÖRNER H., GAGARSKI A.M., PETROV G.A., PETUKHOV A.K., ABELE H., BÄßLER S., STÖFERLE T., SOLOVIEV S.M. Search for quantum states of the neutron in a gravitational field: Gravitational levels.
Nuclear Instruments and Methods in Physics Research A **440**, 754-759 (2000)

NESVIZHEVSKY V.V., LYCHAGIN E.V., MUZYCHKA A.Y., NEKHAEV G.V., STRELKOV A.V. About interpretation of experiments on small increase in energy of UCN in traps.
Physics Letters B **479**, 353-357 (2000)

NEUEFEIND J., FISCHER H.E., SCHRÖER W. EPMC versus RMC modelling: The structure of supercritical $HCF_3$.
Physica B **276-278**, 481-482 (2000)

NEUEFEIND J., FISCHER H.E., SCHRÖER W. The structure of fluid trifluoromethane and methylfluoride.
Journal of Physics Condensed Matter **12**, 8765-8776 (2000)

NÖLDEKE C., ASMUSSEN B., PRESS W., BÜTTNER H.G., KEARLEY G., LECHNER R.E., RUFFLE B. Hydrogen dynamics in $[Me(H_2O)_6](ClO_4)_2$ with Me=Mg, Mn, Fe, Ni and Zn investigated with quasielastic neutron scattering.
Journal of Chemical Physics **113**, 3219-3225 (2000)

ODA R., WEBER V., LINDNER P., PINE D.J., MENDES E., SCHOSSELER F. Time-resolved small-angle neutron scattering study of shear-thickening surfactant solutions after the cessation of flow.
Langmuir **16**, 4859-4863 (2000)

OGRIN F.Y., LEE S.L., AGER C., AEGERTER C.M., FORGAN E.M., LLOYD S.H., KEALEY P.G., RISEMAN T.M., CUBITT R., WIRTH G. Vortex studies in heavy-ion irradiated $Bi_{2.15}Sr_{1.85}CaCu_2O_{8+\delta}$ probed by μSR and small-angle neutron scattering.
Physica B **289-290**, 355-359 (2000)

OLEINEK P., ISNARD O., CONVERT P., MÜLLER K.H., LOEWENHAUPT M., SCHULTZ L. In situ neutron diffraction study of the reaction of the compounds $NdFe_{10.75}V_{1.25}$ and $NdFe_{11}Ti$ with nitrogen.
Journal of Alloys and Compounds **298**, 220-225 (2000)

OSBORN R., GOREMYCHKIN E.A., RAINFORD B.D., SASHIN I.L., MURANI A.P. Anomalous magnetic response of $Ce_{1-x}La_xAl_2$.
Journal of Applied Physics **87**, 5131-5133 (2000)

OULADDIAF B., RITTER C., BALLOU R., DEPORTES J. Magnetic ordering of $GdMn_2$.
Physica B **276-278**, 670-671 (2000)

PAGNIER T., CHARRIER-COUGOULIC I., RITTER C., LUCAZEAU G. A neutron diffraction study of $BaCe_xZr_{1-x}O_3$.
European Physical Journal Applied Physics **9**, 1-9 (2000)

PAIXAO J.A., RAMOS SILVA M., SØRENSEN S.A., LEBECH B., LANDER G.H., BROWN P.J., LANGRIDGE S., TALIK E., GONCALVES A.P. Neutron-scattering study of the magnetic structure of $DyFe_4Al_8$ and $HoFe_4Al_8$.
Physical Review B **61**, 6176-6188 (2000)

PAOLASINI L., LANDER G.H. Iron magnetism in cubic Laves phase itinerant ferromagnets.
Journal of Alloys and Compounds 303-304, 232-238 (2000)

PAUL-BONCOUR V., LATROCHE M., PERCHERON-GUEGAN A., ISNARD O. Study of phase transformations in $YFe_2D_{3.75}$ deuterides by in situ neutron diffraction.
Physica B **276-278**, 278-279 (2000)

PAVESE A., FERRARIS G., PISCHEDDA V., RADAELLI P. Further study of the cation ordering in phengite 3*T* by neutron powder diffraction.
Mineralogical Magazine **64**, 11-18 (2000)

PEPIN DONAT B., LAIREZ D., GEYER A. DE, VIALLAT A. Light and small angle neutron scattering studies of well-defined conducting gels.
Synthetic Metals **101**, 471-472 (1999)

PERINO-GALLICE L., BELLET-AMALRIC E., BRASLAU A., CHARITAT T., DAILLANT J., FRAGNETO G., GRANER F. Adsorbed and free lipid bilayers at the solid-liquid interface viewed by specular and off-specular reflectivity.
Progress in Colloid and Polymer Science **115**, 171-173 (2000)

PETRI I., SALMON P.S., FISCHER H.E. Defects in a disordered world: The structure of glassy $GeSe_2$.
Physical Review Letters **84**, 2413-2416 (2000)

PETRI I., SALMON P.S., FISCHER H.E. Structure of molten GeSe by neutron diffraction: The Ge coordination environment.
Journal of Non-Crystalline Solids **250-252**, 405-409 (1999)

PETRILLO C., SACCHETTI F., DORNER B., SUCK J.B. High-resolution neutron scattering measurement of the dynamic structure factor of heavy water.
Physical Review E **62**, 3611-3618 (2000)

PFLEIDERER T., WALDNER I., BERTAGNOLLI H., TÖDHEIDE K., FISCHER H.E. The structure of liquid and supercritical deuterium fluoride from neutron scattering using high-pressure techniques.
Journal of Chemical Physics **113**, 3690-3696 (2000)

PICHLMAIER A., BUTTERWORTH J., GELTENBORT P., NAGEL H., NESVIZHEVSKY V.V., NEUMAIER S., SCHRECKENBACH K., STEICHELE E., VARLAMOV V. MAMBO II: Neutron lifetime measurement with storage of ultra-cold neutrons.
Nuclear Instruments and Methods in Physics Research A **440**, 517-521 (2000)

PIGNOL D., AYVAZIAN L., KERFELEC B., TIMMINS P.A., CRENON I., HERMOSO J., FONTECILLA-CAMPS J.C., CHAPUS C. Critical role of micelles in pancreatic lipase activation revealed by small angle neutron scattering.
Journal of Biological Chemistry **275**, 4220-4224 (2000)

PINSTON J.A., FOIN C., GENEVEY J., BERAUD R., CHABANAT E., FAUST H., OBERSTEDT S., WEISS B. Microsecond isomers in $^{125,127,129}$Sn.
Physical Review C **61**, 024312-1-024312-6 (2000)

PIQUER C., PALACIOS E., ARTIGAS M., BARTOLOME J., RUBIN J., CAMPO J., HOFMANN M. Neutron powder diffraction study of the $RFe_{11.5}Ta_{0.5}$ (R ≡Lu, Er, Ho, Dy, and Tb) compounds.
Journal of Physics Condensed Matter **12**, 2265-2278 (2000)

PISTOLESI F., MANINI N. Geometric phases and multiple degeneracies in harmonic resonators.
Physical Review Letters **85**, 1585-1589 (2000)

PLAKHTY V.P., KULDA J., VISSER D., MOSKVIN E., WOSNITZA J. Chiral critical exponents in the triangular-lattice antiferromagnet $CsMnBr_3$ as determined by polarized neutron scattering.
Physical Review Letters **85**, 3942-3945 (2000)

PLAKHTY V.P., MALEYEV S.V., KULDA J., WOSNITZA J., VISSER D., MOSKVIN E. Inelastic polarised neutron scattering in the triangular-lattice antiferromagnet $CsMnBr_3$: An experimental proof of the chiral universality.
Europhysics Letters **48**, 215-220 (1999)

PLAZANET M., JOHNSON M.R., GALE J.D., YILDIRIM T., KEARLEY G.J., FERNANDEZ-DIAZ M.T., SANCHEZ-PORTAL D., ARTACHO E., SOLER J.M., ORDEJON P., GARCIA A., TROMMSDORFF H.P. The structure and dynamics of crystalline durene by neutron scattering and numerical modelling using density functional methods.
Chemical Physics **261**, 189-203 (2000)

PLAZANET M., JOHNSON M.R., KEARLEY G.J. Single-molecule dynamics in a molecular cluster - A semi-emprical approach.
Physica B **276-278**, 228-229 (2000)

PLAZANET M., NEUMANN M.A., TROMMSDORFF H.P. Methyl group rotational tunneling in vibrational spectra of crystals at low temperatures.
Chemical Physics Letters **320**, 651-657 (2000)

PONTILLON Y., AKITA T., GRAND A., KOBAYASHI K., LELIEVRE-BERNA E., PECAUT J., RESSOUCHE E., SCHWEIZER J. Experimental and theoretical spin density in a ferromagnetic molecular complex.
Molecular Crystals and Liquid Crystals **334**, 211-220 (1999)

PONTILLON Y., BENCINI A., CANESCHI A., DEI A., GATTESCHI D., GILLON B., SANGREGORIO C., STRIDE J., TOTTI F. Spin-density map of the triplet ground state of a titanium(IV) complex with schiff-base diquinone radical ligands: An investigation using polarized-neutron diffraction and denstity-functional theory.
Angewandte Chemie International Edition English **39**, 1786-1788 (2000)

PONTILLON Y., GRAND A., ISHIDA T., LELIEVRE-BERNA E., NOGAMI T., RESSOUCHE E., SCHWEIZER J. Spin density of a ferromagnetic TEMPO derivative: Polarized neutron investigation and *ab initio* calculation.
Journal of Materials Chemistry **10**, 1539-1546 (2000)

PONTILLON Y., ISHIDA T., LELIEVRE-BERNA E., NOGAMI T., RESSOUCHE E., SCHWEIZER J. Spin density of a ferromagnetic tempo derivative.
Molecular Crystals and Liquid Crystals **334**, 359-367 (1999)

PÖTSCHKE D., BALLAUFF M., LINDNER P., FISCHER M., VÖGTLE F. Analysis of the structure of dendrimers in solution by small-angle neutron scattering using contrast variation.
Journal of Applied Crystallography **33**, 605-608 (2000)

POUGETS. La spectrométrie à écho de spins de neutrons.
Journal de Physique IV **10**, Pr1-45-Pr1-58 (2000)

PRASSIDES K., BROWN C.M., MARGADONNA S., KORDATOS K., TANIGAKI K., SUARD E., DIANOUX A.J., KNUDSEN K.D. Powder diffraction and inelastic neutron scattering studies of the $Na_2RbC_{60}$ fulleride.
Journal of Materials Chemistry **10**, 1443-1449 (2000)

PREM M., KREXNER G. Martensitic phase transitions *hcp-dhcp* and *dhcp-fcc* in Co 0.85 at% Fe.
Physica B **276-278**, 927-928 (2000)

PREM M., KREXNER G., BLASCHKO O. Investigation of the two martensitic phase transition hcp-dhcp and dhcp-fcc in Co-0.85 at% Fe by neutron scattering.
Materials Science and Engineering A **273-275**, 491-493 (1999)

PRIGENT G., BELLISSENT R., CEOLIN R., FISCHER H.E., GASPARD J.P. Local order and metal–non-metal transition in $Cd_xTe_{1-x}$ : a neutron diffraction study.
Journal of Non-Crystalline Solids **250-252**, 297-300 (1999)

PYKA N.M., D'ASTUTO M., METZA., IVANOV A.S., LOEWENHAUPT M., CASALTA H., PETITGRAND D., BOURGES P. High-resolution study of the supposed fourfold Nd spin-wave degeneracy of $Nd_2CuO_4$.
Physical Review B **61**, 14311-14314 (2000)

PYKA N.M., LOEWENHAUPT M., METZ A., SCHMIDT W. The momentum space distribution of the low-energy magnetic response in $Nd_{1.85}Ce_{0.15}CuO_4$ at $T_{0.1}$ K and up to 5.7 T.
Physica B **292**, 191-193 (2000)

RADLINSKI A.P., BOREHAM C.J., LINDNER P., RANDL O., WIGNALL G.D., HINDE A., HOPE J.M. Small angle neutron scattering signature of oil generation in artificially and naturally matured hydrocarbon source rocks.
Organic Geochemistry **31**, 1-14 (2000)

RADLINSKI A.P., RADLINSKA E.Z., AGAMALIAN M., WIGNALL G.D., LINDNER P., RANDL O.G. The fractal microstructure of ancient sedimentary rocks.
Journal of Applied Crystallography **33**, 860-862 (2000)

RAT E., HEHLEN B., KULDA J., YONENAGA I., CASALTA H., COURTENS E., FORET M., VACHER R. Disorder broadening of the acoustic branches in $Si_xGe_{1-x}$ mixed crystals.
Physica B **276-278**, 429-430 (2000)

RAYMOND S., HAEN P., CALEMCZUK R., KAMBE S., FÅK B., LEJAY P., FUKUHARA T., FLOUQUET J. From heavy fermion antiferromagnetism to localized ferromagnetism: Competition of two ground states in $CeRu_2Ge_2$ on cooling.
Journal of Physics Condensed Matter **11**, 5547-5560 (1999)

REAT V., DUNN R., FERRAND M., FINNEY J.L., DANIEL R.M., SMITH J.C. Solvent dependence of dynamic transitions in protein solutions.
Proceedings of the National Academy of Sciences of the USA **97**, 9961-9966 (2000)

REGNAULT L.P., LORENZO J.E., BOUCHER J.P., GRENIER B., HIESS A., CHATTERJI T., JEGOUDEZ J., REVCOLEVSCHI A. Charge ordering and spin dynamics in $NaV_2O_5$.
Physica B **276-278**, 626-627 (2000)

REGNAULT L.P., TASSET F., LORENZO J.E., ROBERTS T., DHALENNE G., REVCOLEVSCHI A. Nature of magnetic excitations in $CuGeO_3$.
Physica B **276-278**, 708-709 (2000)

REICH J., ABELE H., ASTRUC HOFFMANN M., BÄßLER S., BÜLOW P.V., DUBBERS D., NESVIZHEVSKY V.V., PESCHKE U., ZIMMER O. A measurement of the beta asymmetry in neutron decay with PERKEO II.
Nuclear Instruments and Methods in Physics Research A **440**, 535-538 (2000)

RENKER B., SCHOBER H., FERNANDEZ-DIAZ M.T., HEID R. Structure and dynamics of $C_{60}$ intercalation compounds: $N_2C_{60}$ and $O_2C_{60}$.
Physical Review B **61**, 13960-13968 (2000)

REQUARDT H., NAD F.Y., MONCEAU P., CURRAT R., LORENZO J.E., RIDEAU D., SMILGIES D., GRÜBEL G. Space- and time-resolved X-ray diffraction from pinned and sliding charge-density-waves in $NbSe_3$.
Journal de Physique IV **9**, Pr10-133-Pr10-137 (1999)

RESPAUD M., BROTO J.M., RAKOTO H., GOIRAN M., LLOBET A., FRONTERA C., GARCIA-MUNOZ J.L., VANACKEN J. Stability of charge-ordering and *H-T* diagrams of $Ln_{1-x}Ca_xMnO_3$ manganites in pulsed magnetic field up to 50T.
Journal of Magnetism and Magnetic Materials **211**, 128-132 (2000)

RESPAUD M., LLOBET A., FRONTERA C., RITTER C., BROTO J.M., RAKOTO H., GOIRAN M., GARCIA-MUNOZ J.L. High magnetic field study of lattice and magnetic effects on the charge-melting transition in $La_{1/2}Ca_{1/2}MnO_3$ perovskites.
Physical Review B **61**, 9014-9018 (2000)

RIDEAU D., MONCEAU P., REQUARDT H., CURRAT R., NAD F., LORENZO J.E., BRAZOVSKII S., KIROVA N., SMILGIES D., GRÜBEL G. Phase slippage at the interface: Normal metal/sliding charge-density wave.
Physica B **280**, 317-322 (2000)

RIGHI L., AMBOAGE M., GUTIERREZ J., BARANDIARAN J.M., FERNANDEZ BARQUIN L., FERNANDEZ-DIAZ M.T. Magnetic and nuclear structure of the perovskite-like oxides $(LaBi)_{0.7}Ca_{0.3}MnO_3$.
Physica B **276-278**, 718-719 (2000)

RINALDI R., ARTIOLI G., WILSON C.C., MCINTYRE G.J. Octahedral cation ordering in olivine at high temperature. I: In situ neutron single-crystal diffraction studies on natural mantle olivines (Fa12 and Fa10).
Physics and Chemistry of Minerals **27**, 623-629 (2000)

RITTER C., IBARRA M.R., MORELLON L., BLASCO J., GARCIA J., DE TERESA J.M. Structural and magnetic properties of double perovskites $AA'FeMoO_6$ (AA' = $Ba_2$, BaSr, $Sr_2$ and $Ca_2$).
Journal of Physics Condensed Matter **12**, 8295-8308 (2000)

RITTER C., MAHENDIRAN R., IBARRA M.R., MORELLON L., MAIGNAN A., RAVEAU B., RAO C.N.R. Direct evidence of phase segregation and magnetic-field-induced structural transition in $Nd_{0.7}Sr_{0.3}MnO_3$ by neutron diffraction (Rapid communications).
Physical Review B **61**, R9229-R9232 (2000)

ROBINSON R.A., BROWN P.J., ARGYRIOU D.N., HENDRICKSON D.N., AUBIN S.M.J. Internal magnetic structure of $Mn_{12}$ acetate by polarized neutron diffraction.
Journal of Physics Condensed Matter **12**, 2805-2810 (2000)

ROLS S., ANGLARET E., SAUVAJOL J.L., CODDENS G., SCHOBER H., DIANOUX A.J. Structure and dynamics of single-wall-carbon nanotubes probed by neutron scattering.
Physica B **276-278**, 276-277 (2000)

ROLS S., BENES Z., ANGLARET E., SAUVAJOL J.L., PAPANEK P., FISCHER J.E., CODDENS G., SCHOBER H., DIANOUX A.J. Phonon density of states of single-wall carbon nanotubes.
Physical Review Letters **85**, 5222-5225 (2000)

ROMERO DE PAZ J., HERNANDEZ VELASCO J., FERNANDEZ-DIAZ M.T., PORCHER P., MARTINEZ J.L., SAEZ PUCHE R. Structural and magnetic characterization of $NdCaCrO_4$ oxide.
Journal of Solid State Chemistry **148**, 361-369 (1999)

RÖßLE M., MANAKOVA E., HOLZINGER J., VANATALU K., MAY R.P., HEUMANN H. Time-resolved small-angle neutron scattering of proteins in solution.
Physica B **276-278**, 532-533 (2000)

RÖßLE M., MANAKOVA E., LAUER L., NAWROTH T., HOLZINGER J., NARAYANAN T., BERNSTORFF S., AMENTSCH H., HEUMANN H. Time-resolved small angle scattering: Kinetic and structural data from proteins in solution.
Journal of Applied Crystallography **33**, 548-551 (2000)

ROTTER M., LINDBAUM A., GRATZ E., HILSCHER G., SASSIK H., FISCHER H.E., FERNANDEZ-DIAZ M.T., ARONS R., SEIDL E. The magnetic structure of $GdCu_2$.
Journal of Magnetism and Magnetic Materials **214**, 281-290 (2000)

ROTTER M., LOEWENHAUPT M., KRAMP S., REIF F., PYKA N.M., SCHMIDT W., VAN DE KAMP R. Anisotropic magnetic exchange in orthorhombic $RCu_2$ compounds (R = rare earth).
European Physical Journal B **14**, 29-42 (2000)

ROTTER M., SCHNEIDEWIND A., LOEWENHAUPT M., DOERR M., STUNAULT A., HIESS A., LINDBAUM A., GRATZ E., HILSCHER G., SASSIK H. Magnetic scattering on $GdCu_2$.
Physica B **284-288**, 1329-1330 (2000)

RUBIO D., MESOT J., CONDER K., JANSSEN S., MUTKA H., FURRER A. Doping and isotope dependence of the pseudogap in high-$T_c$ cuprates observed by neutron crystal-field spectroscopy: A fast local probe.
Journal of Superconductivity **13**, 727-730 (2000)

RUBIO TEMPRANO D., FURRER A., CONDER K., MUTKA H. A neutron crystal-field study of the pseudogap in the underdoped high-$T_c$ superconductor $HoBa_2CuO_{6.6}$.
Physica B **276-278**, 762-763 (2000)

RUBIO TEMPRANO D., MESOT J., JANSSEN S., CONDER K., FURRER A., MUTKA H., MÜLLER K.A. Large isotope effect on the pseudogap in the high-temperature superconductor $HoBa_2Cu_3O_{6.6}$.
Physical Review Letters **84**, 1990-1993 (2000)

RUBIO TEMPRANO D., MESOT J., JANSSEN S., FURRER A., CONDER K., MUTKA H., MÜLLER K.A. Pseudogap in the underdoped high-temperature superconductor $HoBa_2Cu_3O_{6.6}$: A neutron crystal-field study of the oxygen isotope effect.
Physica C **341-348**, 905-906 (2000)

SANTINI P., AMORETTI G., CACIUFFO R., BOURDAROT F., FÅK B. Field-dependent energy scales in $URu_2Si_2$.
Physical Review Letters **85**, 654-657 (2000)

SANTISTEBAN J.R., CUELLO G.J., DAWIDOWSKI J., FAINSTEIN A., PERETTI H.A., IVANOV A.S., BERMEJO F.J. Vibrational spectrum of magnesium hydride.
Physical Review B **62**, 37-40 (2000)

SAROUN J., KULDA J., WILDES A., HIESS A. Monte Carlo simulation of neutron fluxes on an absolute scale - Comparison to experiments.
Physica B **276-278**, 148-149 (2000)

SATO T.J., TAKAKURA H., TSAI A.P., SHIBATA K., OHOYAMA K., ANDERSEN K.H. Antiferromagnetic spin correlations in the Zn-Mg-Ho icosahedral quasicrystal.
Physical Review B **61**, 476-486 (2000)

SAVIOT L., DUVAL E., DIANOUX A.J., JAL J.F. Fast relaxational motions in polycarbonate glass.
Physica B **276-278**, 435-436 (2000)

SAVIOT L., DUVAL E., JAL J.F., DIANOUX A.J. Very fast relaxation in polycarbonate glass.
European Physical Journal B **17**, 661-666 (2000)

SCHEFER J., BÖHM M., KELLER L., MEDARDE M., HORISBERGER M., FISCHER P., POMJAKUSHIN V., DÖNNI A. Application of composite germanium neutron monochromators at SINQ: Neutron powder diffraction (HRPT) and single crystal diffraction (TriCS).
Physica B **283**, 302-304 (2000)

SCHICK E., LEWITZKI E., MAY R.P., KRIECHBAUM M., LAGGNER P., GRELL E. Micellar Na,K-ATPase: Mechanism of formation, functional properties and structural studies employing small-angle neutron and X-ray scattering.
In: 'Na/K-ATPase and Related ATPases', TANIGUCHI K., KAYA S. (Eds.) (2000) pp. 445-448

SCHIEBEL P., BURGER K., BÜTTNER H.G., KEARLEY G.J., LEHMANN M.S., PRANDL W. $ND_3$-density distribution in orientationally disordered $Ni(ND_3)_6Cl_2$ observed by means of neutron Laue diffraction.
Journal of Physics Condensed Matter **12**, 8567-8576 (2000)

SCHMIDT U., ABELE H., BOUCHER A., KLEIN M., STELLMACH C., GELTENBORT P. Neutron polarization induced by radio frequency radiation.
Physical Review Letters **84**, 3270-3273 (2000)

SCHNEIDER J.J., HAGEN J., CZAP N., KRÜGER C., MASON S.A., BAU R., ENSLING J., GÜTLICH P., WRACKMEYER B. Hydrido hydrido complexes of iron and cobalt (Sn–Fe–Sn, Sn–Co–Sn): Probing agostic Sn–H–M interactions in solution and in the solid state.
Chemistry - A European Journal **6**, 625-635 (2000)

SCHNEIDER J.M., SCHÖNFELD B., DEME B., KOSTORZ G. Shape of precipitates in Ni-Al-Mo single crystals.
Journal of Applied Crystallography **33**, 465-468 (2000)

SCHNEIDER R., CHATTERJI T., HOFFMANN J.U., HOHLWEIN D. Paramagnetic short-range order in holmium.
Physica B **276-278**, 610-611 (2000)

SCHOBER H., DIANOUX A.J., COOK J.C., MEZEI F. Upgrade of the IN5 cold neutron time-of-flight spectrometer.
Physica B **276-278**, 164-165 (2000)

SCHOBER H., KOZA M.M., TÖLLE A., MASCIOVECCHIO C., SETTE F., FUJARA F. Crystal-like high frequency phonons in the amorphous phases of solid water.
Physical Review Letters **85**, 4100-4103 (2000)

SCHOBER H., LOSERT C., MEZEI F., COOK J.C. Chopper cascades: An analytic treatment of the contamination problem.
Journal of Neutron Research **8**, 175-185 (2000)

SCHOBINGER-PAPAMANTELLOS P., BUSCHOW K.H.J., DE GROOT C.H., DE BOER F.R., RITTER C. Magnetic ordering of the $R_2Fe_{17}Sn$ (R = Nd, Pr) compounds studied by neutron diffraction.
Journal of Magnetism and Magnetic Materials **218**, 31-41 (2000)

SELLMANN R., FRITZSCHE H., MALETTA H., LEINER V., SIEBRECHT R. Thickness- and temperature-driven spin-reorientation-transition in ultrathin epitaxial Co-films.
Physica B **276-278**, 578-579 (2000)

SEMADENI F., ROESSLI B., BÖNI P., VORDERWISCH P., CHATTERJI T. Critical fluctuations in the weak itinerant ferromagnet $Ni_2Al$: A comparison between self-consistent renormalization and mode-mode coupling theory.
Physical Review B **62**, 1083-1088 (2000)

SERDYUK I., ULITIN A., KOLESNIKOV I., VASILIEV V., AKSENOV V., ZACCAI G., SVERGUN D., KOZIN M., WILLUMEIT R. Structure of a beheaded 30 S ribosomal subunit from *Thermus thermophilus*.
Journal of Molecular Biology **292**, 633-639 (1999)

SEREBROV A., MITYUKHLYAEV V., ZAKHAROV A., KHARITONOV A., SHUSTOV V., KUZMINOV V., LASAKOV M., TALDAEV R., ALDUSHCHENKOV A., VARLAMOV V., VASILEV A., SAZHIN M., GREENE G., BOWLES T., HILL R., SEESTROM S., GELTENBORT P. Studies of a solid-deuterium source for ultra-cold neutrons.
Nuclear Instruments and Methods in Physics Research A **440**, 658-665 (2000)

SEREBROV A., VASILIEV A., LASAKOV M., RUDNEV Y., KRASNOSHEKOVA I., GELTENBORT P., BUTTERWORTH J., BOWLES T., MORRIS C., SEESTROM S., SMITH D., YOUNG A.R. Depolarization of UCN stored in material traps.
Nuclear Instruments and Methods in Physics Research A **440**, 717-721 (2000)

SERERO Y., JACOBSEN V., BERRET J.F., MAY R.P. Evidence of nonlinear chain stretching in the rheology of transient networks.
Macromolecules **33**, 1841-1847 (2000)

SKRIPOV A.V., COMBET J., GRIMM H., HEMPELMANN R., KOZHANOV V.N. Quasielastic neutron scattering study of H motion in the hydrogen-stabilized C15-type phases $HfTi_2H_x$ and $ZrTi_2H_x$.
Journal of Physics Condensed Matter **12**, 3313-3324 (2000)

SOLDNER T., BECK L., SCHRECKENBACH K., BUSSIERE A., KOSSAKOWSKI R., LIAUD P., ZIMMER O. Test of time reversal invariance with TRINE.
Nuclear Instruments and Methods in Physics Research A **440**, 643-647 (2000)

SONDERGELD P., FUESS H., MASON S.A., ISHIHARA H., SCHMAHL W.W. Pseudo-symmetries of the phases of $(Et_4N)_2ZnBr_4$.
Zeitschrift für Naturforschung A **55**, 801-809 (2000)

SONNEVILLE-AUBRUN O., BERGERON V., GULIKKRZYWICKI T., JÖNSSON B., WENNERSTRÖM H., LINDNER P., CABANE B. Surfactant films in biliquid foams.
Langmuir **16**, 1566-1579 (2000)

SOUBEYROUX J.L., FRUCHART D., BIRIS A.S. Structural studies of Laves phases $ZrCo(V_{1-x}Cr_x)$ with $0 \le x \le 1$ and their hydrides.
Journal of Alloys and Compounds **293-295**, 88-92 (1999)

STAUB U., SODERHOLM L., SKANTHAKUMAR S., OSBORN R., FAUTH F., RITTER C. The magnetic properties of Pr in the $Pb_2Sr_2PrCu_3O_{8+\delta}$ cuprate.
Physica C **333**, 13-22 (2000)

STEINER T., MASON S.A. Short $N^+$—H···Ph hydrogen bonds in ammonium tetraphenylborate characterized by neutron diffraction.
Acta Crystallographica B **56**, 254-260 (2000)

STEINER T., MASON S.A., WILSON C.C., MAJERZ I. Neutronendiffraktionsstudie von sehr kurzen O-H···N und N-H···O Brücken.
Zeitschrift für Kristallographie Supplement **17**, 68 (2000)

STELLBRINK J., ALLGAIER J., MONKENBUSCH M., RICHTER D., LANG A., LIKOS C.N., WATZLAWEK M., LÖWEN H., EHLERS G., SCHLEGER P. Neither Gaussian chains nor hard spheres — star polymers seen as ultrasoft colloids.
Progress in Colloid and Polymer Science **115**, 88-92 (2000)

STELLMACH C., ABELE H., BOUCHER A., DUBBERS D., SCHMIDT U., GELTENBORT P. On the Anderson-localization of ultra-cold neutrons.
Nuclear Instruments and Methods in Physics Research A **440**, 744-749 (2000)

STEWART J.R., ANDERSEN K.H., CYWINSKI R., MURANI A.P. Magnetic diffuse scattering in disordered systems studied by neutron polarization analysis (Invited).
Journal of Applied Physics **87**, 5425-5430 (2000)

STIEWE A., SONNTAG R., TROYANOV S.I., HANSEN T., KEMNITZ E. Synthesis and structure determination of $Rb_2(HSO_4)(H_2PO_4)$ and $Rb_3(HSO_4)_2(H_2PO_4)$ by X-ray single crystal and neutron powder diffraction.
Journal of Solid State Chemistry **149**, 9-15 (2000)

STRELKOV A.V., NESVIZHEVSKY V.V., GELTENBORT P., KARTASHOV D.G., KHARITONOV A.G., LYCHAGIN E.V., MUZYCHKA A.Y., PENDLEBURY J.M., SCHRECKENBACH K., SHVETSOV V.N., SEREBROV A.P., TALDAEV R.R., YAIDJIEV P. Identification of a new escape channel for UCN from traps.
Nuclear Instruments and Methods in Physics Research A **440**, 695-703 (2000)

STRIDE J.A., JAYASOORIYA U.A., NJAGI MBOGO, WHITE R.P., KEARLEY G.J., LONGEVILLE S. Restricted proton mobility in the self-organising system 3,5-dimethylpyrazole.
Physica B **276-278**, 308-309 (2000)

STRIFFLER T., STUHR U., WIPF H., HAHN H., EGELHAAF S. The microstructure of hydrogen- and deuterium-doped nanocrystalline palladium studied by small-angle neutron scattering.
European Physical Journal B **17**, 245-251 (2000)

STRITT N., JOLIE J., JENTSCHEL M., BÖRNER H.G., DOLL C. Study of interatomic potentials using the crystal-GRID method on oriented single crystals of Ni, Fe, and Cr.
Journal of Research of the National Institute of Standards and Technology **105**, 71-80 (2000)

STUHR U., CORNELL K., WIPF H. Coherency stresses and deuterium diffusion in $NbD_{0.37}$.
Journal of Alloys and Compounds **293-295**, 289-291 (1999)

STUHR U., WIPF H., ANDERSEN K.H., HAHN H. Neutron scattering study of the vibrational behaviour of H-doped nanocrystalline Pd.
Physica B **276-278**, 882-883 (2000)

SUARD E., FAUTH F., CAIGNAERT V. Rhombohedral distortion in the new disordered $LaBaCo_2O_6$ perovskite.
Physica B **276-278**, 254-255 (2000)

SUARD E., FAUTH F., CAIGNAERT V., MIREBEAU I., BALDINOZZI G. Charge ordering in the layered Co-based perovskite $HoBaCo_2O_5$ (Rapid communications).
Physical Review B **61**, R11871-R11874 (2000)

SULLIVAN D.M., NEILSON G.W., FISCHER H.E., RENNIE A.R. Small angle neutron scattering from $D_2O$ in the critical region.
Journal of Physics Condensed Matter **12**, 3531-3542 (2000)

SUNDARESAN A., THOLENCE J.L., MAIGNAN A., MARTIN C., HERVIEU M., RAVEAU B., SUARD E. Jahn-Teller distortion and magnetoresistance in electron doped $Sr_{1-x}Ce_xMnO_3$ ($x = 0.1, 0.2, 0.3$ and $0.4$).
European Physical Journal B **14**, 431-438 (2000)

SURYANARAYANAN R., DHALENNE G., REVCOLEVSCHI A., PRELLIER W., RENARD J.P., DUPAS C., CALIEBE W., CHATTERJI T. Colossal magnetoresistance and re-entrant charge ordering in single crystalline two layer Mn perovskite $LaSr_2Mn_2O_7$.
Solid State Communications **113**, 267-271 (2000)

SWALLOWE G.M., WIMPORY R.C. Neutron diffraction studies for the measurement of strains and stresses.
In: 'International Conference on Nuclear Energy in Central Europe. Proceedings Volume 2 Embedded Meeting Neutron Imaging Methods to Detect Defects in Materials' (Nuclear Society of Slovenia, 1999) pp. 695-702

SYROMYATNIKOV V.G., TOPERVERG B.P., SIEBRECHT R., MENELLE A., PLESHANOV N.K., PUSENKOV V.M., SCHEBETOV A.F., SOROKO Z.N., ULYANOV V.A. Observation of peculiarities in magnetic off-specular polarized neutron scattering from rough interfaces in Co/Ti periodic multilayer.
Physica B **276-278**, 700-701 (2000)

TELLING M.T.F., RITTER C., CYWINSKI R. Evolution of magnetic order in $(Tb_{1-x}Ho_x)Mn_2$ and $(Tb_{1-x}Dy_x)Mn_2$.
Physica B **276-278**, 740-741 (2000)

TOLLA B., DEMOURGUES A., ISNARD O., MENETRIER M., POUCHARD M., RABARDEL L., SEGUELONG T. Structural investigation of oxygen insertion within the $Ce_2Sn_2O_7$—$Ce_2Sn_2O_8$ pyrochlore solid solution by means of *in situ* neutron diffraction experiments.
Journal of Materials Chemistry **9**, 3131-3136 (1999)

TÖLLE A., ZIMMERMANN H., FUJARA F., PETRY W., SCHMIDT W., SCHOBER H., WUTTKE J. Vibrational states of glassy and crystalline ortho-terphenyl.
European Physical Journal B **16**, 73-80 (2000)

TOMKA G.J., RITTER C., RIEDI P.C., ADROJA D.T., LORD J.S., KAPUSTA C., ZUKROWSKI J. Magnetic structure of $^{154}SmMn_2(Ge_{0.9}Si_{0.1})_2$ as a function of temperature and pressure.
Physica B **291**, 317-323 (2000)

TOPERVERG B., LAUTER-PASYUK V., LAUTER H.J., NIKONOV O., AUSSERRE D., GALLOT Y. Morphology of off-specular neutron scattering pattern from islands on a lamellar film.
Physica B **283**, 60-64 (2000)

TOPERVERG B., LAUTER-PASYUK V., LAUTER H.J., NIKONOV O., AUSSERRE D., GALLOT Y. Off-specular neutron scattering from islands on a lamellar film.
Physica B **276-278**, 355-356 (2000)

TOPERVERG B., VOROBYEV A., GORDEYEV G., NICKEL B., DONNER W., DOSCH H., REKVELDT T. Reflectivity and off-specular neutron scattering from ferrofluid.
Physica B **283**, 203-207 (2000)

TOPERVERG B.P., FELCHER G.P., METLUSHKO V.V., LEINER V., SIEBRECHT R., NIKONOV O. Grazing incidence neutron diffraction from large scale 2D structures.
Physica B **283**, 149-152 (2000)

TOPERVERG B.P., SCHÄRPF O., ANDERSON I.S. Optical theorem for neutron scattering from rough interfaces.
Physica B **276-278**, 954-955 (2000)

TRIOLO F., TRIOLO A., TRIOLO R., BETTS D.E., MCCLAIN J.B., DE SIMONE J.M., STEYTLER D.C., WIGNALL G.D., DEME B., HEENAN R.K. Critical micellisation density: A SAS structural study of the unimer-aggregate transition of block-copolymers in supercritical $CO_2$.
Journal of Applied Crystallography **33**, 641-644 (2000)

TUINIER R., HOLT C., TIMMINS P.A., DE KRUIF K. Small-angle neutron scattering of aggregated whey protein colloids with an exocellular polysaccharide.
Journal of Applied Crystallography **33**, 540-543 (2000)

VACHER R., COURTENS E., FORET M., HEHLEN B., RAT E., CASALTA H., DORNER B. Brillouin scattering of neutrons and X-rays from glasses.
Physica B **276-278**, 427-428 (2000)

VAN DER MAAREL J.R.C., GROENEWEGEN W., EGELHAAF S.U., LAPP A. Salt-induced contraction of polyelectrolyte diblock copolymer micelles.
Langmuir **19**, 7510-7519 (2000)

VAN DER ZOUW G., WEBER M., FELBER J., GÄHLER R., GELTENBORT P., ZEILINGER A. Aharonov-Bohm and gravity experiments with the very-cold-neutron interferometer.
Nuclear Instruments and Methods in Physics Research A **440**, 568-574 (2000)

VAN DIJK N.H., FÅK B., CHARVOLIN T., LEJAY P., MIGNOT J.M. Magnetic excitations in heavy-fermion $CePd_2Si_2$.
Physical Review B **61**, 8922-8931 (2000)

VAQUEIRO P., BOLD M., POWELL A.V., RITTER C. Structural, magnetic, and electronic properties of vanadium-substituted nickel chromium sulfide.
Chemistry of Materials **12**, 1034-1041 (2000)

VERT R., BOUOUDINA M., FRUCHART D., GIGNOUX D., GIRARD S., KALYCHAK Y., OULADDIAF B., SKOLOZDRA R.V. Study of exchange and anisotropy parameters versus insertion of H and C in the $RFe_{11.35}Nb_{0.65}$ compounds (R = Ho, Lu).
Journal of Alloys and Compounds **296**, 293-302 (2000)

VIALLON M., BERTHEZENE Y., CALLOT V., BOURGEOIS M., HUMBLOT H., BRIGUET A., CREMILLIEUX Y. Dynamic imaging of hyperpolarized $^3$He distribution in rat lungs using interleaved-spiral scans.
NMR in Biomedicine **13**, 207-213 (2000)

VIALLON M., BERTHEZENE Y., DECORPS M., WIART M., CALLOT V., BOURGEOIS M., HUMBLOT H., BRIGUET A., CREMILLIEUX Y. Laser-polarized $^3$He as a probe for dynamic regional measurements of lung perfusion and ventilation using magnetic resonance imaging.
Magnetic Resonance in Medicine **44**, 1-4 (2000)

VIVES F., HAMBSCH F.J., BAX H., OBERSTEDT S. Investigation of the fission fragment properties of the reaction $^{238}U(n,f)$ at incident neutron energies up to 5.8 MeV.
Nuclear Physics A **662**, 63-92 (2000)

WAGEMANS C., SEROT O., GELTENBORT P., ZIMMER O. Experimental determination of the $^{238}U(n_{th},f)$ cross section.
Nuclear Science and Engineering **136**, 415-418 (2000)

WAGEMANS J., WAGEMANS C., GOEMINNE G., GELTENBORT P. Experimental determination of the $^{14}N(n,p)^{14}C$ reaction cross section for thermal neutrons.
Physical Review C **61**, 064601-1-064601-5 (2000)

WANDERLINGH U.N., GIORDANO R., SCIORTINO M.T., DIANOUX A.J. Dynamics of proteins, IQENS study on $D_2O$ hydrate Crambin.
Physica B **276-278**, 522-523 (2000)

WANDERLINGH U.N., GIORDANO R., SCIORTINO M.T., DIANOUX A.J. Protein and solvent dynamics in hydrated Crambin.
Journal de Physique IV **10**, Pr7-325-Pr7-328 (2000)

WASSE J.C., HAYAMA S., SKIPPER N.T., FISCHER H.E. Structure of a metallic solution of lithium in ammonia.
Physical Review B **61**, 11993-11997 (2000)

WECHSLER D., ZSIGMOND G., STREFFER F., MEZEI F. VITESS: Virtual instrumentation tool for pulsed and continuous sources.
Neutron News **11**, 25-28 (2000)

WEITKAMP J., NEUEFEIND J., FISCHER H.E., ZEIDLER M.D. Hydrogen bonding in liquid methanol at ambient conditions and at high pressure.
Molecular Physics **98**, 125-134 (2000)

WILDES A.R., COWLAM N., AL-HENITI S., KISS L.F., KEMENY T. A polarised neutron scattering study of two samples of $Fe_{90}Zr_{10}$.
Physica B **276-278**, 712-713 (2000)

WILDES A.R., SAROUN J., FARHI E., ANDERSON I., HØGHØJ P., BROCHIER A. A comparison of Monte-Carlo simulations using RESTRAX and McSTAS with experiment on IN14.
Physica B **276-278**, 177-178 (2000)

WILKINSON C., SCHOBINGER-PAPAMANTELLOS P., MYLES D., TUNG L.D., BUSCHOW K.H.J. On the modulated structure of $La_2Co_{1.7}$: A neutron Laue diffraction study.
Journal of Magnetism and Magnetic Materials **217**, 55-64 (2000)

WILLNER L., POPPE A., ALLGAIER J., MONKENBUSCH M., LINDNER P., RICHTER D. Micellization of amphiphilic diblock copolymers: Corona shape and mean-field to scaling crossover.
Europhysics Letters **51**, 628-634 (2000)

WILLS A.S., HARRISON A., RITTER C., SMITH R.I. Magnetic properties of pure and diamagnetically doped jarosites: Model *kagomé* antiferromagnets with variable coverage of the magnetic lattice.
Physical Review B **61**, 6156-6169 (2000)

WISCHNEWSKI A., RICHTER D., MONKENBUSCH M., WILLNER L., FARAGO B., EHLERS G., SCHLEGER P. Reptation in polyethylene-melts with different molecular weights.
Physica B **276-278**, 337-338 (2000)

WOODCOCK D.A., LIGHTFOOT P., RITTER C. Negative thermal expansion in $Y_2(WO_4)_3$.
Journal of Solid State Chemistry **149**, 92-98 (2000)

ZABEL H., SIEBRECHT R., SCHREYER A. Neutron reflectometry on magnetic thin films.
Physica B **276-278**, 17-21 (2000)

ZACCAI G. How soft is a protein? A protein dynamics force constant measured by neutron scattering.
Science **288**, 1604-1607 (2000)

ZACCAI G., TEHEI M., SCHERBAKOVA I., SERDYUK I., GEREZ C., PFISTER C. Incoherent elastic neutron scattering as a function of temperature: A fast way to characterise *in-situ* biological dynamics in complex solutions.
Journal de Physique IV **10**, Pr7-283-Pr7-287 (2000)

ZEYEN C.M.E., OTAKE Y. Neutron EDM search using crystal techniques.
Nuclear Instruments and Methods in Physics Research A **440**, 489-490 (2000)

ZHELUDEV A., MASLOV S., SHIRANE G., TSUKADA I., MASUDA T., UCHINOKURA K., ZALIZNYAK I., ERWIN R., REGNAULT L.P. Magnetic anisotropy and low-energy spin waves in the Dzyaloshinskii-Moriya spiral magnet $Ba_2CuGe_2O_7$.
Physical Review B **59**, 11432-11444 (1999)

ZIMMER O. A method of magnetic storage of ultracold neutrons for a precise measurement of the neutron lifetime.
Journal of Physics G: Nuclear and Particle Physics **26**, 67-77 (2000)

ZIMMER O., BYRNE J., VAN DER GRINTEN M.G.D., HEIL W., GLÜCK F. "aspect" - A new spectrometer for the measurement of the angular correlation coefficient *a* in neutron beta decay.
Nuclear Instruments and Methods in Physics Research A **440**, 548-556 (2000)

ZIMMER O., HAUTLE P., HEIL W., HOFMANN D., HUMBLOT H., KRASNOSCHEKOVA I., LASAKOV M., MÜLLER T.M., NESVIZHEVSKY V.V., REICH J., SEREBROV A., SOBOLEV Y., VASSILEV A. Spin filters and supermirrors: A comparison study of two methods of high-precision neutron polarisation analysis.
Nuclear Instruments and Methods in Physics Research A **440**, 764-771 (2000)

ZORN R., RICHTER D., HARTMANN L., KREMER F., FRICK B. Inelastic neutron scattering experiments on the fast dynamics of a glass forming liquid in mesoscopic confinements.
Journal de Physique IV **10**, Pr7-83-Pr7-86 (2000)

## Theses and Habilitations

ANDERSON C.R. The effects of introducing static and dynamic disorder on the low-energy excitations of superfluid $^3$He.
Thesis submitted with the requirements of the University of Liverpool for the degree of Doctor of Philosophy, University of Liverpool, Great Britain - Institut Laue-Langevin, Grenoble, France (2000)

CLEGG P.S. The chemical and magnetic structures of rare earth alloys and superlattices.
Thesis submitted for the degree of Doctor of Philosophy, Wolfson College, University of Oxford, Great Britain (2000)

GONZALEZ GONZALEZ M.A. Estructura y dinámica de las fases condensadas del etanol.
Universidad Complutense de Madrid, Facultad de Ciencias Quimicas, Madrid, Spain / Institut Laue Langevin, Grenoble, France (1999)

JOHNSON M.R. De l'effet tunnel des protons à la modélisation de la surface d'énergie potentielle.
Mémoire présenté pour un diplôme d'habilitation à diriger les recherches, Université Joseph Fourier - Grenoble I, France (1999)

MONDELLI C. Fluctuations, frustration and dilution in the $SrCr_xGa_{12-x}O_{19}$ compounds. Neutron scattering investigation in a broad dynamical range.
Thèse présentée pour obtenir le grade de Docteur de l'Université Joseph Fournier - Grenoble I, France (2000)

PLAZANET M. Structure et dynamique quantique de cristaux moléculaires: Spectroscopie et modélisation numérique.
Thèse présentée pour obtenir le grade de Docteur de l'Université Joseph Fourier - Grenoble I, France (2000)

WIMPORY R.C. Aspects of neutron residual stress analysis.
A doctoral thesis submitted in partial fulfilment of the requirements for the award of the degree Doctor of Philosophy of Loughborough University, Great Britain (1999)

Editors: Giovanna Cicognani, Christian Vettier
Design and Typesetting: PARALLELES – studio@paralleles.fr
Photography by S. Claisse (ILL) and Artechnique – artechnique@wanadoo.fr
Photo DNA molecule page 56: © CNRS/Université de Montpellier 2
Printing: Imprimerie du Pont-de-Claix
April 2001

Acknowledgement
We would like to thank all the people who helped make this report.

Further copies can be obtained from:
Institut Laue-Langevin
Scientific Coordination Office (SCO)
BP 156 - F-38042 Grenoble Cedex 9 (France)
Tel: +33 (0)4 76 20 72 40 - Fax: +33 (0)4 76 48 39 06
email: kjenkins@ill.fr or sco@ill.fr
WEB: www.ill.fr

NEUTRONS
FOR SCIENCE

NEUTRONS
FOR SCIENCE

6, RUE JULES HOROWITZ - BP 156 - 38042 GRENOBLE CEDEX 9 - FRANCE
Web site: www.ill.fr